

# 20

## Solar Thermal Energy Conversion

---

T. Agami Reddy

*Drexel University*

Riccardo Battisti

*University of Rome "La Sapienza"*

Hans Schweiger

*Active Solar System Group*

Werner Weiss

*AEE INTEC*

Jeffrey H. Morehouse

*University of South Carolina*

Sanjay Vijayaraghavan

*Intel Technology India Pvt. Ltd.*

D. Yogi Goswami

*University of South Florida*

20.1	Active Solar Heating Systems .....	20-1
	Introduction • Solar Collectors • Long-Term Performance of Solar Collectors • Solar Systems • Controls • Thermal Storage Systems • Solar System Simulation • Solar System Sizing Methodology • Solar System Design Methods • Design Recommendations and Costs	
	References.....	20-48
20.2	Solar Heat for Industrial Processes .....	20-49
	The Potential for Solar Process Heat • Solar Thermal Systems in Industrial Processes: Integration and Basic Design Guidelines • Overview of Existing Solar Process Heat Plants	
	References.....	20-59
20.3	Passive Solar Heating, Cooling, and Daylighting .....	20-59
	Introduction • Solar Thermosyphon Water Heating • Passive Solar Heating Design Fundamentals • Passive Space Cooling Design Fundamentals • Daylighting Design Fundamentals	
	Glossary.....	20-119
	References.....	20-119
	For Further Information.....	20-121
20.4	Solar Cooling.....	20-121
	Vapor Compression Cycle • Absorption Air Conditioning • Solar Desiccant Dehumidification • Liquid-Desiccant Cooling System	
	References.....	20-133

### 20.1 Active Solar Heating Systems

---

*T. Agami Reddy*

#### 20.1.1 Introduction

This section defines the scope of the entire chapter and presents a brief overview of the types of applications that solar thermal energy can potentially satisfy.

##### 20.1.1.1 Motivation and Scope

Successful solar system design is an iterative process involving consideration of many technical, practical, reliability, cost, code, and environmental considerations (Mueller Associates 1985). The success of a

project involves identification of and intelligent selection among trade-offs, for which a proper understanding of goals, objectives, and constraints is essential. Given the limited experience available in the solar field, it is advisable to keep solar systems as simple as possible and not be lured by the promise of higher efficiency offered by more complex systems. Because of the location-specific variability of the solar resource, solar systems offer certain design complexities and concerns not encountered in traditional energy systems.

The objective of this chapter is to provide energy professionals with a fundamental working knowledge of the scientific and engineering principles of solar collectors and solar systems relevant to both the prefeasibility study and the feasibility study of a solar project. Conventional equipment such as heat exchangers, pumps, and piping layout are but briefly described. Because of space limitations, certain equations/correlations had to be omitted, and proper justice could not be given to several concepts and design approaches. Effort has been made to provide the reader with pertinent references to textbooks, manuals, and research papers.

A detailed design of solar systems requires in-depth knowledge and experience in (i) the use of specially developed computer programs for detailed simulation of solar system performance, (ii) designing conventional equipment, controls, and hydronic systems, (iii) practical aspects of equipment installation, and (iv) economic analysis. These aspects are not addressed here, given the limited scope of this chapter. Readers interested in acquiring such details can consult manuals such as Mueller Associates (1985) or SERI (1989).

The lengthy process outlined above pertains to large solar installations. The process is much less involved when a small domestic hot-water system, or unitary solar equipment or single solar appliances such as solar stills, solar cookers, or solar dryers are to be installed. Not only do such appliances differ in engineering construction from region to region, there are also standardized commercially available units whose designs are already more or less optimized by the manufacturers, normally as a result of previous experimentation, both technical or otherwise. Such equipment is not described in this chapter for want of space.

The design concepts described in this chapter are applicable to domestic water heating, swimming pool heating, active space heating, industrial process heat, convective drying systems, and solar cooling systems.

## **20.1.2 Solar Collectors**

### **20.1.2.1 Collector Types**

A solar thermal collector is a heat exchanger that converts radiant solar energy into heat. In essence this consists of a receiver that absorbs the solar radiation and then transfers the thermal energy to a working fluid. Because of the nature of the radiant energy (its spectral characteristics, its diurnal and seasonal variability, changes in diffuse to global fraction, etc.), as well as the different types of applications for which solar thermal energy can be used, the analysis and design of solar collectors present unique and unconventional problems in heat transfer, optics, and material science. The classification of solar collectors can be made according to the type of working fluid (water, air, or oils) or the type of solar receiver used (nontracking or tracking).

Most commonly used working fluids are water (glycol being added for freeze protection) and air. [Table 20.1](#) identifies the relative advantages and potential disadvantages of air and liquid collectors and associated systems. Because of the poorer heat transfer characteristics of air with the solar absorber, the air collector may operate at a higher temperature than a liquid-filled collector, resulting in greater thermal losses and, consequently, a lower efficiency. The choice of the working fluid is usually dictated by the application. For example, air collectors are suitable for space heating and convective drying applications, while liquid collectors are the obvious choice for domestic and industrial hot-water applications. In certain high-temperature applications, special types of oils are used that provide better heat transfer characteristics.

The second criterion of collector classification is according to the presence of a mechanism to track the sun throughout the day and year in either a continuous or discreet fashion (see [Table 20.2](#)). The

**TABLE 20.1** Advantages and Disadvantages of Liquid and Air Systems

Characteristics	Liquid	Air
Efficiency	Collectors generally more efficient for a given temperature difference	Collectors generally operate at slightly lower efficiency
System configuration	Can be readily combined with service hot-water and cooling systems	Space heat can be supplied directly but does not adapt easily to cooling. Can preheat hot-water
Freeze protection	May require antifreeze and heat exchangers that add cost and reduce efficiency	None needed
Maintenance	Precautions must be taken against leakage, corrosion and boiling	Low maintenance requirements. Leaks repaired readily with duct tape, but leaks may be difficult to find
Space requirements	Insulated pipes take up nominal space and are more convenient to install in existing buildings	Duct work and rock storage units are bulky, but ducting is a standard HVAC installation technique
Operation	Less energy required to pump liquids	More energy required by blowers to move air; noisier operation
Cost	Collectors cost more	Storage costs more
State of the art	Has received considerable attention from solar industry	Has received less attention from solar industry

Source: From SERI, *Engineering Principles and Concepts for Active Solar Systems*, Hemisphere Publishing Company, New York, 1989.

stationary flat-plate collectors are rigidly mounted, facing toward the equator with a tilt angle from the horizontal roughly equal to the latitude of the location for optimal year-round operation. The compound parabolic concentrators (CPCs) can be designed either as completely stationary devices or as devices that need seasonal adjustments only. On the other hand, Fresnel reflectors, paraboloids, and heliostats need two-axis tracking. Parabolic troughs have one axis tracking either along the east–west direction or the north–south direction. These collector types are described by Kreider (1979a, 1979b) and Rabl (1985).

A third classification criterion is to distinguish between nonconcentrating and concentrating collectors. The main reason for using concentrating collectors is not that *more energy* can be collected but that the thermal energy is obtained at higher temperatures. This is done by decreasing the area from which heat losses occur (called the receiver area) with respect to the aperture area (i.e., the area that intercepts the solar radiation). The ratio of the aperture to receiver area is called the *concentration ratio*.

## 20.1.2.2 Flat-Plate Collectors

### 20.1.2.2.1 Description

The flat-plate collector is the most common conversion device in operation today, since it is most economical and appropriate for delivering energy at temperatures up to about 100°C. The construction of flat-plate collectors is relatively simple, and many commercial models are available.

Figure 20.1 shows the physical arrangements of the major components of a conventional flat-plate collector with a liquid working fluid. The blackened absorber is heated by radiation admitted via the transparent cover. Thermal losses to the surroundings from the absorber are contained by the cover,

**TABLE 20.2** Types of Solar Thermal Collectors

Nontracking Collectors	Tracking Collectors
Basic flat-plate	Parabolic troughs
Flat-plate enhanced with side reflectors or V-troughs	Fresnel reflectors
Tubular collectors	Paraboloids
Compound parabolic concentrators (CPCs)	Heliostats with central receivers

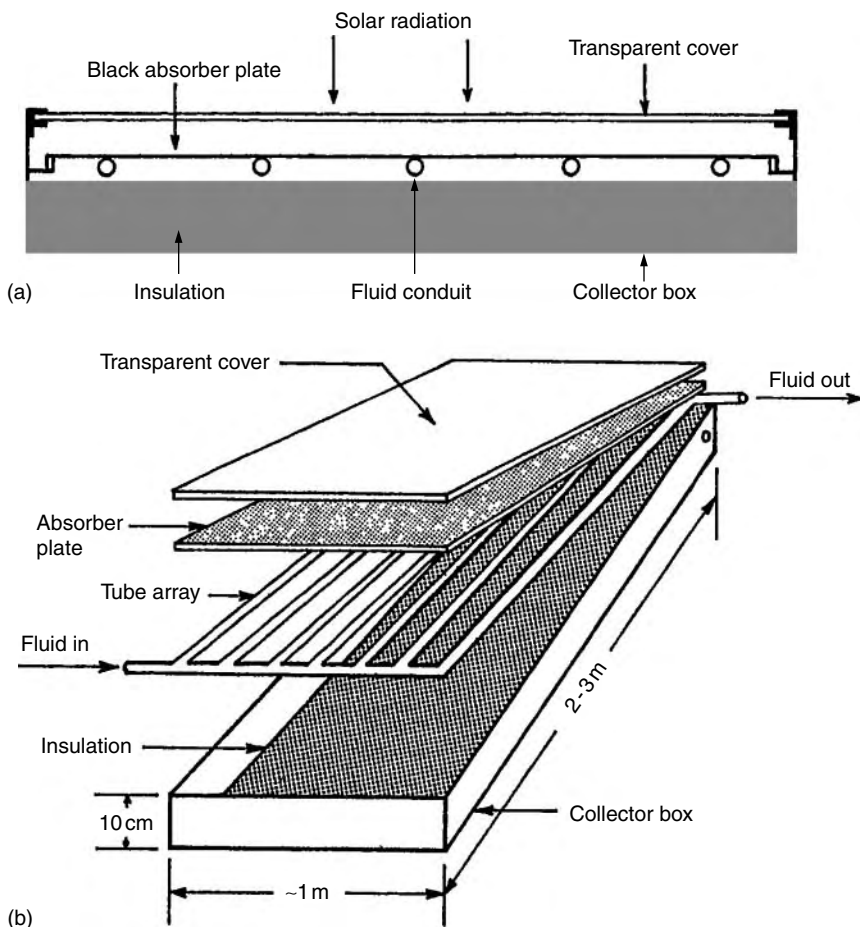
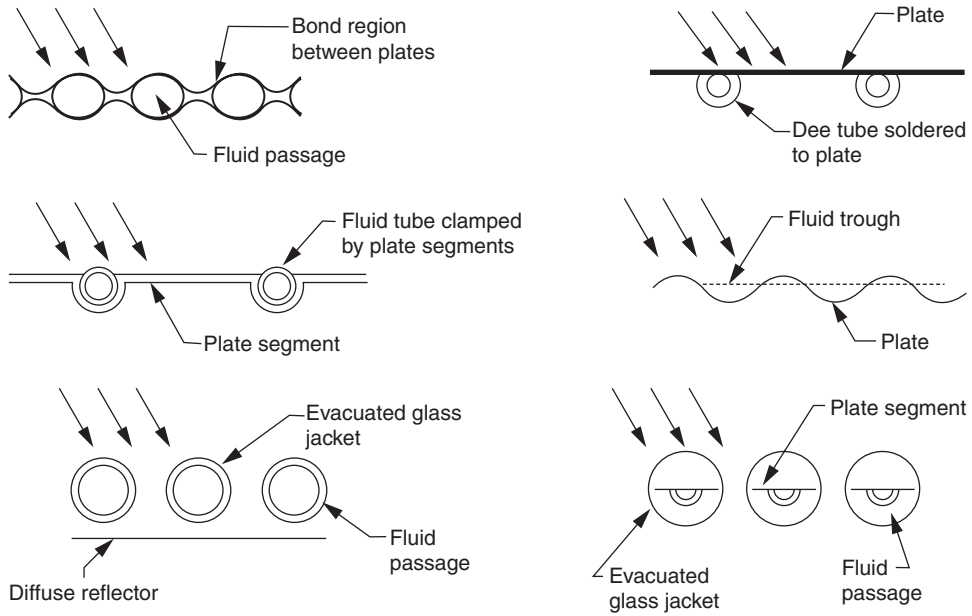


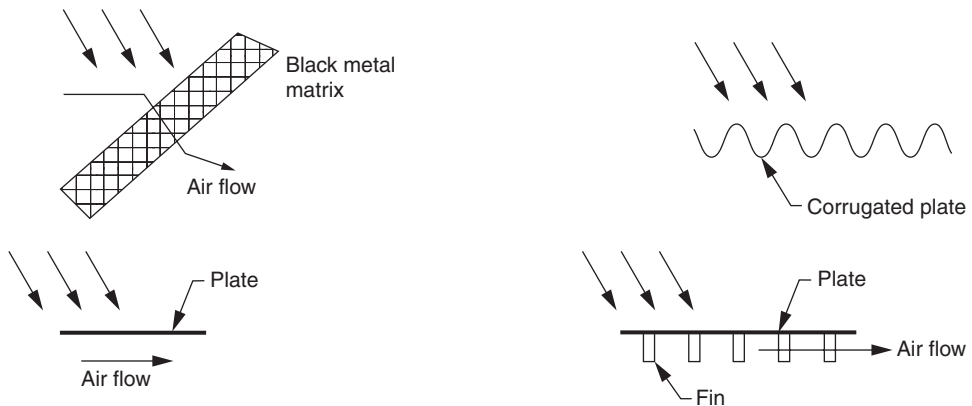
FIGURE 20.1 Cross-section and isometric view of a flat-plate collector.

which acts as a black body to the infrared radiation (this effect is called the *greenhouse* effect), and by insulation provided under the absorber plate. Passages attached to the absorber are filled with a circulating fluid, which extracts energy from the hot absorber. The simplicity of the overall device makes for long service life.

The absorber is the most complex portion of the flat-plate collector, and a great variety of configurations are currently available for liquid and air collectors. Figure 20.2 illustrates some of these concepts in absorber design for both liquid and air absorbers. Conventional materials are copper, aluminum, and steel. The absorber is either painted with a dull black paint or can be coated with a *selective surface* to improve performance (see “Improvements to Flat-Plate Collector Performance” for more details). Bonded plates having internal passageways perform well as absorber plates because the hydraulic passageways can be designed for optimal fluid and thermal performance. Such collectors are called *roll-bond* collectors. Another common absorber consists of tubes soldered or brazed to a single metal sheet, and mechanical attachments of the tubes to the plate have also been employed. This type of collector is called a *tube-and-sheet* collector. Heat pipe collectors have also been developed, though these are not as widespread as the previous two types. The so-called *trickle type* of flat-plate collector, with the fluid flowing directly over the corrugated absorber plate, dispenses entirely with fluid passageways. Tubular collectors have also been used because of the relative ease by which air can be evacuated from such collectors, thereby reducing convective heat losses from the absorber to the ambient air.



(a) Liquid collectors



(b) Air collectors

FIGURE 20.2 Typical flat-plate absorber configurations.

The absorber in an air collector normally requires a larger surface than in a liquid collector because of the poorer heat transfer coefficients of the flowing air stream. Roughness elements and producing turbulence by way of devices such as expanded metal foil, wool, and overlapping plates have been used as a means for increasing the heat transfer from the absorber to the working fluid. Another approach to enhance heat transfer is to use packed beds of expanded metal foils or matrices between the glazing and the bottom plate.

**20.1.2.2.2 Modeling**

A particular modeling approach and the corresponding degree of complexity in the model are dictated by the objective as well as by experience gained from past simulation work. For example, it has been found that transient collector behavior has insignificant influence when one is interested in determining the

long-term performance of a solar thermal system. For complex systems or systems meant for nonstandard applications, detailed modeling and careful simulation of system operation are a must initially, and simplifications in component models and system operation can subsequently be made. However, in the case of solar thermal systems, many of the possible applications have been studied to date and a backlog of experience is available not only concerning system configurations but also with reference to the degree of component model complexity.

Because of low collector time constants (about 5–10 min), heat capacity effects are usually small. Then the instantaneous (or hourly, because radiation data are normally available in hourly time increments only) steady-state useful energy  $q_C$  in watts delivered by a solar flat-plate collector of surface area  $A_C$  is given by

$$q_C = A_C F' [I_T \eta_0 - U_L (T_{Cm} - T_a)]^+ \tag{20.1}$$

where  $F'$  is the plate efficiency factor, which is a measure of how good the heat transfer is between the fluid and the absorber plate;  $\eta_0$  is the optical efficiency, or the product of the transmittance and absorptance of the cover and absorber of the collector;  $U_L$  is the overall heat loss coefficient of the collector, which is dependent on collector design only and is normally expressed in  $W/(m^2\text{ }^\circ\text{C})$ ;  $T_{Cm}$  is the mean fluid temperature in the collector (in  $^\circ\text{C}$ ); and  $I_T$  is the radiation intensity on the plane of the collector (in  $W/m^2$ ). The + sign denotes that negative values are to be set to zero, which physically implies that the collector should not be operated when  $q_C$  is negative (i.e., when the collector loses more heat than it can collect).

However, because  $T_{Cm}$  is not a convenient quantity to use, it is more appropriate to express collector performance in terms of the fluid inlet temperature to the collector ( $T_{Ci}$ ). This equation is known as the classical Hottel–Whillier–Bliss (HWB) equation and is most widely used to predict instantaneous collector performance:

$$q_C = A_C F_R [I_T \eta_0 - U_L (T_{Ci} - T_a)]^+ \tag{20.2}$$

where  $F_R$  is called the heat removal factor and is a measure of the solar collector performance as a heat exchanger, since it can be interpreted as the ratio of actual heat transfer to the maximum possible heat transfer. It is related to  $F'$  by

$$\frac{F_R}{F'} = \frac{(m c_p)_C}{A_C F' U_L} \left\{ 1 - \exp \left[ - \frac{A_C U_L F'}{(m c_p)_C} \right] \right\} \tag{20.3}$$

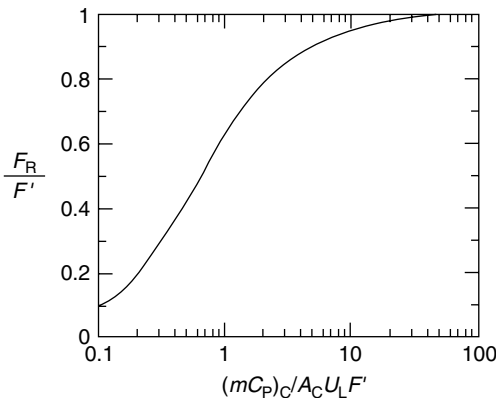


**FIGURE 20.3** Variation of  $F_R/F'$  as a function of  $[(m c_p)_C / (A_C U_L F')]$ . (From Duffie, J. A. and Beckman, W. A., *Solar Engineering of Thermal Processes*, Wiley Interscience, New York, 1980.)

where  $m_C$  is the total fluid flow rate through the collectors and  $c_{pc}$  is the specific heat of the fluid flowing through the collector. The variation of  $(F_R/F')$  with  $[(m c_p)_C / A_C U_L F']$  is shown graphically in Figure 20.3. Note the asymptotic behavior of the plot, which suggests that increasing the fluid flow rate more than a certain amount results in little improvement in  $F_R$  (and hence in  $q_C$ ) while causing a quadratic increase in the pressure drop.

Factors influencing solar collector performance are of three types: (i) constructional, that is, related to collector design and materials used, (ii) climatic, and (iii) operational, that is, fluid temperature, flow rate, and so on. The plate efficiency factor  $F'$  is a factor that depends on the physical constructional features and is

essentially a constant for a given liquid collector. (This is not true for air collectors, which require more careful analysis.) Operational features involve changes in  $m_C$  and  $T_{Ci}$ . While changes in  $m_C$  affect  $F_R$  as per Equation 20.3, we note from Equation 20.2 that to enhance  $q_C$ ,  $T_{Ci}$  needs to be kept as low as possible. For solar collectors that are operated under more or less constant flow rates, specifying  $F_R \eta_0$  and  $F_R U_L$  is adequate to predict collector performance under varying climatic conditions.

There are a number of procedures by which collectors have been tested. The most common is a *steady-state procedure*, where transient effects due to collector heat capacity are minimized by performing tests only during periods when radiation and ambient temperature are steady. The procedure involves simultaneous and accurate measurements of the mass flow rate, the inlet and outlet temperatures of the collector fluid, and the ambient conditions (incident solar radiation, air temperature, and wind speed). The most widely used test procedure is the ASHRAE Standard 93-77 (1978), whose test setup is shown in Figure 20.4. Though a solar simulator can be used to perform indoor testing, outdoor testing is always more realistic and less expensive. The procedure can be used for nonconcentrating collectors using air or liquid as the working fluid (but not two phase mixtures) that have a single inlet and a single outlet and contain no integral thermal storage.

Steady-state procedures have been in use for a relatively long period and though the basis is very simple the engineering setup is relatively expensive (see Figure 20.4). From an overall heat balance on the collector fluid and from Equation 20.2, the expressions for the instantaneous collector efficiency under normal solar incidence are

$$\eta_C \equiv \frac{q_C}{A_C I_T} = \frac{(m c_p)_C (T_{Co} - T_{Ci})}{A_C I_T} \quad (20.4)$$

$$= \left[ F_R \eta_n - F_R U_L \left( \frac{T_{Ci} - T_a}{I_T} \right) \right] \quad (20.5)$$

where  $\eta_n$  is the optical efficiency at normal solar incidence.

From the test data, points of  $\eta_c$  against reduced temperature  $[(T_{Ci} - T_a)/I_T]$  are plotted as shown in Figure 20.5. Then a linear fit is made to these data points by regression, from which the values of  $F_R \eta_n$  and  $F_R U_L$  are easily deduced. It will be noted that if the reduced term were to be taken as  $[(T_{Cm} - T_a)/I_T]$ , estimates of  $F' \eta_n$  and  $F' U_L$  would be correspondingly obtained.

### 20.1.2.2.3 Incidence Angle Modifier

The optical efficiency  $\eta_0$  depends on the collector configuration and varies with the angle of incidence as well as with the relative values of diffuse and beam radiation. The incidence angle modifier is defined as  $K_\eta \equiv (\eta_0/\eta_n)$ . For flat-plate collectors with 1 or 2 glass covers,  $K_\eta$  is almost unchanged up to incidence angles of  $60^\circ$ , after which it abruptly drops to zero.

A simple way to model the variation of  $K_\eta$  with incidence angle for flat-plate collectors is to specify  $\eta_n$ , the optical efficiency of the collector at normal beam incidence, to assume the entire radiation to be beam, and to use the following expression for the angular dependence (ASHRAE 1978)

$$K_\eta = 1 + b_0 \left( \frac{1}{\cos \theta} - 1 \right) \quad (20.6)$$

where  $\theta$  is the solar angle of incidence on the collector plate (in degrees) and  $b_0$  is a constant called the incidence angle modifier coefficient. Plotting  $K_\eta$  against  $[(1/\cos \theta) - 1]$  results in linear plots (see Figure 20.6), thus justifying the use of Equation 20.6. We note that for one-glass and two-glass covers, approximate values of  $b_0$  are  $-0.10$  and  $-0.17$ , respectively.

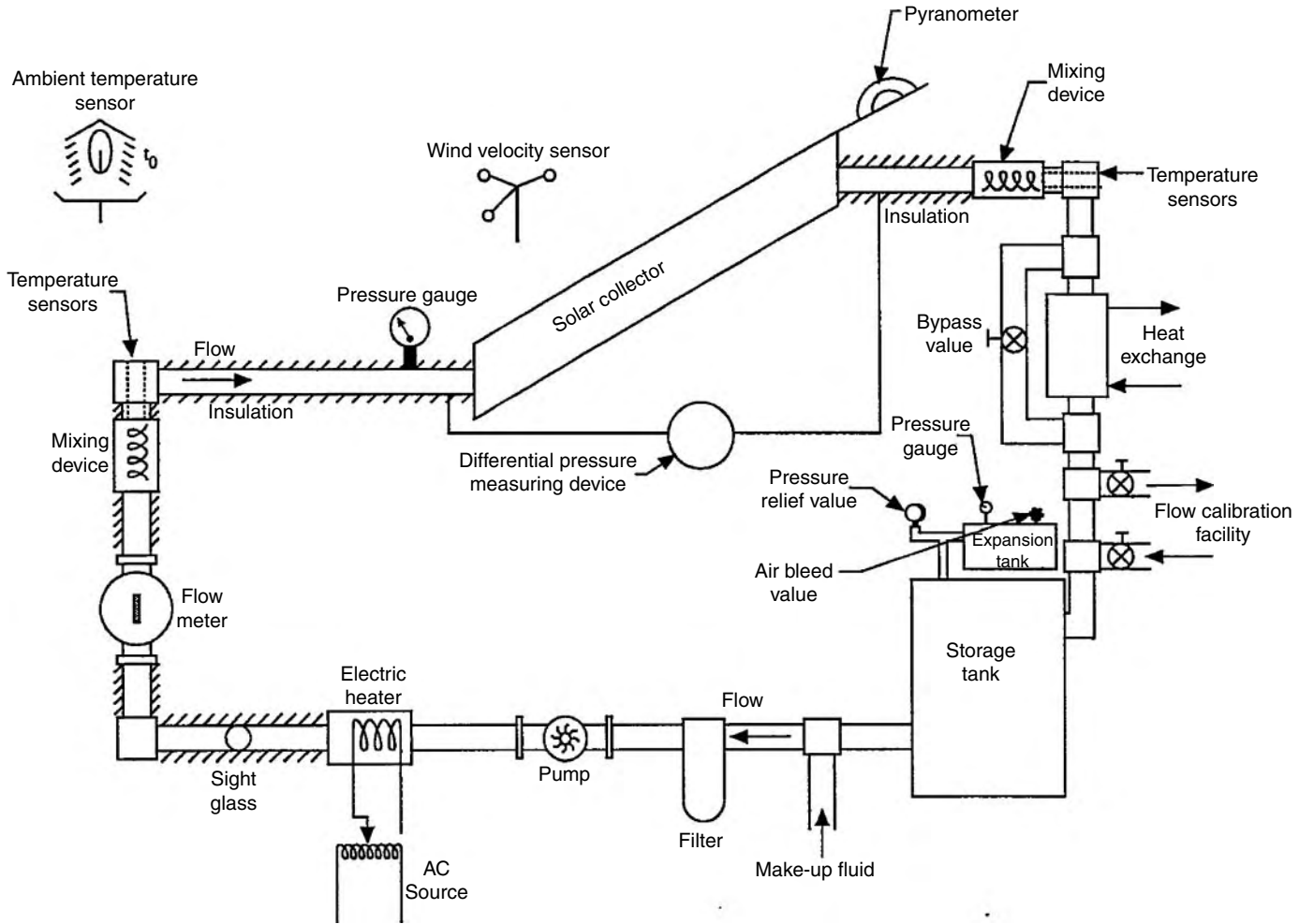
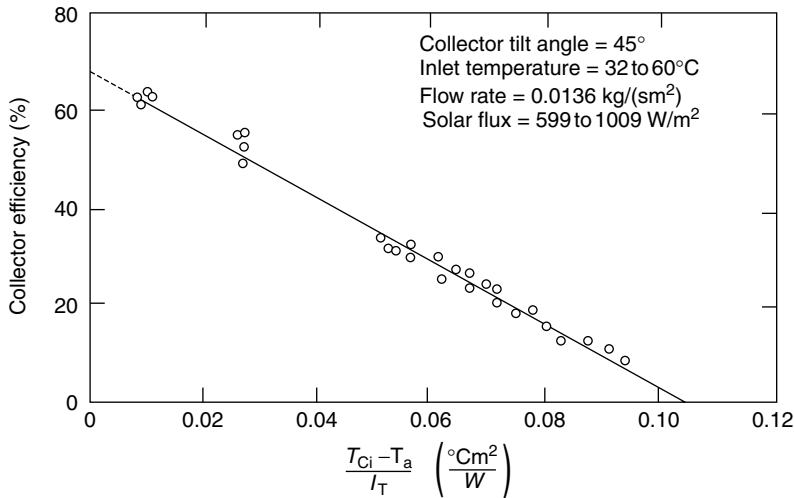


FIGURE 20.4 Set up for testing liquid collectors according to ASHRAE Standard 93-72.





**FIGURE 20.5** Thermal efficiency curve for a double glazed flat-plate liquid collector. Test conducted outdoors on a 1.2 m by 1.25 m panel with 10.2 cm of glass fiber back insulation and a flat copper absorber with black coating of emissivity of 0.97. (From ASHRAE Standard 93-77, *Methods of Testing to Determine the Thermal Performance of Solar Collectors*, American Society of Heating, Refrigeration and Air Conditioning Engineers, New York, 1978.)

In case the diffuse solar fraction is high, one needs to distinguish between beam, diffuse, and ground-reflected components. Diffuse radiation, by its very nature, has no single incidence angle. One simple way is to assume an equivalent incidence angle of  $60^\circ$  for diffuse and ground-reflected components. One would then use Equation 20.6 for the beam component along with its corresponding value of  $\theta$  and account for the contribution of diffuse and ground reflected components by assuming a value of  $\theta = 60^\circ$  in Equation 20.6. For more accurate estimation, one can use the relationship between the effective diffuse solar incidence angle versus collector tilt given in Duffie and Beckman (1980). It should be noted that the preceding equation gives misleading results with incidence angles close to  $90^\circ$ . An alternative functional form for the incidence angle modifier for both flat-plate and concentrating collectors has been proposed by Rabl (1981).

### Example 20.1.1

From the thermal efficiency curve given in Figure 20.5 determine the performance parameters of the corresponding solar collector.

Extrapolating the curve yields  $y$ -intercept = 0.69,  $x$ -intercept = 0.105 ( $\text{m}^2\text{C}/\text{W}$ ). Since the reduced temperature in Figure 20.5 is in terms of the inlet fluid temperature to the collector, Equation 20.5 yields  $F_R \eta_n = 0.69$  and  $F_R U_L = 0.69/0.105 = 6.57 \text{ W}/(\text{m}^2\text{C})$ . Alternatively, the collector parameters in terms of the plate efficiency factor can be deduced. From Figure 20.5, the collector area =  $1.22 \times 1.25 = 1.525 \text{ m}^2$ , while the flow rate ( $m/A_C$ ) =  $0.0136 \text{ kg}/(\text{s m}^2)$ . From Equation 20.3,

$$F'/F_R = -(0.0136 \times 4190/6.57) \ln[-6.57/(0.0136 \times 4190)] = 1.0625$$

Thus  $F' U_L = 6.57 \times 1.0625 = 6.98 \text{ W}/(\text{m}^2\text{C})$  and  $F' \eta_n = 0.69 \times 1.0625 = 0.733$ .

### Example 20.1.2

How would the optical efficiency be effected at a solar incidence angle of  $60^\circ$  for a flat-plate collector with two glass covers?

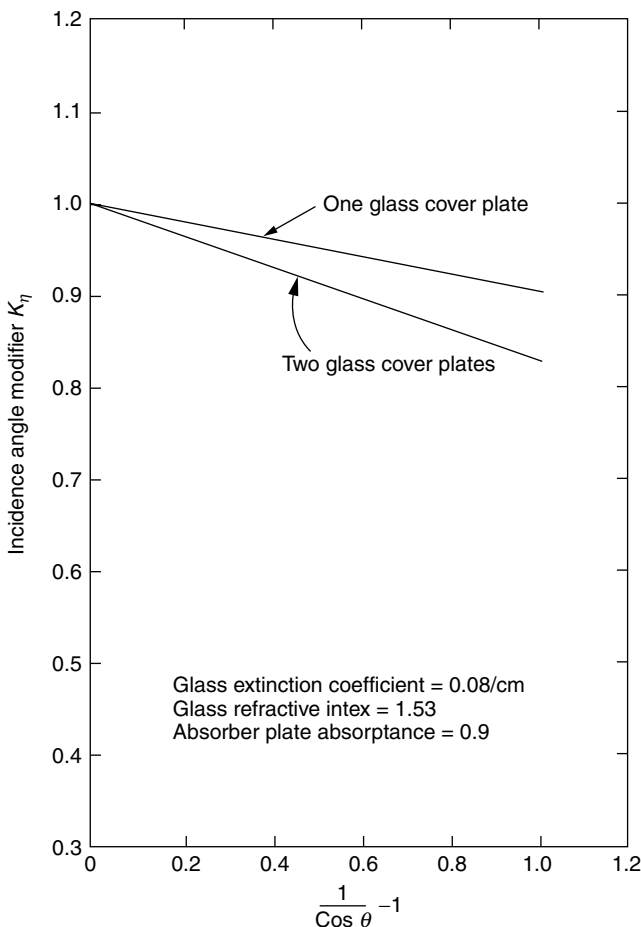


**FIGURE 20.6** Incidence angle modifiers for two flat-plate collectors with nonselective coating on the absorber. (Adapted From ASHRAE Standard 93-77, *Methods of Testing to Determine the Thermal Performance of Solar Collectors*, American Society of Heating, Refrigeration and Air Conditioning Engineers, New York, 1978.)

Assume a value of  $b_0 = -0.17$ . From Equation 20.6,  $K_\eta = 0.83$ . Thus

$$F_R \eta_0 = F_R \eta_n K_\eta = 0.69 \times 0.83 = 0.57$$

#### 20.1.2.2.4 Other Collector Characteristics

There are three collector characteristics that a comprehensive collector testing process should also address. The collector *time constant* is a measure that determines how intermittent sunshine affects collector performance and is useful in defining an operating control strategy for the collector array that avoids instability. Collector performance is usually enhanced if collector time constants are kept low. ASHRAE 93-77 also includes a method for determining this value. Commercial collectors usually have time constants of about 5 min or less, and this justifies the use of the HWB model (see Equation 20.2).

Another quantity to be determined from collector tests is the collector *stagnation temperature*. This is the equilibrium temperature reached by the absorber plate when no heat is being extracted from the collector. Determining the maximum stagnation temperature, which occurs under high  $I_T$  and  $T_a$  values, is useful in order to safeguard against reduced collector life due to thermal damage to collectors (namely irreversible thermal expansion, sagging of covers, physical deterioration, optical changes, etc.) in the field

when not in use. Though the stagnation temperature could be estimated from Equation 20.2 by setting  $q_C=0$  and solving for  $T_{C_i}$ , it is better to perform actual tests on collectors before field installation.

The third collector characteristic of interest is the *pressure drop* across the collector for different fluid flow rates. This is an important consideration for liquid collectors, and more so for air collectors, in order to keep parasitic energy consumption (namely electricity to drive pumps and blowers) to a minimum in large collector arrays.

### 20.1.2.3 Improvements to Flat-Plate Collector Performance

There are a number of ways by which the performance of the basic flat-plate collectors can be improved. One way is to enhance optical efficiency by treatment of the glass cover thereby reducing reflection and enhancing performance. As much as a 4% increase has been reported (Anderson 1977). Low-iron glass can also reduce solar absorption losses by a few percent.

These improvements are modest compared to possible improvements from reducing losses from the absorber plate. Essentially, the infrared upward reradiation losses from the heated absorber plate have to be decreased. One could use a second glass cover to reduce the losses, albeit at the expense of higher cost and lower optical efficiency. Usually for water heating applications, radiation accounts for about two-thirds of the losses from the absorber to the cover with convective losses making up the rest (conduction is less than about 5%). The most widely used manner of reducing these radiation losses is to use selective surfaces whose emissivity varies with wavelength (as against matte-black painted absorbers, which are essentially gray bodies). Note that 98% of the solar spectrum is at wavelengths less than  $3.0\ \mu\text{m}$ , whereas less than 1% of the black body radiation from a  $200^\circ\text{C}$  surface is at wavelengths less than  $3.0\ \mu\text{m}$ . Thus selective surfaces for solar collectors should have high-solar absorptance (i.e., low reflectance in the solar spectrum) and low long-wave emittance (i.e., high reflectance in the long-wave spectrum). The spectral reflectance of some commonly used selective surfaces is shown in Figure 20.7. Several commercial collectors for water heating or low-pressure steam (for absorption cooling or process heat applications) are available that use selective surfaces.

Another technique to simultaneously reduce both convective and radiative losses between the absorber and the transparent cover is to use honeycomb material (Hollands 1965). The honeycomb material can be reflective or transparent (the latter is more common) and should be sized properly. Glass honeycombs have had some success in reducing losses in high-temperature concentrating receivers, but plastics are

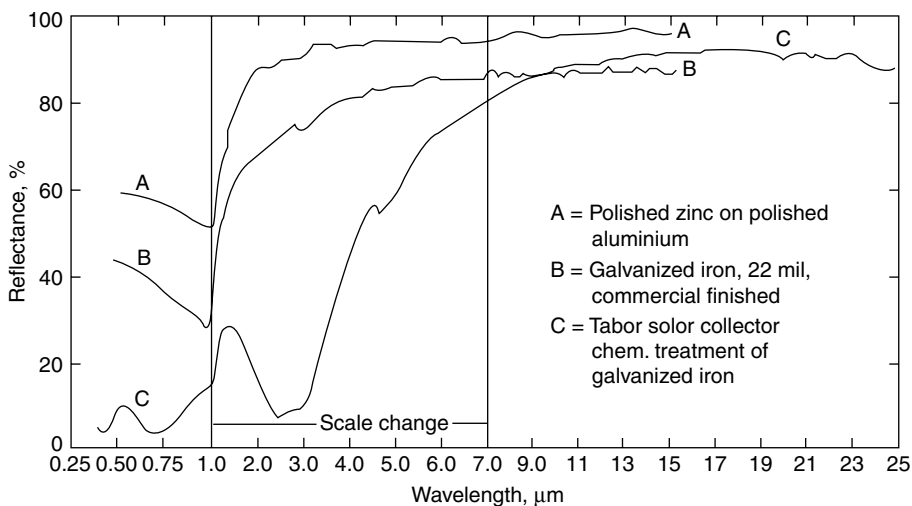


**FIGURE 20.7** Spectral reflectance of several surfaces. (From Edwards, D. K., Nelson, K. E., Roddick, R. D., and Gier, J. T., Basic Studies on the Use of Solar Energy, Report no. 60-93, Department of Engineering, University of California at Los Angeles, CA, 1960.)

usually recommended for use in flat-plate collectors. Because of the poor thermal aging properties, honeycomb flat-plate collectors have had little commercial success. Currently the most promising kind seems to be the simplest (both in terms of analysis and construction), namely collectors using horizontal rectangular slats (Meyer 1978). Convection can be entirely suppressed provided the slats with the proper aspect ratio are used.

Finally, collector output can be enhanced by using side reflectors, for instance a sheet of anodized aluminum. The justification in using these is their low cost and simplicity. For instance, a reflector placed in front of a tilted collector cannot but increase collector performance because losses are unchanged and more solar radiation is intercepted by the collector. Reflectors in other geometries may cast a shadow on the collector and reduce performance. Note also that reflectors would produce rather nonuniform illumination over the day and during the year, which, though not a problem in thermal collectors, may drastically penalize the electric output of photovoltaic modules. Whether reflectors are cost-effective depends on the particular circumstances and practical questions such as aesthetics and space availability. The complexity involved in the analysis of collectors with planar reflectors can be reduced by assuming the reflector to be long compared to its width and treating the problem in two dimensions only. How optical performance of solar collectors are affected by side planar reflectors is discussed in several papers, for example Larson (1980), Chiam (1981).

#### 20.1.2.4 Other Collector Types

##### 20.1.2.4.1 Evacuated Tubular Collectors

One method of obtaining temperatures between 100 and 200°C is to use evacuated tubular collectors. The advantage in creating and being able to maintain a vacuum is that convection losses between glazing

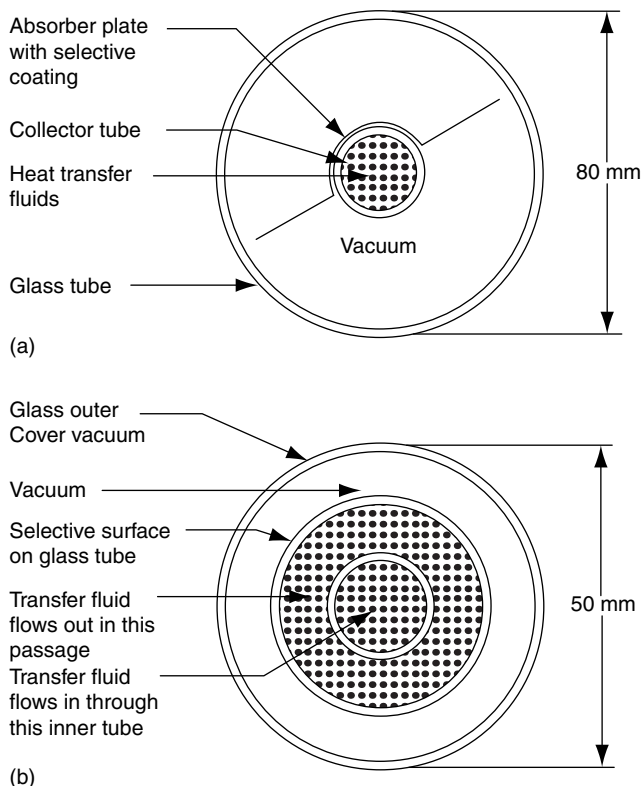


**FIGURE 20.8** Evacuated tubular collectors. (From Charters, W. W. S. and Pryor, T. L., *An Introduction to the Installation of Solar Energy Systems*, Victoria Solar Energy Council, Melbourne, Australia, 1982.)

and absorber can be eliminated. There are different possible arrangements of configuring evacuated tubular collectors. Two designs are shown in Figure 20.8. The first is like a small flat-plate collector with the liquid to be heated making one pass through the collector tube. The second uses an all-glass construction with the glass absorber tube being coated selectively. The fluid being heated passes up the middle of the absorber tube and then back through the annulus. Evacuated tubes can collect both direct and diffuse radiation and do not require tracking. Glass breakage and leaking joints due to thermal expansion are some of the problems which have been experienced with such collector types. Various reflector shapes (like flat-plate, V-groove, circular, cylindrical, involute, etc.) placed behind the tubes are often used to usefully collect some of the solar energy, which may otherwise be lost, thus providing a small amount of concentration.

#### 20.1.2.4.2 Compound Parabolic Concentrators

The CPC collector, discovered in 1966, consists of parabolic reflectors that funnel radiation from aperture to absorber rather than focusing it. The right and left halves belong to different parabolas (hence the name *compound*) with the edges of the receiver being the foci of the opposite parabola (see Figure 20.9). It has been proven that such collectors are *ideal* in that any solar ray, be it beam or diffuse, incident on the aperture within the acceptance angle will reach the absorber while all others will bounce back to and fro and reemerge through the aperture. CPCs are also called *nonimaging* concentrators because they do not form clearly defined images of the solar disk on the absorber surface as achieved in classical concentrators. CPCs can be designed both as low-concentration devices with large acceptance angles or as high-concentration devices with small acceptance angles. CPCs with low-concentration ratios (of about 2) and with east–west axes can be operated as stationary devices throughout the year or at most

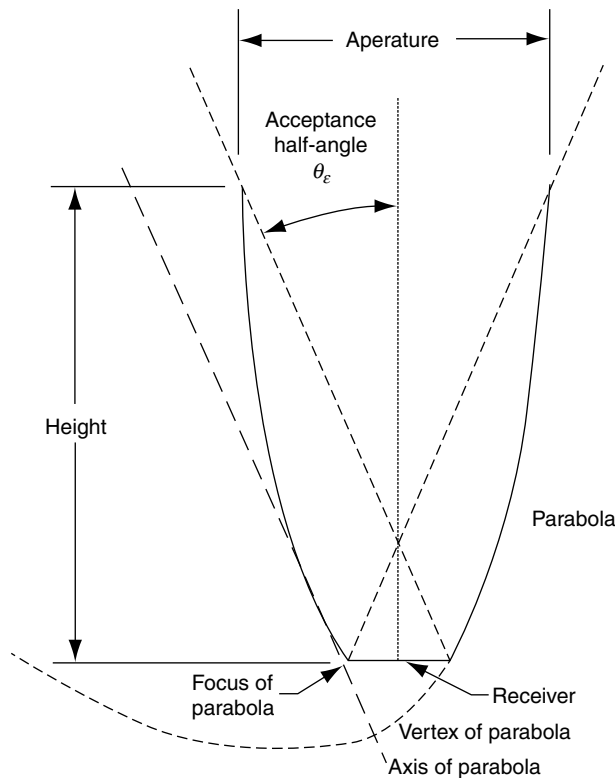


**FIGURE 20.9** Cross-section of a symmetrical nontruncated CPC. (From Duffie, J. A. and Beckman, W. A., *Solar Engineering of Thermal Processes*, Wiley Interscience, New York, 1980.)

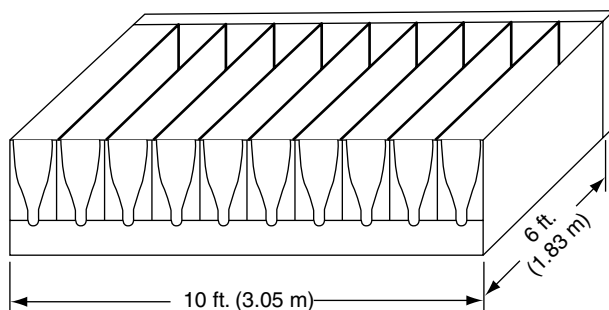


**FIGURE 20.10** A CPC collector module. (From SERI, *Engineering Principles and Concepts for Active Solar Systems*, Hemisphere Publishing Company, New York, 1989.)

with seasonal adjustments only. CPCs, unlike other concentrators, are able to collect all the beam and a large portion of the diffuse radiation. Also they do not require highly specular surfaces and can thus better tolerate dust and degradation. A typical module made up of several CPCs is shown in Figure 20.10. The absorber surface is located at the bottom of the trough, and a glass cover may also be used to encase the entire module. CPCs show considerable promise for water heating close to the boiling point and for low-pressure steam applications. Further details about the different types of absorber and receiver shapes used, the effect of truncation of the receiver and the optics, can be found in Rabl (1985).

### 20.1.3 Long-Term Performance of Solar Collectors

#### 20.1.3.1 Effect of Day-to-Day Changes in Solar Insolation

Instantaneous or hourly performance of solar collectors has been discussed in “Flat-Plate Collectors.” For example, one would be tempted to use the HWB Equation 20.2 to predict long-term collector performance at a prespecified and constant fluid inlet temperature  $T_{Ci}$  merely by assuming average hourly values of  $I_T$  and  $T_a$ . Such a procedure would be erroneous and lead to underestimation of collector output because of the presence of the control function, which implies that collectors are turned on only when  $q_C > 0$ , that is, when radiation  $I_T$  exceeds a certain critical value  $I_C$ . This critical radiation value is found by setting  $q_C$  in Equation 20.2 to zero:

$$I_C = U_L(T_{Ci} - T_a)/\eta_0 \quad (20.7a)$$

To be more rigorous, a small increment  $\delta$  to account for pumping power and stability of controls can also be included if needed by modifying the equation to

$$I_C = U_L(T_{Ci} + \delta - T_a)/\eta_0 \quad (20.7b)$$

Then, Equation 20.2 can be rewritten in terms of  $I_C$  as

$$q_C = A_C F_R \eta_0 [I_T - I_C]^+ \quad (20.8)$$

Why one cannot simply assume a mean value of  $I_T$  in order to predict the mean value of  $q_C$  will be illustrated by the following simple concept (Klein 1978). Consider the three identical day sequences shown in sequence A of Figure 20.11. If  $I_{C1}$  is the critical radiation intensity and if it is constant over the whole day, the useful energy collected by the collector is represented by the sum of the shaded areas. If a higher critical radiation value shown as  $I_{C2}$  in Figure 20.11 is selected, we note that no useful energy is collected at all. Actual weather sequences would not look like that in sequence A but rather like that in sequence B, which is comprised of an excellent, a poor, and an average day. Even if both sequences have

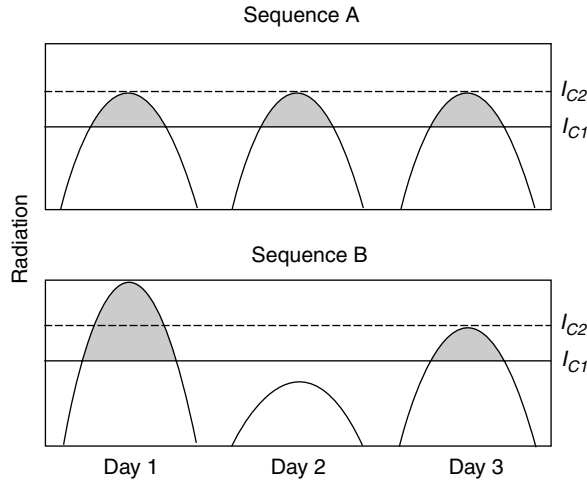


**FIGURE 20.11** Effect of radiation distribution on collector long-term performance. (From Klein, S. A., Calculation of flat-plate collector utilizability, *Solar Energy*, 21, 393, 1978.)

the same average radiation over 3 days, a collector subjected to sequence B will collect useful energy when the critical radiation is  $I_{C2}$ . Thus, neglecting the variation of radiation intensity from day-to-day over the long term and dealing with mean values would result in an underestimation of collector performance.

Loads are to a certain extent repetitive from day-to-day over a season or even the year. Consequently, one can also expect collectors to be subjected to a known diurnal repetitive pattern or mode of operation, that is, the collector inlet temperature  $T_{Ci}$  has a known repetitive pattern.

**20.1.3.2 Individual Hourly Utilizability**

In this mode,  $T_{Ci}$  is assumed to vary over the day but has the same variation for all the days over a period of  $N$  days (where  $N=30$  days for monthly and  $N=365$  for yearly periods). Then from Equation 20.8, total useful energy collected over  $N$  days during individual hour  $i$  of the day is

$$q_{CN}(i) = A_C F_R \bar{\eta}_0 \bar{I}_{Ti} \sum_{i=1}^N \frac{[I_{Ti} - I_C]^+}{\bar{I}_{Ti}} \tag{20.9}$$

Let us define the radiation ratio

$$X_i = I_{Ti} / \bar{I}_{Ti} \tag{20.10}$$

and the critical radiation ratio

$$X_C = I_C / \bar{I}_{Ti}$$

The modified HWB Equation 20.8 can be rewritten as

$$q_{CN}(i) = A_C F_R \bar{\eta}_0 \bar{I}_{Ti} N \phi_i(x_c) \tag{20.11}$$

where the individual hourly utilizability factor  $\phi_i$  is identified as

$$\phi_i(X_C) = \frac{1}{N} \sum_{i=1}^N (X_i - X_C)^+ \tag{20.12}$$

Thus  $\phi_i$  can be considered to be the fraction of the incident solar radiation that can be converted to useful heat by an ideal collector (i.e., whose  $F_R \eta_0 = 1$ ). The utilizability factor is thus a *radiation statistic* in the sense that it depends solely on the radiation values at the specific location. As such, it is in no way dependent on the solar collector itself. Only after the radiation statistics have been applied is a collector dependent significance attached to  $X_c$ .

Hourly utilizability curves on a *monthly* basis that are independent of location were generated by Liu and Jordan (1963) over 30 years ago for flat-plate collectors (see Figure 20.12). The key climatic parameter which permits generalization is the *monthly clearness index*  $\bar{K}$  of the location defined as

$$\bar{K} = \bar{H}/\bar{H}_0 \tag{20.13}$$

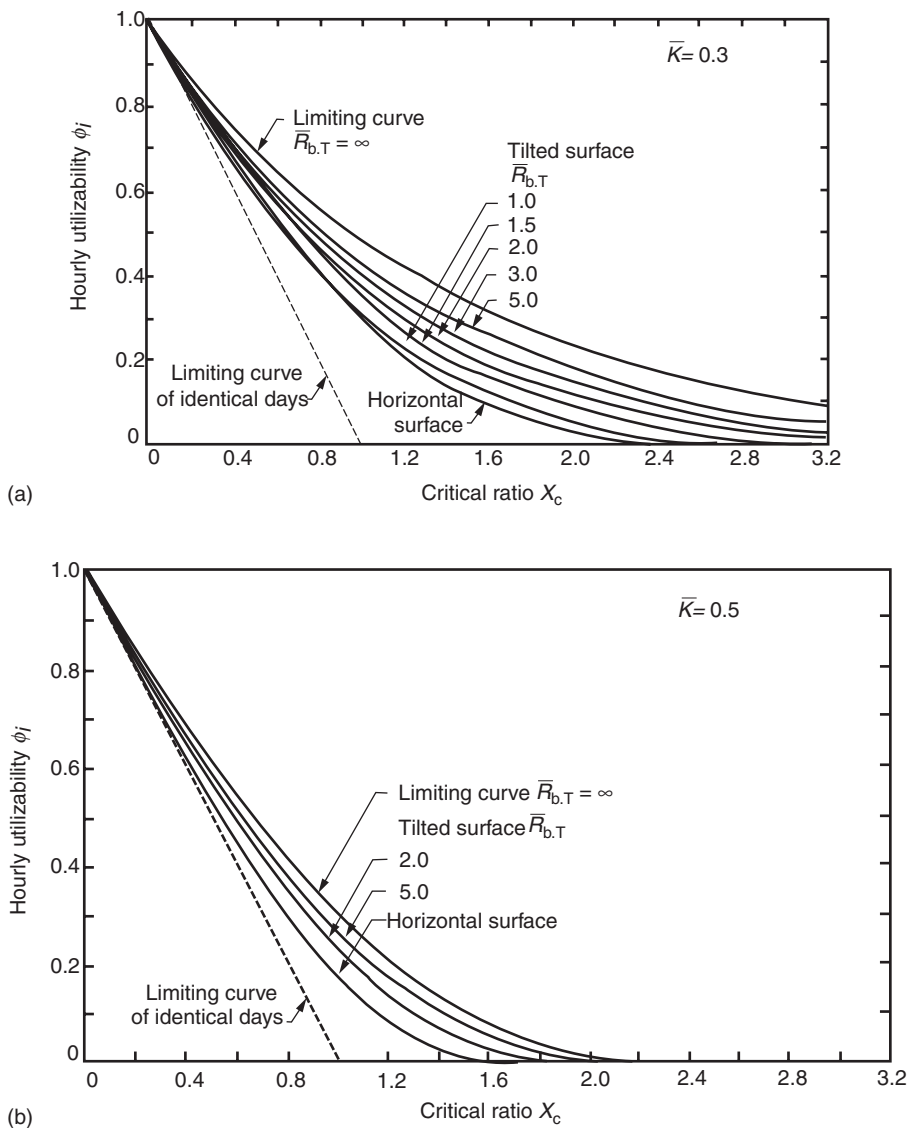


**FIGURE 20.12** Generalized hourly utilizability curves of Liu and Jordan (1963) for three different monthly mean clearness indices  $\bar{K}$ . (a)  $\bar{K} = 0.3$ , (b)  $\bar{K} = 0.5$ , (c)  $\bar{K} = 0.7$ . (From Liu, B. Y. H. and Jordan, R. C., A rational procedure for predicting the long-term average performance of flat-plate solar energy collectors, *Solar Energy*, 7, 53, 1963.)



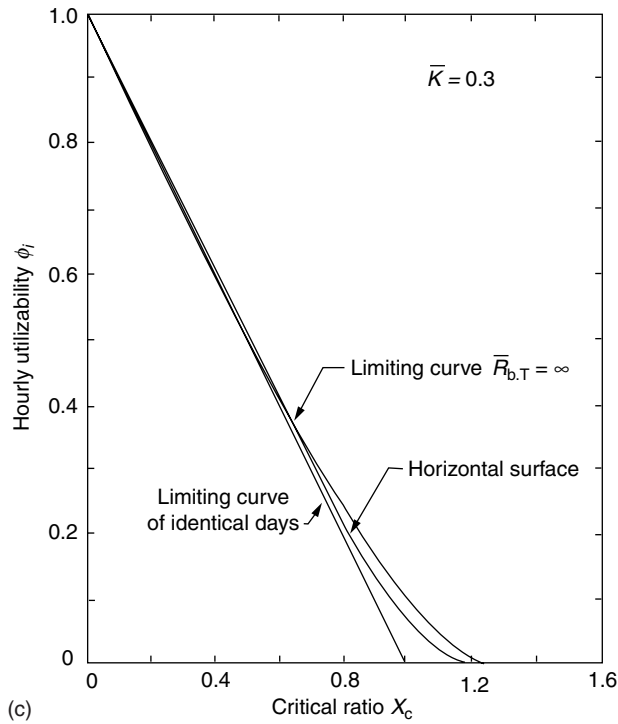


FIGURE 20.12 (continued)

where  $\bar{H}$  is the monthly mean daily global radiation on the horizontal surface and  $\bar{H}_0$  is the monthly mean daily extraterrestrial radiation on a horizontal surface.

Extensive tables giving monthly values of  $\bar{K}$  for several different locations worldwide can be found in several books, for example, Duffie and Beckman (1980) or Reddy (1987). The curves apply to equator-facing tilted collectors with the effect of collector tilt accounted for by the factor  $\bar{R}_{b,T}$  which is the ratio of the monthly mean daily extraterrestrial radiation on the tilted collector to that on a horizontal surface. Monthly mean daily calculations can be made using the 15th of the month, though better accuracy is achieved using slightly different dates (Reddy 1987). Clark, Klein, and Beckman (1983), working from measured data from several U.S. cities, have proposed the following correlation for individual hourly utilizability over monthly time scales applicable to flat-plate collectors only:

$$\begin{aligned}
 \phi_i &= 0 \quad \text{for } X_C \geq X_{\max} \\
 &= (1 - X_C/X_{\max})^2 \quad \text{for } X_{\max} = 2 \\
 &= \left| a - [a^2 + (1 + 2a)(1 - X_C/X_{\max})^2]^{1/2} \right| \quad \text{otherwise}
 \end{aligned}
 \tag{20.14}$$

where

$$a = (X_{\max} - 1)(2 - X_{\max})
 \tag{20.15}$$

and

$$X_{\max} = 1.85 + 0.169(\bar{r}_T/\bar{k}^2) - 0.0696 \cos \beta/\bar{k}^2 - 0.981\bar{k}/(\cos \delta)^2
 \tag{20.16}$$

where  $\bar{k}$  is the monthly mean hourly clearness index for the particular hour,  $\delta$  is the solar declination,  $\beta$  is the tilt angle of the collector plane with respect to the horizontal, and  $\bar{r}_T$  is the ratio of monthly average hourly

global radiation on a tilted surface to that on a horizontal surface for that particular hour. For an isotropic sky assumption,  $\bar{r}_T$  is given by

$$\bar{r}_T = (1 - \bar{I}_d \bar{I}) r_{b,T} + \left( \frac{1 + \cos \beta}{2} \right) \bar{I}_d \bar{I} + \left( \frac{1 - \cos \beta}{2} \right) \rho \quad (20.17)$$

where  $\bar{I}_d$  and  $\bar{I}$  are the hourly diffuse and global radiation on the horizontal surface,  $r_{b,T}$  is the ratio of hourly beam radiation on the tilted surface to that on a horizontal surface (this is a purely astronomical quantity and can be calculated accurately from geometric considerations), and  $\rho$  is the ground albedo.

### Example 20.1.3

Compute the total energy collected during 11:30–12:30 for the month of September in New York, NY (latitude:  $40.75^\circ\text{N}$ ,  $T_a = 20^\circ\text{C}$ ) by a flat-plate solar collector of  $5 \text{ m}^2$  area having zero tilt. The collector performance parameters are  $F_R \eta_0 = 0.54$  and  $F_R U_L = 3.21 \text{ W}/(\text{m}^2\text{C})$  and the collector inlet temperature is  $80^\circ\text{C}$ . The corresponding hourly mean clearness index  $\bar{k}$  is 0.44, and the monthly mean hourly radiation on a horizontal surface  $\bar{I}_{Ti}$  (11:30–12:30) is  $6.0 \text{ MJ}/(\text{m}^2 \text{ h})$ .

From Equation 20.7a, critical radiation  $I_C = 3.21 \times (80 - 20)/0.54 = 356.7 \text{ W}/\text{m}^2 = 1.28 \text{ MJ}/(\text{m}^2 \text{ h})$ . For the average day of September, solar declination  $\delta = 2.2^\circ$ . Also, because the collector is horizontal  $\bar{r}_T = 1$  and  $\beta = 0$ . Thus from Equation 20.16

$$X_{\max} = 1.85 + 0.169/0.44^2 - 0.0696/0.44^2 - 0.981 \times 0.44/(\cos 2.2)^\circ = 1.93.$$

Also from Equation 20.15,  $a = (1.93 - 1)/(2 - 1.93) = 13.29$ .

The critical radiation ratio  $X_C = 1.28/1.93 = 0.663$ .

Because  $X_C < X_{\max}$ , from Equation 20.14 we have

$$\phi_i(X_C) = |13.29 - [13.29^2 + (1 + 2 \times 13.29)(1 - 0.663/1.93)^2]^{1/2}| = |13.29 - 13.73| = 0.44.$$

Finally, the total energy collected is given by Equation 20.11

$$q_{CN}(11 : 30 - 12 : 30) = 5 \times 0.54 \times 60 \times 30 \times 0.44 = 214 \text{ MJ/h}$$

## 20.1.3.3 Daily Utilizability

### 20.1.3.3.1 Basis

In this mode,  $T_{Ci}$ , and hence the critical radiation level, is assumed constant during all hours of the day. The *total* useful energy over  $N$  days that can be collected by solar collectors operated all day over  $n$  hours is given by

$$Q_{CN} = A_C F_R \bar{\eta}_0 \bar{H}_T N \bar{\phi} \quad (20.18)$$

where  $\bar{H}_T$  is the average daily global radiation on the collector surface, and  $\bar{\phi}$  (called Phibar) is the daily utilizability factor, defined as

$$\bar{\phi} = \frac{1}{Nn} \sum_{N=1}^N \sum_{n=1}^n (I_T - I_C)^+ / \sum_{N=1}^N \sum_{n=1}^n I_T = \frac{1}{Nn} \sum_{N=1}^N \sum_{n=1}^n (X_i - X_C)^+ \quad (20.19)$$

Generalized correlations have been developed both at monthly time scales and for annual time scales based on the parameter  $\bar{K}$ . Generalized (i.e., location and month independent) correlations for  $\bar{\phi}$  on a *monthly* time scale have been proposed by Theilacker and Klein (1980). These are strictly applicable for flat-plate collectors only. Collares-Pereira and Rabl (1979) have also proposed generalized correlations

for  $\bar{\phi}$  on a monthly time scale which, though a little more tedious to use are applicable to concentrating collectors as well. The reader may refer to Rabl (1985) or Reddy (1987) for complete expressions.

### 20.1.3.3.2 Monthly Time Scales

The Phibar method of determining the daily utilizability fraction proposed by Theilacker and Klein (1980) correlates  $\bar{\phi}$  to the following factors:

1. A geometry factor  $\bar{R}_T/\bar{r}_{T,\text{noon}}$ , which incorporates the effects of collector orientation, location, and time of year.  $\bar{R}_T$  is the ratio of monthly average global radiation on the tilted surface to that on a horizontal surface.  $\bar{r}_{T,\text{noon}}$  is the ratio of radiation at noon on the tilted surface to that on a horizontal surface for the average day of the month. Geometrically,  $\bar{r}_{T,\text{noon}}$  is a measure of the maximum height of the radiation curve over the day, whereas  $\bar{R}_T$  is a measure of the enclosed area. Generally the value  $(\bar{R}_T/\bar{r}_{T,\text{noon}})$  is between 0.9 and 1.5.
2. A dimensionless critical radiation level  $\bar{X}_{C,K}$  where

$$\bar{X}_{C,K} = I_C/\bar{I}_{T,\text{noon}} \quad (20.20)$$

with  $\bar{I}_{T,\text{noon}}$ , the radiation intensity on the tilted surface at noon, given by

$$\bar{I}_{T,\text{noon}} = \bar{r}_{\text{noon}}\bar{r}_{T,\text{noon}}\bar{H} \quad (20.21)$$

where  $\bar{r}_{\text{noon}}$  is the ratio of radiation at noon to the daily global radiation on a horizontal surface during the mean day of the month which can be calculated from the following correlation proposed by Liu and Jordan (1960):

$$r(W) = \frac{I(W)}{H} = \frac{\pi}{24} (a + b \cos W) \frac{(\cos W - \cos W_S)}{(\sin W_S - \frac{\pi}{180} W_S \cos W_S)} \quad (20.22)$$

with

$$a = 0.409 + 0.5016 \sin(W_S - 60)$$

$$b = 0.6609 - 0.4767 \sin(W_S - 60)$$

where  $W$  is the hour angle corresponding to the midpoint of the hour (in degrees) and  $W_S$  is the sunset hour angle given by

$$\cos W_S = -\tan L \tan \delta \quad (20.23)$$

where  $L$  is the latitude of the location. The fraction  $r$  is the ratio of hourly to daily global radiation on a horizontal surface. The factors  $\bar{r}_{T,\text{noon}}$  and  $\bar{r}_{\text{noon}}$  can be determined from Equation 20.17 and Equation 20.22, respectively, with  $W=0^\circ$ .

The Theilacker and Klein correlation for the daily utilizability for equator-facing flat-plate collectors is

$$\bar{\phi}(X_{C,K}) = \exp\{[a' + b'(\bar{r}_{T,\text{noon}}/\bar{R}_T)][X_{C,K} + c'X_{C,K}^2]\} \quad (20.24)$$

where

$$a' = 7.476 - 20.00\bar{K} + 11.188\bar{K}^2$$

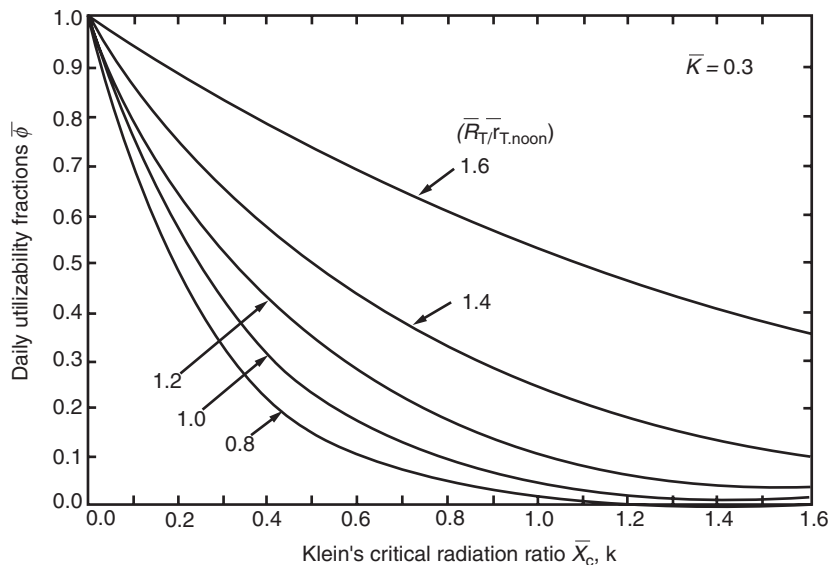
$$b' = -8.562 + 18.679\bar{K} - 9.948\bar{K}^2 \quad (20.25)$$

$$c' = -0.722 + 2.426\bar{K} + 0.439\bar{K}^2$$

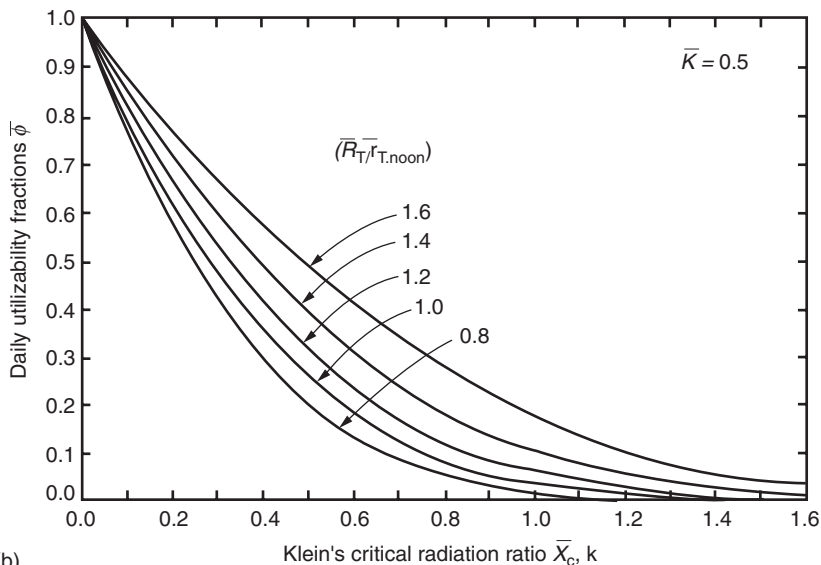
How  $\bar{\phi}$  varies with the critical radiation ratio  $\bar{X}_{C,K}$  for three different values of  $\bar{K}$  is shown in [Figure 20.13](#).

**Example 20.1.4**

A flat-plate collector operated horizontally at Fort Worth, Texas ( $L = 32.75^\circ\text{N}$ ), has a surface area of  $20 \text{ m}^2$ . It is used to heat  $10 \text{ kg/min.}$  of water entering the collector at a constant temperature of  $80^\circ\text{C}$  each day from 6 a.m. to 6 p.m. The collector performance parameters are  $F_R \eta_0 = 0.70$  and  $F_R U_L = 5.0 \text{ W/(m}^2\text{C)}$ . Use Klein's correlation to compute the energy collected by the solar collectors during September.



(a)



(b)

**FIGURE 20.13** Generalized daily utilizability curves of Theilacker and Klein (1980) for three different K values. (a)  $\bar{K} = 0.3$ , (b)  $\bar{K} = 0.5$ , (c)  $\bar{K} = 0.7$ . (From Theilacker, J. C. and Klein, S. A., Improvements in the utilizability relationships, *American Section of the International Solar Energy Society Meeting Proceedings*, p. 271. Phoenix, AZ, 1980.)

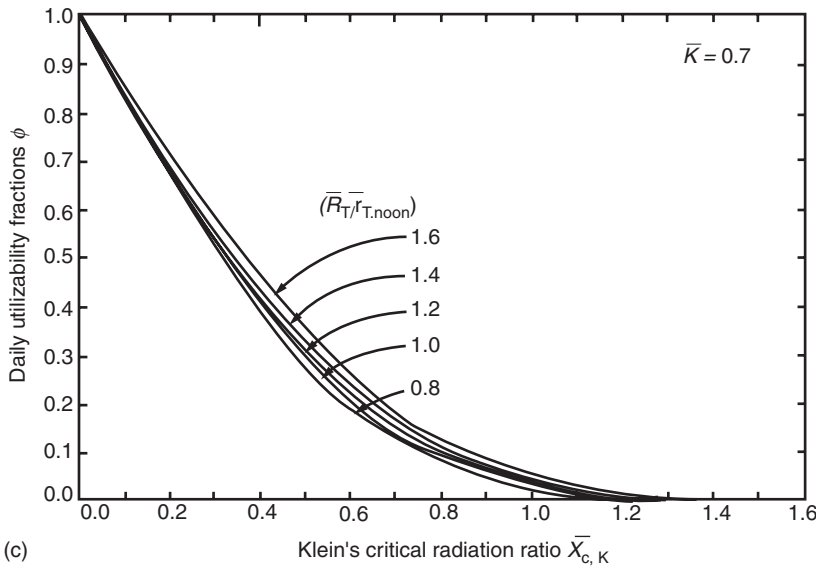


FIGURE 20.13 (continued)

Assume  $\bar{H} = 18.28 \text{ MJ}/(\text{m}^2\text{d})$ ,  $\bar{K} = 0.57$  and  $\bar{T}_a = 25^\circ\text{C}$ . Assume the mean sunset hour angle for September to be  $90^\circ$ .

The critical radiation is calculated first:

$$I_c = (5/0.7)(80 - 25) = 393 \text{ W}/\text{m}^2 = 1.414 \text{ MJ}/(\text{m}^2\text{h})$$

For a horizontal surface,  $\bar{R}_T = \bar{r}_{T,\text{noon}} = 1$ . From Equation 20.22,  $r(W = 0) = \pi/24(a + b) = 0.140$ . Klein's critical radiation ratio (20.1.20)  $\bar{X}_{C,K} = 1.414/(18.28 \times 0.140) = 0.553$ . From Equation 20.24,  $\bar{\phi} = 0.318$ . Finally, from Equation 20.18, the total monthly energy collected by the solar collectors is  $Q_{CM} = 20 \times 0.7 \times 30 \times 0.318 \times 18.28 = 2.44 \text{ GJ}/\text{month}$ .

**20.1.3.3.3 Annual Time Scales**

Generalized expressions for the *yearly* average energy delivered by the principal collector types with constant radiation threshold (i.e., when the fluid inlet temperature is constant for all hours during the day over the entire year) have been developed by Rabl (1981) based on data from several U.S. locations. The correlations are basically quadratic of the form

$$\frac{Q_{CY}}{A_C F_R \eta_n} = \tilde{a} + \tilde{b} I_C + \tilde{c} I_C^2 \tag{20.26}$$

where the coefficients  $\tilde{a}$ ,  $\tilde{b}$ , and  $\tilde{c}$  are functions of collector type and/or tracking mode, climate, and in some cases, latitude. The complete expressions as revised by Gordon and Rabl (1982) are given in Reddy (1987). Note that the yearly *daytime* average value of  $T_a$  should be used to determine  $I_C$ . If this is not available, the yearly mean *daily* average value can be used. Plots of  $Q_{CY}$  versus  $I_C$  for flat-plate collectors that face the equator with tilt equal to the latitude are shown in Figure 20.14. The solar radiation enters these expressions as  $\tilde{I}_{bn}$ , the annual average beam radiation at normal incidence. This can be estimated from the following correlation

$$\tilde{I}_{bn} = 1.37\bar{K} - 0.34 \tag{20.27}$$

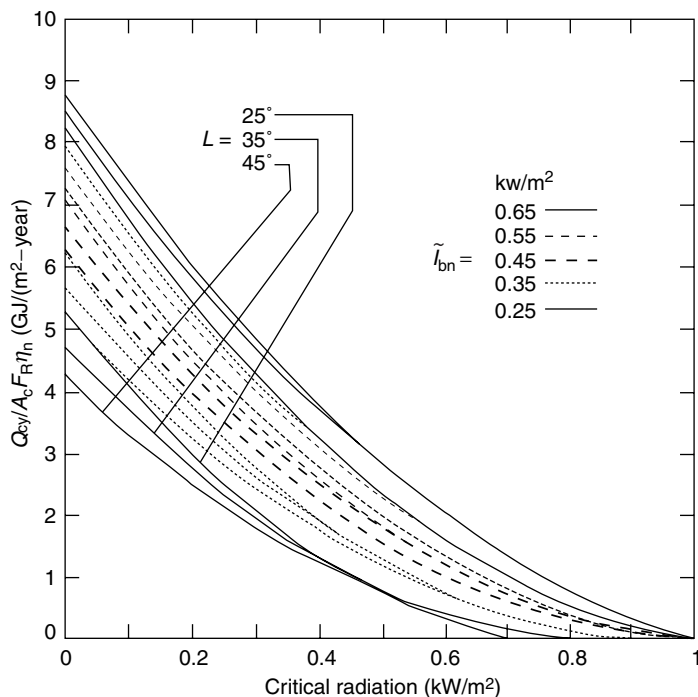


**FIGURE 20.14** Yearly total energy delivered by flat-plate collectors with tilt equal to latitude. (From Gordon, J. M. and Rabl, A., Design, analysis and optimization of solar industrial process heat plants without storage, *Solar Energy*, 28, 519, 1982.)

where  $\tilde{I}_{bn}$  is in  $\text{kW/m}^2$  and  $\tilde{K}$  is the annual average clearness index of the location. Values of  $\tilde{K}$  for several locations worldwide are given in Reddy (1987).

This correlation is strictly valid for latitudes ranging from 25 to 48°. If used for lower latitudes, the correlation is said to lead to overprediction. Hence, it is recommended that for such lower latitudes a value of 25° be used to compute  $Q_{Cy}$ .

A direct comparison of the yearly performance of different collector types is given in Figure 20.15 (from Rabl 1981). A latitude of 35°N is assumed and plots of  $Q_{Cy}$  U.S. ( $T_{Ci} - T_a$ ) have been generated in a sunny climate with  $I_{bn} = 0.6 \text{ kW/m}^2$ . Relevant collector performance data are given in Figure 20.15. The crossover point between flat-plate and concentrating collectors is approximately 25°C above ambient temperature whether the climate is sunny or cloudy.

## 20.1.4 Solar Systems

### 20.1.4.1 Classification

Solar thermal systems can be divided into two categories: standalone or solar supplemented. They can be further classified by means of energy collection as active or passive, by their use as residential or industrial. Further, they can be divided by collector type into liquid or air systems, and by the type of storage they use into seasonal or daily systems.

#### 20.1.4.1.1 Standalone and Solar Supplemented Systems

*Standalone systems* are systems in which solar energy is the only source of energy input used to meet the required load. Such systems are normally designed for applications where a certain amount of tolerance is permissible concerning the load requirement; in other words, where it is not absolutely imperative that

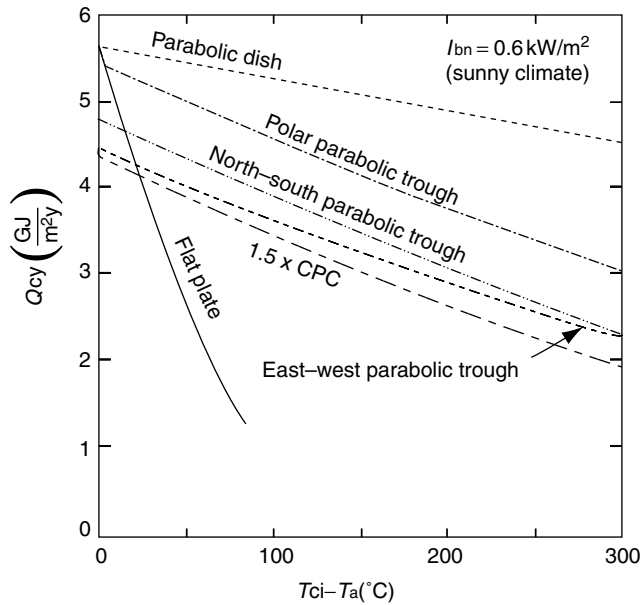


**FIGURE 20.15** Figure illustrating the comparative performance (yearly collectible energy) of different collector types as a function of the difference between collector inlet temperature and ambient collector performance parameters  $F'\eta_0$  and  $F'U_L$  in  $W/(m^2 \cdot ^\circ C)$  are: flat plate (0.70 and 5.0), CPC (0.60 and 0.75), parabolic trough (0.65 and 0.67), and parabolic dish (0.61 and 0.27). (From Rabl, A., Yearly average performance of the principal solar collector types, *Solar Energy*, 27, 215, 1981.)

the specified load be met each and every instant. This leniency is generally admissible in the case of certain residential and agricultural applications. The primary reasons for using such systems are their low cost and simplicity of operation.

*Solar-supplemented systems*, widely used for both industrial and residential purposes, are those in which solar energy supplies part of the required heat load, the rest being met by an auxiliary source of heat input. Due to the daily variations in incident solar radiation, the portion of the required heat load supplied by the solar energy system may vary from day-to-day. However, the auxiliary source is so designed that at any instant it is capable of meeting the remainder of the required heat load. It is normal practice to incorporate an auxiliary heat source large enough to supply the entire heat load required. Thus, the benefit in the solar subsystem is not in its capacity credit (i.e., not that a smaller capacity conventional system can be used), but rather that a part of the conventional fuel consumption is displaced. The solar subsystem thus acts as a fuel economizer.

Solar-supplemented energy systems will be the primary focus of this chapter. Designing such systems has acquired a certain firm scientific rationale, and the underlying methodologies have reached a certain maturity and diversity, which may satisfy professionals from allied fields. On the other hand, unitary solar apparatus are not discussed here, since these are designed and sized based on local requirements, material availability, construction practices, and practical experience. Simple rules of thumb based on prior experimentation are usually resorted to for designing such systems.

#### 20.1.4.1.2 Active and Passive Systems

*Active systems* are those systems that need electric pumps or blowers to collect solar energy. It is evident that the amount of solar energy collected should be more than the electrical energy used. Active systems are invariably used for industrial applications and for most domestic and commercial applications as well. *Passive systems* are those systems that collect or use solar energy without direct recourse to any

source of conventional power, such as electricity, to aid in the collection. Thus, either such systems operate by natural thermosyphon (for example, domestic water heating systems) between collector, storage, and load or, in the case of space heating, the architecture of the building is such as to favor optimal use of solar energy. Use of a passive system for space heating applications, however, in no way precludes the use of a backup auxiliary system. This chapter deals with active solar systems only.

### **20.1.4.1.3 Residential and Industrial Systems**

Basically, the principles and the components used in these two types of systems are alike, the difference being in the load distribution, control strategies, and relative importance of the components with respect to each other. Whereas *residential* loads have sharp peaks in the early morning or in the evening and have significant seasonal variations, industrial loads tend to be fairly uniform over the year. Constant loads favor the use of solar energy because good equipment utilization can be achieved. Because of differences in load distribution, the role played by the storage differs for both applications. Residential loads often occur at times when solar radiation is no longer available. Thus the collector and the storage subsystems interact in a mode without heat withdrawal from the storage. Finally, for economic reasons, many residential systems are designed to operate by natural thermosyphon, in which case no pumps or controls are needed.

On the other hand, for *industrial and commercial* applications, there is no a priori relationship between the time dependence of the load and the period of sunshine. Moreover, a high reliability has to be assured, so the solar system will have to be combined with a conventional system. Very often, a significant portion of the load can be directly supplied by the solar system even without storage. Another option is to use buffer storage for short periods, on the order of a few hours, in case of discontinuous batch process loads. Thus, the proper design of the storage component has to be given adequate consideration. At present, due to economic constraints as well as the fact that proper awareness of the various installations and operational difficulties associated with larger solar thermal systems is still lacking, solar thermal systems are normally designed either (i) with the no-storage option, or (ii) with buffer storage where a small fraction of the total heat demand is only supplied by the solar system.

#### **20.1.4.1.4 Liquid and Air Collectors**

Although air has been the primary fluid for space heating and drying applications, solar air heating systems have until recently been relegated to second place, mainly as a result of the engineering difficulties associated with such systems. Also, applications involving hot air are probably less common than those needing hot water. Air systems for space heating are well described by Löff (1981).

Even with liquid solar collectors, various configurations are possible, and these can be classified basically as *nontracking* (which include flat-plate collectors and CPCs) or *tracking* collectors (which include various types of concentrating collectors). For low-grade thermal heat, for which solar energy is most suited, flat-plate collectors are far more appropriate than concentrating collectors, not only because of their lower cost but also because of their higher thermal efficiencies at low temperature levels. Moreover, their operation and maintenance costs are lower. Finally, for locations having a high fraction of diffuse radiation, as in the tropics, flat-plate collectors are considered to be thermally superior because they can make use of diffuse radiation as well as beam radiation. Although the system design methodologies presented in this chapter explicitly assume flat-plate collector systems, these design approaches can be equally used with concentrating collectors.

#### **20.1.4.1.5 Daily and Seasonal Storage**

By *daily storage* is meant systems having capacities equivalent to at most a few days of demand (i.e., just enough to tide over day-to-day climatic fluctuations). In *seasonal storage*, solar energy is stored during the summer for use in winter. Industrial demand loads, which are more or less uniform over the year, are badly suited for seasonal-storage systems. This is also true of air-conditioning for domestic and commercial applications because the load is maximum when solar radiation is also maximum, and



vice versa. The present-day economics of seasonal storage units do not usually make such systems an economical proposition except for community heating in cold climates.

#### 20.1.4.2 Closed-Loop and Open-Loop Systems

The two possible configurations of solar thermal systems with daily storage are classified as closed-loop or open-loop systems. Though different authors define these differently, we shall define these as follows. A *closed-loop system* has been defined as a circuit in which the performance of the solar collector is directly dependent on the storage temperature. Figure 20.16 gives a schematic of a closed-loop system in which the fluid circulating in the collectors does not mix with the fluid supplying thermal energy to the load. Thus, these two subsystems are distinct in the sense that any combination of fluids (water or air) is theoretically feasible (a heat exchanger, as shown in the figure, is of course imperative when the fluids are different). However, in practice, only water-water, water-air, or air-air combinations are used. From the point of system performance, the storage temperature normally varies over the day and, consequently, so does collector performance. Closed-loop system configurations have been widely used to date for domestic hot water and space heating applications. The flow rate per unit collector area is generally around  $50 \text{ kg}/(\text{h m}^2)$  for liquid collectors. The storage volume makes about 5–10 passes through the collector during a typical sunny day, and this is why such systems are called *multipass* systems. The temperature rise for each pass is small, of the order of  $2^\circ\text{C}$ – $5^\circ\text{C}$  for systems with circulating pumps and about  $10^\circ\text{C}$  for thermosyphon systems. An expansion tank and a check valve to prevent reverse thermosyphoning at nights, although not shown in the figure, are essential for such system configurations.

Figure 20.17 illustrates one of the possible configurations of *open-loop systems*. Open-loop systems are defined as systems in which the collector performance is independent of the storage temperature. The working fluid may be rejected (or a heat recuperator can be used) if contaminants are picked up during its passage through the load. Alternatively, the working fluid could be directly recirculated back to the entrance of the solar collector field. In all these open-loop configurations, the collector is subject to a given or known inlet temperature specified by the load requirements.

If the working fluid is water, instead of having a continuous flow rate (in which case the outlet temperature of the water will vary with isolation), a solenoid valve can be placed just at the exit of the collector, set so as to open when the desired temperature level of the fluid in the collector is reached. The water is then discharged into storage, and fresh water is taken into the collector. The solar collector will thus operate in a discontinuous manner, but this will ensure that the temperature in the storage is always at the desired level. An alternative way of ensuring uniform collector outlet temperature is to vary the flow rate according to the incident radiation. One can collect a couple of percent more energy

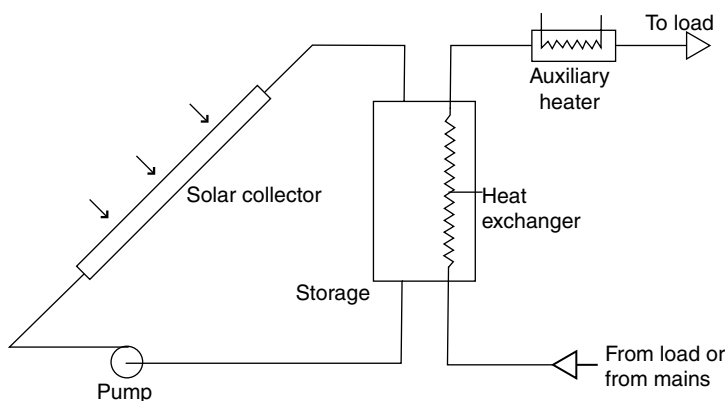


FIGURE 20.16 Schematic of a closed-loop solar system.

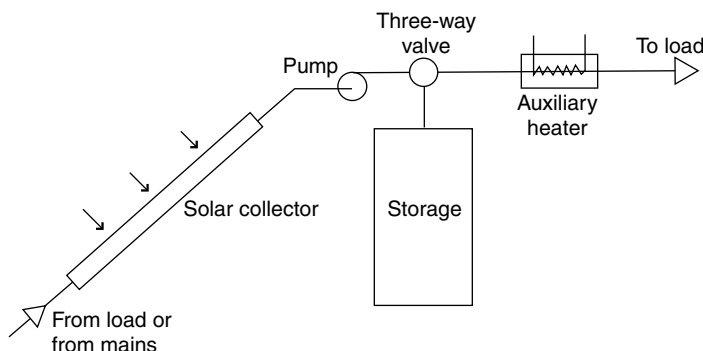


FIGURE 20.17 Schematic of an open-loop solar system.

than with constant rate single-pass designs (Gordon and Zarmi 1985). However, this entails changing the flow rate of the pump more or less continuously, which is injurious to the pump and results in reduced life. Of all the three variants of the open-loop configuration, the first one, namely the single-pass open-loop solar thermal system configuration with constant flow rate and without a solenoid valve, is the most common.

As stated earlier, closed-loop systems are appropriate for domestic applications. Until recently, industrial process heat systems were also designed as large solar domestic hot-water systems with high collector flow rates and with the storage tank volume making several passes per day through the collectors. Consequently, the storage tank tends to be fairly well mixed. Also the tank must be strong enough to withstand the high pressure from the water mains. The open-loop single-pass configuration, wherein the required average daily fluid flow is circulated just once through the collectors with the collector inlet temperature at its lowest value, has been found to be able to deliver as much as 40% more yearly energy for industrial process heat applications than the multipass designs (Collares-Pereira et al. 1984). Finally, in a closed-loop system where an equal amount of fresh water is introduced into storage whenever a certain amount of hot water is drawn off by the load, it is not possible to extract the entire amount of thermal energy contained in storage since the storage temperature is continuously reduced due to mixing. This *partial depletion effect* in the storage tank is not experienced in open-loop systems. The penalty in yearly energy delivery ranges typically from about 10% for daytime-only loads to around 30% for nighttime-only loads compared to a closed-loop multipass system where the storage is depleted every day. Other advantages of open-loop systems are (i) the storage tank need not be pressurized (and hence is less costly), and (ii) the pump size and parasitic power can be lowered.

A final note of caution is required. The single-pass design is not recommended for *variable* loads. The tank size is based on yearly daily load volumes, and efficient use of storage requires near-total depletion of the daily collected energy each day. If the load draw is markedly lower than its average value, the storage would get full relatively early the next day and solar collection would cease. It is because industrial loads tend to be more uniform, both during the day and over the year, than domestic applications that the single-pass open-loop configuration is recommended for such applications.

#### 20.1.4.2.1 Description of a Typical Closed-Loop System

Figure 20.18 illustrates a typical closed-loop solar-supplemented liquid heating system. The useful energy is often (but not always) delivered to the storage tank via a collector-heat exchanger, which separates the collector fluid stream and the storage fluid. Such an arrangement is necessary either for antifreeze protection or to avoid corrosion of the collectors by untreated water containing gases and salts. A safety relief valve is provided because the system piping is normally nonpressurized, and any steam produced in the solar collectors will be let off from this valve. When this happens, energy dumping is said to take place.

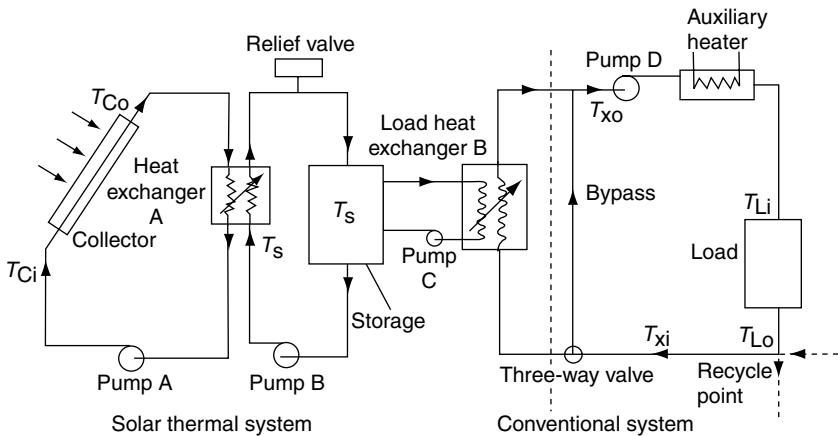


**FIGURE 20.18** Schematic of a typical closed-loop system with auxiliary heater placed in series (also referred to as a topping-up type).

Fluid from storage is withdrawn and made to flow through the load-heat exchanger when the load calls for heat. Whenever possible, one should withdraw fluid directly from the storage and pass it through the load, and avoid incorporating the load-heat exchanger, since it introduces additional thermal penalties and involves extra equipment and additional parasitic power use. Heat is withdrawn from the storage tank at the top and reinjected at the bottom in order to derive maximum benefit from the thermal stratification that occurs in the storage tank. A bypass circuit is incorporated prior to the load heat exchanger and comes into play

1. when there is no heat in the storage tank (i.e., storage temperature  $T_s$  is less than the fluid temperature entering the load heat exchanger  $T_{Xi}$ )
2. when  $T_s$  is such that the temperature of the fluid leaving the load heat exchanger is greater than that required by the load (i.e.,  $T_{Xo} > T_{Li}$ , in which case the three-way valve bypasses part of the flow so that  $T_{Xo} = T_{Li}$ ). The bypass arrangement is thus a differential control device which is said to modulate the flow such that the above condition is met. Another operational strategy for maintaining  $T_{Xo} = T_{Li}$  is to operate the pump in a “bang-bang” fashion (i.e., by short cycling the pump). Such an operation is not advisable, however, since it would lead to premature pump failure.

An auxiliary heater of the *topping-up type* supplies just enough heat to raise  $T_{Xo}$  to  $T_{Li}$ . After passing through the load, the fluid (which can be either water or air) can be recirculated or, in case of liquid contamination through the load, fresh liquid can be introduced. The auxiliary heater can also be placed in parallel with the load (see Figure 20.19), in which case it is called an *all-or-nothing type*. Although such an arrangement is thermally less efficient than the topping-up type, this type is widely used during the solar retrofit of heating systems because it involves little mechanical modifications or alterations to the auxiliary heater itself.

It is obvious that there could also be solar-supplemented energy systems that do not include a storage element in the system. Figure 20.20 shows such a system configuration with the auxiliary heater installed in series. The operation of such systems is not very different from that of systems with storage, the primary difference being that whenever instantaneous solar energy collection exceeds load requirements (i.e.,  $T_{Co} > T_{Li}$ ), energy dumping takes place. It is obvious that by definition there cannot be a closed-loop, no-storage solar thermal system. Solar thermal systems without storage are easier to construct and operate, and even though they may be effective for 8–10 h a day, they are appropriate for applications such as process heat in industry.

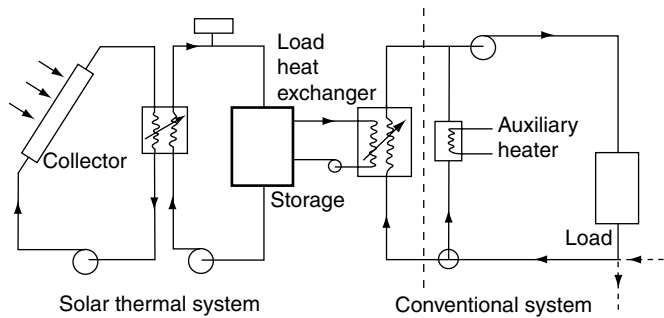


FIGURE 20.19 Schematic of a typical closed-loop system with auxiliary heater placed in parallel (also referred to as an all-or-nothing type).

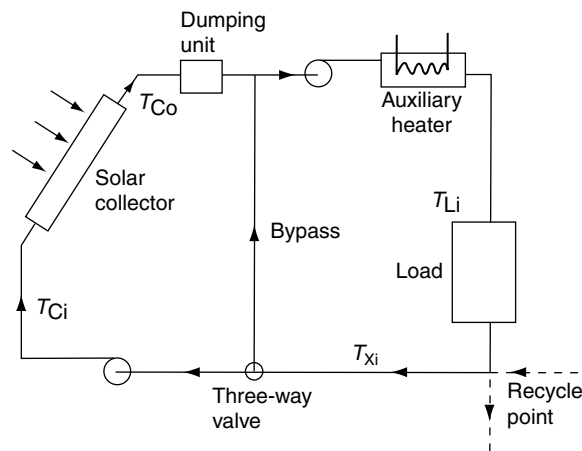
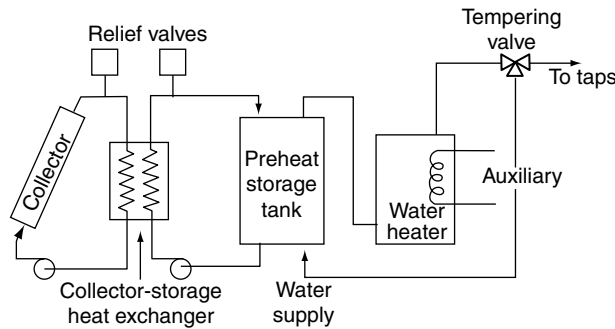


FIGURE 20.20 Simple solar thermal system without storage.

Active closed-loop solar systems as described earlier are widely used for service hot-water systems, that is, for domestic hot water and process heat applications as well as for space heat. There are different variants to this generic configuration. A system without the collector-heat exchanger is referred to having collectors *directly coupled* to the storage tank (as against *indirect coupling* as in Figure 20.16). For domestic hot-water systems, the system can be simplified by placing the auxiliary heater (which is simply an electric heater) directly inside the storage tank. One would like to maintain stratification in the tank so that the coolest fluid is at the bottom of the storage tank, thereby enhancing collection efficiency. Consequently, the electric heater is placed at about the upper third portion of the tank so as to assure good collection efficiency while assuring adequate hot water supply to the load. A more efficient but expensive option is widely used in the United States: the *double tank system*, shown in Figure 20.21. Here the functions of solar storage and auxiliary heating are separated, with the solar tank acting as a preheater for the conventional gas or electric unit. Note that a further system simplification can be achieved for domestic applications by placing the load heat exchanger directly inside the storage tank. In certain cases, one can even eliminate the heat exchanger completely.

Another system configuration is the *drain-back* (also called drain-out) system, where the collectors are emptied each time the solar system shuts off. Thus the system invariably loses collector fluid at least once, and often several times, each day. No collector-heat exchanger is needed, and freeze protection is inherent in such a configuration. However, careful piping design and installation, as well as a two-speed pump, are



**FIGURE 20.21** Schematic of a standard domestic hot-water system with double tank arrangement. (From Duffie, J. A. and Beckman, W. A., *Solar Engineering of Thermal Processes*, Wiley Interscience, New York, 1980.)

needed for the system to work properly (Newton and Gilman 1981). The drain-back configuration may be either open (vented to atmosphere) or closed (for better corrosion protection). Long-term experience in the United States with the drain-back system has shown it to be very reliable if engineered properly. A third type of system configuration is the *drain-down* system, where the fluid from the collector array is removed only when adverse conditions, such as freezing or boiling, occur. This design is used when freezing ambient temperatures are only infrequently encountered.

Active solar systems of the type described above are mostly used in countries such as the United States and Canada. Countries such as Australia, India, and Israel (where freezing is rare) usually prefer thermosyphon systems. No circulating pump is needed, the fluid circulation being driven by density difference between the cooler water in the inlet pipe and the storage tank and the hotter water in the outlet pipe of the collector and the storage tank. The low fluid flow in thermosyphon systems enhances thermal stratification in the storage tank. The system is usually fail-proof, and a study by Liu and Fanny (1980) reported that a thermosyphon system performed better than several pumped service hot-water systems. If operated properly, thermosyphon and active solar systems are comparable in their thermal performance. A major constraint in installing thermosyphon systems in already existing residences is the requirement that the bottom of the storage tank be at least 20 cm or more higher than the top of the solar collector in order to avoid reverse thermosyphoning at night. To overcome this, spring-loaded one-way valves have been used, but with mixed success.

### 20.1.5 Controls

There are basically five categories to be considered when designing automatic controls (Mueller Associates 1985): (i) collection to storage, (ii) storage to load, (iii) auxiliary energy to load, (iv) miscellaneous (i.e., heat dumping, freeze protection, overheating, etc.), and (v) alarms. The three major control system components are sensors, controllers, and actuating devices. Sensors are used to detect conditions (such as temperatures, pressures, etc.). Controllers receive output from the sensors, select a course of action, and signal a system component to adjust the condition. Actuated devices are components such as pumps, valves, and alarms that execute controller commands and regulate the system.

The sensors for the controls must be set, operated, and located correctly if the solar system is to collect solar energy effectively, reduce operating time, wear and tear of active components, and minimize auxiliary and parasitic energy use. Moreover, sensors also need to be calibrated frequently. For diagnostic purposes, it may be advisable to add extra sensors and data acquisition equipment in order to verify system operation and keep track of long-term system operation. Potential problems can be then rectified in time. The reader may refer to manuals by Mueller Associates (1985) or by SERI (1989) for more details on controls pertaining to solar energy systems.

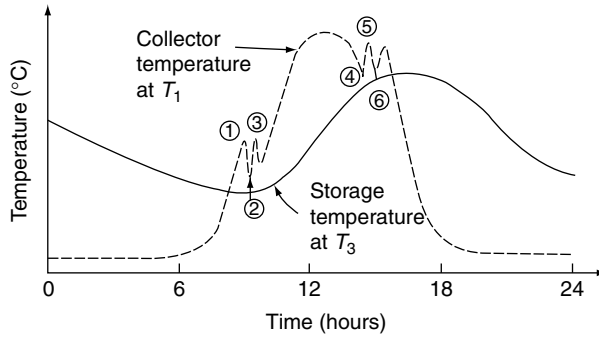


**FIGURE 20.22** Typical diurnal variation of collector and storage temperatures. (From CSU, Solar Heating and Cooling of Residential Buildings—Design of Systems, manual prepared by the Solar Energy Applications Laboratory, Colorado State University, 1980.)

Though single-point temperature controllers or solar-cell-activated controls have been used for activated solar collectors, the best way to do so is by differential temperature controllers. Temperature sensors are used to measure the fluid temperature at collector outlet and at the bottom of the storage tank. When the difference is greater than a set amount, say 5°C, then the controller turns the pump on. If the pump is running and the temperature difference falls below another preset value, say 1°C, the controller stops the pump. The temperature deadband between switching-off and reactivating levels should be set with care, since too high a deadband would adversely affect collection efficiency and too low a value would result in short cycling of the collector pump. Figure 20.22 taken from CSU (1980), shows typical diurnal temperature variations of the liquids at collector exit  $T_1$  and in the storage bottom  $T_3$  as a result of heat withdrawal and/or heat losses from the storage. At about 8:30 a.m.,  $T_1 > T_3$  and, since there is no flow in the collector,  $T_1$  increases rapidly until the difference ( $T_1 - T_3$ ) reaches the preset activation level (shown as point 1). The collector pump A comes on, and liquid circulation through the collector begins. Because of this cold water surge,  $T_1$  decreases, resulting in a drop of ( $T_1 - T_3$ ) to the preset deactivating level (shown as point 2). The pump switches off, and liquid flow through the collectors stops. Gradually  $T_1$  increases again, and so on. The number of on-off cycles at system start-up depends on solar intensity, fluid flow rate, volume of water in the collector loop, and the differential controller setting. A similar phenomenon of cycling also occurs in the afternoon. However, the error introduced in solar collector long-term performance predictions by neglecting this cycling effect in the modeling equations is usually small.

**20.1.5.1 Corrections to Collector Performance Parameters**

**20.1.5.1.1 Combined Collector-Heat Exchanger Performance**

The use of the heat exchanger A in Figure 20.18 imposes a penalty on the performance of the solar system because  $T_{Ci}$  is always higher than  $T_s$ , thereby decreasing  $q_C$  (see Figure 20.23). The collector-heat exchanger can be implicitly accounted for by suitably modifying the collector performance parameters. Recall from basic heat transfer the concept of heat exchanger effectiveness  $E$  defined as the ratio of the actual heat transfer rate to the maximum possible heat transfer rate, that is,

$$E = (mc_p)_a(T_{ai} - T_{ao}) / (mc_p)_{\min}(T_{ai} - T_{bi}) \tag{20.28a}$$

$$= (mc_p)_b(T_{bo} - T_{bi}) / (mc_p)_{\min}(T_{ai} - T_{bi}) \tag{20.28b}$$

where  $(mc_p)_x$  = capacitance rate of fluid  $X$  (with  $X = a$  for the warmer fluid, or  $X = b$  for the cooler fluid) and  $(mc_p)_{\min}$  is the lower heat capacitance value of either stream. The advantage of this modeling approach is that, to a good approximation,  $E$  can be considered constant in spite of variations in

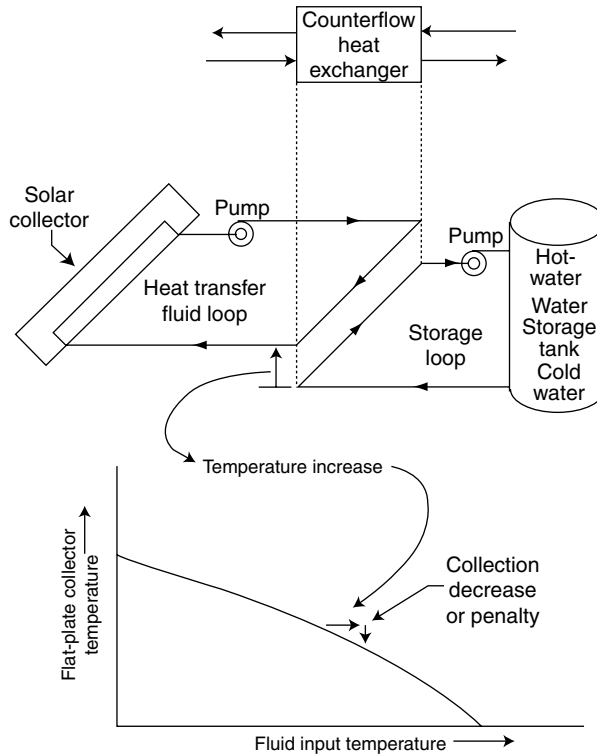


**FIGURE 20.23** Heat collection decrease caused by double-loop heat exchangers. (From Cole, R. L., Nield, K. J., Rohde, R. R., and Wolosewicz, R. M. eds., *Design and Installation Manual for Thermal Energy Storage*, ANL-79-15, Argonne National Laboratory, Argonne, IL, 1979.)

temperature levels provided the mass flow rates of both fluids remain constant. Thus knowing the two flow rates,  $E$ ,  $T_{ai}$ , and  $T_{bi}$ , both the exit fluid temperatures can be conveniently deduced. De Winter (1975) has shown that the combined performance of the solar collector and the heat exchanger can be conveniently modeled by replacing the collector heat removal factor  $F_R$  by a combined collector-exchanger heat removal factor  $F'_R$  such that

$$\frac{F'_R}{F_R} = \left[ 1 + \frac{F_R U_L A_C}{(mC_p)_C} \left\{ \frac{(mC_p)_C}{E_A (mC_p)_{\min}} - 1 \right\} \right]^{-1} \quad (20.29)$$

where  $(mC_p)_C$  is the capacitance rate of the fluid through the collector and  $E_A$  is the effectiveness of heat exchanger A. The variation of  $F'_R/F_R$  is shown in Figure 20.24. The plots exhibit the same type of asymptotic behavior with mass flow rate as in Figure 20.3.

The design of the collector-heat exchanger also requires care if the penalty imposed by it on the solar collection is to be minimized. Using a large heat exchanger increases the effectiveness and lowers this penalty; that is, the ratio  $(F'_R/F_R)$  is high, but the associated initial and operating costs may be higher. Both these considerations need to be balanced for optimum design (see Figure 20.25). Optimum heat exchanger area  $A_X$  can be found from the following equation proposed by Cole et al. (1979):

$$A_X = A_C \left[ \frac{F_R U_L C_C}{U_X C_X} \right]^{1/2} \quad (20.30)$$

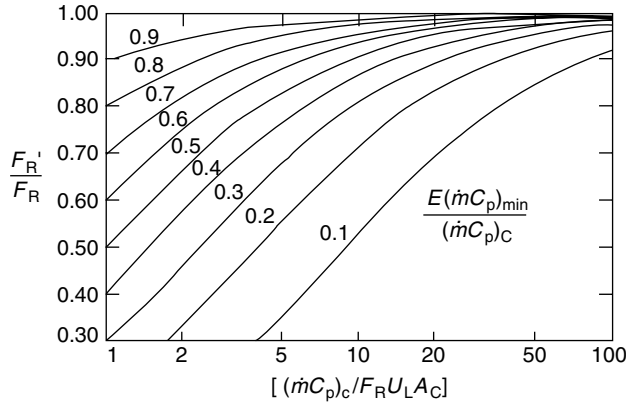


FIGURE 20.24 Variation of collector-heat exchanger correction factor. (From Duffie, J. A. and Beckman, W. A., *Solar Engineering of Thermal Processes*, Wiley Interscience, New York, 1980.)

where  $A_C$  is the collector area,  $C_C$  is the cost per unit collector area,  $C_X$  is the cost per unit heat exchanger area, and  $U_X$  is the heat loss per unit area of the heat exchanger.

**20.1.5.1.2 Collector Piping and Shading Losses**

Other corrections that can be applied to collector performance parameters include those for thermal losses from the piping (or from ducts) between the collection subsystem and the storage unit. Beckman (1978) has shown that these losses can be conveniently taken into consideration by suitably modifying the  $\eta_n$  and  $U_L$  terms of the solar collectors as follows:

$$\frac{\eta'_n}{\eta_n} = \left[ 1 + \frac{u_d A_0}{(mC_p)_C} \right]^{-1} \quad \text{and} \quad \frac{U'_L}{U_L} = \frac{1 - \frac{U_d A_i}{(mC_p)_C} + \frac{U_d (A_i + A_0)}{A_C F_R U_L}}{1 + \frac{U_d A_0}{(mC_p)_C}} \quad (20.31)$$

where  $U_d$  is the heat coefficient from the pipe or duct,  $A_0$  is the heat loss area of the outlet pipe or duct, and  $A_i$  is the heat loss area of the inlet pipe or duct.

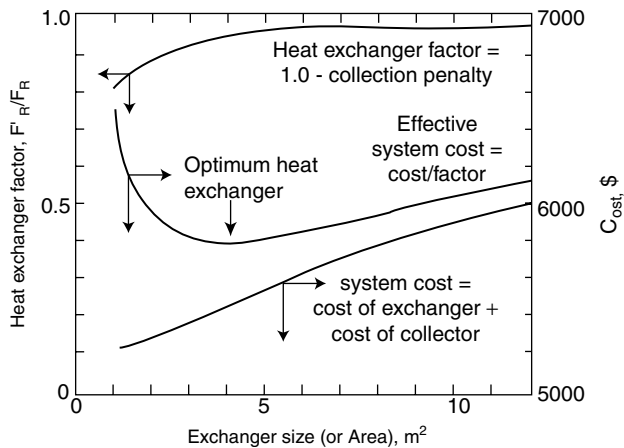


FIGURE 20.25 Typical heat-exchanger optimization plot. (From Cole, R. L., Nield, K. J., Rohde, R. R., and Wolosewicz, R. M. eds., *Design and Installation Manual for Thermal Energy Storage*, ANL-79-15, Argonne National Laboratory, Argonne, IL, 1979.)



When large collector arrays are mounted on flat roofs or level ground, multiple rows of collectors are usually arranged in a sawtooth fashion. These multiple rows must be spaced so that they do not shade each other at low sun angles. Unlimited space is rarely available, and it is desirable to space the rows as close as possible to minimize piping and to keep land costs low. Some amount of shading, especially during early mornings and late evenings during the winter months is generally acceptable. Detailed analysis of shading losses is cumbersome though not difficult and equations presented in standard text books such as Duffie and Beckman (1980) can be used directly.

### 20.1.6 Thermal Storage Systems

Low-temperature solar thermal energy can be stored in liquids, solids, or phase change materials (PCMs). Water is the most frequently used liquid storage medium because of its low cost and high specific heat. The most widely used solid storage medium is rocks (usually of uniform circular size 25–40 mm in diameter). PCM storage is much less bulky because of the high-latent heat of the PCM material, but this technology has yet to become economical and safe for widespread use.

Water storage would be the obvious choice when liquid collectors are used to supply hot water to a load. When hot air is required (for space heat or for convective drying), one has two options: an air collector with a pebble-bed storage or a system with liquid collectors, water storage, and a load heat exchanger to transfer heat from the hot water to the working air stream. Though a number of solar air systems have been designed and operated successfully (mainly for space heating), water storage is very often the medium selected. Water has twice the heat capacity of rock, so water storage tanks will be smaller than rock-bed containers. Moreover, rock storage systems require higher parasitic energy to operate, have higher installation costs, and require more sophisticated controls. Water storage permits simultaneous charging and discharging while such an operation is not possible for rock storage systems. The various types of materials used as containers for water and rock-bed storage and the types of design, installation, and operation details one needs to take care of in such storage systems are described by Mueller Associates (1985), SERI (1989).

Sensible storage systems, whether water or rock-bed, exhibit a certain amount of thermal stratification. Standard textbooks present relevant equations to model such effects. In the case of active closed-loop multipass hot-water systems, storage stratification effects can be neglected for long-term system performance with little loss of accuracy. Moreover, this leads to conservative system design (i.e., solar contribution is underpredicted if stratification is neglected). A designer who wishes to account for the effect of stratification in the water storage can resort to a formulation by Phillips and Dave (1982), who showed that this effect can be fairly well modeled by introducing a *stratification coefficient* (which is a system constant that needs to be determined only once) and treating the storage subsystem as fully mixed. However, this approach is limited to the specific case of no (or very little) heat withdrawal from storage during the collection period. Even when water storage systems are highly stratified, simulation studies seem to indicate that modeling storage as a one-dimensional plug-flow three-node heat transfer problem yields satisfactory results of long-term solar system performance.

The thermal losses  $q_w$  from the storage tank can be modeled as

$$q_w = (UA_S)(T_S - T_{env}) \quad (20.32)$$

where  $(UA_S)$  is the storage overall heat loss per unit temperature difference and  $T_{env}$  is the temperature of the air surrounding the storage tank. Note that  $(UA_S)$  depends (i) on the storage size, which is a parameter to be sized during system design, and (ii) on the configuration of the storage tank (i.e., on the length by diameter ratio in case of a cylindrical tank). For storage tanks, this ratio is normally in the range of 1.0–2.0.

### 20.1.7 Solar System Simulation

A system model is nothing but an assembly of appropriate component modeling equations that are to be solved over time subject to certain forcing functions (i.e., the meteorological data and load data). The resulting set of simultaneous equations can be solved either analytically or numerically.

The analytical method of resolution is appropriate, or possible, only for simplified system configurations and operating conditions. This approach has had some success in the analysis and design of open-loop systems (refer to Reddy 1987, and Gordon and Rabl 1986, for more details). On the other hand, numerical simulation can be performed for any system configuration and operating strategy, however, complex. However, this is time-consuming and expensive in computer time and requires a high level of operator expertise.

We shall illustrate the approach of numerical simulation by considering the simple solar system shown in Figure 20.18. Assuming a fully mixed storage tank, the instantaneous energy balance equation is

$$(Mc_p)_s(dT_s/dt) = q_c - q_u - q_w \quad (20.33)$$

where

$q_c$  is the useful energy delivered by the solar collector (given by Equation 20.2.)

$q_w$  is the thermal loss from the storage tank (given by Equation 20.32)

$q_u$  is the useful heat transferred through the load heat exchanger, which can be determined as follows:

The maximum hourly rate of energy transfer through the load heat exchanger is

$$q_{\max} = E_B(mc_p)_{\min}(T_s - T_{Xi})\delta_L \quad (20.34)$$

where  $\delta_L$  is a control function whose value is either 1 or 0 depending upon whether there is a heat demand or not. Since  $q_{\max}$  can be greater than the amount of thermal energy  $q_L$  actually required by the load, the bypass arrangement can be conveniently modeled as

$$q_u = \min(q_{\max}, q_L) \quad (20.35)$$

where

$$q_L = (mc_p)_L(T_{Li} - T_{Xi}) \quad (20.36)$$

for water heating and industrial process heat loads. Space heating and cooling loads can be conveniently determined by one of the several variants of the bin-type methods (ASHRAE 1985).

The amount of energy  $q_{\max}$  supplied by a topping-up type of auxiliary heater is

$$q_{\max} = q_L - q_u \quad (20.37)$$

Assuming  $T_{\text{env}} = T_a$ , Equation 20.33 can be expanded into

$$(Mc_p)_s \frac{dT_s}{dt} - A_C F_R [I_T \eta_0 - U_L(T_s - T_a)]^+ - (mc_p)_s(T_s - T_{Xi})\delta_L - (UA)_s(T_s - T_a) \quad (20.38)$$

The presence of control functions and time dependence of  $I_T$  and  $T_a$  prevent a general analytical treatment, though, as mentioned earlier, specific cases can be handled. The numerical approach involves expressing this differential equation in finite difference form. After rearranging, one gets

$$= T_{S,b} + \frac{\Delta t}{(Mc_p)_s} \{A_C F_R [I_T \eta_0 - U_L(T_{S,b} - T_a)]^+ - (mc_p)_s(T_{S,b} - T_{Xi})\delta_L - (UA)_s(T_{S,b} - T_a)\} T_{S,f} \quad (20.39)$$

where  $T_{S,b}$  and  $T_{S,f}$  are the storage temperatures at the beginning and the end of the time step  $\Delta t$ . The time step is sufficiently small (say 1 h) that  $I_T$  and  $T_a$  can be assumed constant. This equation is repeatedly

used over the time period in question (day, month, or year), and the total energy supplied by the collector or to the load can be estimated.

Such methods of simulation, referred as stepwise steady-state simulations, implicitly assume that the solar thermal system operates in a steady-state manner during one time step, at the end of which it undergoes an abrupt change in operating conditions as a result of changes in the forcing functions, and thereby attains a new steady-state operating level. Although in reality, the system performance varies smoothly over time and is consequently different from that outlined earlier, it has been found that, in most cases, taking time steps of the order of 1 h yields acceptable results of long-term performance.

The objective of solar-supplemented energy systems is to displace part of the conventional fuel consumption of the auxiliary heater. The index used to represent the contribution of the solar thermal system is the *solar fraction*, which is the fraction of the total energy required by the load that is supplied by the solar system. The solar fraction could be expressed over any time scale, with month and year being the most common. Two commonly used definitions of the monthly solar fraction are

1. Thermal solar fraction:

$$f_Y = Q_{UM}/Q_{LM} = 1 - Q_{aux,M}/Q_{LM} \quad (20.40)$$

where

$Q_{UM}$  is the monthly total thermal energy supplied by the solar system

$Q_{LM}$  is the monthly total thermal requirements of the load

$Q_{aux,M}$  is the monthly total auxiliary energy consumed

2. Energy solar fraction (i.e., thermal plus parasitic energy):

$$f'_M = Q'_{UM}/Q'_{LM} \quad (20.41)$$

where  $Q'_{UM}$  is  $Q_{UM}$  minus the parasitic energy consumed by the solar system and  $Q'_{LM}$  is  $Q_{LM}$  plus the parasitic energy consumed by the load.

### Example 20.1.5

Simulate the closed-loop solar thermal system shown in Figure 20.18 for each hour of a day assuming both collector and load heat exchangers to be absent (i.e.,  $E_A = E_B = 1$ ). Assume the following data as input for the simulation:  $A_C = 10 \text{ m}^2$ ,  $F_R U_L = 5.0 \text{ W/m}^2\text{°C}$ ,  $F_R \eta_0 = 0.7$ ,  $(Mc_p) = 2.0 \text{ MJ/°C}$  and  $(UA)_S = 3 \text{ W/°C}$ . Water is withdrawn to meet a load from 9 a.m. to 7 p.m. (solar time) at a constant rate of 60 kg/h and is replenished from the mains at a temperature of 25°C. The storage temperature at the start (i.e., at 6 a.m.) is 40°C, and the environment temperature is equal to the ambient temperature. The temperature of the water entering the load should not exceed 55°C. The hourly values of the solar radiation on the plane of the collector are given in column 2 of Table 20.3 and the ambient temperature is assumed constant over the day and equal to 25°C. The variation of the optical efficiency with angle of incidence can be neglected.

The results of the simulation are given in Table 20.3. The following equations should permit the reader to verify for himself the results obtained. Simulating the system entails solving the following equations in the sequence given here:

*Column 4.* Useful energy delivered by the collector (Equation 20.2)

$$q_C = 10[0.7I_T - 5(3,600/10^6)T_{S,b} - 25]^+ \text{ (MJ/h)}$$

The term  $(3600/10^6)$  is introduced to convert  $\text{W/m}^2$  (the units in which  $I_T$  is expressed) into  $\text{MJ}/(\text{h m}^2)$ . Note that  $T_{S,b}$  is taken to be equal to  $T_{S,f}$  of the final hour.

*Column 5.* Thermal losses from the storage tank (Equation 20.32)

$$q_w = 3(3,600/10^6)(T_{S,b} - 25) \text{ (MJ/h)}$$

**TABLE 20.3** Simulation Results of Example 20.1.5

(1) Solar Time (h)	(2) $I_T$ (MJ/m <sup>2</sup> h)	(3) $T_{s,f}$ (°C)	(4) $q_C$ (MJ/h)	(5) $q_w$ (MJ/h)	(6) $q_{max}$ (MJ/h)	(7) $q_L$ (MJ/h)	(8) $q_U$ (MJ/h)	(9) $q_{aux}$ (MJ/h)
Start		40.00						
6–7	0.37	39.92	0.00	0.16	0.00	0.00	0.00	0.00
7–8	0.95	41.82	3.96	0.16	0.00	0.00	0.00	0.00
8–9	1.54	45.61	7.75	0.18	0.00	0.00	0.00	0.00
9–10	2.00	48.05	10.29	0.22	5.18	754	5.18	2.36
10–11	2.27	50.90	11.74	0.25	5.79	7.54	5.79	1.75
11–12	2.46	53.78	12.56	0.28	6.51	7.54	6.51	1.03
12–13	2.50	56.17	12.32	0.31	7.24	7.54	7.24	0.31
13–14	2.24	57.26	10.07	0.34	7.84	7.54	7.54	0.00
14–15	2.12	57.84	9.03	0.35	8.11	7.54	7.54	0.00
15–16	1.37	55.73	3.68	0.35	8.25	7.54	7.54	0.00
16–17	0.76	51.79	0.00	0.33	7.72	7.54	7.54	0.00
17–18	0.23	48.28	0.00	0.29	6.73	7.54	6.73	0.81
18–19	0.00	45.23	0.00	0.25	5.85	7.54	5.85	1.69
Total	18.81	—	81.41	3.48	69.24	75.40	67.48	7.94

*Column 6.* The maximum rate of energy that can be transferred from the load can be calculated from Equation 20.34

$$q_{max} = 60(4,190/10^6)(T_{s,b} - 25) \text{ (MJ/h)}$$

*Column 7.* The thermal energy required by the load (from Equation 20.36)

$$q_L = 60(4,190/10^6)(55 - 25) = 7.54 \text{ MJ/h}$$

*Column 8.* The actual amount of heat withdrawn from storage (Equation 20.35)

$$q_w = \min[\text{column 6, column 7}]$$

*Column 9.* The amount of energy supplied by the auxiliary heater (Equation 20.2.37)

$$q_{aux} = \text{column 7} - \text{column 8}$$

The final storage temperature  $T_{s,f}$  is now calculated from Equation 20.39

$$T_{s,f} = T_{s,b} + [\text{column 4} - \text{column 8} - \text{column 5}]/2.0$$

From Table 20.3, we note that the solar collector efficiency over the entire day is  $[81.41/(18.81 \times 10)] = 0.43$ . The corresponding daily solar fraction  $= (67.48/75.40) = 0.895$ .

## 20.1.8 Solar System Sizing Methodology

Sizing of solar systems primarily involves determining the collector area and storage size that are most cost effective. Standalone and solar-supplemented systems have to be treated separately since the basic design problem is somewhat different. The interested reader can refer to Gordon (1987) for sizing standalone systems.

### 20.1.8.1 Solar-Supplemented Systems

#### 20.1.8.1.1 Production Functions

Because of the annual variation of incident solar radiation, it is not normally economical to size a solar subsystem such that it provides 100% of the heat demand. Most solar energy systems follow the *law of*

*diminishing returns*. This implies that increasing the size of the solar collector subsystem results in a less than proportional increase in the annual fuel savings (or alternatively, in the annual solar fraction).

Any model has two types of variables: exogenous and endogenous. The *exogenous parameters* are also called the input variables, and these in turn may be of two kinds. *Variable exogenous parameters* are the collector area  $A_C$ , the collector performance parameters  $F_R\eta_n$  and  $F_RU_L$ , the collector tilt, the thermal storage capacity  $(Mc_p)_S$ , the heat exchanger size, and the control strategies of the solar thermal system. On the other hand, the climatic data specified by radiation and the ambient temperature, as well as the end use thermal demand characteristics, are called *constrained exogenous parameters* because they are imposed externally and cannot be changed. The *endogenous parameters* are the output parameters whose values are to be determined, the annual solar fraction being one of the parameters most often sought.

Figure 20.26 illustrates the law of diminishing results. The annual solar fraction  $f_Y$  is seen to increase with collector area but at a decreasing rate and at a certain point will reach saturation. Variation of any of the other exogenous parameters also exhibits a similar trend. The technical relationship between  $f_Y$  and one or several variable exogenous parameters for a given location is called the *yearly production function*.

It is only for certain simple types of solar thermal systems that an analytical expression for the production can be deduced directly from theoretical considerations. The most common approach is to carry out computer simulations of the particular system (solar plus auxiliary) over the complete year for several combinations of values of the exogenous parameters. The production function can subsequently be determined by an empirical curve fit to these discrete sets of points.

### Example 20.1.6

Kreider (1979a, 1979b) gives the following expression for the production function of an industrial solar water heater for a certain location:

$$f_Y = Q_{UY}/Q_{LY} = \left(0.35 - \frac{F_R U_L}{100 F_R \eta_n}\right) \ln \left(1 + \frac{20 F_R \eta_n A_C}{Q_{LY}}\right) \quad (20.42)$$

where  $Q_{UY}$  is the thermal energy delivered by the solar thermal system over the year in GJ/y;  $Q_{LY}$  is the yearly thermal load demand, also in GJ/y; and  $F_R U_L$  is in  $W/(m^2\text{C})$ . Note that only certain solar system exogenous parameters figure explicitly in this expression, thereby implying that other exogenous parameters (for example, storage volume) have not been varied during the study. As an illustration,

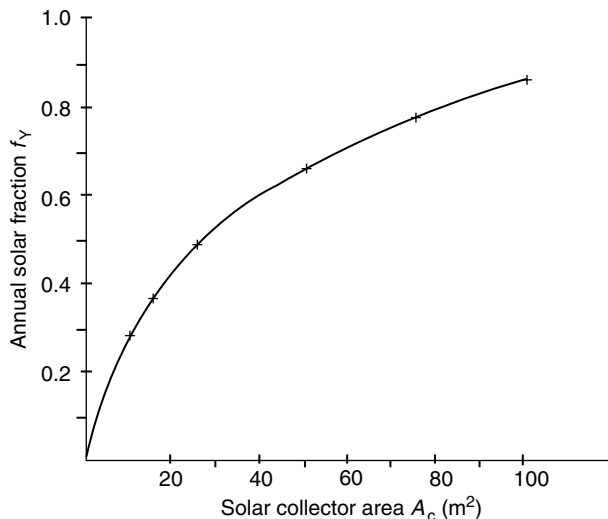


FIGURE 20.26 A typical solar system production function (see Example 20.3.6).

let us assume the following nominal values:  $Q_{LY} = 100$  GJ/y,  $F_R U_L = 2.0$  W/(m<sup>2</sup>°C), and  $F_R \eta_n = 0.7$ . For a 1% increase in collector area  $A_C$ , the corresponding percentage increase in  $Q_{UY}$  (called elasticity) can be determined:

$$\frac{dQ_{UY}}{Q_{UY}} = \frac{dA_C}{A_C} \left[ \left( \frac{Q_{LY}}{20F_R \eta_n A_C} + 1 \right) \ln \left( 1 + \frac{20F_R \eta_n A_C}{Q_{LY}} \right) \right]^{-1} \quad (20.43)$$

From this, we obtain the expression for *marginal productivity*

$$\frac{dQ_{UY}}{dA_C} = \frac{Q_{UY}}{A_C} \left[ \left( \frac{Q_{LY}}{20F_R \eta_n A_C} + 1 \right) \ln \left( 1 + \frac{20F_R \eta_n A_C}{Q_{LY}} \right) \right]^{-1} \quad (20.44)$$

Numerical values can be obtained from the preceding expression. Though  $Q_{UY}$  increases with  $A_C$ , the marginal productivity of  $Q_{UY}$  goes on decreasing with increasing  $A_C$ , thus illustrating the law of diminishing returns. A qualitative explanation of this phenomenon is that as  $A_C$  increases, the mean operating temperature level of the collector increases, thus leading to decreasing solar collection rates. Figure 20.26 illustrates the variation of  $f_Y$  with  $A_C$  as given by Equation 20.42 when the preceding numerical values are used.

The objective of the sizing study in its widest perspective is to determine, for a given specific thermal end use, the size and configuration of the solar subsystem that results in the most economical operation of the entire system. This economical optimum can be determined using the production function along with an appropriate economic analysis. Several authors—for example, Duffie and Beckman (1980) or Rabl (1985)—have presented fairly rigorous methodologies of economic analysis, but a simple approach is adequate to illustrate the concepts and for preliminary system sizing.

### 20.1.8.1.2 Simplified Economic Analysis

It is widely recognized that *discounted cash flow analysis* is most appropriate for applications such as sizing an energy system. This analysis takes into account both the initial cost incurred during the installation of the system and the annual running costs over its entire life span.

The economic objective function for optimal system selection can be expressed in terms of either the energy cost incurred or the energy savings. These two approaches are basically similar and differ in the sense that the objective function of the former has to be minimized while that of the latter has to be maximized. In our analysis, we shall consider the latter approach, which can further be subdivided into the following two methods:

1. Present worth or life cycle savings, wherein all running costs are discounted to the beginning of the first year of operation of the system.
2. Annualized life cycle savings, wherein the initial expenditure incurred at the start as well as the running costs over the life of the installation are expressed as a yearly mean value.

## 20.1.9 Solar System Design Methods

### 20.1.9.1 Classification

Design methods may be separated into three generic classes. The *simple* category, usually associated with the prefeasibility study phase involves quick manual calculations of solar collector/system performance and rule-of-thumb engineering estimates. For example, the generalized yearly correlations proposed by Rabl (1981) and described in Section 20.1.2 could be conveniently used for year-round, more or less constant loads. The approach is directly valid for open-loop solar systems, while it could also be used for closed-loop systems if an *average* collector inlet temperature could be determined. A simple manner of selecting this temperature  $\bar{T}_m$  for domestic closed-loop multipass systems is to assume the following

empirical relation:

$$\bar{T}_m - T_{\text{mains}}/3 + (2/3)T_{\text{set}} \quad (20.45)$$

where  $T_{\text{mains}}$  is the average annual supply temperature and  $T_{\text{set}}$  is the required hot-water temperature (about 60°C–80°C in most cases).

These manual methods often use general guidelines, graphs, and/or tables for sizing and performance evaluation. The designer should have a certain amount of knowledge and experience in solar system design in order to make pertinent assumptions and simplifications regarding the operation of the particular system.

*Mid-level* design methods are resorted to during the feasibility phase of a project. The main focus of this chapter has been toward this level, and a few of these design methods will be presented in this section. A personal computer is best suited to these design methods because they could be conveniently programmed to suit the designer's tastes and purpose (spreadsheet programs, or better still one of the numerous equation-solver software packages, are most convenient). Alternatively, commercially available software packages such as f-chart (Beckman, Klein, and Duffie 1977) could also be used for certain specific system configurations.

*Detailed* design methods involve performing hourly simulations of the solar system over the entire year from which accurate optimization of solar collector and other equipment can be performed. Several simulation programs for active solar energy systems are available, TRNSYS (Klein et al. 1975, 1979) developed at the University of Wisconsin–Madison being perhaps the best known. This public-domain software has technical support and is being constantly upgraded. TRNSYS contains simulation models of numerous subsystem components (solar radiation, solar equipment, loads, mechanical equipment, controls, etc.) that comprise a solar energy system. A user can conveniently hook up components representative of a particular solar system to be analyzed and then simulate that system's performance at a level of detail that the user selects. Thus TRNSYS provides the design with large flexibility, diversity, and convenience of usage.

As pointed out by Rabl (1985), the detailed computer simulations approach, though a valuable tool, has several problems. Judgment is needed both in the selection of the input and in the evaluation of the output. The very flexibility of big simulation programs has drawbacks. So many variables must be specified by the user that errors in interpretation or specification are common. Also, learning how to use the program is a time-consuming task. Because of the numerous system variables to be optimized, the program may have to be run for numerous sets of combinations, which adds to expense and time. The inexperienced user can be easily misled by the second-order details while missing first-order effects. For example, uncertainties in load, solar radiation, and economic variables are usually very large, and long-term performance simulation results are only accurate to within a certain degree. Nevertheless, detailed simulation programs, if properly used by experienced designers, can provide valuable information on system design and optimization aspects at the final stages of a project design.

There are basically three types of mid-level design approaches: the empirical correlation approach, the analytical approach, and the one-day repetitive methods (described fully in Reddy 1987). We shall illustrate their use by means of specific applications.

### 20.1.9.2 Active Space Heating

The solar system configuration for this particular application has become more or less standardized. For example, for a liquid system, one would use the system shown in [Figure 20.27](#). One of the most widely used design methods is the f-chart method (Beckman, Klein, and Duffie 1977; Duffie and Beckman 1980), which is applicable for standardized liquid and air heating systems as well as for standardized domestic hot-water systems. The f-chart method basically involves using a simple algebraic correlation that has been deduced from numerous TRNSYS simulation runs of these standard solar systems subject to a wide range of climates and solar system parameters (see [Figure 20.28](#)). Correlations were

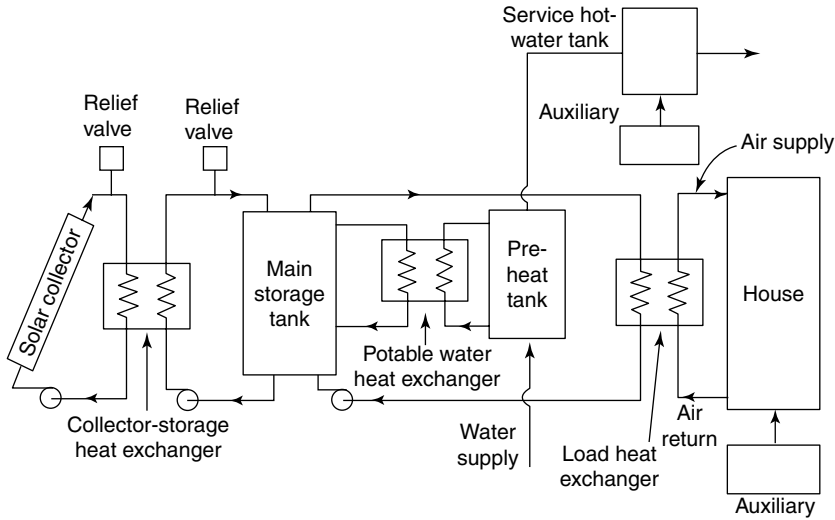


FIGURE 20.27 Schematic of the standard space heating liquid system configuration for the f-chart method. (From Duffie, J. A. and Beckman, W. A., *Solar Engineering of Thermal Processes*, Wiley Interscience, New York, 1980.)

developed between monthly solar fractions and two easily calculated dimensionless variables  $X$  and  $Y$ , where

$$X = (A_C F'_R U_L (T_{Ref} - \bar{T}_a) \Delta t) / Q_{LM} \tag{20.46}$$

$$Y = A_C F'_R \bar{\eta}_0 \bar{H}_T N / Q_{LM} \tag{20.47}$$

where

$A_C$  collector area ( $m^2$ )

$F'_R$  collector-heat exchanger heat removal factor (given by Equation 20.29)

$U_L$  collector overall loss coefficient ( $W/(m^2 \cdot C)$ )

$\Delta t$  total number of seconds in the month =  $3600 \times 24 \times N = 86,400 \times N$

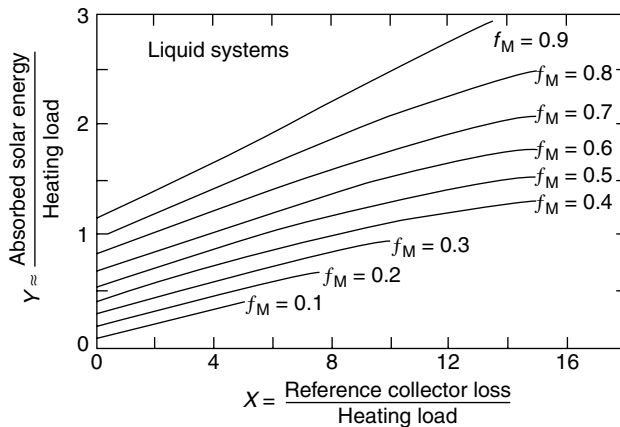


FIGURE 20.28 The f-chart correlation for liquid system configuration. (From Duffie, J. A. and Beckman, W. A., *Solar Engineering of Thermal Processes*, Wiley Interscience, New York, 1980.)



- $\bar{T}_a$  monthly average ambient temperature ( $^{\circ}\text{C}$ )  
 $T_{\text{Ref}}$  an empirically derived reference temperature, taken as  $100^{\circ}\text{C}$   
 $Q_{\text{LM}}$  monthly total heating load for space heating and/or hot water (J)  
 $\bar{H}_T$  monthly average daily radiation incident on the collector surface per unit area ( $\text{J}/\text{m}^2$ )  
 $N$  number of days in the month  
 $\bar{\eta}_0$  monthly average collector optical efficiency

The dimensionless variable  $X$  is the ratio of reference collector losses over the entire month to the monthly total heat load; the variable  $Y$  is the ratio of the monthly total solar energy absorbed by the collectors to the monthly total heat load. It will be noted that the collector area and its performance parameters are the predominant exogenous variables that appear in these expressions. For changes in secondary exogenous parameters, the following corrective terms  $X_C$  and  $Y_C$  should be applied for liquid systems:

1. for changes in storage capacity:

$$X_C/X = (\text{actual storage capacity}/\text{standard storage capacity})^{-0.25} \quad (20.48)$$

where the standard storage volume is  $75 \text{ L}/\text{m}^2$  of collector area.

2. for changes in heat exchanger size:

$$Y_C/Y = 0.39 + 0.65 \exp[-(0.139(UA)_B/(E_L(mc_p)_{\min}))] \quad (20.49)$$

The monthly solar fraction for liquid space heating can then be determined from the following empirical correlation:

$$f_M = 1.029Y - 0.065X - 0.245Y^2 + 0.0018X^2 + 0.0215Y^3 \quad (20.50)$$

subject to the conditions that  $0 \leq X \leq 15$  and  $0 \leq Y \leq 3$ . This empirical correlation is shown graphically in Figure 20.28.

A similar correlation has also been proposed for space heating systems using air collectors and pebble-bed storage. The procedure for exploiting the preceding empirical correlations is as follows. For a predetermined location, specified by its 12 monthly radiation and ambient temperature values, Equation 20.50 is repeatedly used for each month of the year for a particular set of variable exogenous parameters. The monthly solar fraction  $f_M$  and thence the annual thermal energy delivered by the solar thermal system are easily deduced. Subsequently, the entire procedure is repeated for different values and combinations of variable exogenous parameters. Finally, an economic analysis is performed to determine optimal sizes of various solar system components. Care must be exercised that the exogenous parameters considered are not outside the range of validity of the f-chart empirical correlations.

### Example 20.1.7

(Adapted from Duffie and Beckman 1980). A solar heating system is to be designed for Madison, Wisconsin (latitude  $43^{\circ}\text{N}$ ) using one-cover collectors with  $F_R \eta_n = 0.74$  and  $F_R U_L = 4 \text{ W}/(\text{m}^2\text{C})$ . The collector faces south with a slope of  $60^{\circ}$  from the horizontal. The average daily radiation on the tilted surface in January is  $12.9 \text{ MJ}/\text{m}^2$ , and the average ambient temperature is  $-7^{\circ}\text{C}$ . The heat load is  $36 \text{ GJ}$  for space heating and hot water. The collector-heat exchanger correction factor is  $0.97$  and the ratio of monthly average to normal incidence optical efficiency is  $0.96$ . Calculate the energy delivered by the solar system in January if  $50 \text{ m}^2$  of collector area is to be used.

From Equation 20.46 and Equation 20.47, with  $A_C = 50 \text{ m}^2$ ,

$$X = 4.0 \times 0.97[100 - (-7)]31 \times 86,400 \times 50/(36 \times 10^9) = 1.54$$

$$Y = 0.74 \times 0.97 \times 0.96 \times 12.9 \times 10^6 \times 31 \times 50/(36 \times 10^9) = 0.38$$

From Equation 20.50, the solar fraction for January is  $f_M = 0.26$ . Thus the useful energy delivered by the solar system  $= 0.26 \times 36 = 9.4 \text{ GJ}$ .

In an effort to reduce the tediousness involved in having to perform 12 monthly calculations, two analogous approaches that enable the annual solar fraction to be determined directly have been developed by Barley and Winn (1978), Lameiro and Bendt (1978). These involve the computation of a few site-specific empirical coefficients, thereby rendering the approach less general. For example, the *relative-area* method suggested by Barley and Winn enable the designer to directly calculate the annual solar fraction of the corresponding system using four site-specific empirical coefficients. The approach involves curve fits to simulation results of the f-chart method for specific locations in order to deduce a correlation such as:

$$f = c_1 + c_2 \ln(A/A_{0.5}) \quad (20.51)$$

where  $c_1$  and  $c_2$  are location-specific parameters that are tabulated for several United States locations, and  $A_{0.5}$  is the collector area corresponding to an annual solar fraction of 0.5 given by

$$A_{0.5} = A_S(UA)/(F'_R \eta_0 - F'_R U_L Z) \quad (20.52)$$

where  $A_S$  and  $Z$  are two more location specific parameters,  $UA$  is the overall heat loss coefficient of the building, and  $F'_R \eta_0$  and  $F'_R U_L$  are the corresponding solar collector performance parameters corrected for the effect of the collector-heat exchanger.

Barley and Winn also proposed a simplified economic life-cycle analysis whereby the optimal collector area could be determined directly. Another well-known approach is the *Solar Load Ratio* (SLR) method for sizing residential space heating systems (Hunn 1980).

### 20.1.9.3 Domestic Water Heating

The f-chart correlation (Equation 20.50) can also be used to predict the monthly solar fraction for domestic hot-water systems represented by Figure 20.21 provided the water mains temperature  $T_{\text{mains}}$  is between 5 and 20°C and the minimum acceptable hot-water temperature drawn from the storage for end use (called the set water temperature  $T_w$ ) is between 50 and 70°C. Further, the dimensionless parameter  $X$  must be corrected by the following ratio

$$X_w/X = (11.6 + 1.8T_w + 3.86T_{\text{mains}} - 2.32\bar{T}_a)/(100 - \bar{T}_a) \quad (20.53)$$

In case the domestic hot-water load is much smaller than the space heat load, it is recommended that Equation 20.50 be used without the above correction.

### 20.1.9.4 Industrial Process Heat

As discussed in “Description of a Typical Closed-Loop System,” two types of solar systems for industrial process heat are currently used: the closed-loop multipass systems (with an added distinction that the auxiliary heater may be placed either in series or in parallel (see Figure 20.18 and Figure 20.19) and the open-loop singlepass system. How such systems can be designed will be described next.

### 20.1.9.4.1 Closed-Loop Multipass Systems

*Auxiliary Heater in Parallel.* The Phibar-f chart method (Klein and Beckman 1979; Duffie and Beckman 1980; Reddy 1987) is a generalization of the f-chart method in the sense that no restrictions need be imposed on the temperature limits of the heated fluid in the solar thermal system. However, three basic criteria for the thermal load have to be satisfied for the Phibar-f chart method to be applicable: (i) the thermal load must be constant and uniform over each day and for at least a month, (ii) the thermal energy supplied to the load must be above a minimum temperature that completely specifies the temperature level of operation of the load, and (iii) either there is no conversion efficiency in the load (as in the case of hot water usage) or the efficiency of conversion is constant (either because the load temperature level is constant or because the conversion efficiency is independent of the load temperature level). The approach is strictly applicable to solar systems with the auxiliary heater in parallel (Figure 20.19).

A typical application for the Phibar-f chart method is absorption air-conditioning. The hot water inlet temperature from the collectors to the generator must be above a minimum temperature level (say, 80°C) for the system to use solar heat. If the solar fluid temperature is less (even by a small amount), the entire energy to heat up the water to 80°C is supplied by the auxiliary system.

As a result of continuous interaction between storage and collector in a closed-loop system, the variation of the storage temperature and hence the fluid inlet temperature to the collectors) over the day and over the month is undetermined. The Phibar-f chart method implicitly takes this into account and reduces these temperature fluctuations down to a monthly mean equivalent storage temperature  $\bar{T}_S$ . The determination of this temperature in conjunction with the daily utilizability approach is the basis of the design approach.

The basic empirical correlation of the Phibar-f chart method, shown graphically in Figure 20.29, is as follows:

$$f_M = Y\bar{\phi} - a[\exp(bf_M) - 1][1 - \exp(cX)] \quad (20.54)$$

with  $0 < X < 20$  and  $0 < Y < 1.6$ , and  $\bar{\phi}$  is the Klein daily utilizability fraction described in “Daily Utilizability” and given by Equation 20.24.  $Y$  is given by Equation 20.47, and  $X$  is now slightly different from Equation 20.46 and is defined as:

$$X = A_C F_R U_L \Delta t (100^\circ\text{C}) / Q_{LM} \quad (20.55)$$

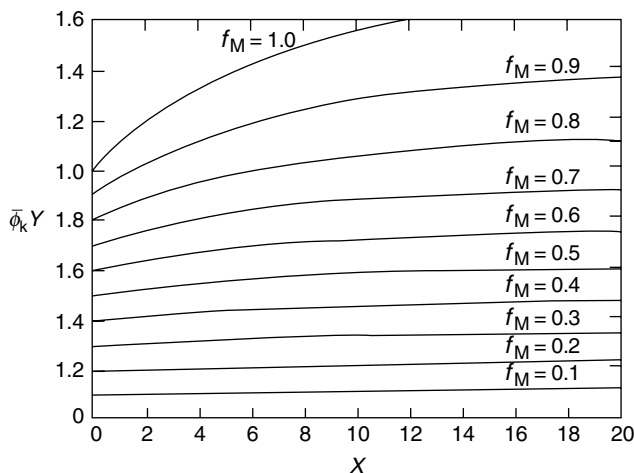


**FIGURE 20.29** The Phibar-f chart correlation for a storage capacity of 350 kJ/m<sup>2</sup> and for a 12 h per day thermal load. (From Duffie, J. A. and Beckman, W. A., *Solar Engineering of Thermal Processes*, Wiley Interscience, New York, 1980.)

The values of the constants  $a$ ,  $b$ , and  $c$  are given by the following:

1. for an end use load operating between 6 a.m. and 6 p.m. every day of the month,

$$a = 0.015[(Mc_p)_s/350 \text{ kJ}/(\text{m}^2\text{C})]^{-0.76} \quad \text{for} \quad 175 \leq [(Mc_p)_s/A_C] \leq 1,400 \text{ kJ}/(\text{m}^2\text{C}) \quad (20.56)$$

and  $b = 3.85$  and  $c = -0.15$

2. for an end use load operating 24 h per day over the entire month,

$$a = 0.043 \quad \text{only for} [(Mc_p)_s/A_C] = 350 \text{ kJ}/(\text{m}^2\text{C}), \quad b = 2.81, \quad \text{and} \quad c = -0.18 \quad (20.57)$$

It will be noted that  $(Y\bar{\phi})$  denotes the maximum solar fraction that would have resulted had  $T_{Ci}$ , the inlet temperature to the collector, been equal to  $T_{Li}$  throughout the month. The term in Equation 20.54 that is subtracted from  $(Y\bar{\phi})$  represents the decrease in the solar fraction as a result of  $T_{Ci} > T_{Xi}$ . The solar fraction computed from Equation 20.54 has to be corrected for the effect of thermal losses from the storage as well as the presence of the load-heat exchanger, both of which will decrease the solar fraction. For complete details, refer to Duffie and Beckman (1980) or Reddy (1987). Note that Equation 20.54 needs to be solved for  $f_m$  in an iterative manner.

*Auxiliary Heater in Series.* The Phibar- $f$  chart method has also been modified to include solar systems with the auxiliary heater in series as shown in Figure 20.18. This configuration leads to higher solar fractions but retrofit to existing systems may be more costly.

In this case, the empirical correlation given by Equation 20.54 has been modified by Braun, Klein, and Pearson (1983) as follows:

$$f_M = Y\bar{\phi} - a[\exp(bf_M) - 1][1 - \exp(cX)]\exp(-1.959Z) \quad (20.58)$$

with  $Z = Q_{LM}/(C_L \times 100^\circ\text{C})$  and (i) when there is no load-heat exchanger,  $C_L$  is the monthly total load heat capacitance, which is the product of the monthly total mass of water used and the specific heat capacity of water, and (ii) when there is a load-heat exchanger present  $C_L = E_L \times C_{\min}$ , where  $E_L$  is the effectiveness of the load-heat exchanger and  $C_{\min}$  is the monthly total heat capacitance, which is the lesser of the two fluids rates across the load heat exchanger.

The modified Phibar- $f$  chart is similar to the original method in respect to load uniformity on a day-to-day basis over the month and in assuming no conversion efficiency. The interested may refer to Braun, Klein, and Pearson (1983) or Reddy (1987) for complete details.

#### 20.1.9.4.2 Open-Loop Single-Pass Systems

The advantages offered by open-loop single-pass systems over closed-loop multipass systems for meeting constant loads has been described in "Closed-Loop and Open-Loop Systems." Because industrial loads operate during the entire sun-up hours or even for 24 h daily, the simplest solar thermal system is one with no heat storage (Figure 20.20). A sizable portion (between 25 and 70%) of the daytime thermal load can be supplied by such systems and consequently, the sizing of such systems will be described below (Gordon and Rabl 1982). We shall assume that  $T_{Li}$  and  $T_{Xi}$  are constant for all hours during system operation. Because no storage is provided, excess solar energy collection (whenever  $T_{Ci} > T_{Li}$ ) will have to be dumped out.

The maximum collector area  $\hat{A}_C$  for which energy dumping does not occur at any time of the year can be found from the following instantaneous heat balance equation:

$$P_L = \hat{A}_C \hat{F}_R [I_{\max} \eta_n - U_L (T_{Ci} - T_a)] \quad (20.59)$$

where  $P_L$ , the instantaneous thermal heat demand of the load (say, in kW) is given by

$$P_L = m_L c_p (T_{Li} - T_{Xi}) \quad (20.60)$$

and  $F_R$  is the heat removal factor of the collector field when its surface area is  $\hat{A}_C$ . Since  $\hat{A}_C$  is as yet unknown, the value of  $\hat{F}_R$  is also undetermined. (Note that though the *total* fluid flow rate is known, the flow rate per unit collector area is not known.) Recall that the plate efficiency factor  $F'$  for liquid collectors can be assumed constant and independent of fluid flow rate per unit collector area. Equation 20.59 can be expressed in terms of critical radiation level  $I_C$ :

$$P_L = \hat{A}_C \hat{F}_R \eta_n (I_{\max} - I_C) \quad (20.61a)$$

or

$$\hat{A}_C \hat{F}_R \eta_n = P_L / (I_{\max} - I_C) \quad (20.61b)$$

Substituting Equation 20.3 in lieu of  $F_R$  and rearranging yields

$$\hat{A}_C = -(m_L c_p / F' U_L) \ln[1 - P_L U_L / (\eta_n (I_{\max} - I_C) m_L c_p)] \quad (20.62)$$

If the actual collector area  $A_C$  exceeds this value, dumping will occur as soon as the radiation intensity reaches a value  $I_D$ , whose value is determined from the following heat balance:

$$P_L = A_C F_R \eta_n (I_D - I_C) \quad (20.63a)$$

Hence

$$I_D = I_C + P_L / (A_C F_R \eta_n) \quad (20.63b)$$

Note that the value of  $I_D$  decreases with increasing collector area  $A_C$ , thereby indicating that increasing amounts of solar energy will have to be dumped out.

Since the solar thermal system is operational during the entire sunshine hours of the year, the yearly total energy collected can be directly determined by the Rabl correlation given by Equation 20.26. Similarly, the yearly total solar energy collected by the solar system which has got to be dumped out is

$$Q_{DY} = A_C F_R \eta_n (\bar{a} + \bar{b} I_D + \bar{c} I_D^2) \quad (20.64)$$

The yearly total solar energy delivered to the load is

$$\begin{aligned} Q_{UY} &= Q_{CY} - Q_{DY} \\ &= A_C F_R \eta_n [\bar{b}(I_C - I_D) + \bar{c}(I_C^2 - I_D^2)] \end{aligned} \quad (20.65)$$

$$\begin{aligned} &= -(\bar{b} + 2\bar{c} I_C) P_L - \bar{c} P_L^2 / (A_C F_R \eta_n) \\ &= -(\bar{b} + 2\bar{c} I_C) P_L - \bar{c} P_L^2 / (A_C F_R \eta_n) \end{aligned} \quad (20.66)$$

Replacing the value of  $F_R$  given by Equation 20.3, the annual production function in terms of  $A_C$  is

$$Q_{UY} = -(\bar{b} + 2\bar{c} I_C) P_L - \frac{\bar{c} P_L^2}{\left(\frac{F' \eta_n}{F' U_L}\right) (m_L c_p) \left[1 - \exp\left(-\frac{F' U_L A_C}{m_L c_p}\right)\right]} \quad (20.67)$$

subject to the condition that  $A_C > \hat{A}_C$ . If the thermal load is not needed during all days of the year due to holidays or maintenance shutdown, the production function can be reduced proportionally. This is illustrated in the following example.

**Example 20.1.8**

Obtain the annual production function of an open-loop solar thermal system without storage that is to be set up in Boston, Massachusetts according to the following load specifications: industrial hot water load for 12 h a day (6 a.m.–6 p.m.) and during 290 days a year, mass flow rate  $m_L = 0.25$  kg/s, required inlet temperature  $T_{Li} = 60^\circ\text{C}$ . Contaminants are picked up in the load, so that all used water is to be rejected and fresh water at ambient temperature is taken in. Flat-plate collectors with tilt equal to latitude with the following parameters are used  $F'\eta_n = 0.75$  and  $F'U_L = 5.5$  W/(m<sup>2</sup>°C). The latitude of Boston is  $42.36^\circ\text{N} = 0.739$  radians. The yearly  $\tilde{K} = 0.45$  and  $\tilde{T}_a = 10.9^\circ\text{C}$ . Use the following Gordon and Rabl (1981) correlation:

$$Q_{CY}/A_c F_R \eta_n = [(5.215 + 6.973I_{bn}) + (-5.412 + 4.293I_{bn})L + (1.403 - 0.899I_{bn})L^2] + \\ [(-18.596 - 5.931I_{bn}) + (15.468 + 18.845I_{bn})L + (-0.164 - 35.510I_{bn})L^2]I_C + \\ [(-14.601 - 3.570I_{bn}) + (13.675 - 15.549I_{bn})L + (-1.620 + 30.564I_{bn})L^2]I_C^2$$

From Equation 20.27,  $\tilde{I}_{bn} = 1.37 \times 0.45 - 0.34 = 0.276$  kW/m<sup>2</sup>. The critical radiation level  $I_C = 0$ , since  $T_{Ci} = T_a$ . Consequently, Equation 20.26, using the above expression reduces to

$$Q_{CY}/(A_c F_R \eta_n) = 5.215 + 6.973 \times 0.276 + (-5.412 + 4.293 \times 0.276)0.739 + (1.403 - 0.899 \\ \times 0.276)0.739^2 \\ = 4.646 \text{ GJ}/(\text{m}^2\text{y}).$$

The expression for the dumped out energy is found from Equation 20.64 and the previous expression by replacing  $I_C$  by  $I_D$ :

$$Q_{CY,dump}/(A_c F_R \eta_n) = 4.646 + [(-18.596 - 5.931 \times 0.276) + (15.468 + 18.845 \times 0.276)0.739 + \\ (-0.164 - 35.510 \times 0.276)0.739^2]I_D + [(14.601 - 3.57 \times 0.276) + \\ (-13.675 - 15.549 \times 0.276)0.739 + (1.620 + 30.564 \times 0.276)0.739^2]I_D^2 \\ = 4.646 - 10.40I_D + 5.83I_D^2 \text{ (GJ}/\text{m}^2\text{y)}$$

The thermal energy demand  $P_L = 0.25 \times 4.19(60 - 10.9) = 51.43$  kW.

The annual production function is

$$Q_{UY}(365/290) = -(-10.40 + 2\tilde{c} \times 0)51.43 - (5.83 \times 51.43^2) \{ (0.75/5.5)(0.25 \times 4.19) \\ [1 - \exp[-(5.5 \times A_c)/(0.25 \times 4190)]] \} \\ \text{or } Q_{UY} = 424.96 - 85.78/[1 - \exp(-A_c/190.45)] \text{ (GJ}/\text{y)}$$

Complete details as well as how this approach can be extended to solar systems with storage (see [Figure 20.30](#)) can be found in Rabl (1985) or Reddy (1987).

**20.1.10 Design Recommendations and Costs****20.1.10.1 Design Recommendations**

As mentioned earlier, design methods reduce computational effort compared to detailed computer simulations. Even with this decrease, the problem of optimal system design and sizing remains formidable because of

- a. The presence of several solar thermal system configuration alternatives.
- b. The determination of optimal component sizes for a given system.

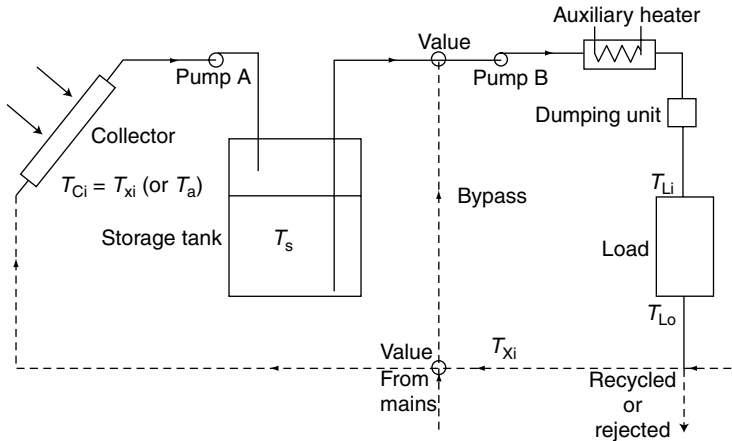


FIGURE 20.30 Open-loop solar industrial hot-water system with storage.

- c. The presence of certain technical and economic constraints.
- d. The choice of proper climatic, technical, and economic input parameters.
- e. The need to perform sensitivity analysis of both technical and economic parameters.

For most practical design work, a judicious mix of theoretical expertise and practical acumen is essential. Proper focus right from the start on the important input variables as well as the restriction of the normal range of variation would lead to a great decrease in design time and effort several examples of successful case studies and system design recommendations are described in the published literature (see, for example, Kutcher et al. 1982).

### 20.1.10.2 Solar System Costs

How the individual components of the solar system contribute to the total cost can be gauged from Table 20.4. We note that collectors constitute the major fraction (from 15 to 30%), thus suggesting that collectors should be selected and sized with great care. Piping costs are next with other collector-related costs like installation and support structure being also important.

TABLE 20.4 Percentage of Total System Cost by Component

Cost Component	Percentage Range
Collectors	15–30
Collector installation	5–10
Collector support structure	5–20 <sup>a</sup>
Storage tanks	5–7
Piping and specialties	10–30
Pumps	1–3
Heat exchangers	0–5 <sup>b</sup>
Chiller	5–10
Miscellaneous	2–10
Instrumentation	1–3
Insulation	2–8
Control subsystem	4–9
Electrical	2–6

<sup>a</sup> For collectors mounted directly on a tilted roof.

<sup>b</sup> For systems without heat exchangers.

Source: From Mueller Associates. 1985. Active Solar Thermal Design Manual, funded by U.S. DOE (no. EG-77-C-01-4042), SERI (XY-2-02046-1) and ASHRAE (project no. 40). Baltimore, MD.

## References

---

- Anderson, B. 1977. *Solar Energy: Fundamentals in Building Design*, McGraw-Hill, New York.
- ASHRAE Standard 93-77. 1978. *Methods of Testing to Determine the Thermal Performance of Solar Collectors*. American Society of Heating, Refrigeration and Air Conditioning Engineers, New York.
- ASHRAE. 1985. *Fundamentals*, American Society of Heating, Refrigeration and Air Conditioning Engineers, New York.
- Barley, C. D. and Winn, C. B. 1978. Optimal sizing of solar collectors by the method of relative areas. *Solar Energy*, 21, 279.
- Beckman, W. A. 1978. Technical note: Duct and pipe losses in solar energy systems. *Solar Energy*, 21, 531.
- Beckman, W. A., Klein, S. A., and Duffie, J. A. 1977. *Solar Heating Design by the f-Chart Method*, Wiley Interscience, New York.
- Braun, J. E., Klein, S. A., and Pearson, K. A. 1983. An improved design method for solar water heating systems. *Solar Energy*, 31, 597.
- Charters, W. W. S. and Pryor, T. L. 1982. In *An Introduction to the Installation of Solar Energy Systems*, pp. 503–127. Victoria Solar Energy Council, Melbourne, Australia.
- Chiam, H. F. 1981. Planar concentrators for flat-plate solar collectors, *Solar Energy*, 26, 503.
- Clark, D. R., Klein, S. A., and Beckman, W. A. 1983. Algorithm for evaluating the hourly radiation utilizability function. *ASME Journal of Solar Energy Engineering*, 105, 281.
- Cole, R. L., Nield, K. J., Rohde, R. R., and Wolosewicz, R. M. eds. 1979. *Design and Installation Manual for Thermal Energy Storage*, ANL-79-15, pp. 223–397. Argonne National Laboratory, Argonne, IL.
- Collares-Pereira, M. and Rabl, A. 1979. Derivation of method for predicting the long-term average energy delivery of solar collectors. *Solar Energy*, 23, 223.
- Collares-Pereira, M., Gordon, J. M., Rabl, A., and Zarmi, Y. 1984. Design and optimization of solar industrial hot water systems with storage. *Solar Energy*, 32, 121.
- CSU. 1980. *Solar Heating and Cooling of Residential Buildings—Design of Systems*, manual prepared by the Solar Energy Applications Laboratory, Colorado State University. Colorado State University, Fort Collins, CO.
- de Winter, F. 1975. Heat exchanger penalties in double loop solar water heating systems. *Solar Energy*, 17, 335.
- Duffie, J. A. and Beckman, W. A. 1980. *Solar Engineering of Thermal Processes*, Wiley Interscience, New York.
- Edwards, D. K., Nelson, K. E., Roddick, R. D., and Gier, J. T. 1960. Basic Studies on the Use of Solar Energy, Report no. 60-93. Department of Engineering. University of California, Los Angeles, CA.
- Gordon, J. M. and Rabl, A. 1982. Design, analysis and optimization of solar industrial process heat plants without storage. *Solar Energy*, 28, 519.
- Gordon, J. M. and Zarmi, Y. 1985. An analytic model for the long-term performance of solar thermal systems with well-mixed storage. *Solar Energy*, 35, 55.
- Gordon, J. M. and Rabl, A. 1986. Design of solar industrial process heat systems, In *Reviews of Renewable Energy Sources* chapter 6. Sodha, M. S. Mathur, S. S. Malik, M. A.S and Kandpal, T. C. eds., pp. 55–177. Wiley Eastern, New Delhi.
- Gordon, J. M. 1987. Optimal sizing of stand-alone photovoltaic systems. *Solar Cells*, 20, 295.
- Hollands, K. G. T. 1965. Honeycomb devices in flat-plate solar collectors. *Solar Energy*, 9, 159.
- Hunn, B. D. 1980. A simplified method for sizing active solar space heating systems, In *Solar Energy Technology Handbook, Part B: Applications, System Design and Economics*, Dickinson, W. C. and Cheremisinoff, P. N. eds., pp. 639–255. Marcel Dekker, New York.
- Klein, S. A., Cooper, P. I., Freeman, T. L., Beekman, D. M., Beckman, W. A. and Doffie, J. A. 1975. A method of simulation of solar processes and its applications. *Solar Energy*, 17, 29.
- Klein, S. A. 1978. Calculation of flat-plate collector utilizability. *Solar Energy*, 21, 393.
- Klein, S. A. et al. 1979. TRNSYS-A Transient System Simulation User's Manual, University of Wisconsin-Madison Engineering Experiment Station Report. University of Wisconsin-Madison Engineering Experiment Station Report 38-10.



- Klein, S. A. and Beckman, W. A. 1979. A general design method for closed-loop solar energy systems. *Solar Energy*, 22, 269.
- Kreider, J. F. 1979. Medium and High Temperature Solar Energy Processes. Academic Press, New York.
- Kutcher, C. F., Davenport, R. L., Dougherty, D. A., Gee, R. C., Masterson, P. M., and May, E. K. 1982. Design Approaches for Solar Industrial Process Heat Systems, SERI/TR-253-1356. Solar Energy Research Institute, Golden, CO.
- Lameiro, G. F. and Bendt, P., 1978. The GFL method for designing solar energy space heating and domestic hot water systems, In Proceedings of American Solar Energy Society Conference, Vol. 2, p. 113. Boulder, CO.
- Larson, D. C. 1980. Optimization of flat-plate collector flat mirror system. *Solar Energy*, 24, 203.
- Larson, R. W., Vignola, F., and West, R. 1992a. *Economics of Solar Energy Technologies*. American Solar Energy Society Report, Boulder, CO.
- Liu, B. Y. H. and Jordan, R. C. 1960. The inter-relationship and characteristic distribution of direct, diffuse and total solar radiation. *Solar Energy*, 4, 1.
- Liu, B. Y. H. and Jordan, R. C. 1963. A rational procedure for predicting the long-term average performance of flat-plate solar energy collectors. *Solar Energy*, 7, 53.
- Liu, S. T. and Fanney, A. H. 1960. Comparing experimental and Computer-predicted performance for solar hot water systems, *ASHRAE Journal*, 22, 5, 34.
- Löf, G. O. G. 1981. Air based solar systems for space heating, In *Solar Energy Handbook*, J. F. Kreider and F. Kreith, eds., pp. 39–44. McGraw-Hill, New York.
- Meyer, B. A. 1978. Natural convection heat transfer in small and moderate aspect ratio enclosures—An application to flat-plate collectors, In *Thermal Storage and Heat Transfer in Solar Energy Systems*, Kreith, F. Boehm, R. Mitchell, J. and Bannerot, R. eds., pp. 555–558. American Society of Mechanical Engineers, New York.
- Mitchell, J. C., Theilacker, J. C., and Klein, S. A. 1981. Technical note: Calculation of monthly average collector operating time and parasitic energy requirements. *Solar Energy*, 26, 555–558.
- Mueller Associates. 1985. *Active Solar Thermal Design Manual*, funded by U. S. DOE (no. EG-77-C-01-4042). SERI(XY-2-02046-1) and ASHRAE (project no. 40). Baltimore, MD.
- Newton, A. B. and Gilman, S. H. 1981. *Solar Collector Performance Manual*, funded by U. S. DOE (no. EG-77-C-01-4042), SERI(XH-9-8265-1) and ASHRAE (project no. 32, Task 3).
- Phillips, W. F. and Dave, R. N. 1982. Effect of stratification on the performance of liquid-based solar heating systems. *Solar Energy*, 29, 111.
- Rabl, A. 1981. Yearly average performance of the principal solar collector types. *Solar Energy*, 27, 215.
- Rabl, A. 1985. *Active Solar Collectors and Their Applications*. Oxford University Press, New York.
- Reddy, T.A. 1987. *The Design and Sizing of Active Solar Thermal Systems*. Oxford University Press, Oxford, U.K.
- SERI 1989. Engineering Principles and Concepts for Active Solar Systems. Hemisphere Publishing Company, New York.
- Theilacker, J. C. and Klein, S. A. 1980. Improvements in the utilizability relationships. *American Section of the International Solar Energy Society Meeting Proceedings*, p. 271. Phoenix, AZ.
- Liu, S. T. and Fanney, A. H. 1980. Comparing experimental and computer-predicted performance for solar hot water systems. *ASHRAE Journal*, 22, 5, 34.
- Klein, S. A., Cooper, P. I., Freeman, T. L., Beekman, D. M., Beckman, W. A. and Doffie, J. A. 1975. A method of simulation of solar processes and its applications, *Solar Energy*, 17, 29.

## 20.2 Solar Heat for Industrial Processes

---

*Riccardo Battisti, Hans Schweiger, and Werner Weiss*

### 20.2.1 The Potential for Solar Process Heat

Currently, the widespread use of residential solar thermal energy has focused almost exclusively on swimming pools, domestic hot water preparation, and space heating, while its use in the service

sector and in industrial applications is insignificant. On the other hand, the industrial sector accounts for a large share of the total energy consumption in the OECD (Organization for Economic Co-operation and Development) countries at approximately 30%, and a significant portion of industrial heat demand falls within a temperature range compatible with solar thermal collectors.

As a matter of fact, 30%–50% of the thermal energy needed in commercial and industrial companies for production processes is below 250°C (Kreider 1979; European Commission 2001). In this temperature range, the heat demand in the European Union (EU) for industrial processes can be estimated with about 300 TWh, or 7% of the total energy demand. The total potential for industrial process heat at below 150°C was estimated to be 202.8 TWh for the 12 countries that formed the EU in 1994 (Laue and Reichert 1994).

Studies for the application potential for industrial solar thermal systems were carried out in Austria (Müller 2004), Germany and Greece (PROCESOL 2000), Italy (IEA 2005), Netherlands (KWA 2001), Portugal and Spain (European Commission 2001). The potential for solar low temperature heat ranges between 3% and 4% of the total industrial heat demand in Italy, Spain, Portugal, and Austria. These studies primarily showed that solar thermal plants can readily provide the required low- and medium-temperature process heat.

The most promising industrial sectors and processes are shown in Table 20.5, and the distribution of heat demand by temperature range is shown in Figure 20.31.

Another important result showed by the studies is that the available surface area on factory roofs is often a limiting factor for the installation of a solar plant for industrial use.

**TABLE 20.5** Industrial Sectors and Processes Suitable for Solar Thermal Use

Sector	Processes	Temperature (°C)
Brewing and malting	Wort boiling	100
	Bottle washing	60
	Drying	90
	Cooling	60
Milk	Pasteurization	60–85
	Sterilization	130–150
Food preservation	Pasteurization	110–125
	Sterilization	< 80
	Cooking	70–100
	Scalding	95–100
Meat	Bleaching	< 90
	Washing, sterilization, cleaning	< 90
Wine and beverage	Cooking	90–100
	Bottle washing	60–90
Textile	Cooling (single effect absorption cooling)	85
	Washing, bleaching, dyeing	< 90
Automobile	Cooking	140–200
	Paint drying	160–220
Paper	Degreasing	35–55
	Paper pulp: cooking	170–180
	Boiler feed water	< 90
	Bleaching	130–150
Tanning	Drying	130–160
	Water heating for damp processes	165–180 (steam)
Cork	Drying, cork baking	40–155

Source: From European Commission, *The Potential of Solar Heat for Industrial Processes*, Final report, EC Project, Contract No. NNE5-1999-0308, 2001, <http://www.solarpaces.org>. With permission.

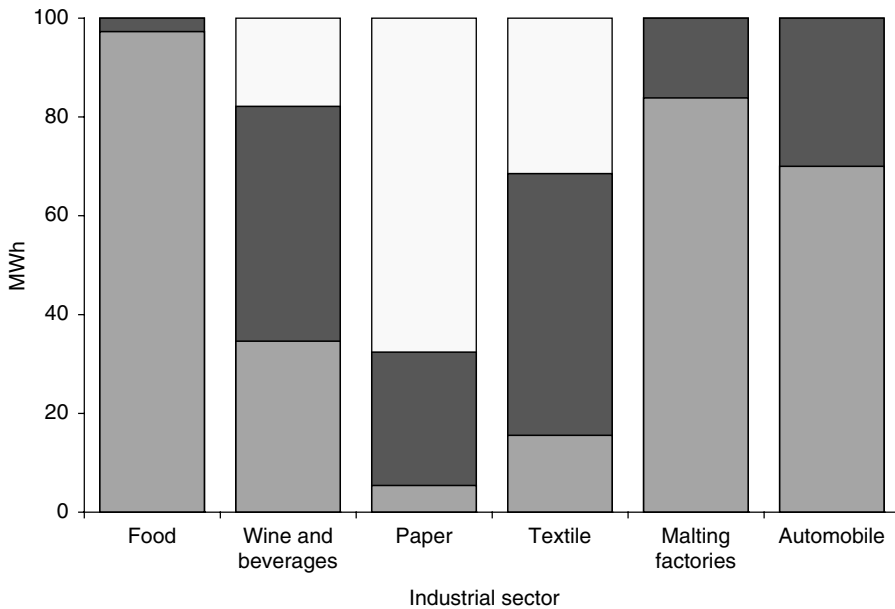


**FIGURE 20.31** Distribution of the heat demand by temperature range in some selected companies studied within the POSHIP project, grouped by industrial sectors. (From European Commission, *The Potential of Solar Heat for Industrial Processes*, Final Report, EC Project, Contract No. NNE5-1999-0308, 2001, <http://www.aiguasol.com/poship.htm>. With permission.)

## 20.2.2 Solar Thermal Systems in Industrial Processes: Integration and Basic Design Guidelines

### 20.2.2.1 Which Solar Collectors?

For process temperatures up to about 60°C, flat-plate collectors with selective absorbers would be most appropriate and could be the most economical solution even up to a temperature range of 90°C. For temperatures above this range, other collector types should be considered: evacuated tubes, high efficiency flat plate, CPC or line-axis concentrating collectors. In the framework of IEA Task 33/IV, “Solar Heat for Industrial Processes,” which is carried out within the Solar Heating and Cooling Program of the IEA, new “medium temperature collectors” (i.e., with operating temperatures between 80 and 250°C) are being developed, including:

- Improved flat-plate collectors
- Stationary low-concentration collectors
- Small parabolic trough collectors

Different collector technologies already available on the market can be used for applications in the 80°C–120°C temperature range. For example, flat-plate collectors with double antireflection glazings and hermetically sealed collectors with inert-gas fillings, or even a combination of both, reduce collector heat losses without significantly sacrificing the optical performance. Figure 20.32 shows estimated efficiency curves of single-, double-, and triple-glazed flat-plate collectors when newly developed antireflection glazings (AR-glass) are used.

Another solution for medium temperature collectors is to reduce heat losses by concentration by, for example, using stationary CPC collector without vacuum and with a low concentration factor (in the range of two).

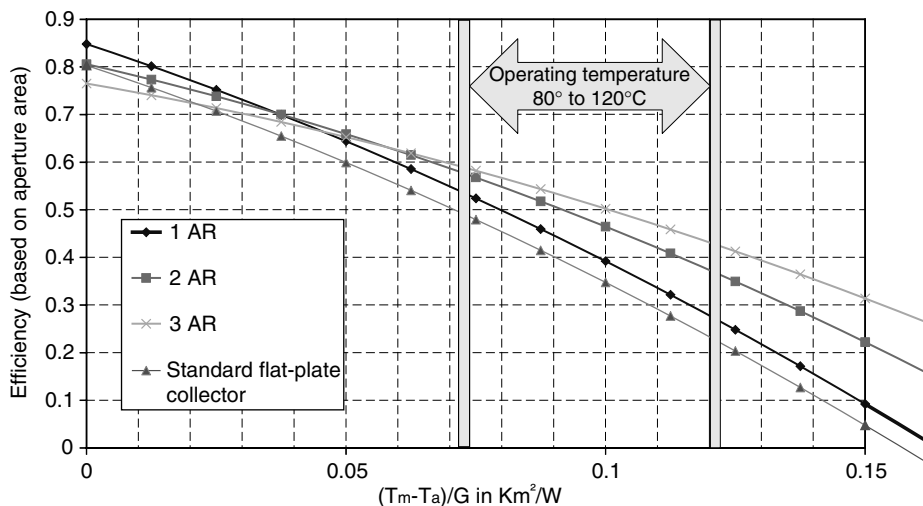


**FIGURE 20.32** Efficiency curves of a single-, double-, and triple-glazed antireflection collector in comparison with a standard flat-plate collector with ordinary solar glass. (From IEA., *Task 33/IV, Solar Heat for Industrial Processes*, International Energy Agency, 2005.)

Between 150 and 250°C, it is appropriate to consider the parabolic trough collector technology. Much is known about high-temperature applications (400°C–600°C) using parabolic trough collectors for electric power production, but adjustments must be made for the medium temperature range. Current developments involved in Task 33/IV have been carried out in Spain, Austria, and Germany. The first results showed that parabolic troughs could even be an appropriate alternative for large systems at low temperatures (about 60°C). It is noteworthy that small parabolic trough are readily available in the market and are a reliable technology (e.g., in the U.S., some plants have been operating since the early 1990s).

### 20.2.2.2 Coupling the Solar Thermal System with the Processes

The integration of solar heat into industrial production processes is challenging for both the process engineer and the solar designer. Existing heating systems based on steam or hot water from boilers are normally designed for much higher temperatures (150°C–180°C) compared to those that the processes need (100°C or lower) to keep temperature differences small. On the contrary, the solar thermal system should always be coupled to the existing heat supply at the lowest possible temperature. Nevertheless, for fluid preheating, solar heat should be introduced only after preheating by waste heat recovery systems, and not as an alternative to these systems (Figure 20.33).

Even if the waste heat recovery raises the working temperature in the solar thermal system, the combination of both systems yields better results than a solar thermal system at lower temperature but without heat recovery.

Today, one of the most used heat recovery assessment methodologies is the “pinch” analysis. The discovery of the heat recovery “pinch” was a major breakthrough in the development of design methods for energy efficient industrial processes. Based on the analysis of hot and cold streams within the process, the pinch methodology gives fundamental hints about the possibility and the right position of heat exchangers for waste heat recovery. This allows developing integral solutions for solar thermal energy applications in given industrial processes. From the point of view of energy, the streams that constitute a process flow sheet may be classified into two groups: “hot” streams, i.e., streams that must be cooled, and “cold” streams, i.e., streams that must be heated.

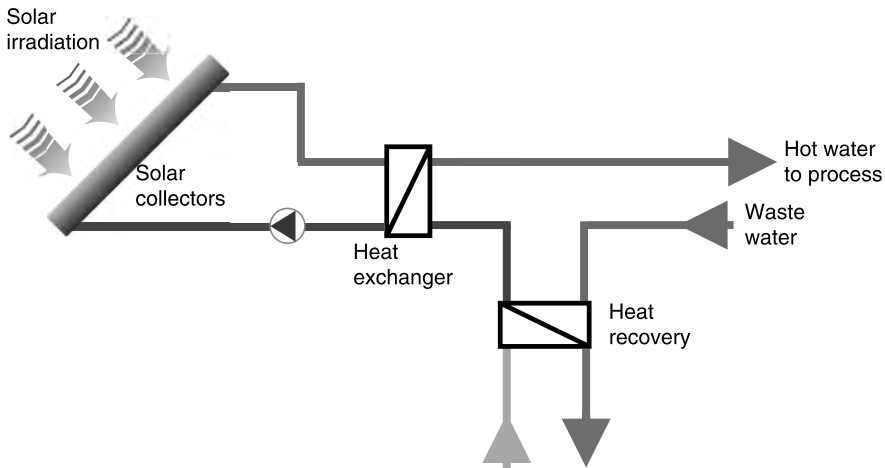


**FIGURE 20.33** Combination of solar thermal system and waste heat recovery. (From European Commission, *The Potential of Solar Heat for Industrial Processes*, Final Report, EC Project, Contract No. NNE5-1999-0308, 2001, <http://www.aiguasol.com/poship.htm>. With permission.)

When there are a large number of streams, the selection of the best match between these streams is not obvious. The pinch methodology provides a systematic way to find the optimal solutions for the implementation of heat recovery techniques.

The solar thermal system may be coupled with the conventional heat supply system in several ways, including direct coupling to a specific process, preheating of water, and steam generation in the central system (Figure 20.34).

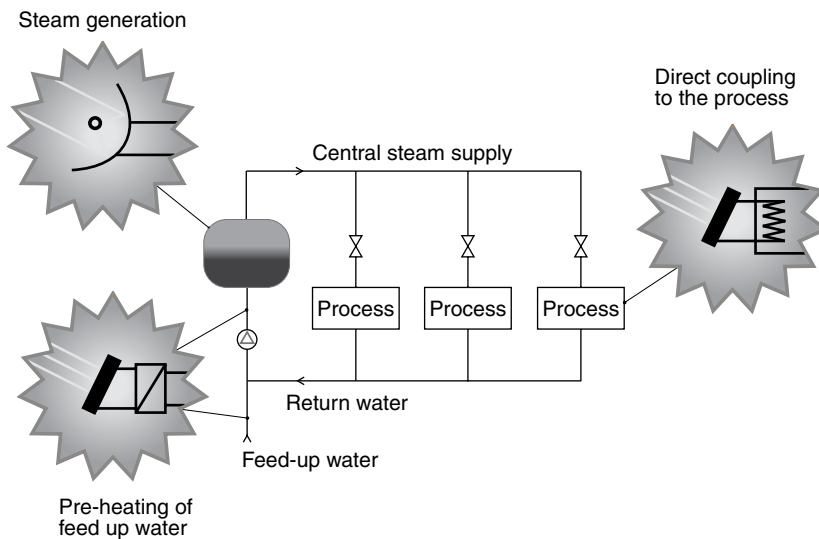


**FIGURE 20.34** Coupling the solar thermal system with the conventional heat supply. (From European Commission, *The Potential of Solar Heat for Industrial Processes*, Final Report, EC Project, Contract No. NNE5-1999-0308, 2001, <http://www.aiguasol.com/poship.htm>. With permission.)

Whenever possible, a direct coupling of the solar thermal systems to one or several processes is preferred because the working temperatures are lower. Direct coupling to a process can mainly be carried out in the following two ways:

- Preheating of a circulating fluid (e.g., feed-up water, return of closed circuits, air preheating). This solution is feasible if fluid circulation is either continuous or periodic (e.g., periodic replacement of bath water). If circulation is discontinuous, a storage tank must be introduced. The mean working temperature of the solar thermal system is lower than the required final process temperature. The smaller the solar fraction, the lower the mean working temperature. For very low solar fractions, the mean working temperature may be close to the fluid inlet (or return) temperature.
- Heating of liquid baths or hot (e.g., drying) chambers. The energy demand is both for heating-up at the operational start-up, either concentrated in the early morning hours or periodically each time the used fluid is replaced with fresh fluid, and for maintaining the operating temperature, which is generally a nearly constant load.

The existing heat exchangers for bath heating generally require steam at temperatures that are too high for a solar thermal system. The introduction of additional heat exchangers with a larger exchange area into existing baths is not always possible due to lack of space or other technical restrictions. In some cases, an external heat exchanger in combination with a circulation pump can be used.

If the process baths are well-insulated, they can be used for solar heat storage. For example, maintaining the temperature of the solar thermal system during a weekend without operation can reduce the heat demand for start-up on Monday morning.

In almost all industries, coupling of a solar thermal system to the central heat supply system is possible. This can be done either by preheating the feed-up water for the steam boilers (the temperature level rises with increasing condensate recovery) or by a solar steam generator. The latter is only recommended at sites with a high level of solar radiation and if concentrating collectors are used.

### 20.2.2.3 Heat Demand and Storage

Another challenge in applying solar thermal energy to industrial production processes is the time dependency of the solar energy supply and the heat demand of the processes (Figure 20.35). Very few

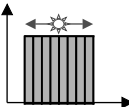
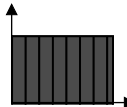
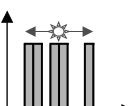
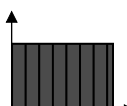
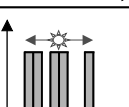
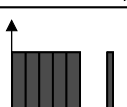
	Demand profile		Storage size
	Daily	Weekly	
Constant daily demand in sunny hours (7 days/week)			No storage needed
Fluctuating daily demand in sunny hours (7 days/week)			20–80 l/m <sup>2</sup> (depending on consumption profile)
Fluctuating daily demand in sunny hours (5 days/week)			80–150 l/m <sup>2</sup>

FIGURE 20.35 Heat storage size depending on daily and weekly heat demand profiles.

production lines run at constant load throughout the day. Most processes in smaller companies run for one or two shifts per day and show a batch operation mode.

When the process heat demand is continuous during sunny hours with no weekend breaks, the load is always higher than the solar gains. Therefore, the solar thermal system can be designed without storage allowing the solar heat to be fed directly to the process or to the heat supply system. This enables building lower cost solar thermal systems by eliminating storage related costs.

In case the total weekly demand is constant, but there are strong fluctuations in the daily demand during operational periods (e.g., demand peaks, short breaks of operation), storage of 20–80 l/m<sup>2</sup> of collectors is necessary, depending on the process heat demand profile.

If the daily fluctuations come together with weekend breaks (five days of operation per week), then the storage size is recommended to be 80–150 l/m<sup>2</sup>. Weekend storage is generally not recommended for small systems. The larger the system size, the more effective the heat storage over longer periods (e.g., weekends). A weekend storage becomes economic for systems with an installed capacity of about 350 kW<sub>th</sub>, corresponding to 500 m<sup>2</sup> or more of collector array.

Storage for longer periods (seasonal storage) can only be considered for very large systems (greater than 3.5 MW<sub>th</sub>), but systems with only seasonal utilization (less than six months of operation a year) are generally not economically viable.

From the previous considerations, key criteria for the feasibility of a solar process heat plant can be drawn:

- Temperature level: solar heat at temperatures above 150°C is technically feasible but economically reasonable only at favorable locations; applications at low temperature (less than 60°C) offer the best economics
- Continuous or quasicontinuous demand (otherwise storage is needed and plant costs increase)
- Technical possibility of introducing a heat exchanger in the existing equipment or heat supply circuit for the solar thermal system

The different possible schemes of solar thermal plants for process heat production are summarized in [Figure 20.36](#). This classification scheme, currently under development and improvement, allows choosing the most suitable plant scheme depending on key process features (open/closed, collector fluid same as or different from heat distribution fluid, need for storage). The scheme is divided into three parts: energy supply (both solar and conventional), heat transfer/storage, and process load. For each column corresponding to a class of processes, two possibilities are given depending on the heat distribution medium: water/air or steam. These concepts are currently being developed and tested in demonstration plants.

### 20.2.3 Overview of Existing Solar Process Heat Plants

Since the 1980s, several solar thermal systems for industrial applications have been developed and are currently operating. At present, 84 plants are reported worldwide, with a total installed thermal power of about 24 MW<sub>th</sub> (34,000 m<sup>2</sup>).

The majority of the operational plants are in the sectors of food and beverage, textile, and transport (e.g., washing and painting of car components). The main applications differ among countries. In Greece, for instance, several “solar dairies” are operating, whereas in Germany the most common application is for car-washing facilities.

Most of the reported plants supply heat at temperature levels between 60 and 100°C and therefore, standard flat-plate collectors are suitable. As a matter of fact, flat-plate collectors are used in about 65% of the operational systems. Some plants are working at temperatures above 160°C, whereas there is only one project operating in the intermediate range from 100 to 160°C. Analysis of the reported plants reveals that they appear to encompass a broad range of working temperatures, but with no significant correlation with the solar field size. [Figure 20.37](#) through [Figure 20.40](#) show some examples of solar industrial process heat plants.

# SHIP-Systematics of system concepts

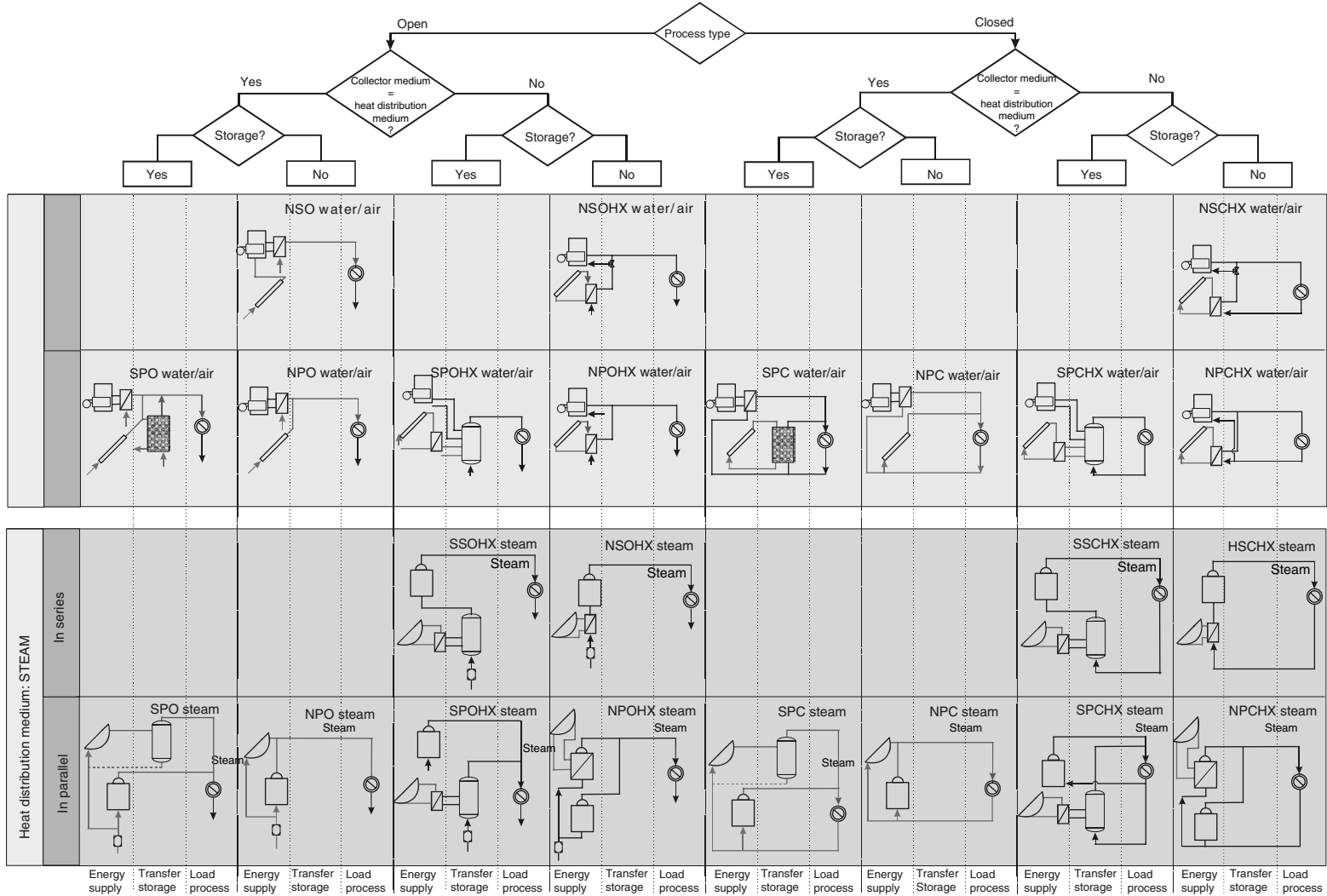


FIGURE 20.36 Systematic of systems concepts. (From IEA., Task 33/IV, Solar Heat for Industrial Processes, International Energy Agency, 2005.)





**FIGURE 20.37** El NASR Pharmaceutical Chemicals, Egypt. Installed capacity: 1.33 MW<sub>th</sub>. (From Fichtner Solar GmbH, Germany. With permission.)



**FIGURE 20.38** Alpino SA, dairy industry, Greece. Installed capacity: 518 kW<sub>th</sub>. (From Alpino SA, Greece. With permission.)



**FIGURE 20.39** Wine cooling and bottle washing, Austria. Installed capacity: 70 kW<sub>th</sub>. (From S.O.L.I.D. GmbH, Austria. With permission.)



**FIGURE 20.40** Parking service Castellbisbal SA, container washing, Spain. Installed capacity: 357 kW<sub>th</sub>. (From Aiguasol Engineering, Spain. With permission.)

## References

---

- European Commission. 2001. The Potential of Solar Heat for Industrial Processes. Final Report, EC Project, Contract No. NNE5-1999-0308, 2001, <http://www.aiguasol.com/poship.htm> (accessed on 2006/10/11).
- IEA (International Energy Agency). 2005. *Task 33/IV. Solar heat for industrial processes*, International Energy Agency.
- Kreider, J. F. 1979. *Medium and High Temperature Solar Energy Processes*, Academic Press, New York.
- KWA. 2001. Bedrijfsadviseurs B. V., *Onderzoek naar het potentieel van zonthermische energie in de industrie*. Relatienummer 8543.00, Rapportnummer 2009740DR01.DOC.
- Laue, H. J. and Reichert, J. 1994. *Potential for medium and large sized industrial heat pumps in Europe*. Contract No. XVII/7001/90-8, Final report, European Commission, Directorate General for Energy (DGXII).
- Müller, T. et al. 2004. *PROMISE-Produzieren mit Sonnenenergie, Projekt im Rahmen der Programmlinien "Fabrik der Zukunft" des Bundesministeriums für Verkehr*. Innovation und Technologie, Endbericht, Gleisdorf.
- PROCESOL. 2000. *Solar Thermal Process Heating in Industrial Applications: A Stimulate Plan*, Final Report, EC ALTENTER Project, Contract No 4.1030/Z/98-205.

## 20.3 Passive Solar Heating, Cooling, and Daylighting

---

Jeffrey H. Morehouse

### 20.3.1 Introduction

Passive systems are defined, quite generally, as systems in which the thermal energy flow is by natural means: by conduction, radiation, and natural convection. A *passive heating system* is one in which the sun's radiant energy is converted to heat upon absorption by the building. The absorbed heat can be transferred to thermal storage by natural means or used to directly heat the building. *Passive cooling systems* use natural energy flows to transfer heat to the environmental sinks: the ground, air, and sky.

If one of the major heat transfer paths employs a pump or fan to force flow of a heat transfer fluid, then the system is referred to as having an active component or subsystem. Hybrid systems—either for heating or cooling—are ones in which there are both passive and active energy flows. The use of the sun's radiant energy for the natural illumination of a building's interior spaces is called *daylighting*. Daylighting design approaches use both solar beam radiation (referred to as *sunlight*) and the diffuse radiation scattered by the atmosphere (referred to as *skylight*) as sources for interior lighting, with historical design emphasis on utilizing skylight.

#### 20.3.1.1 Distinction Between a Passive System and Energy Conservation

A distinction is made between energy conservation techniques and passive solar measures. Energy conservation features are designed to reduce the heating and cooling energy required to thermally condition a building: the use of insulation to reduce either heating and cooling loads, and the use of window shading or window placement to reduce solar gains, reducing summer cooling loads. Passive features are designed to increase the use of solar energy to meet heating and lighting loads, plus the use of ambient "coolth" for cooling. For example, window placement to enhance solar gains to meet winter heating loads and/or to provide daylighting is passive solar use, and the use of a thermal chimney to draw air through the building to provide cooling is also a passive cooling feature.

### 20.3.1.2 Key Elements of Economic Consideration

The distinction between passive systems, active systems, or energy conservation is not critical for economic calculations, as they are the same in all cases: a trade-off between the life-cycle cost of the energy saved (performance) and the life-cycle cost of the initial investment, operating, and maintenance costs (cost).

#### 20.3.1.2.1 Performance: Net Energy Savings

The key performance parameter to be determined is the net annual energy saved by the installation of the passive system. The basis for calculating the economics of any solar energy system is to compare it against a “normal” building; thus, the actual difference in the annual cost of fuel is the difference in auxiliary energy that would be used with and without solar. Therefore, the energy saved rather than energy delivered, energy collected, useful energy, or some other energy measure, must be determined.

#### 20.3.1.2.2 Cost: Over and Above “Normal” Construction

The other significant part of the economic trade-off involves determining the difference between the cost of construction of the passive building and of the “normal” building against which it is to be compared. The convention, adopted from the economics used for active solar systems, is to define a “solar add-on cost.” Again, this may be a difficult definition in the case of passive designs because the building can be significantly altered compared to typical construction since, in many cases, it is not just a one-to-one replacement of a wall with a different wall, but it is more complex and involves assumptions and simulations concerning the “normal” building.

#### 20.3.1.2.3 General System Application Status and Costs

Almost 500,000 buildings in the U.S. were constructed or retrofitted with passive features in the 20 years after 1980. Passive heating applications are primarily in single-family dwellings and secondarily in small commercial buildings. Daylighting features that reduce lighting loads and the associated cooling loads are usually more appropriate for large office buildings.

A typical passive heating design in a favorable climate might supply up to one-third of a home’s original load at a cost of \$5 to \$10 per million Btu net energy saved. An appropriately designed daylighting system can supply lighting at a cost of 2.5–5 ¢ per kWh (Larson, Vignola, and West 1992a, 1992b, 1992c).

## 20.3.2 Solar Thermosyphon Water Heating

Solar hot-water heating systems are composed of a collector and a storage tank. When the flow between the collector and tank is by natural circulation, these passive solar hot-water systems are referred to as *thermosyphon systems*. This ability of thermosyphon systems to heat water without an externally powered pump has spurred its use in both regions where power is unavailable and where power is very expensive.

### 20.3.2.1 Thermosyphon Concept

The natural tendency of a less dense fluid to rise above a more dense fluid can be used in a simple solar water heater to cause fluid motion through a collector. The density difference is created within the solar collector where heat is added to increase the temperature and decrease the density of the liquid. This collection concept is called a *thermosyphon*, and [Figure 20.41](#) schematically illustrates the major components of such a system.

The flow pressure drop in the fluid loop ( $\Delta P_{\text{FLOW}}$ ) must equal the buoyant force “pressure difference” ( $\Delta P_{\text{BUOYANT}}$ ) caused by the differing densities in the “hot” and “cold” legs of the fluid loop:

$$\begin{aligned} \Delta P_{\text{FLOW}} &= \Delta P_{\text{BUOYANT}} \\ &= \rho_{\text{stor}}gH - \left[ \int_O^L \rho(x)g \, dx + \rho_{\text{out}}g(H-L) \right], \end{aligned} \quad (20.68)$$

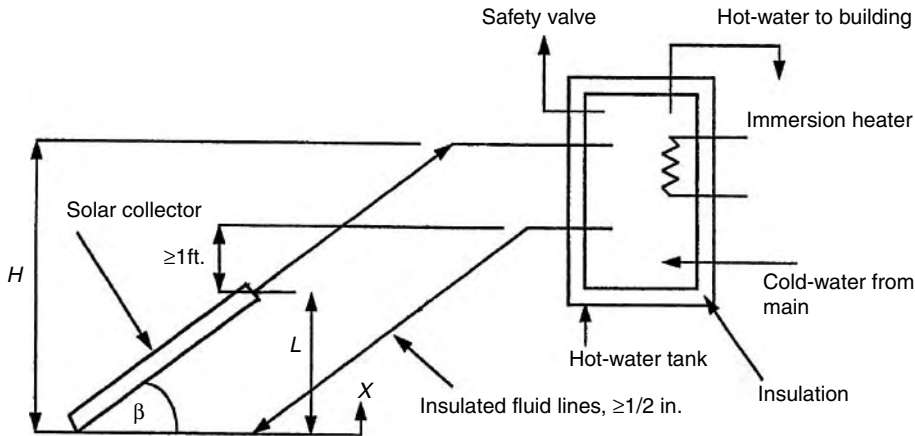


**FIGURE 20.41** Schematic diagram of thermosyphon loop used in a natural circulation, service water-heating system. The flow pressure drop in the fluid loop must equal the bouyant force “pressure”  $[\int g\rho(x)dx - \rho_{stor}gL]$  where  $\rho(x)$  is the local collector fluid density and  $\rho_{stor}$  is the tank fluid density, assumed uniform.<sup>0</sup>

where  $H$  is the height of the “legs,”  $L$  is the height of the collector (see Figure 20.41),  $\rho(x)$  is the local collector fluid density,  $\rho_{stor}$  is the tank fluid density, and  $\rho_{out}$  is the collector outlet fluid density; the latter two densities are assumed to be uniform. The flow pressure term,  $\Delta P_{FLOW}$ , is related to the flow loop system headloss that is in turn directly connected to friction and fitting losses and the loop flow rate:

$$\Delta P_{FLOW} = \oint_{LOOP} \rho d(h_L), \tag{20.69}$$

where  $h_L = KV^2$ , with  $K$  being the sum of the component loss “velocity” factors (see any fluid mechanics text), and  $V$  is the flow velocity.

### 20.3.2.2 Thermo-Fluid System Design Considerations

Because the driving force in a thermosyphon system is only a small density difference and not a pump, larger than normal plumbing fixtures must be used to reduce pipe friction losses. In general, one pipe size larger than would be used with a pump system is satisfactory. Under no conditions should piping smaller than 1/2-in (12-mm) national pipe thread (NPT) be used. Most commercial thermosyphons use 1-in (25-mm) NPT pipe. The flow rate through a thermosyphon system is about 1 gal/ft.<sup>2</sup> h (40 L/m<sup>2</sup> h) in bright sun, based on collector area.

Because the hot-water system loads vary little during a year, the best angle to tilt the collector is that equal to the local latitude. The temperature difference between the collector inlet water and the collector outlet water is usually 15–20°F (8–11°C) during the middle of a sunny day (Close 1962). After sunset, a thermosyphon system can reverse its flow direction and lose heat to the environment during the night. To avoid reverse flow, the top header of the absorber should be at least 1 ft. (30 cm) below the cold leg fitting on the storage tank, as shown.

To provide heat during long cloudy periods, an electrical immersion heater can be used as a backup for the solar system. The immersion heater is located near the top of the tank to enhance stratification and so that the heated fluid is at the required delivery temperature at the delivery point. Tank stratification is desirable in a thermosyphon to maintain flow rates as high as possible. Insulation must be applied over

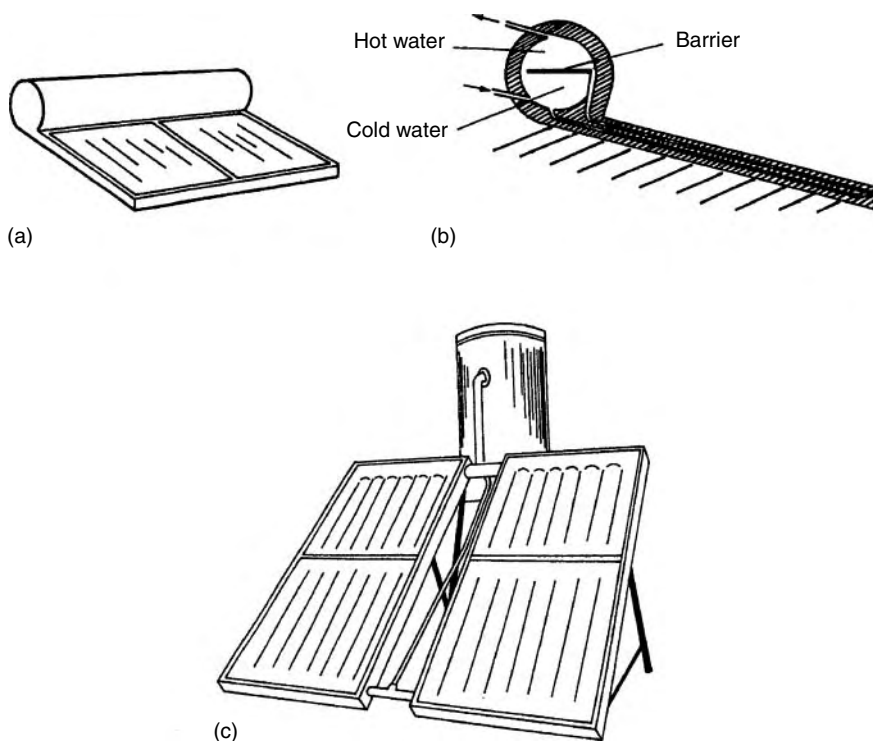


**FIGURE 20.42** Passive solar water heaters; (a) compact model using combined collector and storage, (b) section view of the compact model, and (c) tank and collector assembly.

the entire tank surface to control heat loss. Figure 20.42 illustrates two common thermosyphon system designs.

Several features inherent in the thermosyphon design limit its utility. If it is to be operated in a freezing climate, a nonfreezing fluid must be used, which in turn requires a heat exchanger between collector and potable water storage. (If potable water is not required, the collector can be drained during cold periods instead.) Heat exchangers of either the shell-and-tube type or the immersion-coil type require higher flow rates for efficient operation than a thermosyphon can provide. Therefore, the thermosyphon is generally limited to nonfreezing climates. A further restriction on thermosyphon use is the requirement for an elevated tank. In many cases structural or architectural constraints prohibit raised-tank locations. In residences, collectors are normally mounted on the roof, and tanks mounted above the high point of the collector can easily become the highest point in a building. Practical considerations often do not permit this application.

### Example 20.3.1

Determine the “pressure difference” available for a thermosyphon system with 1-m high collector and 2-m high “legs.” The water temperature input to the collector is 25°C and the collector output temperature is 35°C. If the overall system loss velocity factor ( $K$ ) is 15.6, estimate the system flow velocity.

**Solution.** Equation 20.68 is used to calculate the pressure difference, with the water densities being found from the temperatures (in steam tables):

$$\rho_{\text{stor}}(25^{\circ}\text{C}) = 997.009 \text{ kg/m}^3;$$

$$\rho_{\text{out}}(35^{\circ}\text{C}) = 994.036 \text{ kg/m}^3;$$

$$\rho_{\text{coll.ave.}}(30^{\circ}\text{C}) = 996.016 \text{ kg/m}^3$$

(note: average collector temperature used in “temperature”) and with  $H=2$  m and  $L=1$  m,

$$\begin{aligned}\Delta P_{\text{BUOYANT}} &= (997.009)9.81(2) - [(996.016)9.81(1) + (994.036)9.81(1)] \\ &= 38.9 \text{ N/m}^2(\text{Pa}).\end{aligned}$$

The system flow velocity is estimated from the “system  $K$ ” given, the pressure difference calculated above, taking the average density of the water around the loop (at  $30^{\circ}\text{C}$ ), and substituting into Equation 20.69:

$$\begin{aligned}\Delta P_{\text{BUOYANT}} &= (\rho_{\text{loop.ave}})(h_L)_{\text{loop}} = (\rho_{\text{loop.ave}})KV^2, \\ V^2 &= 38.9/(996.016)(15.6), \\ V &= 0.05 \text{ m/s}.\end{aligned}$$

### 20.3.3 Passive Solar Heating Design Fundamentals

Passive heating systems contain the five basic components of all solar systems, as described in the previous chapter on Active Solar Systems. Typical passive realizations of these components are:

1. Collector: windows, walls and floors
2. Storage: walls and floors, large interior masses (often these are integrated with the collector absorption function)
3. Distribution system: radiation, free convection, simple circulation fans
4. Controls: moveable window insulation, vents both to other inside spaces or to ambient
5. Backup system: any nonsolar heating system

The design of passive systems requires the strategic placement of windows, storage masses, and the occupied spaces themselves. The fundamental principles of solar radiation geometry and availability are instrumental in the proper location and sizing of the system’s “collectors” (windows). Storage devices are usually more massive than those used in active systems and are frequently an integral part of the collection and distribution system.

#### 20.3.3.1 Types of Passive Heating Systems

A commonly used method of cataloging the various passive system concepts is to distinguish three general categories: direct, indirect, and isolated gain. Most of the physical configurations of passive heating systems are seen to fit within one of these three categories.

For direct gain (Figure 20.43), sunlight enters the heated space and is converted to heat at absorbing surfaces. This heat is then distributed throughout the space and to the various enclosing surfaces and room contents.

For indirect gain category systems, sunlight is absorbed and stored by a mass interposed between the glazing and the conditioned space. The conditioned space is partially enclosed and bounded by this thermal storage mass, so a natural thermal coupling is achieved. Examples of the indirect approach are the thermal storage wall, the thermal storage roof, and the northerly room of an attached sunspace.

In the thermal storage wall (Figure 20.44), sunlight penetrates the glazing and is absorbed and converted to heat at a wall surface interposed between the glazing and the heated space. The wall is usually masonry (Trombe wall) or containers filled with water (water wall), although it might contain phase-change material. The attached sunspace (Figure 20.45) is actually a two-zone combination of direct gain and thermal storage wall. Sunlight enters and heats a direct gain southerly “sunspace” and also heats a

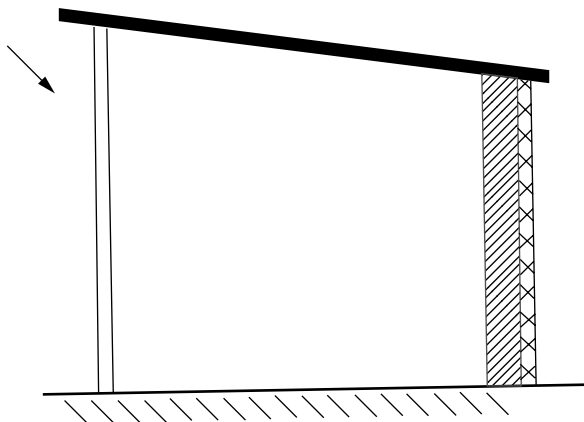


FIGURE 20.43 Direct gain.

mass wall separating the northerly buffered space, which is heated indirectly. The “sunspace” is frequently used as a greenhouse, in which case, the system is called an “attached greenhouse.” The thermal storage roof (Figure 20.46) is similar to the thermal storage wall except that the interposed thermal storage mass is located on the building roof.

The isolated gain category concept is an indirect system, except that there is a distinct thermal separation (by means of either insulation or physical separation) between the thermal storage and the heated space. The convective (thermosyphon) loop, as depicted in Figure 20.41, is in this category and, while often used to heat domestic water, is also used for building heating. It is most akin to conventional active systems in that there is a separate collector and separate thermal storage. The thermal storage wall, thermal storage roof, and attached sunspace approaches can also be made into isolated systems by insulating between the thermal storage and the heated space.

### 20.3.3.2 Fundamental Concepts for Passive Heating Design

Figure 20.47 is an equivalent thermal circuit for the building illustrated in Figure 20.44, the Trombe wall-type system. For the heat transfer analysis of the building, three temperature nodes can be identified: room temperature, storage wall temperature, and the ambient temperature. The circuit responds to

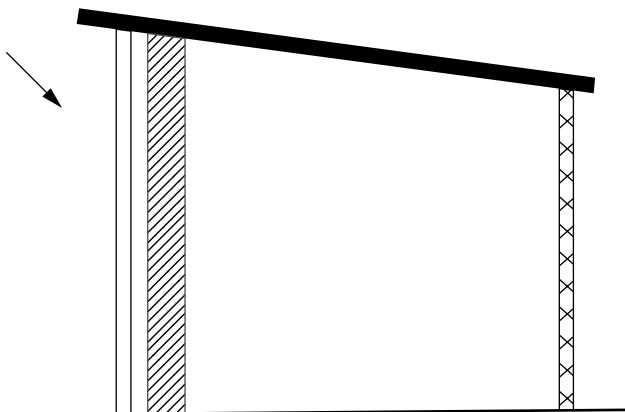


FIGURE 20.44 Thermal storage wall.



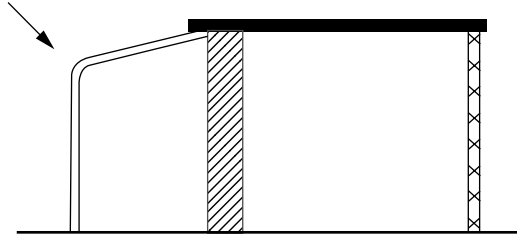


FIGURE 20.45 Attached sunspace.

climatic variables represented by a current injection  $I_s$  (solar radiation) and by the ambient temperature  $T_a$ . The storage temperature,  $T_s$ , and room temperature,  $T_r$ , are determined by current flows in the equivalent circuit. By using seasonal and annual climatic data, the performance of a passive structure can be simulated and the results of many such simulations correlated to give the design approaches described below.

### 20.3.3.3 Passive Design Approaches

Design of a passive heating system involves selection and sizing of the passive feature type(s), determination of thermal performance, and cost estimation. Ideally, a cost/performance optimization would be performed by the designer. Owner and architect ideas usually establish the passive feature type, with general size and cost estimation available. However, the thermal performance of a passive heating system has to be calculated.

There are several “levels” of methods that can be used to estimate the thermal performance of passive designs. First-level methods involve a rule of thumb and/or generalized calculation to get a starting estimate for size and/or annual performance. A second-level method involves climate, building, and passive system details, which allow annual performance determination, plus some sensitivity to passive system design changes. Third-level methods involve periodic calculations (hourly, monthly) of performance and permit more detailed variations of climatic, building, and passive solar system design parameters.

These three levels of design methods have a common basis in that they all are derived from correlations of a multitude of computer simulations of passive systems (PSDH 1980, 1984). As a result, a similar set of defined terms is used in many passive design approaches:

- $A_p$ , solar projected area,  $m^2$  ( $ft.^2$ ): the net south-facing passive solar glazing area projected onto a vertical plane

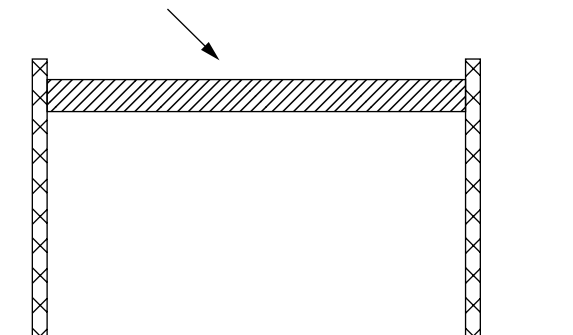


FIGURE 20.46 Thermal storage roof.

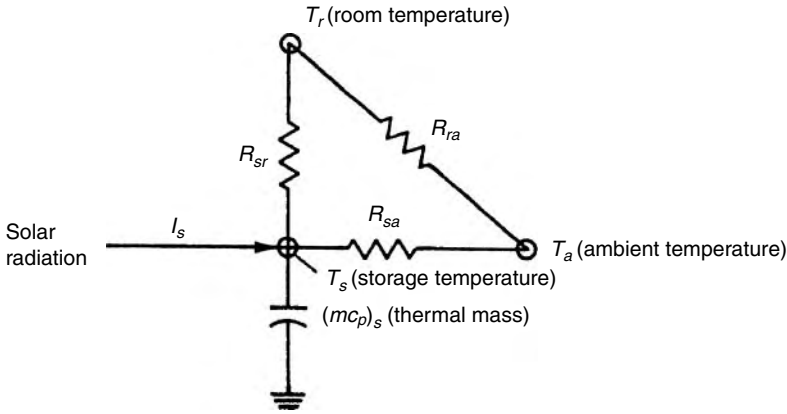


FIGURE 20.47 Equivalent thermal circuit for passively heated solar building in Figure 20.44.

- NLC, net building load coefficient, kJ/CDD (Btu/FDD): net load of the nonsolar portion of the building per degree day of indoor–outdoor temperature difference. The CDD and FDD terms refer to Celsius and Fahrenheit degree days, respectively
- $Q_{net}$ , net reference load, Wh (Btu): heat loss from nonsolar portion of building as calculated by

$$Q_{net} = NLC \times (\text{Number of degree days}). \tag{20.70}$$

- LCR, load collector ratio, kJ/m<sup>2</sup> CDD (Btu/ft.<sup>2</sup> FDD): ratio of NLC to  $A_p$ ,

$$LCR = NLC/A_p \tag{20.71}$$

- SSF, solar savings fraction, %: percentage reduction in required auxiliary heating relative to net reference load,

$$SSF = 1 - \frac{\text{Auxiliary heat required } (Q_{aux})}{\text{Net reference load } (Q_{net})} \tag{20.72}$$

Therefore, using Equation 20.70, the auxiliary heat required,  $Q_{aux}$ , is given by

$$Q_{aux} = (1 - SSF) \times NLC \times (\text{Number of degree days}). \tag{20.73}$$

The amount of auxiliary heat required is often a basis of comparison between possible solar designs as well as being the basis for determining building energy operating costs. Thus, many of the passive design methods are based on determining SSF, NLC, and the number of degree days in order to calculate the auxiliary heat required for a particular passive system by using Equation 20.73.

**20.3.3.4 The First Level: Generalized Methods**

A first estimate or starting value is needed to begin the overall passive system design process. Generalized methods and rules of thumb have been developed to generate initial values for solar aperture size, storage size, solar savings fraction, auxiliary heat required, and other size and performance characteristics. The following rules of thumb are meant to be used with the defined terms presented above.

### 20.3.3.5 Load

A rule of thumb used in conventional building design is that a design heating load of 120–160 kJ/CDD per m<sup>2</sup> of floor area (6–8 Btu/FDD ft.<sup>2</sup>) is considered an energy conservative design. Reducing these non-solar values by 20% to solarize the proposed south-facing solar wall gives rule-of-thumb NLC values per unit of floor area:

$$\text{NLC/Floor area} = 100\text{--}130 \text{ kJ/CDD m}^2 \text{ (4.8--6.4 Btu/FDD ft.}^2\text{)}. \quad (20.74)$$

### 20.3.3.6 Solar Savings Fraction

A method of getting starting-point values for the solar savings fraction is presented in Figure 20.48 (PSDH 1984). The map values represent optimum SSF (in percent) for a particular set of conservation and passive-solar costs for different climates across the United States. With the  $Q_{\text{net}}$  generated from the NLC rule of thumb (see above) and the SSF read from the map, the  $Q_{\text{aux}}$  can be determined.

### 20.3.3.7 Load Collector Ratio (LCR)

The  $A_p$  can be determined using the NLC from above if the LCR is known. The rule of thumb associated with “good” values of LCR (PSDH 1984) differs depending on whether the design is for a “cold” or “warm” climate:

$$\text{"Good" LCR} = \begin{cases} \text{For cold climate : } 410 \text{ kJ/m}^2 \text{ CDD (20 Btu/ft.}^2 \text{ FDD)} \\ \text{For warm climate : } 610 \text{ kJ/m}^2 \text{ CDD (30 Btu/ft.}^2 \text{ FDD)} \end{cases} \quad (20.75)$$

### 20.3.3.8 Storage

Rules of thumb for thermal mass storage relate storage material total heat capacity to the solar projected area (PSDH 1984). The use of the storage mass is to provide for heating on cloudy days and to regulate sunny day room air temperature swing. When the thermal mass directly absorbs the solar radiation, each

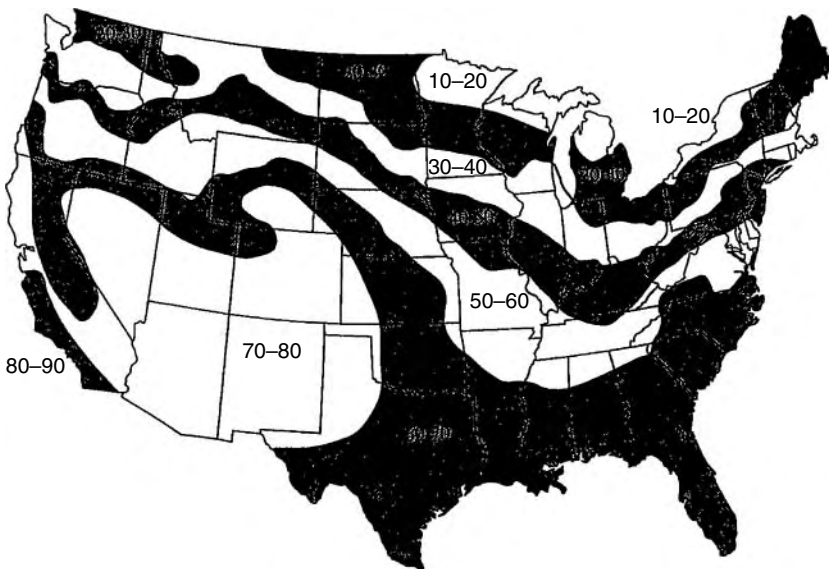


**FIGURE 20.48** Starting-point values of solar savings fraction (SSF) in percent. (From PSDH, *Passive Solar Design Handbook*. Part One: Total Environmental Action, Inc., Part Two: Los Alamos Scientific Laboratory, Part Three: Los Alamos National Laboratory. Van Nostrand Reinhold, New York, 1984.)

square meter of the projected glazing area requires enough mass to store 613 kJ/°C. If the storage material is not in direct sunlight, but heated from room air only, then four times as much mass is needed. In a room with a directly sunlight-heated storage mass, the room air temperature swing will be approximately one-half the storage mass temperature swing. For room air heated storage, the air temperature swing is twice that of the storage mass.

### Example 20.3.2

A Denver, Colorado, building is to have a floor area of 195 m<sup>2</sup> (2100 ft.<sup>2</sup>). Determine rule-of-thumb size and performance characteristics.

**Solution.** From Equation 20.72, the NLC is estimated as

$$\begin{aligned} \text{NLC} &= (115 \text{ kJ/CDD m}^2) \times (195 \text{ m}^2) \\ &= 22,400 \text{ kJ/CDD (11,800 Btu/FDD)}. \end{aligned}$$

Using the “cold” LCR value and Equation 20.71, the passive solar projected area is

$$\begin{aligned} A_p &= \text{NLC}/\text{LCR} = (22,400 \text{ kJ/CDD})/(410 \text{ kJ/m}^2 \text{ CDD}) \\ &= 54.7 \text{ m}^2(588 \text{ ft.}^2) \end{aligned}$$

Locating Denver on the map of [Figure 20.48](#) gives an SSF value in the 70%–80% range (use 75%). An annual °C-degree-day value can be found in city climate tables (PSDH 1984; NCDC 1992), and is 3491 CDD (6283 FDD) for Denver. Thus, the auxiliary heat required,  $Q_{\text{aux}}$ , is found using Equation 20.73:

$$\begin{aligned} Q_{\text{aux}} &= (1 - 0.75)(22,400 \text{ kJ/CDD})(3491 \text{ CDD}) \\ &= 19,600 \text{ MJ (18.5} \times 10^6 \text{ Btu) annually.} \end{aligned}$$

The thermal storage can be sized using directly solar-heated and/or room air heated mass by using the projected area. Assuming brick with a specific heat capacity of 840 J/kg°C, the storage mass is found by

$$\begin{aligned} A_p \times (613 \text{ kJ/C}) &= m \times (840 \text{ J/kg}^\circ\text{C}); \\ m_d &= 40,000 \text{ kg (88,000 lbm) [Direct sun]} \\ \text{or } m_a &= 160,000 \text{ kg (351,000 lbm) [Air heated]} \end{aligned}$$

A more location-dependent set of rules of thumb is presented in PSDH (1980). The first rule of thumb relates solar projected area as a percentage of floor area to solar savings fraction, with and without night insulation of the solar glazing:

“A solar projected area of (B1)% to (B2)% of the floor area can be expected to produce a SSF in (location) of (S1)% to (S2)%, or, if R9 night insulation is used, of (S3)% to (S4)%.”

The values of B1, B2, S1, S2, S3 and S4 are found using [Table 20.6](#) for the location. The thermal storage mass rule of thumb is again related to the solar projected area:

“A thermal storage wall should have 14 kg × SSF (%) of water or 71 kg × SSF (%) of masonry for each square meter of solar projected area. For a direct gain space, the mass above should be used with a surface area of at least three times the solar projected area, and masonry no thicker than 10–15 cm. If the mass is located in back rooms, then four times the above mass is needed.”

**TABLE 20.6** Values to Be Used in the Glazing Area and SSF Relations Rules of Thumb

City	B1	B2	S1	S2	S3	S4
Birmingham, Alabama	0.09	0.18	22	37	34	58
Mobile, Alabama	0.06	0.12	26	44	34	60
Montgomery, Alabama	0.07	0.15	24	41	34	59
Phoenix, Arizona	0.06	0.12	37	60	48	75
Prescott, Arizona	0.10	0.20	29	48	44	72
Tucson, Arizona	0.06	0.12	35	57	45	73
Winslow, Arizona	0.12	0.24	30	47	48	74
Yuma, Arizona	0.04	0.09	43	66	51	78
Fort Smith, Arkansas	0.10	0.20	24	39	38	64
Little Rock, Arkansas	0.10	0.19	23	38	37	62
Bakersfield, California	0.08	0.15	31	50	42	67
Baggett, California	0.07	0.15	35	56	46	73
Fresno, California	0.09	0.17	29	46	41	65
Long Beach, California	0.05	0.10	35	58	44	72
Los Angeles, California	0.05	0.09	36	58	44	72
Mount Shasta, California	0.11	0.21	24	38	42	67
Needles, California	0.06	0.12	39	61	49	76
Oakland, California	0.07	0.15	35	55	46	72
Red Bluff, California	0.09	0.18	29	46	41	65
Sacramento, California	0.09	0.18	29	47	41	66
San Diego, California	0.04	0.09	37	61	46	74
San Francisco, California	0.06	0.13	34	54	45	71
Santa Maria, California	0.05	0.11	31	53	42	69
Colorado Springs, Colorado	0.12	0.24	27	42	47	74
Denver, Colorado	0.12	0.23	27	43	47	74
Eagle, Colorado	0.14	0.29	25	35	53	77
Grand Junction, Colorado	0.13	0.27	29	43	50	76
Pueblo, Colorado	0.11	0.23	29	45	48	75
Hartford, Connecticut	0.17	0.35	14	19	40	64
Wilmington, Delaware	0.15	0.29	19	30	39	63
Washington, District Of Columbia	0.12	0.23	18	28	37	61
Apalachicola, Florida	0.05	0.10	28	47	36	61
Daytona Beach, Florida	0.04	0.08	30	51	36	63
Jacksonville, Florida	0.05	0.09	27	47	35	62
Miami, Florida	0.01	0.02	27	48	31	54
Orlando, Florida	0.03	0.06	30	52	37	63
Tallahassee, Florida	0.05	0.11	26	45	35	60
Tampa, Florida	0.03	0.06	30	52	36	63
West Palm Beach, Florida	0.01	0.03	30	51	34	59
Atlanta, Georgia	0.06	0.17	22	36	34	58
Augusta, Georgia	0.06	0.16	24	40	35	60
Macon, Georgia	0.07	0.15	25	41	35	59
Savannah, Georgia	0.06	0.13	25	43	35	60
Boise, Idaho	0.14	0.28	27	38	48	71
Lewiston, Idaho	0.15	0.29	22	29	44	65
Pocatello, Idaho	0.13	0.26	25	35	51	74
Chicago, Illinois	0.17	0.35	17	23	43	67
Moline, Illinois	0.20	0.39	17	22	46	70
Springfield, Illinois	0.15	0.30	19	26	42	67
Evansville, Indiana	0.14	0.27	19	29	37	61
Fort Wayne, Indiana	0.16	0.33	13	17	37	60
Indianapolis, Indiana	0.14	0.28	15	21	37	60
South Bend, Indiana	0.18	0.35	12	15	39	61
Burlington, Iowa	0.18	0.36	20	27	47	71
Des Moines, Iowa	0.21	0.43	19	25	58	75

*(continued)*

TABLE 20.6 (Continued)

City	B1	B2	S1	S2	S3	S4
Mason City, Iowa	0.22	0.44	18	19	56	79
Sioux City, Iowa	0.23	0.46	20	24	53	76
Dodge City, Kansas	0.12	0.23	27	42	46	73
Goodland, Kansas	0.13	0.27	26	39	47	74
Topeka, Kansas	0.14	0.26	24	35	45	71
Wichita, Kansas	0.14	0.26	26	41	45	72
Lexington, Kentucky	0.13	0.27	17	26	35	58
Louisville, Kentucky	0.13	0.27	18	27	35	59
Baton Rouge, Louisiana	0.06	0.12	26	43	34	59
Lake Charles, Louisiana	0.06	0.11	24	41	32	57
New Orleans, Louisiana	0.05	0.11	27	46	35	61
Shreveport, Louisiana	0.08	0.15	26	43	36	61
Caribou, Maine	0.25	0.30	NR	NR	53	74
Portland, Maine	0.17	0.34	14	17	45	69
Baltimore, Maryland	0.14	0.27	19	30	38	62
Boston, Massachusetts	0.15	0.29	17	25	40	64
Alpena, Michigan	0.21	0.42	NR	NR	47	69
Detroit, Michigan	0.17	0.34	13	17	39	61
Flint, Michigan	0.15	0.31	11	12	40	62
Grand Rapids, Michigan	0.19	0.38	12	13	39	61
Sault Ste. Marie, Michigan	0.25	0.50	NR	NR	50	70
Traverse City, Michigan	0.18	0.36	NR	NR	42	62
Duluth, Minnesota	0.25	0.50	NR	NR	50	70
International Falls, Minnesota	0.25	0.50	NR	NR	47	66
Minneapolis-St. Paul, Minnesota	0.25	0.50	NR	NR	55	76
Rochester, Minnesota	0.24	0.49	NR	NR	54	76
Jackson, Mississippi	0.06	0.15	24	48	34	59
Meridian, Mississippi	0.08	0.15	23	39	34	58
Columbia, Missouri	0.13	0.26	20	30	41	66
Kansas City, Missouri	0.14	0.29	22	32	44	70
Saint Louis, Missouri	0.15	0.29	21	33	41	65
Springfield, Missouri	0.13	0.26	22	34	40	65
Billings, Montana	0.16	0.32	24	31	53	76
Cut Bank, Montana	0.24	0.49	22	23	62	81
Dillon, Montana	0.16	0.32	24	32	54	77
Glasgow, Montana	0.25	0.50	NR	NR	55	75
Great Falls, Montana	0.18	0.37	23	26	56	77
Helena, Montana	0.20	0.39	21	25	55	77
Lewistown, Montana	0.19	0.38	21	25	54	76
Miles City, Montana	0.23	0.47	21	23	60	80
Missoula, Montana	0.18	0.36	15	16	47	68
Grand Island, Nebraska	0.18	0.36	24	33	51	76
North Omaha, Nebraska	0.20	0.48	21	29	51	76
North Platte, Nebraska	0.17	0.34	25	36	50	76
Scottsbluff, Nebraska	0.16	0.31	24	36	49	74
Elko, Nevada	0.12	0.25	27	39	52	76
Ely, Nevada	0.12	0.23	27	41	50	77
Las Vegas, Nevada	0.09	0.18	35	56	48	75
Lovelock, Nevada	0.13	0.25	32	48	53	78
Reno, Nevada	0.11	0.22	31	48	49	76
Tonopah, Nevada	0.11	0.23	31	48	51	77
Winnemucca, Nevada	0.13	0.26	28	42	49	75
Concord, New Hampshire	0.17	0.34	13	15	45	68
Newark, New Jersey	0.13	0.25	19	29	39	64
Albuquerque, New Mexico	0.11	0.22	29	47	46	73

(continued)

TABLE 20.6 (Continued)

City	B1	B2	S1	S2	S3	S4
Clayton, New Mexico	0.10	0.20	28	45	45	73
Farmington, New Mexico	0.12	0.24	29	45	49	76
Los Alamos, New Mexico	0.11	0.22	25	40	44	72
Roswell, New Mexico	0.10	0.19	30	49	45	73
Truth or Consequences, New Mexico	0.09	0.17	32	51	46	73
Tucumcari, New Mexico	0.10	0.20	30	48	45	73
Zuni, New Mexico	0.11	0.21	27	43	45	73
Albany, New York	0.21	0.41	13	15	43	66
Binghamton, New York	0.15	0.30	NR	NR	35	56
Buffalo, New York	0.19	0.37	NR	NR	36	57
Massena, New York	0.25	0.50	NR	NR	50	71
New York (Central Park), New York	0.15	0.30	16	25	36	59
Rochester, New York	0.18	0.37	NR	NR	37	58
Syracuse, New York	0.19	0.38	NR	NR	37	59
Asheville, North Carolina	0.10	0.20	21	35	36	61
Cape Hatteras, North Carolina	0.09	0.17	24	40	36	60
Charlotte, North Carolina	0.08	0.17	23	38	36	60
Greensboro, North Carolina	0.10	0.20	23	37	37	63
Raleigh-Durham, North Carolina	0.09	0.19	22	37	36	61
Bismarck, North Dakota	0.25	0.50	NR	NR	56	77
Fargo, North Dakota	0.25	0.50	NR	NR	51	72
Minot, North Dakota	0.25	0.50	NR	NR	52	72
Akron-Canton, Ohio	0.15	0.31	12	16	35	57
Cincinnati, Ohio	0.12	0.24	15	23	35	57
Cleveland, Ohio	0.15	0.31	11	14	34	55
Columbus, Ohio	0.14	0.28	13	18	35	57
Dayton, Ohio	0.14	0.28	14	20	36	59
Toledo, Ohio	0.17	0.34	13	17	38	61
Youngstown, Ohio	0.16	0.32	NR	NR	34	54
Oklahoma City, Oklahoma	0.11	0.22	25	41	41	67
Tulsa, Oklahoma	0.11	0.22	24	38	40	65
Astoria, Oregon	0.09	0.19	21	34	37	60
Burns, Oregon	0.13	0.25	23	32	47	71
Medford, Oregon	0.12	0.24	21	32	38	60
North Bend, Oregon	0.09	0.17	25	42	38	64
Pendleton, Oregon	0.14	0.27	22	30	43	64
Portland, Oregon	0.13	0.26	21	31	38	60
Redmond, Oregon	0.13	0.27	26	38	47	71
Salem, Oregon	0.12	0.24	21	32	37	59
Allentown, Pennsylvania	0.15	0.29	16	24	39	63
Erie, Pennsylvania	0.17	0.34	NR	NR	35	55
Harrisburg, Pennsylvania	0.13	0.26	17	26	38	62
Philadelphia, Pennsylvania	0.15	0.29	19	29	38	62
Pittsburgh, Pennsylvania	0.14	0.28	12	16	33	55
Wilkes-Barre-Scranton, Pennsylvania	0.16	0.32	13	18	37	60
Providence, Rhode Island	0.15	0.30	17	24	40	64
Charleston, South Carolina	0.07	0.14	25	41	34	59
Columbia, South Carolina	0.08	0.17	25	41	36	61
Greenville-Spartanburg, South Carolina	0.08	0.17	23	38	36	60
Huron, South Dakota	0.25	0.50	NR	NR	58	79
Pierre, South Dakota	0.22	0.43	21	23	58	80
Rapid City, South Dakota	0.15	0.30	23	32	51	76
Sioux Falls, South Dakota	0.22	0.45	18	19	57	79
Chattanooga, Tennessee	0.09	0.19	19	32	33	56
Knoxville, Tennessee	0.09	0.18	20	33	33	56

(continued)

TABLE 20.6 (Continued)

City	B1	B2	S1	S2	S3	S4
Memphis, Tennessee	0.09	0.19	22	36	36	60
Nashville, Tennessee	0.10	0.21	19	30	33	55
Abilene, Texas	0.09	0.18	29	47	41	68
Amarillo, Texas	0.11	0.22	29	46	45	72
Austin, Texas	0.06	0.13	27	46	37	63
Brownsville, Texas	0.03	0.06	27	46	32	57
Corpus Christi, Texas	0.05	0.09	29	49	36	63
Dallas, Texas	0.08	0.17	27	44	38	64
Del Rio, Texas	0.06	0.12	30	50	39	66
El Paso, Texas	0.09	0.17	32	53	45	72
Forth Worth, Texas	0.09	0.17	26	44	38	64
Houston, Texas	0.06	0.11	25	43	34	59
Laredo, Texas	0.05	0.09	31	52	39	64
Lubbock, Texas	0.09	0.19	30	49	44	72
Lufkin, Texas	0.07	0.14	26	43	35	61
Midland-Odessa, Texas	0.09	0.18	32	52	44	72
Port Arthur, Texas	0.06	0.11	26	44	34	60
San Angelo, Texas	0.08	0.15	29	48	40	67
San Antonio, Texas	0.06	0.12	28	48	38	64
Sherman, Texas	0.10	0.20	25	41	38	64
Waco, Texas	0.06	0.15	27	45	38	64
Wichita Falls, Texas	0.10	0.20	27	45	41	67
Bryce Canyon, Utah	0.13	0.25	26	39	52	78
Cedar City, Utah	0.12	0.24	28	43	48	75
Salt Lake City, Utah	0.13	0.26	27	39	48	72
Burlington, Vermont	0.22	0.43	NR	NR	46	68
Norfolk, Virginia	0.09	0.19	23	38	37	62
Richmond, Virginia	0.11	0.22	21	34	37	61
Roanoke, Virginia	0.11	0.23	21	34	37	61
Olympia, Washington	0.12	0.23	20	29	38	59
Seattle-Tacoma, Washington	0.11	0.22	21	30	39	59
Spokane, Washington	0.20	0.39	20	24	48	68
Yakima, Washington	0.18	0.36	24	31	49	70
Charleston, West Virginia	0.13	0.25	16	24	32	54
Huntington, West Virginia	0.13	0.25	17	27	34	57
Eau Claire, Wisconsin	0.25	0.50	NR	NR	53	75
Green Bay, Wisconsin	0.23	0.46	NR	NR	53	75
La Crosse, Wisconsin	0.21	0.43	NR	NR	52	75
Madison, Wisconsin	0.20	0.40	15	17	51	74
Milwaukee, Wisconsin	0.18	0.35	15	18	48	71
Casper, Wyoming	0.13	0.26	27	39	53	78
Cheyenne, Wyoming	0.11	0.21	25	39	47	74
Rock Springs, Wyoming	0.14	0.28	26	38	54	79
Sheridan, Wyoming	0.16	0.31	22	30	52	75
Canada						
Edmonton, Alberta	0.25	0.50	NR	NR	54	72
Suffield, Alberta	0.25	0.50	28	30	67	85
Nanaimo, British Columbia	0.13	0.26	26	35	45	66
Vancouver, British Columbia	0.13	0.26	20	28	48	60
Winnipeg, Manitoba	0.25	0.50	NR	NR	54	74
Dartmouth, Nova Scotia	0.14	0.28	17	24	45	70
Moosonee, Ontario	0.25	0.50	NR	NR	48	67
Ottawa, Ontario	0.25	0.50	NR	NR	59	80
Toronto, Ontario	0.18	0.36	17	23	44	68
Normandie, Quebec	0.25	0.50	NR	NR	54	74

Note: NR, not recommended.

Source: From PSDH, *Passive Solar Design Handbook*, U.S. Department of Energy, Washington, DC, 1980.



**Example 20.3.3**

Determine size and performance passive solar characteristics with the location-dependent set of rules of thumb for the house of the previous example.

**Solution.** Using [Table 20.6](#) with the 195 m<sup>2</sup> house in Denver yields:

$$\begin{aligned}\text{Solar projected area} &= 12\% \text{ to } 23\% \text{ of floor area} \\ &= 23.4 \text{ m}^2 \text{ to } 44.9 \text{ m}^2.\end{aligned}$$

$$\text{SSF (no night insulation)} = 27\% \text{ to } 43\%.$$

$$\text{SSF (R9 night insulation)} = 47\% \text{ to } 74\%.$$

Using the rule of thumb for the thermal storage mass:

$$\begin{aligned}m &= 17 \text{ kg} \times 43\% \times 44.9 \text{ m}^2 \\ &= 33,000 \text{ kg (72,000 lbm)}[\text{Thermal wall or direct gain}]\end{aligned}$$

Comparing the results of this example to those of the previous example, the two rules of thumb are seen to produce “roughly” similar answers. General system cost and performance information can be generated with results from rule-of-thumb calculations, but a more detailed level of information is needed to determine design-ready passive system type (direct gain, thermal wall, sunspace), size, performance, and costs.

**20.3.3.9 The Second Level: LCR Method**

The LCR method is useful for making estimates of the annual performance of specific types of passive system(s) combinations. The LCR method was developed by calculating the annual SSF for 94 reference passive solar systems for 219 U.S. and Canadian locations over a range of LCR values. [Table 20.7](#) includes the description of these 94 reference systems for use both with the LCR method and with the SLR method described below. Tables were constructed for each city with LCR versus SSF listed for each of the 94 reference passive systems. (Note that the solar load ratio (SLR) method was used to make the LCR calculations, and this SLR method is described in the next section as the third-level method.) Although the complete LCR tables (PSDH 1984) include 219 locations, [Table 20.8](#) only includes six “representative” cities (Albuquerque, Boston, Madison, Medford, Nashville, Santa Maria), purely due to space restrictions. The LCR method consists of the following steps (PSDH 1984):

1. Determine the building parameters:
  - a. Building load coefficient, NLC
  - b. Solar projected area,  $A_p$
  - c. Load collector ratio,  $\text{LCR} = \text{NLC}/A_p$
2. Find the short designation of the reference system closest to the passive system design ([Table 20.7](#))
3. Enter the LCR Tables ([Table 20.8](#))
  - a. Find the city
  - b. Find the reference system listing
  - c. Determine annual SSF by interpolation using the LCR value from above
  - d. Note the annual heating degree days (Number of degree days)
4. Calculate the annual auxiliary heat required:

$$\text{Auxiliary heat required} = (1 - \text{SSF}) \times \text{NLC} \times (\text{Number of degree days}).$$

If more than one reference solar system is being used, then find the “aperture area weighted” SSF for the combination. Determine each individual reference system SSF using the total aperture area LCR, then take the “area weighted” average of the individual SSFs.

TABLE 20.7 Designations and Characteristics for 94 Reference Systems

(a) Overall System Characteristics						
Masonry Properties						
Thermal conductivity ( $k$ )						
Sunspace floor				0.5 Btu/h/ft./°F		
All other masonry				1.0 Btu/h/ft./°F		
Density ( $Q$ )				150 lb/ft. <sup>3</sup>		
Specific heat ( $c$ )				0.2 Btu/lb/°F		
Infrared emittance of normal surface				0.9		
Infrared emittance of selective surface				0.1		
Solar Absorptances						
Waterwall				1.0		
Masonry, Trombe wall				1.0		
Direct gain and sunspace				0.8		
Sunspace: water containers				0.9		
Lightweight common wall				0.7		
Other lightweight surfaces				0.3		
Glazing Properties						
Transmission characteristics				Diffuse		
Orientation				Due south		
Index of refraction				1.526		
Extinction coefficient				0.5 in. <sup>-1</sup>		
Thickness of each pane				1/8 in.		
Gap between panes				1/2 in.		
Ared emittance				0.9		
Control Range						
Room temperature				65°F–75°F		
Sunspace temperature				45°F–95°F		
Internal heat generation				0		
Thermocirculation Vents (when used)						
Vent area/projected area (sum of both upper and lower vents)				0.06		
Height between vents				8 ft.		
Reverse flow				None		
Nighttime Insulation (when used)						
Thermal resistance				R9		
In place, solar time				5:30 P.M. to 7:30 A.M.		
Solar Radiation Assumptions						
Shading				None		
Ground diffuse reflectance				0.3		
(b) Direct-Gain (DG) System Types						
Designation	Thermal Storage Capacity <sup>a</sup> (Btu/ft. <sup>2</sup> /°F)	Mass Thickness <sup>a</sup> (in.)	Mass-Area-to-Glazing-Area Ratio	No. of Glazings	Nighttime Insulation	
A1	30	2	6	2	No	
A2	30	2	6	3	No	
A3	30	2	6	2	Yes	
B1	45	6	3	2	No	
B2	45	6	3	3	No	
B3	45	6	3	2	Yes	
C1	60	4	6	2	No	
C2	60	4	6	3	No	
C3	60	4	6	2	Yes	

(continued)

TABLE 20.7 (Continued)

(c) Vented Trombe Wall (TW) System Types						
Designation	Thermal Storage Capacity <sup>a</sup> (Btu/ft. <sup>2</sup> /°F)	Wall Thickness <sup>a</sup> (in.)	$\rho ck$ (Btu <sup>2</sup> /h/ft. <sup>4</sup> /°F <sup>2</sup> )	No. of Glazings	Wall Surface	Nighttime Insulation
A1	15	6	30	2	Normal	No
A2	22.5	9	30	2	Normal	No
A3	30	12	30	2	Normal	No
A4	45	18	30	2	Normal	No
B1	15	6	15	2	Normal	No
B2	22.5	9	15	2	Normal	No
B3	30	12	15	2	Normal	No
B4	45	18	15	2	Normal	No
C1	15	6	7.5	2	Normal	No
C2	22.5	9	7.5	2	Normal	No
C3	30	12	7.5	2	Normal	No
C4	45	18	7.5	2	Normal	No
D1	30	12	30	1	Normal	No
D2	30	12	30	3	Normal	No
D3	30	12	30	1	Normal	Yes
D4	30	12	30	2	Normal	Yes
D5	30	12	30	3	Normal	Yes
E1	30	12	30	1	Selective	No
E2	30	12	30	2	Selective	No
E3	30	12	30	1	Selective	Yes
E4	30	12	30	2	Selective	Yes
(d) Unvented Trombe Wall (TW) System Types						
Designation	Thermal Storage Capacity <sup>a</sup> (Btu/ft. <sup>2</sup> /°F)	Wall Thickness <sup>a</sup> (in.)	$\rho ck$ (Btu <sup>2</sup> /h/ft. <sup>4</sup> /°F <sup>2</sup> )	No. of Glazings	Wall Surface	Nighttime Insulation
F1	15	6	30	2	Normal	No
F2	22.5	9	30	2	Normal	No
F3	30	12	30	2	Normal	No
F4	45	18	30	2	Normal	No
G1	15	6	15	2	Normal	No
G2	22.5	9	15	2	Normal	No
G3	30	12	15	2	Normal	No
G4	45	18	15	2	Normal	No
H1	15	6	7.5	2	Normal	No
H2	22.5	9	7.5	2	Normal	No
H3	30	12	7.5	2	Normal	No
H4	45	18	7.5	2	Normal	No
I1	30	12	30	1	Normal	No
I2	30	12	30	3	Normal	No
I3	30	12	30	1	Normal	Yes
I4	30	12	30	2	Normal	Yes
I5	30	12	30	3	Normal	Yes
J1	30	12	30	1	Selective	No
J2	30	12	30	2	Selective	No
J3	30	12	30	1	Selective	Yes
J4	30	12	30	2	Selective	Yes

(continued)

TABLE 20.7 (Continued)

(e) Waterwall (WW) System Types					
Designation	Thermal Storage Capacity <sup>a</sup> (Btu/ft. <sup>2</sup> /°F)	Wall Thickness (in.)	No. of Glazings	Wall Surface	Nighttime Insulation
A1	15.6	3	2	Normal	No
A2	31.2	6	2	Normal	No
A3	46.8	9	2	Normal	No
A4	62.4	12	2	Normal	No
A5	93.6	18	2	Normal	No
A6	124.8	24	2	Normal	No
B1	46.8	9	1	Normal	No
B2	46.8	9	3	Normal	No
B3	46.8	9	1	Normal	Yes
B4	46.8	9	2	Normal	Yes
B5	46.8	9	3	Normal	Yes
C1	46.8	9	1	Selective	No
C2	46.8	9	2	Selective	No
C3	46.8	9	1	Selective	Yes
C4	46.8	9	2	Selective	Yes
(f) Sunspace (SS) System Types					
Designation	Type	Tilt (°)	Common Wall	End Walls	Nighttime Insulation
A1	Attached	50	Masonry	Opaque	No
A2	Attached	50	Masonry	Opaque	Yes
A3	Attached	50	Masonry	Glazed	No
A4	Attached	50	Masonry	Glazed	Yes
A5	Attached	50	Insulated	Opaque	No
A6	Attached	50	Insulated	Opaque	Yes
A7	Attached	50	Insulated	Glazed	No
A8	Attached	50	Insulated	Glazed	Yes
B1	Attached	90/30	Masonry	Opaque	No
B2	Attached	90/30	Masonry	Opaque	Yes
B3	Attached	90/30	Masonry	Glazed	No
B4	Attached	90/30	Masonry	Glazed	Yes
B5	Attached	90/30	Insulated	Opaque	No
B6	Attached	90/30	Insulated	Opaque	Yes
B7	Attached	90/30	Insulated	Glazed	No
B8	Attached	90/30	Insulated	Glazed	Yes
C1	Semienclosed	90	Masonry	Common	No
C2	Semienclosed	90	Masonry	Common	Yes
C3	Semienclosed	90	Insulated	Common	No
C4	Semienclosed	90	Insulated	Common	Yes
D1	Semienclosed	50	Masonry	Common	No
D2	Semienclosed	50	Masonry	Common	Yes
D3	Semienclosed	50	Insulated	Common	No
D4	Semienclosed	50	Insulated	Common	Yes
E1	Semienclosed	90/30	Masonry	Common	No
E2	Semienclosed	90/30	Masonry	Common	Yes
E3	Semienclosed	90/30	Insulated	Common	No
E4	Semienclosed	90/30	Insulated	Common	Yes

<sup>a</sup> The thermal storage capacity is per unit of projected area, or, equivalently, the quantity  $\rho ck$ . The wall thickness is listed only as an appropriate guide by assuming  $\rho c = 30 \text{ Btu/ft.}^3/\text{°F}$ .

Source: From PSDH, Passive Solar Design Handbook. Part One: Total Environmental Action, Inc., Part Two: Los Alamos Scientific Laboratory, Part Three: Los Alamos National Laboratory. Van Nostran Laboratory. Van Nostran Reinhold, New York, 1984.

**TABLE 20.8** LCR Tables for Six Representative Cities (Albuquerque, Boston, Madison, Medford, Nashville, and Santa Maria)

SSF	0.10	0.20	0.30	0.40	0.50	0.60	0.70	0.80	0.90
Santa Maria, California									3053 DD
WW A1	1776	240	119	73	50	35	25	18	12
WW A2	617	259	154	103	74	54	39	28	19
WW A3	523	261	164	114	82	61	45	33	22
WW A4	482	260	169	119	87	65	48	35	24
WW A5	461	263	175	125	92	69	52	38	26
WW A6	447	263	177	128	95	72	54	40	27
WW B1	556	220	128	85	60	43	32	23	15
WW B2	462	256	168	119	88	66	49	36	25
WW B3	542	315	211	151	112	85	64	47	32
WW B4	455	283	197	144	109	83	63	47	32
WW B5	414	263	184	136	103	79	60	45	31
WW C1	569	330	221	159	118	89	67	49	33
WW C2	478	288	197	143	107	81	61	45	31
WW C3	483	318	228	170	130	100	77	57	40
WW C4	426	280	200	149	114	88	68	51	35
TW A1	1515	227	113	70	48	34	24	17	11
TW A2	625	234	134	89	63	46	33	24	16
TW A3	508	231	140	95	68	50	37	27	18
TW A4	431	217	137	95	69	51	38	28	19
TW B1	859	212	112	71	49	35	25	18	12
TW B2	502	209	124	83	59	43	32	23	15
TW B3	438	201	123	84	60	44	33	24	16
TW B4	400	184	112	76	55	40	30	22	14
TW C1	568	188	105	69	48	35	25	18	12
TW C2	435	178	105	70	50	36	27	19	13
TW C3	413	165	97	64	46	33	25	18	12
TW C4	426	146	82	54	38	27	20	14	10
TW D1	403	170	101	67	48	35	25	18	12
TW D2	488	242	152	105	76	57	42	31	21
TW D3	509	271	175	123	90	67	50	36	25
TW D4	464	266	177	127	94	71	53	39	27
TW D5	425	250	169	122	91	69	52	38	26
TW E1	581	309	199	140	102	76	57	42	28
TW E2	512	283	186	132	97	73	55	40	27
TW E3	537	328	225	164	123	94	71	53	36
TW E4	466	287	199	145	109	83	63	47	32
TW F1	713	198	107	68	47	34	25	18	12
TW F2	455	199	120	81	58	42	31	22	15
TW F3	378	190	120	83	60	45	33	24	16
TW F4	311	169	110	77	57	42	32	23	16
TW G1	450	170	98	65	46	33	24	17	12
TW G2	331	163	102	70	51	38	28	20	14
TW G3	278	147	94	66	48	36	27	20	13
TW G4	222	120	78	55	40	30	22	16	11
TW H1	295	137	84	57	41	30	22	16	11
TW H2	226	118	75	52	38	28	21	15	10
TW H3	187	99	64	44	33	24	18	13	9
TW H4	143	75	48	33	24	18	14	10	7
TW I1	318	144	88	59	42	31	23	16	11
TW I2	377	203	132	93	68	51	38	28	19
TW I3	404	226	149	106	78	58	44	32	22
TW I4	387	230	156	113	84	64	48	36	24
TW I5	370	226	155	113	85	65	49	36	25

(continued)

TABLE 20.8 (Continued)

SSF	0.10	0.20	0.30	0.40	0.50	0.60	0.70	0.80	0.90
TW J1	483	271	179	127	94	71	53	39	26
TW J2	422	246	165	119	88	67	50	37	25
TW J3	446	283	199	146	111	85	65	48	33
TW J4	400	254	178	132	100	77	58	43	30
DG A1	392	188	117	79	55	38	26	16	7
DG A2	389	190	121	85	61	45	32	22	14
DG A3	443	220	142	102	77	58	44	31	19
DG B1	384	191	122	86	64	48	35	24	13
DG B2	394	196	127	91	69	53	40	29	19
DG B3	445	222	145	105	80	62	49	37	25
DG C1	451	225	146	104	78	61	47	34	21
DG C2	453	226	148	106	80	63	49	37	25
DG C3	509	254	167	121	92	73	58	45	31
SS A1	1171	396	220	142	98	69	49	34	22
SS A2	1028	468	283	190	135	98	71	50	33
SS A3	1174	380	209	133	91	64	45	31	20
SS A4	1077	481	289	193	136	98	71	50	32
SS A5	1896	400	204	127	86	60	42	29	18
SS A6	1030	468	283	190	135	97	71	50	32
SS A7	2199	359	178	109	72	50	35	24	15
SS A8	1089	478	285	190	133	96	69	48	31
SS B1	802	298	170	111	77	55	40	28	18
SS B2	785	366	224	152	108	79	57	41	27
SS B3	770	287	163	106	74	52	37	26	17
SS B4	790	368	224	152	108	78	57	40	26
SS B5	1022	271	144	91	62	44	31	22	14
SS B6	750	356	219	149	106	77	56	40	26
SS B7	937	242	127	80	54	38	27	19	12
SS B8	750	352	215	146	103	75	55	39	25
SS C1	481	232	144	99	71	52	39	28	19
SS C2	482	262	170	120	88	66	49	36	24
SS C3	487	185	107	71	50	36	27	19	13
SS C4	473	235	147	102	74	55	41	30	20
SS D1	1107	477	282	188	132	95	68	48	31
SS D2	928	511	332	232	169	125	92	66	43
SS D3	1353	449	248	160	110	78	56	39	25
SS D4	946	500	319	222	160	117	86	61	40
SS E1	838	378	227	153	108	78	56	40	26
SS E2	766	419	272	190	138	102	75	54	36
SS E3	973	322	178	115	79	56	40	28	18
SS E4	780	393	247	170	122	89	65	47	31
Albuquerque, New Mexico									4292 DD
WW A1	1052	130	62	38	25	18	13	9	6
WW A2	354	144	84	56	39	29	21	15	10
WW A3	300	146	90	62	45	33	24	18	12
WW A4	276	146	93	65	47	35	26	19	13
WW A5	264	148	97	69	50	38	28	21	14
WW A6	256	148	99	70	52	39	30	22	15
WW B1	293	111	63	41	28	20	15	11	7
WW B2	270	147	96	67	49	37	28	20	14
WW B3	314	179	119	84	62	47	35	26	18
WW B4	275	169	116	85	64	49	37	28	19
WW B5	252	159	110	81	61	47	36	27	19
WW C1	333	190	126	89	66	50	38	28	19
WW C2	287	171	115	83	62	47	36	27	18
WW C3	293	191	136	101	77	59	46	34	24

(continued)

TABLE 20.8 (Continued)

SSF	0.10	0.20	0.30	0.40	0.50	0.60	0.70	0.80	0.90
WW C4	264	172	122	91	69	54	41	31	22
TW A1	900	124	60	37	25	17	12	9	6
TW A2	361	130	73	48	33	24	18	13	8
TW A3	293	129	77	52	37	27	20	15	10
TW A4	249	123	76	52	38	28	21	15	10
TW B1	502	117	60	38	26	18	13	9	6
TW B2	291	118	68	45	32	23	17	12	8
TW B3	254	114	68	46	33	24	18	13	9
TW B4	233	104	63	42	30	22	16	12	8
TW C1	332	106	58	37	26	19	14	10	6
TW C2	255	101	58	39	27	20	15	11	7
TW C3	243	94	54	36	25	18	13	10	7
TW C4	254	84	46	30	21	15	11	8	5
TW D1	213	86	50	33	23	17	12	9	6
TW D2	287	139	86	59	43	32	24	17	12
TW D3	294	153	97	68	49	37	27	20	14
TW D4	281	158	104	74	55	41	31	23	16
TW D5	260	151	101	73	54	41	31	23	16
TW E1	339	177	113	78	57	43	32	23	16
TW E2	308	168	109	77	56	42	32	23	16
TW E3	323	195	133	96	72	55	42	31	21
TW E4	287	175	120	88	66	50	38	28	20
TW F1	409	108	57	36	24	17	13	9	6
TW F2	260	110	65	43	31	22	17	12	8
TW F3	216	106	66	45	33	24	10	13	9
TW F4	178	95	61	42	31	23	17	13	9
TW G1	256	93	53	34	24	17	13	9	6
TW G2	189	91	56	38	27	20	15	11	7
TW G3	159	82	52	36	26	20	15	11	7
TW G4	128	68	43	30	22	16	12	9	6
TW H1	168	76	45	31	22	16	12	9	6
TW H2	130	66	41	29	21	15	11	8	6
TW H3	108	56	35	25	8	13	10	7	5
TW H4	83	42	27	19	13	10	7	5	4
TW I1	166	73	43	29	20	15	11	8	5
TW I2	221	117	75	52	30	28	21	16	11
TW I3	234	128	83	59	43	32	24	10	12
TW I4	234	137	92	66	49	37	28	21	14
TW I5	226	136	93	67	50	38	29	22	15
TW J1	282	156	102	72	53	40	30	22	15
TW J2	254	146	97	69	51	39	29	22	15
TW J3	269	169	118	86	65	50	38	29	20
TW J4	247	155	106	80	60	46	35	26	18
DG A1	211	97	57	36	22	13	5	—	—
DG A2	227	107	67	46	32	23	16	10	5
DG A3	274	131	83	59	44	34	25	18	10
DG B1	210	97	60	42	30	21	13	6	—
DG B2	232	110	69	49	37	28	21	14	8
DG B3	277	134	85	61	47	37	28	21	14
DG C1	253	120	74	53	39	30	22	14	—
DG C2	271	130	82	59	45	35	26	19	12
DG C3	318	155	96	71	54	43	34	26	18
SS A1	591	187	101	64	44	31	22	16	10
SS A2	531	232	137	92	65	47	34	25	16
SS A3	566	170	90	56	38	27	19	13	8

(continued)

TABLE 20.8 (Continued)

SSF	0.10	0.20	0.30	0.40	0.50	0.60	0.70	0.80	0.90
SS A4	537	230	135	89	63	45	33	23	15
SS A5	980	187	92	56	37	26	18	13	8
SS A6	529	231	136	91	64	47	34	24	16
SS A7	1103	158	74	44	29	20	14	10	6
SS A8	540	226	131	87	61	44	32	23	15
SS B1	403	141	78	50	35	25	18	13	8
SS B2	412	186	111	75	53	39	28	20	14
SS B3	372	130	71	46	31	22	16	11	7
SS B4	403	181	106	72	51	37	27	20	13
SS B5	518	127	65	40	27	19	13	9	6
SS B6	390	179	106	73	52	38	28	20	13
SS B7	457	108	54	33	22	16	11	8	5
SS B8	379	171	102	69	49	35	26	19	12
SS C1	270	126	77	52	37	27	20	15	10
SS C2	282	150	97	68	49	37	28	20	14
SS C3	276	101	57	37	26	19	14	10	7
SS C4	277	135	83	57	41	31	23	17	11
SS D1	548	225	130	85	59	43	31	22	14
SS D2	474	253	162	113	82	61	45	33	22
SS D3	683	212	113	72	49	35	25	17	11
SS D4	484	248	156	107	77	57	42	30	20
SS E1	410	176	103	68	48	35	25	18	12
SS E2	390	208	133	92	67	50	37	27	18
SS E3	487	151	80	51	35	25	18	12	8
SS E4	400	195	120	82	59	43	32	23	15
Nashville, Tennessee									3696 DD
WW A1	588	60	24	13	8	5	3	2	1
WW A2	192	70	38	23	15	11	7	5	3
WW A3	161	72	42	27	18	13	9	6	4
WW A4	148	72	43	29	20	14	10	7	5
WW A5	141	74	46	31	22	16	11	8	5
WW A6	137	74	47	32	22	16	12	8	5
WW B1	135	41	19	10	6	3	2	—	—
WW B2	152	78	48	33	23	17	12	9	6
WW B3	179	97	61	42	30	22	16	12	8
WW B4	164	97	65	46	34	25	19	14	9
WW B5	153	93	63	45	33	25	19	14	9
WW C1	193	105	67	46	33	24	18	13	8
WW C2	169	97	63	44	32	24	18	13	8
WW C3	181	115	79	58	43	33	25	18	12
WW C4	164	104	72	53	39	30	23	17	11
TW A1	509	59	25	13	8	5	3	2	1
TW A2	199	64	33	20	13	9	6	4	3
TW A3	160	65	36	23	15	11	8	5	3
TW A4	136	62	36	23	16	11	8	6	4
TW B1	282	57	26	15	9	6	4	3	2
TW B2	161	59	32	20	13	9	6	4	3
TW B3	141	58	32	21	14	10	7	5	3
TW B4	131	54	30	19	13	9	7	5	3
TW C1	188	53	27	16	10	7	5	3	2
TW C2	144	52	28	18	12	8	6	4	2
TW C3	139	49	27	17	11	8	5	4	2
TW C4	149	45	23	14	9	7	5	3	2
TW D1	99	33	16	9	5	3	2	1	—
TW D2	164	75	44	29	20	14	10	7	5

(continued)



TABLE 20.8 (Continued)

SSF	0.10	0.20	0.30	0.40	0.50	0.60	0.70	0.80	0.90
TW D3	167	82	49	33	23	17	12	8	5
TW D4	168	91	58	40	29	21	15	11	7
TW D5	160	89	58	40	29	22	16	12	8
TW E1	198	98	59	40	28	20	15	10	7
TW E2	182	95	59	40	29	21	15	11	7
TW E3	197	115	76	54	39	29	22	16	11
TW E4	178	105	70	50	37	27	20	15	10
TW F1	221	50	23	13	8	5	4	2	1
TW F2	139	53	29	18	12	8	6	4	2
TW F3	116	52	30	19	13	9	7	5	3
TW F4	96	47	28	19	13	9	7	5	3
TW G1	137	44	22	13	9	6	4	3	2
TW G2	101	44	25	16	11	8	5	4	2
TW G3	86	41	24	16	11	8	6	4	2
TW G4	69	34	21	14	10	7	5	3	2
TW H1	89	36	20	13	8	6	4	3	2
TW H2	69	33	19	12	9	6	4	3	2
TW H3	59	28	17	11	8	5	4	3	2
TW H4	46	22	13	9	6	4	3	2	1
TW I1	74	26	13	7	4	2	1	—	—
TW I2	125	62	38	25	18	13	9	7	4
TW I3	133	69	43	29	20	15	11	8	5
TW I4	139	78	51	35	26	19	14	10	7
TW I5	137	80	53	37	27	20	15	11	7
TW J1	164	86	54	36	26	19	14	10	6
TW J2	150	82	53	36	26	19	14	10	7
TW J3	165	101	68	49	36	27	20	15	10
TW J4	153	93	63	46	34	25	19	14	10
DG A1	98	34	—	—	—	—	—	—	—
DG A2	130	55	31	19	11	6	—	—	—
DG A3	173	78	47	32	23	16	11	7	2
DG B1	100	36	17	—	—	—	—	—	—
DG B2	134	58	33	22	15	10	6	—	—
DG B3	177	81	49	33	24	18	14	10	6
DG C1	131	52	28	17	9	—	—	—	—
DG C2	161	71	42	28	20	14	10	6	—
DG C3	205	94	57	39	29	22	17	12	8
SS A1	351	100	50	29	19	13	9	6	4
SS A2	328	135	76	49	33	24	17	12	8
SS A3	330	87	41	24	15	10	6	4	2
SS A4	331	133	74	47	32	22	16	11	7
SS A5	595	98	43	24	15	10	7	4	2
SS A6	324	132	75	48	32	23	16	11	7
SS A7	668	79	32	17	10	6	4	2	1
SS A8	330	129	71	45	30	21	15	10	6
SS B1	236	74	38	23	15	10	7	5	3
SS B2	258	110	63	41	28	20	14	10	6
SS B3	212	65	32	19	12	8	5	3	2
SS B4	251	105	60	39	27	19	13	9	6
SS B5	307	65	30	17	10	7	4	3	2
SS B6	241	104	60	39	27	19	14	10	6
SS B7	264	52	23	12	7	5	3	2	—
SS B8	233	98	56	36	25	17	12	9	5
SS C1	141	60	33	21	14	10	7	5	3
SS C2	161	81	50	33	23	17	12	9	6
SS C3	149	48	25	15	10	7	4	3	2

(continued)

TABLE 20.8 (Continued)

SSF	0.10	0.20	0.30	0.40	0.50	0.60	0.70	0.80	0.90
SS C4	160	73	43	28	19	14	10	7	5
SS D1	317	119	64	39	26	18	13	8	5
SS D2	287	147	90	61	43	31	23	16	10
SS D3	405	113	55	33	21	14	10	6	4
SS D4	295	144	87	58	40	29	21	15	10
SS E1	229	89	48	29	19	13	9	6	4
SS E2	233	118	72	48	34	24	18	12	8
SS E3	283	77	37	22	14	9	6	4	2
SS E4	242	111	65	43	29	21	15	11	7
Medford, Oregon									4930 DD
WW A1	708	64	24	11	—	—	—	—	—
WW A2	212	73	38	22	13	7	3	—	—
WW A3	174	75	41	25	16	9	5	2	—
WW A4	158	74	43	27	17	11	6	3	1
WW A5	149	75	45	29	19	12	7	4	2
WW A6	144	75	46	30	20	13	8	4	2
WW B1	154	43	16	—	—	—	—	—	—
WW B2	162	80	48	31	21	14	9	6	3
WW B3	190	100	62	41	28	19	13	8	5
WW B4	171	99	65	45	32	23	16	11	7
WW B5	160	95	63	45	32	23	17	12	7
WW C1	205	108	67	45	31	21	15	10	6
WW C2	178	99	63	43	30	22	15	10	6
WW C3	189	117	80	57	42	31	23	16	10
WW C4	170	106	72	52	38	28	21	15	9
TW A1	607	63	25	12	5	—	—	—	—
TW A2	222	68	33	19	11	6	2	—	—
TW A3	175	67	36	21	13	8	4	2	—
TW A4	147	64	36	22	14	9	5	3	1
TW B1	327	61	27	14	7	3	—	—	—
TW B2	178	62	32	19	12	7	4	2	—
TW B3	154	60	33	20	12	8	4	2	1
TW B4	143	56	31	19	12	8	5	2	1
TW C1	212	56	27	15	9	5	2	—	—
TW C2	159	55	28	17	11	7	4	2	—
TW C3	154	52	27	16	10	6	4	2	1
TW C4	167	48	24	14	9	5	3	2	—
TW D1	112	34	14	—	—	—	—	—	—
TW D2	177	77	44	28	18	12	8	5	3
TW D3	180	85	50	32	21	14	9	6	3
TW D4	177	93	58	39	27	19	13	9	5
TW D5	168	92	58	40	28	20	14	10	6
TW E1	213	101	60	39	26	18	12	8	4
TW E2	194	98	59	39	27	19	13	9	5
TW E3	208	118	77	53	38	27	20	13	8
TW E4	186	108	71	49	36	26	19	13	8
TW F1	256	53	23	12	5	—	—	—	—
TW F2	153	56	29	17	10	5	2	—	—
TW F3	125	54	30	18	11	7	3	1	—
TW F4	102	48	28	18	11	7	4	2	1
TW G1	153	46	22	12	7	—	—	—	—
TW G2	109	46	25	15	9	5	3	1	—
TW G3	92	42	24	15	9	6	3	2	—
TW G4	74	35	20	13	8	5	3	2	—
TW H1	97	38	20	12	7	4	1	—	—

(continued)

TABLE 20.8 (Continued)

SSF	0.10	0.20	0.30	0.40	0.50	0.60	0.70	0.80	0.90
TW H2	75	34	19	12	7	5	3	1	—
TW H3	63	29	17	10	7	4	3	1	—
TW H4	49	23	13	8	5	3	2	1	—
TW I1	83	27	10	—	—	—	—	—	—
TW I2	133	64	38	24	16	11	7	4	2
TW I3	142	71	43	28	19	13	9	5	3
TW I4	146	80	51	35	25	17	12	8	5
TW I5	144	82	53	37	26	19	13	9	6
TW J1	175	89	54	36	24	17	11	7	4
TW J2	158	85	53	36	25	18	12	8	5
TW J3	173	103	69	48	35	26	18	13	8
TW J4	160	96	64	45	33	24	17	12	8
DG A1	110	35	—	—	—	—	—	—	—
DG A2	142	58	32	18	9	—	—	—	—
DG A3	187	82	48	32	22	15	9	5	—
DG B1	110	40	15	—	—	—	—	—	—
DG B2	146	61	35	21	13	7	—	—	—
DG B3	193	84	51	34	24	17	12	7	3
DG C1	144	57	29	13	—	—	—	—	—
DG C2	177	75	44	28	19	12	6	—	—
DG C3	224	98	60	41	29	21	14	10	5
SS A1	415	110	51	28	16	9	4	2	—
SS A2	372	146	79	48	31	21	14	8	5
SS A3	397	96	42	21	10	—	—	—	—
SS A4	379	144	76	46	29	19	12	7	4
SS A5	732	111	45	23	12	5	—	—	—
SS A6	368	143	77	47	30	20	13	8	4
SS A7	846	90	33	14	—	—	—	—	—
SS A8	379	140	73	44	27	17	11	6	3
SS B1	274	81	38	21	12	6	3	—	—
SS B2	288	117	65	40	26	18	12	7	4
SS B3	249	71	33	17	8	—	—	—	—
SS B4	282	113	62	38	25	16	11	7	4
SS B5	368	72	30	15	7	—	—	—	—
SS B6	269	111	62	30	25	17	11	7	4
SS B7	323	58	23	10	—	—	—	—	—
SS B8	262	106	57	35	23	15	9	6	3
SS C1	153	62	33	19	11	5	—	—	—
SS C2	172	83	50	32	22	15	10	6	3
SS C3	166	51	24	13	7	3	—	—	—
SS C4	173	76	43	27	18	12	8	5	3
SS D1	367	129	65	37	22	13	7	3	1
SS D2	318	156	92	60	40	27	18	12	7
SS D3	480	124	57	31	18	10	5	2	—
SS D4	328	153	89	57	38	26	17	11	6
SS E1	262	95	48	27	15	7	—	—	—
SS E2	257	124	73	47	31	21	14	9	5
SS E3	334	84	38	20	10	4	—	—	—
SS E4	269	118	67	42	27	18	12	7	4
Boston, Massachusetts									5621 DD
WW A1	368	28	9	—	—	—	—	—	—
WW A2	119	41	20	12	7	5	3	2	—
WW A3	101	43	24	15	10	6	4	3	1
WW A4	93	44	26	16	11	7	5	3	2
WW A5	89	45	27	18	12	8	6	4	2

(continued)

TABLE 20.8 (Continued)

SSF	0.10	0.20	0.30	0.40	0.50	0.60	0.70	0.80	0.90
WW A6	87	46	28	19	13	9	6	4	3
WW B1	59	—	—	—	—	—	—	—	—
WW B2	103	52	31	21	15	10	7	5	3
WW B3	123	66	41	28	20	14	10	7	5
WW B4	118	70	46	33	24	18	13	9	6
WW B5	113	69	46	33	25	18	14	10	7
WW C1	135	72	46	31	22	16	12	8	5
WW C2	121	68	44	31	22	16	12	9	6
WW C3	136	86	60	44	33	25	19	14	9
WW C4	124	78	54	40	30	23	17	12	8
TW A1	324	30	11	4	—	—	—	—	—
TW A2	126	37	18	10	6	4	2	1	—
TW A3	102	39	21	13	8	5	3	2	1
TW A4	88	38	22	14	9	6	4	3	2
TW B1	180	32	13	7	4	2	—	—	—
TW B2	104	36	19	11	7	5	3	2	1
TW B3	92	36	19	12	8	5	3	2	1
TW B4	86	34	19	12	8	5	4	2	1
TW C1	122	32	15	9	5	3	2	1	—
TW C2	95	33	17	10	7	4	3	2	1
TW C3	93	31	16	10	6	4	3	2	1
TW C4	102	29	15	9	6	4	3	2	1
TW D1	45	—	—	—	—	—	—	—	—
TW D2	112	49	28	18	12	9	6	4	3
TW D3	113	54	32	21	15	10	7	5	3
TW D4	121	64	41	28	20	15	11	8	5
TW D5	118	66	42	30	21	16	12	8	6
TW E1	138	67	40	27	18	13	9	7	4
TW E2	130	66	41	28	20	14	10	7	5
TW E3	146	84	56	39	29	21	16	11	8
TW E4	133	78	52	37	27	20	15	11	7
TW F1	134	25	10	4	—	—	—	—	—
TW F2	86	30	16	9	5	3	2	1	—
TW F3	72	31	17	11	7	4	3	2	1
TW F4	61	29	17	11	7	5	3	2	1
TW G1	83	24	11	6	3	2	—	—	—
TW G2	63	26	14	9	5	4	2	1	—
TW G3	54	25	14	9	6	4	3	2	1
TW G4	45	21	12	8	5	4	3	2	1
TW H1	54	21	11	6	4	2	1	—	—
TW H2	44	20	11	7	5	3	2	1	—
TW H3	38	17	10	6	4	3	2	1	—
TW H4	30	14	8	5	3	2	2	1	—
TW I1	30	—	—	—	—	—	—	—	—
TW I2	84	41	24	16	11	8	6	4	2
TW I3	91	46	28	19	13	9	7	5	3
TW I4	100	56	36	25	18	13	10	7	5
TW I5	101	58	38	27	20	15	11	8	5
TW J1	114	59	37	25	17	12	9	6	4
TW J2	107	58	37	25	18	13	10	7	4
TW J3	123	75	51	36	27	20	15	11	7
TW J4	115	70	47	34	25	19	14	10	7
DG A1	43	—	—	—	—	—	—	—	—
DG A2	85	34	18	9	—	—	—	—	—
DG A3	125	56	33	22	16	11	7	4	—

(continued)

TABLE 20.8 (Continued)

SSF	0.10	0.20	0.30	0.40	0.50	0.60	0.70	0.80	0.90
DG B1	44	—	—	—	—	—	—	—	—
DG B2	87	36	20	12	7	—	—	—	—
DG B3	129	58	35	24	17	13	9	6	3
DG C1	71	23	—	—	—	—	—	—	—
DG C2	109	47	27	17	12	8	4	—	—
DG C3	151	68	41	28	21	16	12	8	5
SS A1	230	61	29	16	10	6	4	2	1
SS A2	231	93	52	33	22	15	11	7	5
SS A3	205	48	20	10	4	—	—	—	—
SS A4	229	90	49	31	20	14	9	6	4
SS A5	389	58	23	11	6	3	—	—	—
SS A6	226	91	50	32	21	15	10	7	4
SS A7	420	40	12	—	—	—	—	—	—
SS A8	226	86	46	28	19	12	8	6	3
SS B1	151	44	21	12	7	4	2	1	—
SS B2	183	77	43	28	19	13	9	6	4
SS B3	129	36	16	8	3	—	—	—	—
SS B4	176	73	41	26	17	12	8	6	4
SS B5	193	36	15	7	3	—	—	—	—
SS B6	169	72	41	26	18	12	9	6	4
SS B7	157	25	7	—	—	—	—	—	—
SS B8	160	66	37	23	16	11	7	5	3
SS C1	84	33	17	10	6	4	2	1	—
SS C2	110	54	33	22	15	11	8	5	3
SS C3	91	26	12	7	4	2	—	—	—
SS C4	109	48	28	18	12	9	6	4	3
SS D1	206	73	38	22	14	9	5	3	2
SS D2	203	103	63	42	29	21	15	10	6
SS D3	264	69	32	18	10	6	4	2	1
SS D4	208	100	60	39	27	19	14	9	6
SS E1	140	51	25	14	8	4	2	—	—
SS E2	161	80	48	32	22	15	11	7	5
SS E3	177	44	19	10	5	2	—	—	—
SS E4	166	75	43	28	19	13	9	6	4
Madison, Wisconsin									7730 DD
WW A1	278	—	—	—	—	—	—	—	—
WW A2	91	27	12	—	—	—	—	—	—
WW A3	77	30	15	8	3	—	—	—	—
WW A4	72	32	17	10	5	—	—	—	—
WW A5	69	33	19	11	7	4	—	—	—
WW A6	67	34	19	12	7	4	2	—	—
WW B1	—	—	—	—	—	—	—	—	—
WW B2	84	41	24	15	10	7	5	3	2
WW B3	102	53	32	21	15	10	7	5	3
WW B4	101	59	39	27	19	14	10	7	5
WW B5	98	59	39	28	20	15	11	8	5
WW C1	113	59	37	25	17	12	8	6	3
WW C2	103	57	37	25	18	13	9	6	4
WW C3	119	75	51	37	28	21	15	11	7
WW C4	109	68	47	34	25	19	14	10	7
TW A1	249	16	—	—	—	—	—	—	—
TW A2	97	26	11	4	—	—	—	—	—
TW A3	79	28	13	7	3	—	—	—	—
TW A4	69	28	15	9	5	3	—	—	—

(continued)

TABLE 20.8 (Continued)

SSF	0.10	0.20	0.30	0.40	0.50	0.60	0.70	0.80	0.90
TW B1	139	20	5	—	—	—	—	—	—
TW B2	81	26	12	6	3	—	—	—	—
TW B3	72	27	13	7	4	2	—	—	—
TW B4	69	26	13	8	5	3	1	—	—
TW C1	96	23	10	4	—	—	—	—	—
TW C2	76	25	12	7	4	2	—	—	—
TW C3	75	24	12	7	4	2	1	—	—
TW C4	84	23	11	6	4	2	1	—	—
TW D1	—	—	—	—	—	—	—	—	—
TW D2	91	39	22	13	9	6	4	2	1
TW D3	93	43	25	16	10	7	5	3	1
TW D4	103	54	34	23	16	12	8	6	4
TW D5	102	56	36	25	18	13	10	7	4
TW E1	115	54	32	21	14	10	7	4	3
TW E2	110	55	34	22	16	11	8	5	3
TW E3	126	72	47	33	24	18	13	9	6
TW E4	116	68	45	32	23	17	13	9	6
TW F1	99	13	—	—	—	—	—	—	—
TW F2	65	20	8	—	—	—	—	—	—
TW F3	55	22	11	5	—	—	—	—	—
TW F4	47	21	11	7	4	2	—	—	—
TW G1	61	14	—	—	—	—	—	—	—
TW G2	47	18	8	4	—	—	—	—	—
TW G3	42	18	9	5	3	—	—	—	—
TW G4	35	16	9	5	3	2	—	—	—
TW H1	41	13	6	—	—	—	—	—	—
TW H2	34	14	7	4	2	—	—	—	—
TW H3	29	13	7	4	2	1	—	—	—
TW H4	24	10	6	3	2	1	—	—	—
TW I1	—	—	—	—	—	—	—	—	—
TW I2	68	32	18	12	8	5	3	2	1
TW I3	75	37	22	14	10	7	4	3	2
TW I4	85	47	30	21	15	11	8	5	3
TW I5	87	50	33	23	16	12	9	6	4
TW J1	95	48	29	19	13	9	6	4	3
TW J2	91	48	30	21	14	10	7	5	3
TW J3	106	65	43	31	23	17	12	9	6
TW J4	100	61	41	29	21	16	12	9	6
DG A1	—	—	—	—	—	—	—	—	—
DG A2	68	25	11	—	—	—	—	—	—
DG A3	109	47	28	18	12	8	5	—	—
DG B1	—	—	—	—	—	—	—	—	—
DG B2	70	27	14	6	—	—	—	—	—
DG B3	114	50	30	20	14	10	7	4	—
DG C1	47	—	—	—	—	—	—	—	—
DG C2	91	37	21	13	7	—	—	—	—
DG C3	133	59	35	24	17	13	9	6	3
SS A1	192	47	20	9	3	—	—	—	—
SS A2	200	78	42	26	17	12	8	5	3
SS A3	166	32	—	—	—	—	—	—	—
SS A4	197	74	39	23	15	10	6	4	2
SS A5	329	42	13	—	—	—	—	—	—
SS A6	195	75	40	25	16	11	7	5	3
SS A7	349	22	—	—	—	—	—	—	—
SS A8	192	69	36	21	13	8	5	3	2

(continued)

TABLE 20.8 (Continued)

SSF	0.10	0.20	0.30	0.40	0.50	0.60	0.70	0.80	0.90
SS B1	122	32	13	5	—	—	—	—	—
SS B2	158	64	36	22	15	10	7	5	3
SS B3	100	22	—	—	—	—	—	—	—
SS B4	150	60	33	29	13	9	6	4	2
SS B5	156	24	—	—	—	—	—	—	—
SS B6	145	59	33	20	13	9	6	4	2
SS B7	122	—	—	—	—	—	1—	—	—
SS B8	136	54	29	18	11	7	5	3	2
SS C1	61	20	7	—	—	—	—	—	—
SS C2	90	43	25	16	11	7	5	3	2
SS C3	67	16	—	—	—	—	—	—	—
SS C4	90	38	22	13	9	6	4	2	1
SS D1	169	56	26	13	6	—	—	—	—
SS D2	175	86	51	34	23	16	11	7	5
SS D3	221	52	21	10	—	—	—	—	—
SS D4	179	84	49	32	21	15	10	7	4
SS E1	108	34	12	—	—	—	—	—	—
SS E2	135	65	38	24	16	11	7	5	3
SS E3	141	29	8	—	—	—	—	—	—
SS E4	140	61	34	21	14	9	6	4	2

Source: From PSDH, *Passive Solar Design Handbook*, Los Alamos National Laboratory, Van Nostrand Reinhold, New York, 1984.

The LCR method allows no variation from the 94 reference passive designs. To treat off-reference designs, sensitivity curves have been produced that illustrate the effect on SSF of varying one or two design variables. These curves were produced for the six “representative” cities, chosen for their wide geographical and climatological ranges. Several of these SSF “sensitivity curves” are presented in [Figure 20.49](#) for storage wall (a, b, c) and sunspace (d) design variations.

### Example 20.3.4

The previously used 2100 ft.<sup>2</sup> building with NLC = 11,800 Btu/FDD is preliminarily designed to be located in Medford, Oregon, with 180 ft.<sup>2</sup> of 12-in thick vented Trombe wall and 130 ft.<sup>2</sup> of direct gain, both systems with double glazing, nighttime insulation, and 30 Btu/ft.<sup>2</sup> thermal storage capacity. Determine the annual auxiliary energy needed by this design.

**Solution.** Step 1 yields:

$$\text{NLC} = 11,800 \text{ Btu/FDD.}$$

$$A_p = 180 + 130 = 320 \text{ ft.}^2$$

$$\text{LCR} = 11,800/320 = 36.8 \text{ Btu/FDD ft.}^2$$

Step 2 yields: From [Table 20.7](#) the short designations for the appropriate systems are

TWD4 (Trombe wall)

DGA3 (Direct gain)

Step 3 yields: From [Table 20.8](#) for Medford, Oregon, with LCR = 36.8,

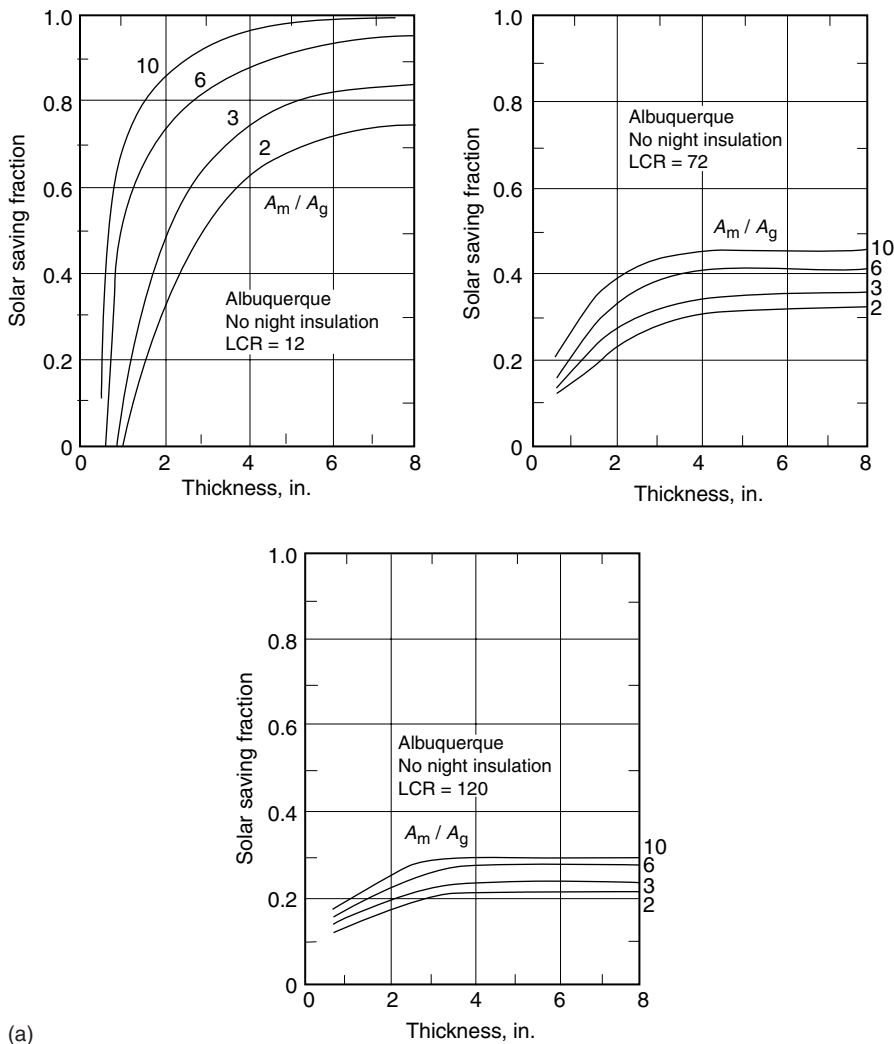


**FIGURE 20.49** (a) Storage wall: Mass thickness. Sensitivity of SSF to Off-Reference conditions. (b) Storage wall:  $\rho ck$  product. (c) Storage wall: Number of glazings. (d) Sunspace : Storage volume to projected area ratio. (From PSDH. *Passive Solar Design Handbook*. Volume One: Passive Solar Design Concepts, DOE/CS-0127/1, March 1980. Prepared by Total Environmental Action, Inc. (B. Anderson, C. Michal, P. Temple, and D. Lewis); Volume Two: *Passive Solar Design Analysis*, DOE/CS-0127/2, January 1980. Prepared by Los Alamos Scientific Laboratory (J. D. Balcomb, D. Barley, R McFarland, J. Perry, W. Wray and S. Noll). U.S. Department of Energy, Washington, DC, 1980.)

$$TWD4 : SSF(TW) = 0.42$$

$$DGA3 : SSF(DG) = 0.37$$

Determine the “weighted area” average SSF:

$$SSF = \frac{180(0.42) + 130(0.37)}{320} = 0.39.$$



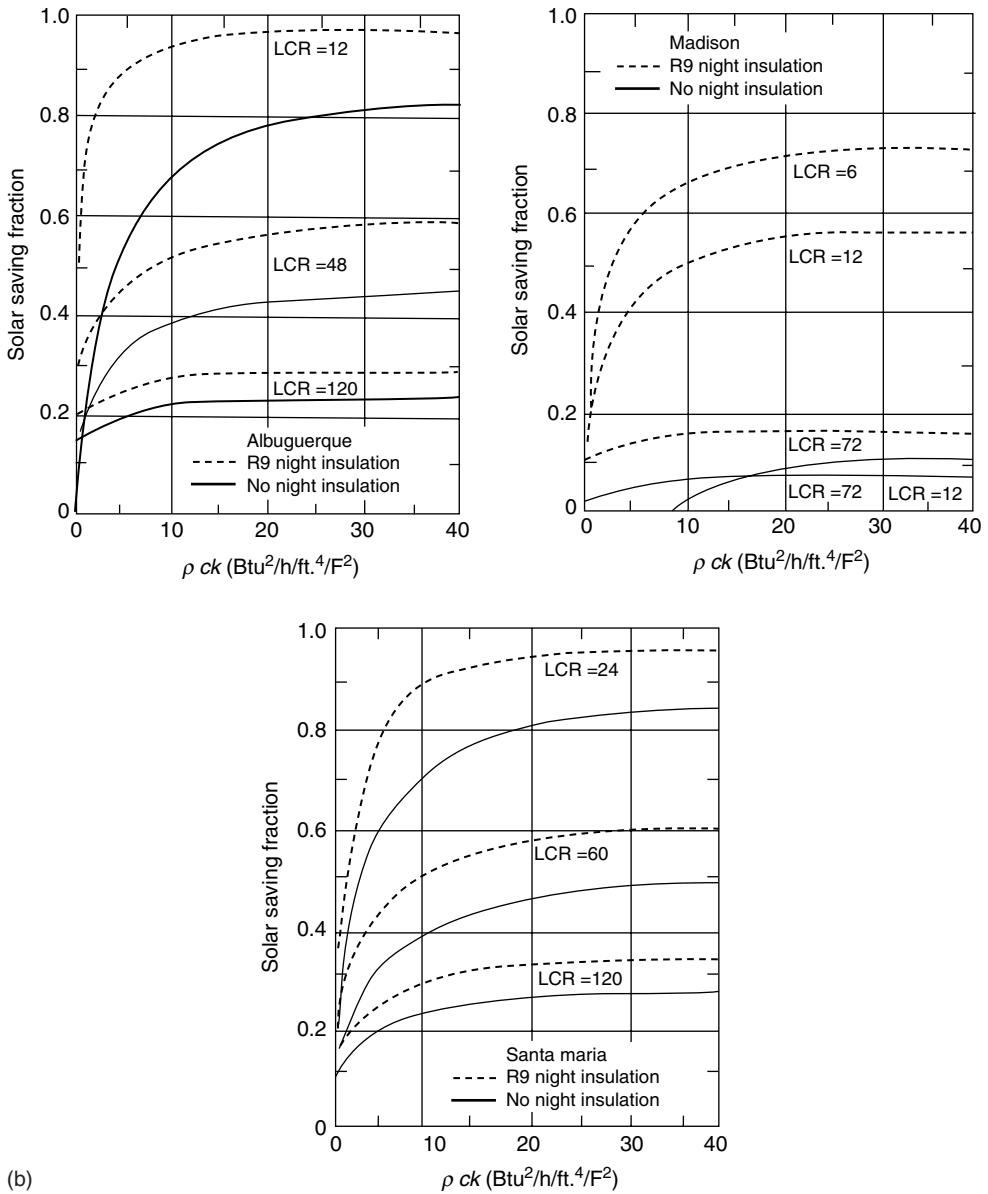


FIGURE 20.49 (continued)

Step 4 yields: Using Equation 20.73 and reading 4930 FDD from Table 20.8,

$$Q_{\text{aux}} = (1 - 0.39) \times 11,800 \text{ Btu} \times 4,930 \text{ FDD} = 35.5 \times 10^6 \text{ Btu annually.}$$

Using the reference system characteristics yields the thermal storage size: Trombe wall ( $\rho ck = 30$ , concrete properties from Table 20.7c):

$$\begin{aligned} m \text{ (TW)} &= \text{density} \times \text{area} \times \text{thickness} \\ &= 150 \text{ lbm/ft}^3 \times 180 \text{ ft}^2 \times 1 \text{ ft.} \\ &= 27,000 \text{ lbm.} \end{aligned}$$

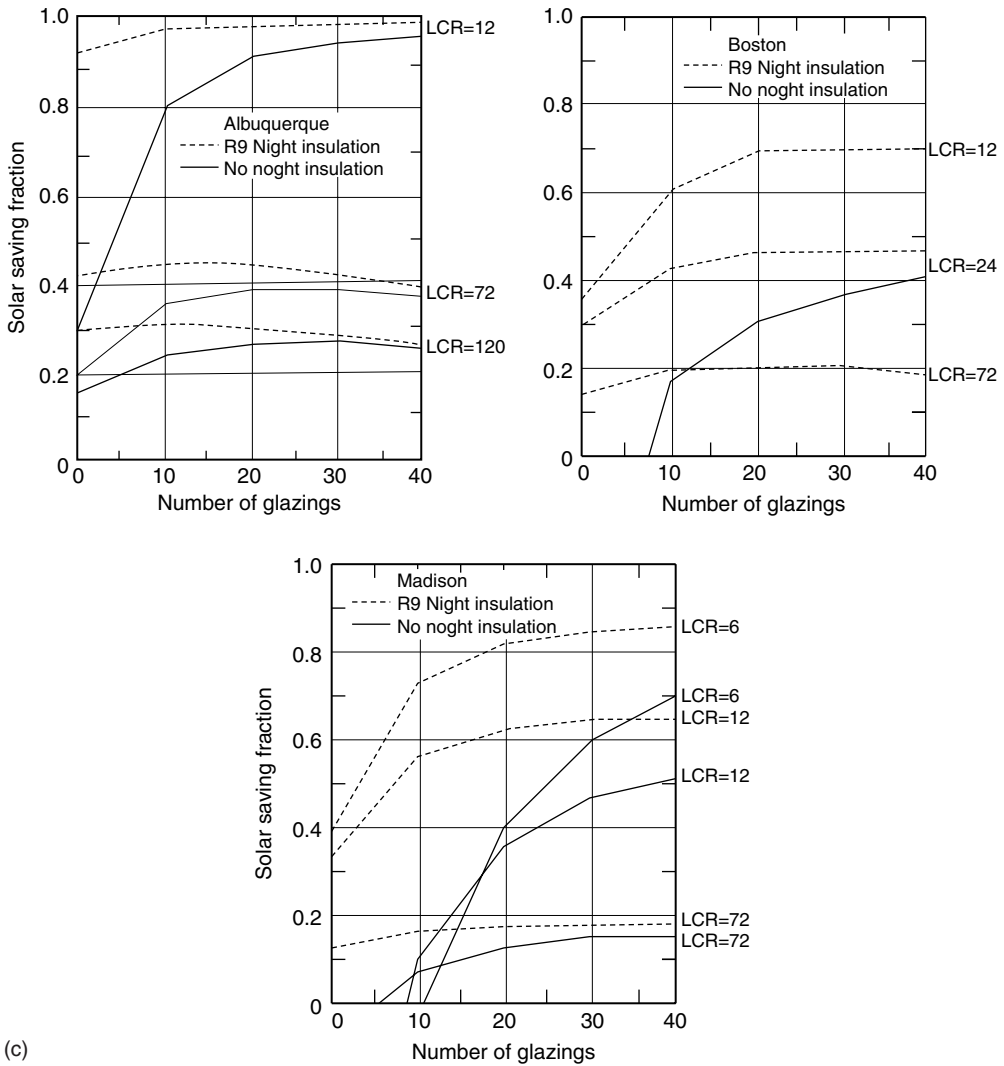


FIGURE 20.49 (continued)

Direct Gain ( $\rho_{ck}=30$ , concrete properties), using mass area to glazing area ratio of 6:

$$\text{mass area} = 6 \times 130 = 780 \text{ ft.}^2 \text{ of } 2'' \text{ thick concrete}$$

$$\begin{aligned} m(\text{DG}) &= 150 \text{ lbm/ft.}^3 \times 780 \text{ ft.}^2 \times 1/6 \text{ ft.} \\ &= 19,500 \text{ lbm} \end{aligned}$$

Using the LCR method allows a basic design of passive system types for the 94 reference systems, and the resulting annual performance. A bit more design variation can be obtained by using the sensitivity curves of Figure 20.49 to modify the SSF of a particular reference system. For instance, a direct gain system SSF of 0.37 would increase by approximately 0.03 if the mass-glazing-area ratio (assumed 6) were increased to 10, and would decrease by about 0.04 if the mass-glazing-area ratio were decreased to 3. This information provides a designer with quantitative information for making trade-offs.

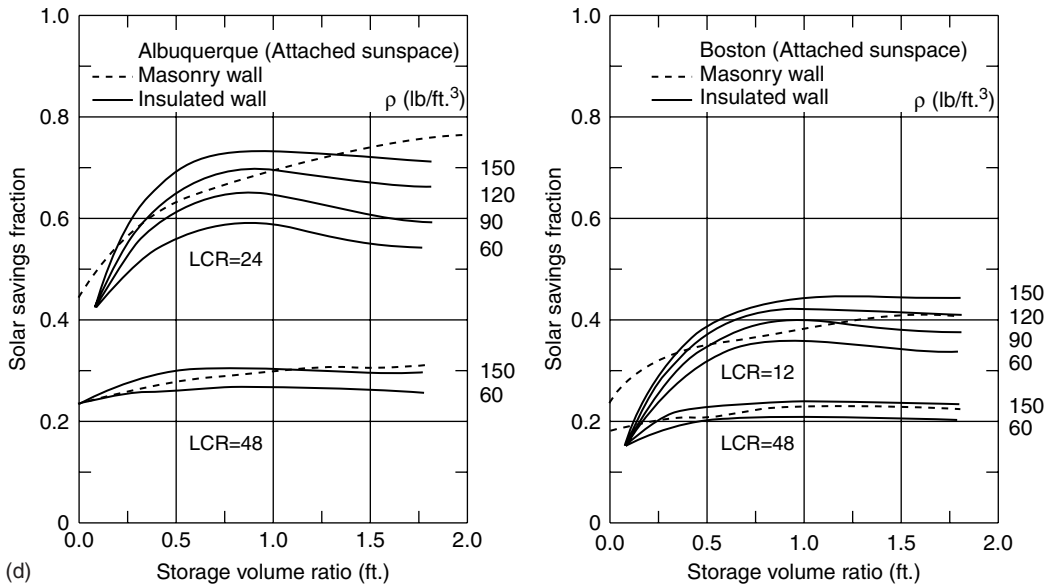


FIGURE 20.49 (continued)

**20.3.3.10 The Third Level: SLR Method**

The solar-load ratio (SLR) method calculates monthly performance, and the terms and values used are monthly based. The method allows the use of specific location weather data and the 94 reference design passive systems (Table 20.7). In addition, the sensitivity curves (Figure 20.49) can again be used to define performance outside the reference design systems. The result of the SLR method is the determination of the monthly heating auxiliary energy required that is then summed to give the annual requirement for auxiliary heating energy. Generally, the SLR method gives annual values within  $\pm 3\%$  of detailed simulation results, but the monthly values may vary more (PSDH 1984; Duffie and Beckman 1991). Thus, the monthly SLR method is more “accurate” than the rule-of-thumb methods, plus providing the designer with system performance on a month-by-month basis.

The SLR method uses equations and correlation parameters for each of the 94 reference systems combined with the insolation absorbed by the system, the monthly degree days, and the system’s LCR to determine the monthly SSF. These correlation parameters are listed in Table 20.9 as A, B, C, D, R, G, H, and LCRs for each reference system (PSDH 1984). The correlation equations are

$$SSF = 1 - K(1 - F), \tag{20.76}$$

where

$$K = 1 + G/LCR, \tag{20.77}$$

$$F = \begin{cases} AX, & \text{when } X < R \\ B - C \exp(-DX), & \text{when } X > R \end{cases} \tag{20.78}$$

$$X = \frac{S/DD - (LCRs) H}{(LCR)K}. \tag{20.79}$$

and X is called the *generalized solar load ratio*. The term S is the monthly insolation absorbed by the system per unit of solar projected area. Monthly average daily insolation data on a vertical south facing

**TABLE 20.9** SLR Correlation Parameters for the 94 Reference Systems

Type	A	B	C	D	R	G	H	LCRs	STDV
WW A1	0.0000	1.0000	0.9172	0.4841	-9.0000	0.00	1.17	13.0	0.053
WW A2	0.0000	1.0000	0.9833	0.7603	-9.0000	0.00	0.92	13.0	0.046
WW A3	0.0000	1.0000	1.0171	0.8852	-9.0000	0.00	0.85	13.0	0.040
WW A4	0.0000	1.0000	1.0395	0.9569	-9.0000	0.00	0.81	13.0	0.037
WW A5	0.0000	1.0000	1.0604	1.0387	-9.0000	0.00	0.78	13.0	0.034
WW A6	0.0000	1.0000	1.0735	1.0827	-9.0000	0.00	0.76	13.0	0.033
WW B1	0.0000	1.0000	0.9754	0.5518	-9.0000	0.00	0.92	22.0	0.051
WW B2	0.0000	1.0000	1.0487	1.0851	-9.0000	0.00	0.78	9.2	0.036
WW B3	0.0000	1.0000	1.0673	1.0087	-9.0000	0.00	0.95	8.9	0.038
WW B4	0.0000	1.0000	1.1028	1.1811	-9.0000	0.00	0.74	5.8	0.034
WW B5	0.0000	1.0000	1.1146	1.2771	-9.0000	0.00	0.56	4.5	0.032
WW C1	0.0000	1.0000	1.0667	1.0437	-9.0000	0.00	0.62	12.0	0.038
WW C2	0.0000	1.0000	1.0846	1.1482	-9.0000	0.00	0.59	8.7	0.035
WW C3	0.0000	1.0000	1.1419	1.1756	-9.0000	0.00	0.28	5.5	0.033
WW C4	0.0000	1.0000	1.1401	1.2378	-9.0000	0.00	0.23	4.3	0.032
TW A1	0.0000	1.0000	0.9194	0.4601	-9.0000	0.00	1.11	13.0	0.048
TW A2	0.0000	1.0000	0.9680	0.6318	-9.0000	0.00	0.92	13.0	0.043
TW A3	0.0000	1.0000	0.9964	0.7123	-9.0000	0.00	0.85	13.0	0.038
TW A4	0.0000	1.0000	1.0190	0.7332	-9.0000	0.00	0.79	13.0	0.032
TW B1	0.0000	1.0000	0.9364	0.4777	-9.0000	0.00	1.01	13.0	0.045
TW B2	0.0000	1.0000	0.9821	0.6020	-9.0000	0.00	0.85	13.0	0.038
TW B3	0.0000	1.0000	0.9980	0.6191	-9.0000	0.00	0.80	13.0	0.033
TW B4	0.0000	1.0000	0.9981	0.5615	-9.0000	0.00	0.76	13.0	0.028
TW C1	0.0000	1.0000	0.9558	0.4709	-9.0000	0.00	0.89	13.0	0.039
TW C2	0.0000	1.0000	0.9788	0.4964	-9.0000	0.00	0.79	13.0	0.033
TW C3	0.0000	1.0000	0.9760	0.4519	-9.0000	0.00	0.76	13.0	0.029
TW C4	0.0000	1.0000	0.9588	0.3612	-9.0000	0.00	0.73	13.0	0.026
TW D1	0.0000	1.0000	0.9842	0.4418	-9.0000	0.00	0.89	22.0	0.040
TW D2	0.0000	1.0000	1.0150	0.8994	-9.0000	0.00	0.80	9.2	0.036
TW D3	0.0000	1.0000	1.0346	0.7810	-9.0000	0.00	1.08	8.9	0.036
TW D4	0.0000	1.0000	1.0606	0.9770	-9.0000	0.00	0.85	5.8	0.035
TW D5	0.0000	1.0000	1.0721	1.0718	-9.0000	0.00	0.61	4.5	0.033
TW E1	0.0000	1.0000	1.0345	0.8753	-9.0000	0.00	0.68	12.0	0.037
TW E2	0.0000	1.0000	1.0476	1.0050	-9.0000	0.00	0.66	8.7	0.035
TW E3	0.0000	1.0000	1.0919	1.0739	-9.0000	0.00	0.61	5.5	0.034
TW E4	0.0000	1.0000	1.0971	1.1429	-9.0000	0.00	0.47	4.3	0.033
TW F1	0.0000	1.0000	0.9430	0.4744	-9.0000	0.00	1.09	13.0	0.047
TW F2	0.0000	1.0000	0.9900	0.6053	-9.0000	0.00	0.93	13.0	0.041
TW F3	0.0000	1.0000	1.0189	0.6502	-9.0000	0.00	0.86	13.0	0.036
TW F4	0.0000	1.0000	1.0419	0.6258	-9.0000	0.00	0.80	13.0	0.032
TW G1	0.0000	1.0000	0.9693	0.4714	-9.0000	0.00	1.01	13.0	0.042
TW G2	0.0000	1.0000	1.0133	0.5462	-9.0000	0.00	0.88	13.0	0.035
TW G3	0.0000	1.0000	1.0325	0.5269	-9.0000	0.00	0.82	13.0	0.031
TW G4	0.0000	1.0000	1.0401	0.4400	-9.0000	0.00	0.77	13.0	0.030
TW H1	0.0000	1.0000	1.0002	0.4356	-9.0000	0.00	0.93	13.0	0.034
TW H2	0.0000	1.0000	1.0280	0.4151	-9.0000	0.00	0.83	13.0	0.030
TW H3	0.0000	1.0000	1.0327	0.3522	-9.0000	0.00	0.78	13.0	0.029
TW H4	0.0000	1.0000	1.0287	0.2600	-9.0000	0.00	0.74	13.0	0.024
TW I1	0.0000	1.0000	0.9974	0.4036	-9.0000	0.00	0.91	22.0	0.038
TW I2	0.0000	1.0000	1.0386	0.8313	-9.0000	0.00	0.80	9.2	0.034
TW I3	0.0000	1.0000	1.0514	0.6886	-9.0000	0.00	1.01	8.9	0.034
TW I4	0.0000	1.0000	1.0781	0.8952	-9.0000	0.00	0.82	5.8	0.032
TW I5	0.0000	1.0000	1.0902	1.0284	-9.0000	0.00	0.65	4.5	0.032
TW J1	0.0000	1.0000	1.0537	0.8227	-9.0000	0.00	0.65	12.0	0.037
TW J2	0.0000	1.0000	1.0677	0.9312	-9.0000	0.00	0.62	8.7	0.035

*(continued)*

TABLE 20.9 (Continued)

Type	A	B	C	D	R	G	H	LCRs	STDV
TW J3	0.0000	1.0000	1.1153	0.9831	-9.0000	0.00	0.44	5.5	0.034
TW J4	0.0000	1.0000	1.1154	1.0607	-9.0000	0.00	0.38	4.3	0.033
DG A1	0.5650	1.0090	1.0440	0.7175	0.3931	9.36	0.00	0.0	0.046
DG A2	0.5906	1.0060	1.0650	0.8099	0.4681	5.28	0.00	0.0	0.039
DG A3	0.5442	0.9715	1.1300	0.9273	0.7068	2.64	0.00	0.0	0.036
DG B1	0.5739	0.9948	1.2510	1.0610	0.7905	9.60	0.00	0.0	0.042
DG B2	0.6180	1.0000	1.2760	1.1560	0.7528	5.52	0.00	0.0	0.035
DG B3	0.5601	0.9839	1.3520	1.1510	0.8879	2.38	0.00	0.0	0.032
DG C1	0.6344	0.9887	1.5270	1.4380	0.8632	9.60	0.00	0.0	0.039
DG C2	0.6763	0.9994	1.4000	1.3940	0.7604	5.28	0.00	0.0	0.033
DG C3	0.6182	0.9859	1.5660	1.4370	0.8990	2.40	0.00	0.0	0.031
SS A1	0.0000	1.0000	0.9587	0.4770	-9.0000	0.00	0.83	18.6	0.027
SS A2	0.0000	1.0000	0.9982	0.6614	-9.0000	0.00	0.77	10.4	0.026
SS A3	0.0000	1.0000	0.9552	0.4230	-9.0000	0.00	0.83	23.6	0.030
SS A4	0.0000	1.0000	0.9956	0.6277	-9.0000	0.00	0.80	12.4	0.026
SS A5	0.0000	1.0000	0.9300	0.4041	-9.0000	0.00	0.96	18.6	0.031
SS A6	0.0000	1.0000	0.9981	0.6660	-9.0000	0.00	0.86	10.4	0.028
SS A7	0.0000	1.0000	0.9219	0.3225	-9.0000	0.00	0.96	23.6	0.035
SS A8	0.0000	1.0000	0.9922	0.6173	-9.0000	0.00	0.90	12.4	0.028
SS B1	0.0000	1.0000	0.9683	0.4954	-9.0000	0.00	0.84	16.3	0.028
SS B2	0.0000	1.0000	1.0029	0.6802	-9.0000	0.00	0.74	8.5	0.026
SS B3	0.0000	1.0000	0.9689	0.4685	-9.0000	0.00	0.82	19.3	0.029
SS B4	0.0000	1.0000	1.0029	0.6641	-9.0000	0.00	0.76	9.7	0.026
SS B5	0.0000	1.0000	0.9408	0.3866	-9.0000	0.00	0.97	16.3	0.030
SS B6	0.0000	1.0000	1.0068	0.6778	-9.0000	0.00	0.84	8.5	0.028
SS B7	0.0000	1.0000	0.9395	0.3363	-9.0000	0.00	0.95	19.3	0.032
SS B8	0.0000	1.0000	1.0047	0.6469	-9.0000	0.00	0.87	9.7	0.027
SS C1	0.0000	1.0000	1.0087	0.7683	-9.0000	0.00	0.76	16.3	0.025
SS C2	0.0000	1.0000	1.0412	0.9281	-9.0000	0.00	0.78	10.0	0.027
SS C3	0.0000	1.0000	0.9699	0.5106	-9.0000	0.00	0.79	16.3	0.024
SS C4	0.0000	1.0000	1.0152	0.7523	-9.0000	0.00	0.81	10.0	0.025
SS D1	0.0000	1.0000	0.9889	0.6643	-9.0000	0.00	0.84	17.8	0.028
SS D2	0.0000	1.0000	1.0493	0.8753	-9.0000	0.00	0.70	9.9	0.028
SS D3	0.0000	1.0000	0.9570	0.5285	-9.0000	0.00	0.90	17.8	0.029
SS D4	0.0000	1.0000	1.0356	0.8142	-9.0000	0.00	0.73	9.9	0.028
SS E1	0.0000	1.0000	0.9968	0.7004	-9.0000	0.00	0.77	19.6	0.027
SS E2	0.0000	1.0000	1.0468	0.9054	-9.0000	0.00	0.76	10.8	0.027
SS E3	0.0000	1.0000	0.9565	0.4827	-9.0000	0.00	0.81	19.6	0.028
SS E4	0.0000	1.0000	1.0214	0.7694	-9.0000	0.00	0.79	10.8	0.027

Source: From PSDH, *Passive Solar Design Handbook*, Los Alamos National Laboratory, Van Nostrand Reinhold, New York, 1984.

surface can be found and/or calculated using various sources (PSDH 1984; McQuiston and Parker 1994) and the  $S$  term can be determined by multiplying by a transmission and an absorption factor and the number of days in the month. Absorption factors for all systems are close to 0.96 (PSDH 1984), whereas the transmission is approximately 0.9 for single glazing, 0.8 for double glazing, and 0.7 for triple glazing.

### Example 20.3.5

For a vented, 180 ft.<sup>2</sup>, double-glazed with night insulation, 12-in thick Trombe wall system (TWD4) in a NLC=11,800 Btu/FDD house in Medford, Oregon, determine the auxiliary energy required in January.

**Solution.** Weather data for Medford, Oregon (PSDH 1984) yields for January ( $N=31$ , days): daily vertical surface insolation=565 Btu/ft.<sup>2</sup> and 880 FDD, so  $S=(31)(565)(0.8)(0.96)=13,452$  Btu/ft.<sup>2</sup> month.

$$\text{LCR} = \text{NLC}/A_p = 11,800/180 = 65.6 \text{ Btu/FDD ft.}^2.$$

From Table 20.9 at TWD4:  $A=0$ ,  $B=1$ ,  $C=1.0606$ ,  $D=0.977$ ,  $R=-9$ ,  $G=0$ ,  $H=0.85$ ,  $\text{LCRs}=5.8 \text{ Btu/FDD ft.}^2$ .

Substituting into Equation 20.77 gives

$$K = 1 + 0/65.6 = 1.$$

Equation 20.79 gives

$$X = \frac{(13,452/880) - (5.8 \times 0.85)}{65.6 \times 1} = 0.16.$$

Equation 20.78 gives

$$F = 1 - 1.0606 e^{-0.977 \times 0.16} = 0.09,$$

and Equation 20.76 gives

$$\text{SSF} = 1 - 1(1 - 0.09) = 0.09.$$

The January auxiliary energy required can be calculated using Equation 20.73:

$$\begin{aligned} Q_{\text{aux}}(\text{Jan}) &= (1 - \text{SSF}) \times \text{NLC} \times (\text{Number of degree days}) \\ &= (1 - 0.09) \times 11,800 \times 880 \\ &= 9,450,000 \text{ Btu.} \end{aligned}$$

As mentioned, the use of sensitivity curves (PSDH 1984) as in Figure 20.49 will allow SSF to be determined for many off-reference system design conditions involving storage mass, number of glazings, and other more esoteric parameters. Also, the use of multiple passive system types within one building would be approached by calculating the SSF for each type system individually using a “combined area” LCR, and then a weighted-area (aperture) average SSF would be determined for the building.

## 20.3.4 Passive Space Cooling Design Fundamentals

Passive cooling systems are designed to use natural means to transfer heat from buildings, including convection/ventilation, evaporation, radiation, and conduction. However, the most important element in both passive and conventional cooling design is to prevent heat from entering the building in the first place. Cooling conservation techniques involve building surface colors, insulation, special window glazings, overhangs and orientation, and numerous other architectural/engineering features.

### 20.3.4.1 Solar Control

Controlling the solar energy input to reduce the cooling load is usually considered a passive (versus conservation) design concern because solar input may be needed for other purposes, such as daylighting throughout the year and/or heating during the winter. Basic architectural solar control is normally “designed in” via the shading of the solar windows, where direct radiation is desired for winter heating and needs to be excluded during the cooling season.

The shading control of the windows can be of various types and “controllability,” ranging from drapes and blinds, use of deciduous trees, to the commonly used overhangs and vertical louvers. A rule of thumb design for determining proper south-facing window overhang for both winter heating and summer

**TABLE 20.10** South-Facing Window Overhang Rule of Thumb

		Length of the Overhang = $\frac{\text{Window Height}}{F}$	
(a) Overhang Factors		(b) Roof Overhang Geometry	
North Latitude	$F^a$		
28	5.6–11.1		
32	4.0–6.3		
36	3.0–4.5		
40	2.5–3.4		
44	2.0–2.7		
48	1.7–2.2		
52	1.5–1.8		
56	1.3–1.5		Properly sized overhangs shade out hot summer sun but allow winter sun (which is lower in the sky) to penetrate windows

<sup>a</sup> Select a factor according to your latitude. Higher values provide complete shading at noon on June 21; lower values, until August 1.

Source: From Halacy, 1984.

shading is presented in Table 20.10. Technical details on calculating shading from various devices and orientations are found in Olgay and Olgay (1976) and ASHRAE (1989, 1993, 1997).

**20.3.4.2 Natural Convection/Ventilation**

Air movement provides cooling comfort through convection and evaporation from human skin. ASHRAE (1989) places the comfort limit at 79°F for an air velocity of 50 ft./min (fpm), 82°F for 160 fpm, and 85°F for 200 fpm. To determine whether or not comfort conditions can be obtained, a designer must calculate the volumetric flow rate,  $Q$ , which is passing through the occupied space. Using the cross-sectional area,  $A_x$ , of the space and the room air velocity,  $V_a$ , required, the flow is determined by

$$Q = A_x V_a. \tag{20.80}$$

The proper placement of windows, “narrow” building shape, and open landscaping can enhance natural wind flow to provide ventilation. The air flow rate through open windows for wind-driven ventilation is given by ASHRAE (1989, 1993, 1997):

$$Q = C_v V_w A_w, \tag{20.81}$$

where  $Q$  is air flow rate ( $m^3/s$ ),  $A_w$  is free area of inlet opening ( $m^2$ ),  $V_w$  is wind velocity ( $m/s$ ), and  $C_v$  is effectiveness of opening that is equal to 0.5–0.6 for wind perpendicular to opening, and 0.25–0.35 for wind diagonal to opening.

The stack effect can induce ventilation when warm air rises to the top of a structure and exhausts outside, while cooler outside air enters the structure to replace it. Figure 20.50 illustrates the solar

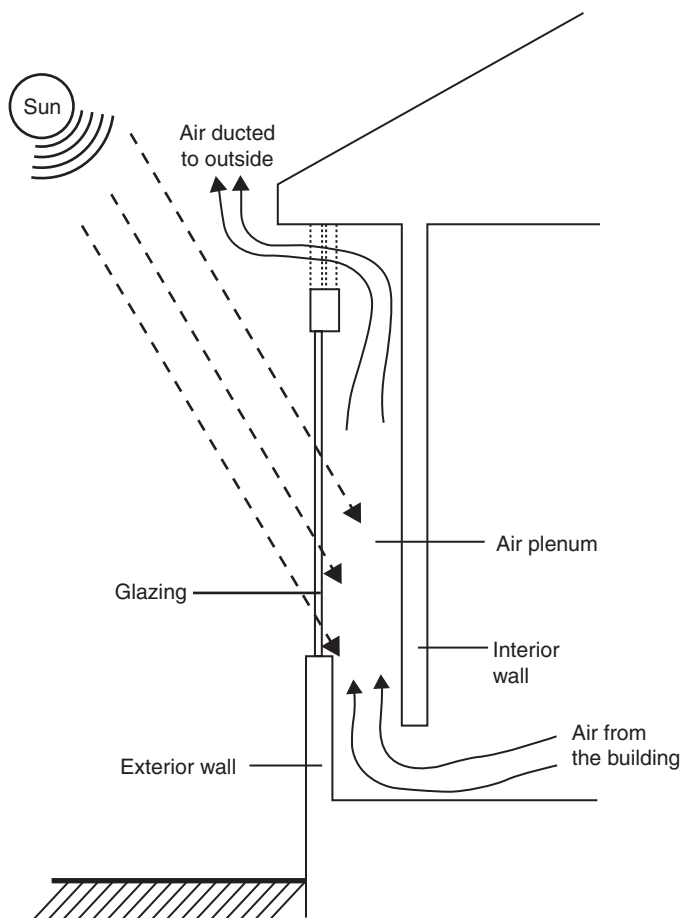


**FIGURE 20.50** The stack-effect/solar chimney concept to induce convection/ventilation. (From PSDH. *Passive Solar Design Handbook*. Volume One: Passive Solar Design Concepts, DOE/CS-0127/1, March 1980. Prepared by Total Environmental Action, Inc. (B. Anderson, C. Michal, P. Temple, and Lewis); Volume Two: *Passive Solar Design Analysis*, DOE/CS-0127/2, January 1980. Prepared by Los Alamos Scientific Laboratory (J. D. Balcomb, D. Barley, R. McFarland, J. Perry, W. Wray and S. Noll). U.S. Department of Energy, Washington, DC, 1980.)

chimney concept, which can easily be adapted to a thermal storage wall system. The greatest stack-effect flow rate is produced by maximizing the stack height and the air temperature in the stack, as given by

$$Q = 0.116 A_j \sqrt{h(T_s - T_o)} \quad (20.82)$$

where  $Q$  is stack flow rate ( $\text{m}^3/\text{s}$ ),  $A_j$  is the area of inlets or outlets, whichever is smaller ( $\text{m}^2$ ),  $h$  is the inlet to outlet height (m),  $T_s$  is the average temperature in stack ( $^{\circ}\text{C}$ ), and  $T_o$  is the outdoor air temperature ( $^{\circ}\text{C}$ ).

If inlet or outlet area is twice the other, the flow rate will increase by 25%, and by 35% if the areas' ratio is 3:1 or larger (Table 20.11).

### Example 20.3.6

A two-story (5-m) solar chimney is being designed to produce a flow of  $0.25 \text{ m}^3/\text{s}$  through a space. The preliminary design features include a  $25 \text{ cm} \times 1.5 \text{ m}$  inlet, a  $50 \text{ cm} \times 1.5 \text{ m}$  outlet, and an estimated  $35^{\circ}\text{C}$  average stack temperature on a sunny  $30^{\circ}\text{C}$  day. Can this design produce the desired flow?



**TABLE 20.11** Ground Reflectivities

Material	$\rho$ (%)
Cement	27
Concrete	20–40
Asphalt	7–14
Earth	10
Grass	6–20
Vegetation	25
Snow	70
Red brick	30
Gravel	15
White paint	55–75

Source: From Murdoch, J. B., *Illumination Engineering—From Edison's Lamp to the Laser*, Macmillan, New York, 1985.

**Solution.** Substituting the design data into Equation 20.82,

$$\begin{aligned} Q &= 0.116(0.25 \times 1.5)[5(5)]^{1/2} \\ &= 0.2 \text{ m}^3/\text{s}. \end{aligned}$$

Because the outlet area is twice the inlet area, the 25% flow increase can be used:

$$Q = 0.2(1.25) = 0.25 \text{ m}^3/\text{s}$$

(answer: Yes, the proper flow rate is obtained).

### 20.3.4.3 Evaporative Cooling

When air with less than 100% relative humidity moves over a water surface, the evaporation of water causes both the air and the water itself to cool. The lowest temperature that can be reached by this direct evaporative cooling effect is the wet-bulb temperature of the air, which is directly related to the relative humidity, with lower wet-bulb temperature associated with lower relative humidity. Thus, dry air (low relative humidity) has a low wet-bulb temperature and will undergo a large temperature drop with evaporative cooling, while humid air (high relative humidity) can only be slightly cooled evaporatively. The wet-bulb temperature for various relative humidity and air temperature conditions can be found via the “psychrometric chart” available in most thermodynamic texts. Normally, an evaporative cooling process cools the air only part of the way down to the wet-bulb temperature. To get the maximum temperature decrease, it is necessary to have a large water surface area in contact with the air for a long time, and interior ponds and fountain sprays are often used to provide this air-water contact area.

The use of water sprays and open ponds on roofs provides cooling primarily via evaporation. The hybrid system involving a fan and wetted mat, the “swamp cooler,” is by far the most widely used evaporative cooling technology. Direct, indirect, and combined evaporative cooling system design features are described in ASHRAE (1989, 1991, 1993, 1995, 1997).

### 20.3.4.4 Nocturnal and Radiative Cooling Systems

Another approach to passive convective/ventilative cooling involves using cooler night air to reduce the temperature of the building and/or a storage mass. Thus, the building/storage mass is prepared to accept part of the heat load during the hotter daytime. This type of convective system can also be combined with evaporative and radiative modes of heat transfer, utilizing air and/or water as the convective fluid. Work in Australia (Close et al. 1968) investigated rock storage beds that were chilled using evaporatively cooled night air. Room air was then circulated through the bed during the day to provide space cooling. The use of encapsulated roof ponds as a thermal cooling mass has been tried by

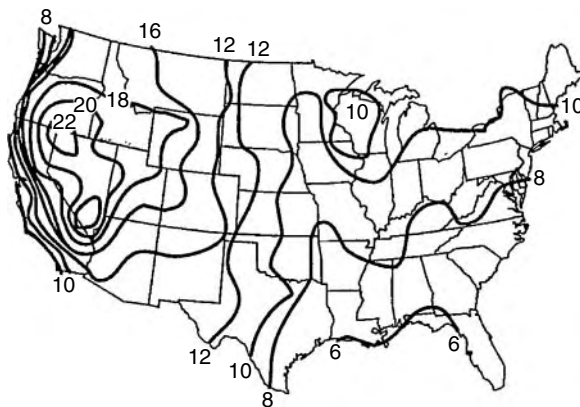


**FIGURE 20.51** Average monthly sky temperature depression ( $I_{\text{AIR}} - I_{\text{SKY}}$ ) for July in °F. (Adapted from Martin, M. and Berdahl, P., *Solar Energy*, 33(314), 321–336, 1984.)

several investigators (Hay and Yellot 1969; Marlatt, Murray, and Squire 1984; Givoni 1994) and is often linked with nighttime radiative cooling.

All warm objects emit thermal infrared radiation; the hotter the body, the more energy it emits. A passive cooling scheme is to use the cooler night sky as a sink for thermal radiation emitted by a warm storage mass, thus chilling the mass for cooling use the next day. The net radiative cooling rate,  $Q_r$ , for a horizontal unit surface (ASHRAE 1989, 1993, 1997) is

$$Q_r = \varepsilon \sigma (T_{\text{body}}^4 - T_{\text{sky}}^4), \quad (20.83)$$

where  $Q_r$  is the net radiative cooling rate,  $\text{W/m}^2$  ( $\text{Btu/h ft.}^2$ ),  $\varepsilon$  is the surface emissivity fraction (usually 0.9 for water),  $\sigma$  is  $5.67 \times 10^{-8} \text{ W/m}^2 \text{ K}^4$  ( $1.714 \times 10^{-9} \text{ Btu/h ft.}^2 \text{ R}^4$ ),  $T_{\text{body}}$  is the warm body temperature, Kelvin (Rankine), and  $T_{\text{sky}}$  is the effective sky temperature, Kelvin (Rankine).

The monthly average air–sky temperature difference has been determined (Martin and Berdahl 1984) and Figure 20.51 presents these values for July (in °F) for the United States.

### Example 20.3.7

Estimate the overnight cooling possible for a  $10 \text{ m}^2$ ,  $85^\circ\text{F}$  water thermal storage roof during July in Los Angeles.

**Solution.** Assume the roof storage unit is black with  $\varepsilon=0.9$ . From Figure 20.51,  $T_{\text{air}} - T_{\text{sky}}$  is approximately  $10^\circ\text{F}$  for Los Angeles. From weather data for LA airport, (PSDH 1984; ASHRAE 1989), the July average temperature is  $69^\circ\text{F}$  with a range of  $15^\circ\text{F}$ . Assuming night temperatures vary from the average ( $69^\circ\text{F}$ ) down to half the daily range ( $15/2$ ), then the average nighttime temperature is chosen as  $69 - (1/2)(15/2) = 65^\circ\text{F}$ . Therefore,  $T_{\text{sky}} = 65 - 10 = 55^\circ\text{F}$ . From Equation 20.83,

$$\begin{aligned} Q_r &= 0.9(1.714 \times 10^{-9})[(460 + 85)^4 - (460 + 55)^4] \\ &= 27.6 \text{ Btu/h ft.}^2. \end{aligned}$$

For a 10-h night and  $10 \text{ m}^2$  ( $107.6 \text{ ft.}^2$ ) roof area,

$$\begin{aligned} \text{Total radiative cooling} &= 27.6(10)(107.6) \\ &= 29,700 \text{ Btu.} \end{aligned}$$

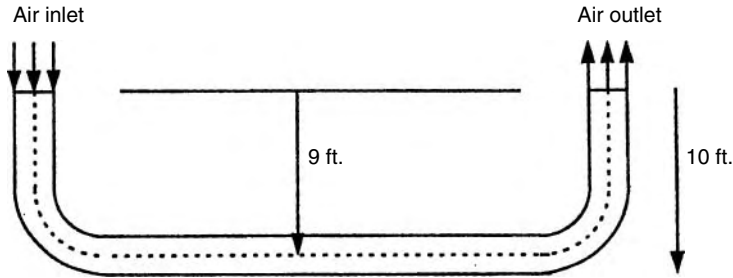


FIGURE 20.52 Open loop underground air tunnel system.

Note that this does not include the convective cooling possible, which can be approximated (at its maximum rate) for still air (ASHRAE 1989, 1993, 1997) by

$$\begin{aligned} \text{Maximum total } Q_{\text{conv}} &= hA(T_{\text{roof}} - T_{\text{air}})(\text{Time}) \\ &= 5(129)(85 - 55)(10) \\ &= 161,000 \text{ Btu.} \end{aligned}$$

This is a maximum since the 85°F storage temperature will drop as it cools; this is also the case for the radiative cooling calculation. However, convection is seen to usually be the more dominant mode of nighttime cooling.

**20.3.4.5 Earth Contact Cooling (or Heating)**

Earth contact cooling or heating is a passive summer cooling and winter heating technique that utilizes underground soil as the heat sink or source. By installing a pipe underground and passing air through the pipe, the air will be cooled or warmed depending on the season. A schematic of an open loop system and a closed loop air-conditioning system are presented in Figure 20.52 and Figure 20.53, respectively (Goswami and Biseli 1994).

The use of this technique can be traced back to 3000 BC when Iranian architects designed some buildings to be cooled by natural resources only. In the nineteenth century, Wilkinson (USDA 1960) designed a barn for 148 cows where a 500-ft. long underground passage was used for cooling during the summertime. Since that time, a number of experimental and analytical studies of this technique have

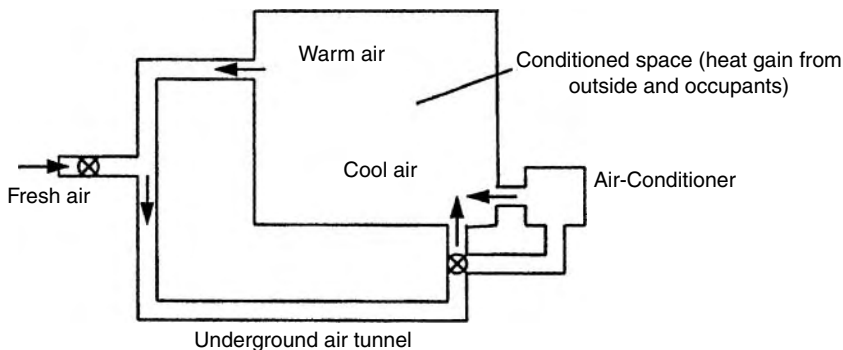


FIGURE 20.53 Schematic of closed loop air-conditioning system using air-tunnel.

continued to appear in the literature (Krarti and Kreider 1996; Hollmuller and Lachal 2001; De Paepe and Janssens 2003). Goswami and Dhaliwal (1985) have given a brief review of the literature, as well as presenting an analytical solution to the problem of transient heat transfer between the air and the surrounding soil as the air is made to pass through a pipe buried underground.

### 20.3.4.5.1 Heat Transfer Analysis

The transient thermal analysis of the air and soil temperature fields (Goswami and Dhaliwal 1985) is conducted using finite elements with the convective heat transfer between the air and the pipe and using semi-infinite cylindrical conductive heat transfer to the soil from the pipe. It should be noted that the thermal resistance of the pipe (whether of metal, plastic or ceramic) is negligible relative to the surrounding soil.

*Air and Pipe Heat Transfer*—The pipe is divided into a large number of elements and a psychrometric energy balance written for each, depending on whether the air leaves the element (1) unsaturated, or (2) saturated.

1. If the air leaves an element as unsaturated, the energy balance on the element is

$$mC_p(T_1 - T_2) = hA_p(T_{\text{air}} - T_{\text{pipe}}). \quad (20.84)$$

$T_{\text{air}}$  can be taken as  $(T_1 + T_2)/2$ . Substituting and simplifying,

$$T_2 = \left[ \left(1 - \frac{U}{2}\right) T_1 + UT_{\text{pipe}} \right] / \left(1 + \frac{U}{2}\right), \quad (20.85)$$

where  $U$  is defined as

$$U = \frac{A_p h}{mC_p}$$

2. If the air leaving the element is saturated, the energy balance is

$$mC_p T_1 + m(W_1 - W_2)H_{\text{fg}} = mC_p T_2 + hA_p(T_{\text{air}} - T_{\text{pipe}}). \quad (20.86)$$

Simplifying gives:

$$T_2 = \left(1 - \frac{U}{2}\right) T_1 + \frac{W_1 - W_2}{C_p} H_{\text{fg}} + UT_{\text{pipe}} / \left(1 + \frac{U}{2}\right). \quad (20.87)$$

The convective heat transfer coefficient  $h$  in the preceding equations depends on Reynolds number, the shape, and roughness of the pipe.

Using the exit temperature from the first element as the inlet temperature for the next element, the exit temperature for the element can be calculated in a similar way. Continuing this way from one element to the next, the temperature of air at the exit from the pipe can be calculated.

*Soil Heat Transfer*—The heat transfer from the pipe to the soil is analyzed by considering the heat flux at the internal radius of a semi-infinite cylinder formed by the soil around the pipe. For a small element the problem can be formulated as

$$\frac{\partial^2 T(r, t)}{\partial r^2} + \frac{1}{r} \frac{\partial T(r, t)}{\partial r} = \frac{1}{\alpha} \frac{\partial T(r, t)}{\partial t}, \quad (20.88)$$

with initial and boundary conditions as

$$T(r, 0) = T_e,$$

$$T(\infty, t) = T_e,$$

$$-K \frac{\partial T}{\partial r}(r, t) = q'',$$

where  $T_e$  is the bulk earth temperature and  $q''$  is also given by the amount of heat transferred to the pipe from the air by convection, i.e.,  $q'' = h(T_{\text{air}} - T_{\text{pipe}})$ .

### 20.3.4.5.2 Soil Temperatures and Properties

Kusuda and Achenback (1965) and Labs (1981) studied the earth temperatures in the United States. According to both of these studies, temperature swings in the soil during the year are dampened with depth below the ground. There is also a phase lag between the soil temperature and the ambient air temperature, and this phase lag increases with depth below the surface. For example, the soil temperature for light dry soil at a depth of about 10 ft. (3.05 m) varies by approximately  $\pm 5^\circ\text{F}$  ( $2.8^\circ\text{C}$ ) from the mean temperature (approximately equal to mean annual air temperature) and has a phase lag of approximately 75 days behind ambient air temperature (Labs 1981).

The thermal properties of the soil are difficult to determine. The thermal conductivity and diffusivity both change with the moisture content of the soil itself, which is directly affected by the temperature of and heat flux from and to the buried pipe. Most researchers have found that using constant property values for soil taken from standard references gives reasonable predictive results (Goswami and Ileslamlou 1990).

### 20.3.4.5.3 Generalized Results from Experiments

Figure 20.54 presents data from Goswami and Biseli (1994) for an open system, 100-ft. long, 12-in diameter pipe, buried 9 ft. deep. The figure shows the relationship between pipe inlet-to-outlet temperature reduction ( $T_{\text{in}} - T_{\text{out}}$ ) and the initial soil temperature with ambient air inlet conditions of  $90^\circ\text{F}$ , 55% relative humidity for various pipe flow rates.

Other relations from this same report which can be used with the Figure 20.54 data include: (1) the effect of increasing pipe/tunnel length on increasing the inlet-to-outlet air temperature difference is fairly

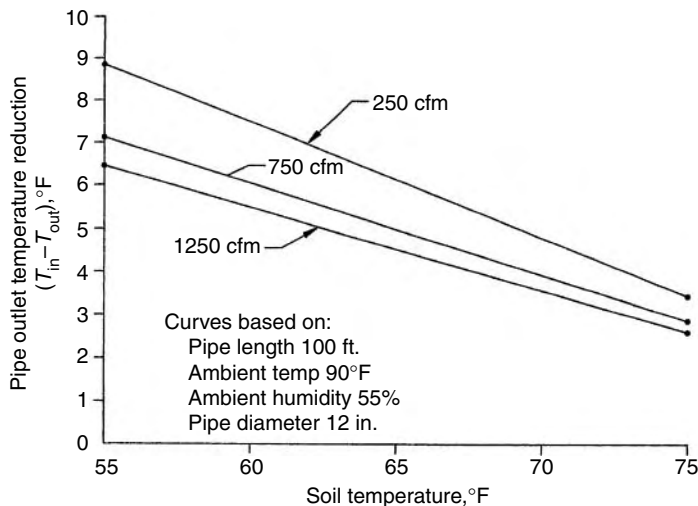


FIGURE 20.54 Air temperature drop through a 100-ft. long, 12-in. diameter pipe buried 9 ft. underground.

linear up to 250 ft.; and (2) the effect of decreasing pipe diameter on lowering the outlet air temperature is slight, and only marginally effective for pipes less than 12-in. in diameter.

### Example 20.3.8

Provide the necessary 12-in diameter pipe length(s) that will deliver 1500 cfm of 75°F air if the ambient temperature is 85°F and the soil at 9 ft. is 65°F.

**Solution.** From Figure 20.54, for 100 ft. of pipe at 65°F soil temperature, the pipe temperature reduction is

$$\begin{aligned} T_{\text{in}} - T_{\text{out}} &= 6^\circ\text{F (at 250 cfm)} \\ &= 5^\circ\text{F (at 750 cfm)} \\ &= 4.5^\circ\text{F (at 1250 cfm)}. \end{aligned}$$

Because the “length versus temperature reduction” is linear (see text above), the 10°F reduction required (85 down to 75) would be met by the 750 cfm case (5°F for 100 ft.) if 200 ft. of pipe is used. Then, two 12-in diameter pipes would be required to meet the 1500-cfm requirement.

*Answer:* Two 12-in diameter pipes, each 200 ft. long. (Note: see what would be needed if the 250 cfm or the 1250 cfm cases had been chosen. Which of the three flow rate cases leads to the “cheapest” installation?)

## 20.3.5 Daylighting Design Fundamentals

Daylighting is the use of the sun’s radiant energy to illuminate the interior spaces in a building. In the 19th century, electric lighting was considered an alternative technology to daylighting. Today the situation is reversed, primarily due to the economics of energy use and conservation. However, there are good physiological reasons for using daylight as an illuminant. The quality of daylight matches the human eye’s response, thus permitting lower light levels for task comfort, better color rendering, and clearer object discrimination (Robbins 1986; McCluney 1998; Clay 2001).

### 20.3.5.1 Lighting Terms and Units

Measurement of lighting level is based on the “standard candle”, where the lumen (lm), the unit of luminous flux ( $\phi$ ), is defined as the rate of luminous energy passing through a 1-m<sup>2</sup> area located 1 m from the candle. Thus, a standard candle generates  $4\pi$  lumens, which radiate away in all directions. The illuminance ( $E$ ) on a surface is defined as the luminous flux on the surface divided by the surface area,  $E = \phi/A$ . Illuminance is measured in either lux (lx), as lm/m<sup>2</sup>, or footcandles (fc), as lm/ft.<sup>2</sup>.

Determination of the daylighting available at a given location in a building space at a given time is important to evaluate the reduction possible in electric lighting and the associated impact on heating and cooling loads. Daylight provides about 110 lm/W of solar radiation, fluorescent lamps about 75 lm/W of electrical input, and incandescent lamps about 20 lm/W; thus daylighting generates only 1/2–1/5 the heating that equivalent electric lighting does, significantly reducing the building cooling load.

### 20.3.5.2 Approach to Daylighting Design

Aperture controls such as blinds and drapes are used to moderate the amount of daylight entering the space, as are the architectural features of the building itself (glazing type, area, and orientation; overhangs and wingwalls; lightshelves; etc.). Many passive and “active” reflective, concentrating, and diffusing devices are available to specifically gather and direct both the direct and diffuse components of

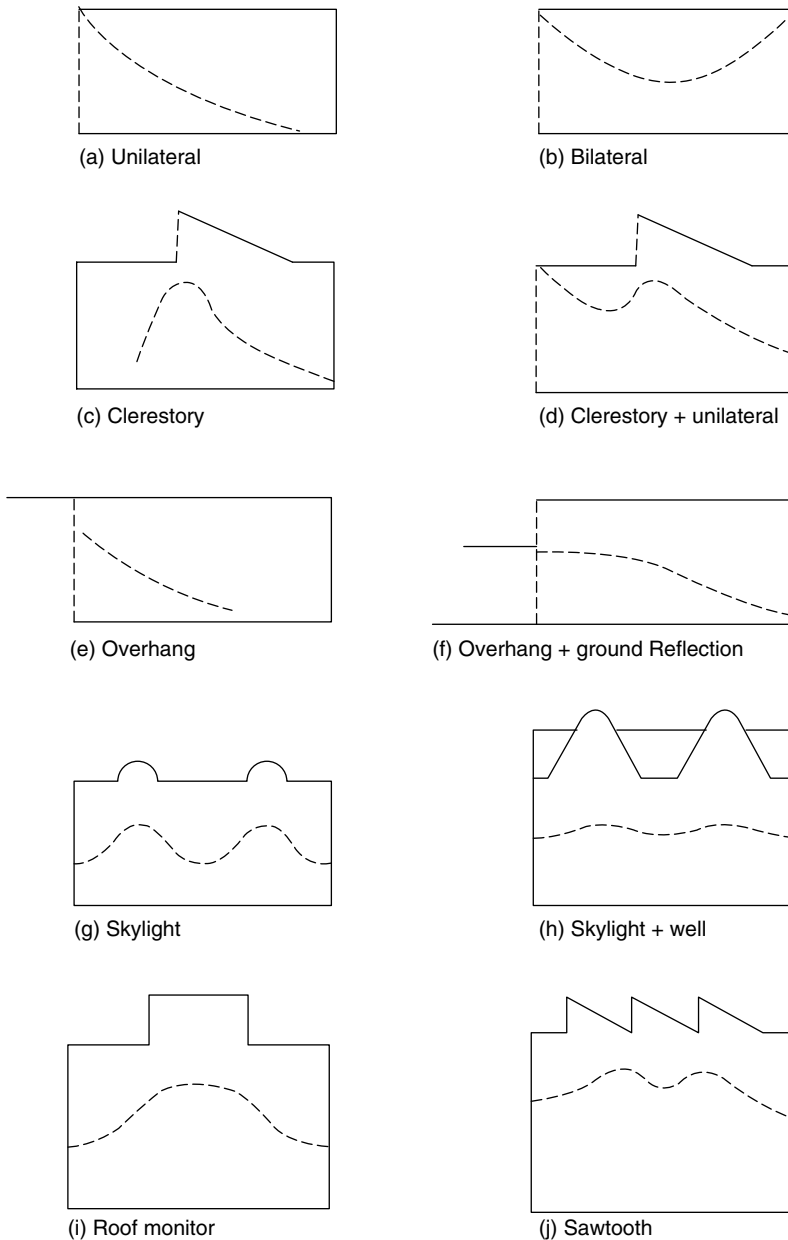


**FIGURE 20.55** Examples of sidelighting and toplighting architectural features (dashed lines represent illuminance distributions). (From Murdoch, J. B., *Illumination Engineering from Edison's Lamp to the Laser*. Macmillan, New York, 1985)

daylight to areas within the space (Kinney et al. 2005). Electric-lighting dimming controls are used to adjust the electric light level based on the quantity of the daylighting. With these two types of controls (aperture and lighting), the electric lighting and cooling energy use and demand, as well as cooling system sizing, can be reduced. However, the determination of the daylighting position and time illuminance value within the space is required before energy usage and demand reduction calculations can be made.

Daylighting design approaches use both solar beam radiation (referred to as sunlight) and the diffuse radiation scattered by the atmosphere (referred to as skylight) as sources for interior lighting, with historical design emphasis being on utilizing skylight. Daylighting is provided through a variety of glazing features, which can be grouped as sidelighting (light enters via the side of the space) and toplighting (light enters from the ceiling area). Figure 20.55 illustrates several architectural forms producing sidelighting and toplighting, with the dashed lines representing the illuminance distribution within the space. The calculation of work-plane illuminance depends on whether sidelighting and/or toplighting features are used, and the combined illuminance values are additive.

### 20.3.5.3 Sun-Window Geometry

The solar illuminance on a vertical or horizontal window depends on the position of the sun relative to that window. In the method described here, the sun and sky illuminance values are determined using the sun's altitude angle ( $\alpha$ ) and the sun-window azimuth angle difference ( $\Phi$ ). These angles need to be determined for the particular time of day, day of year, and window placement under investigation.

#### 20.3.5.3.1 Solar Altitude Angle

The solar altitude angle,  $\alpha$ , is the angle swept out by a person's arm when pointing to the horizon directly below the sun and then raising the arm to point at the sun. The equation to calculate solar altitude,  $\alpha$ , is

$$\sin \alpha = \cos L \cos \delta \cos H + \sin L \sin \delta, \quad (20.89)$$

where  $L$  is the local latitude (degrees),  $\delta$  is the earth-sun declination (degrees) given by  $\delta = 23.45 \sin[360(n - 81)/365]$ ,  $n$  is the day number of the year, and  $H$  is the hour angle (degrees) given by

$$H = \frac{(12 \text{ noon} - \text{time})(\text{in minutes})}{4}; \quad (+ \text{ morning}, - \text{ afternoon}). \quad (20.90)$$

#### 20.3.5.3.2 Sun-Window Azimuth Angle Difference

The difference between the sun's azimuth and the window's azimuth,  $\Phi$ , needs to be calculated for vertical window illuminance. The window's azimuth angle,  $\gamma_w$ , is determined by which way it faces, as measured from south (east of south is positive, westward is negative). The solar azimuth angle,  $\gamma_s$ , is calculated:

$$\sin \gamma_s = \frac{\cos \delta \sin H}{\cos \alpha}. \quad (20.91)$$

The sun-window azimuth angle difference,  $\Phi$ , is given by the absolute value of the difference between  $\gamma_s$  and  $\gamma_w$ :

$$\Phi = |\gamma_s - \gamma_w|. \quad (20.92)$$

### 20.3.5.4 Daylighting Design Methods

To determine the annual lighting energy saved ( $ES_L$ ), calculations using the lumen method described below should be performed on a monthly basis for both clear and overcast days for the space under investigation. Monthly weather data for the site would then be used to prorate clear and overcast lighting energy demands monthly. Subtracting the calculated daylighting illuminance from the design illuminance leaves the supplementary lighting needed, which determines the lighting energy required.

The approach in the method below is to calculate the "sidelighting" and the "skylighting" of the space separately, and then combine the results. This procedure has been computerized (Lumen II/ Lumen Micro) and includes many details of controls, daylighting technologies, and weather. ASHRAE (1989, 1993, 1997) lists many of the methods and simulation techniques currently used with daylighting and its associated energy effects.



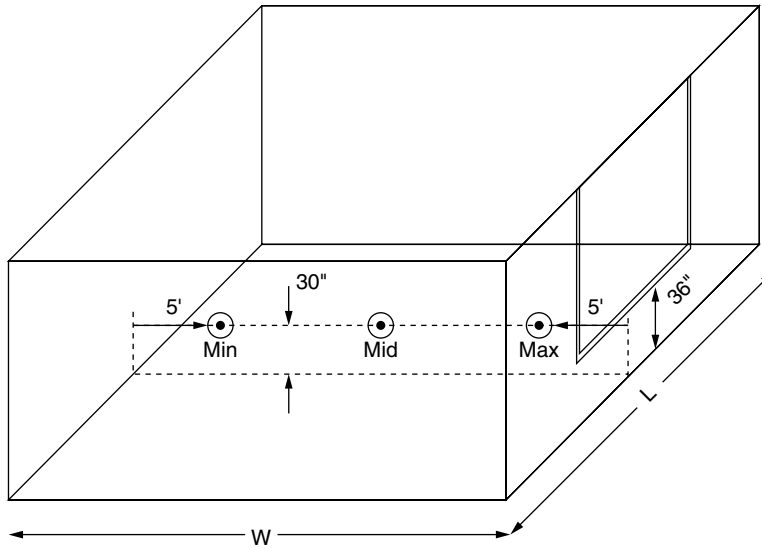


**FIGURE 20.56** Location of illumination points within the room (along centerline of window) determined by lumen method of sidelighting.

#### 20.3.5.4.1 Lumen Method of Sidelighting (Vertical Windows)

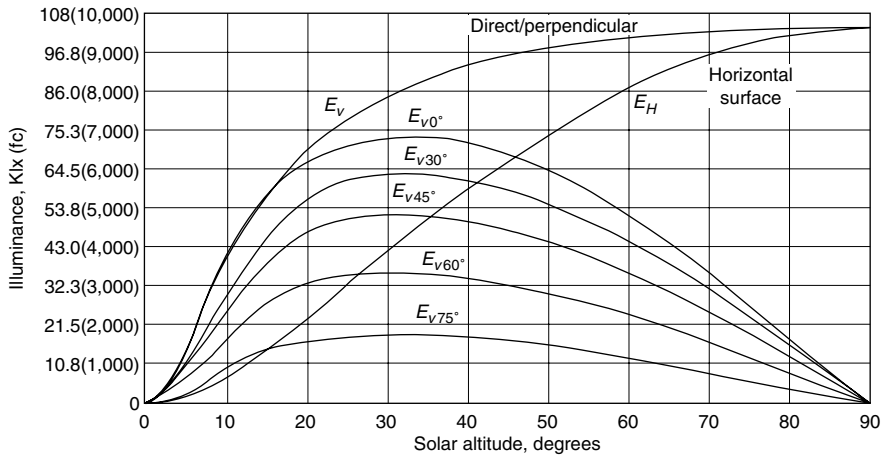
The lumen method of sidelighting calculates interior horizontal illuminance at three points, as shown in Figure 20.56, at the 30-in (0.76-m) work-plane on the room-and-window centerline. A vertical window is assumed to extend from 36 in (0.91 m) above the floor to the ceiling. The method accounts for both direct and ground-reflected sunlight and skylight, so both horizontal and vertical illuminances from sun and sky are needed. The steps in the lumen method of sidelighting are presented next.

As mentioned, the incident direct and ground-reflected window illuminance are normally calculated for both a cloudy and a clear day for representative days during the year (various months), as well as for clear or cloudy times during a given day. Thus, the interior illumination due to sidelighting and skylighting can then be examined for effectiveness throughout the year.

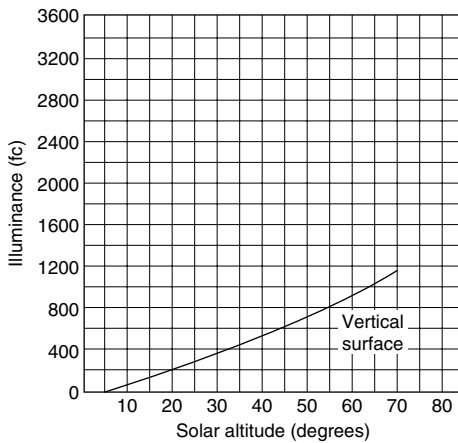
*Step 1: Incident Direct Sky and Sun Illuminances*—The solar altitude and sun-window azimuth angle difference are calculated for the desired latitude, date, and time using Equation 20.89 and Equation 20.92, respectively. Using these two angles, the total illuminance on the window ( $E_{sw}$ ) can be determined by summing the direct sun illuminance ( $E_{uw}$ ) and the direct sky illuminance ( $E_{kw}$ ), each determined from the appropriate graph in Figure 20.57.

*Step 2: Incident Ground-Reflected Illuminance*—The sun illuminance on the ground ( $E_{ug}$ ), plus the overcast or clear sky illuminance ( $E_{kg}$ ) on the ground, make up the total horizontal illuminance on the ground surface ( $E_{sg}$ ). A fraction of the ground surface illuminance is then considered diffusely reflected onto the vertical window surface ( $E_{gw}$ ), where gw indicates from the ground to the window.

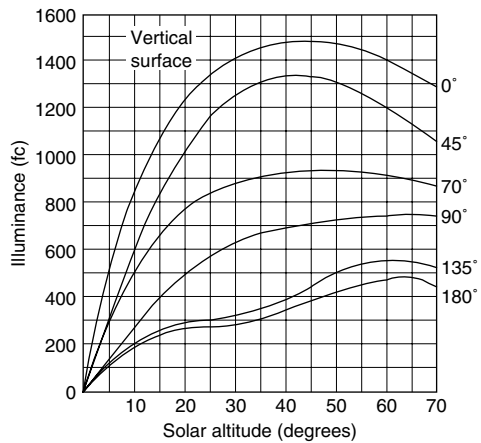
The horizontal ground illuminances can be determined using Figure 20.58, where the clear sky plus sun case and the overcast sky case are functions of solar altitude. The fractions of the ground illuminance diffusely reflected onto the window depends on the reflectivity ( $\rho$ ) of the ground surface (see Table 20.11.) and the window-to-ground surface geometry.



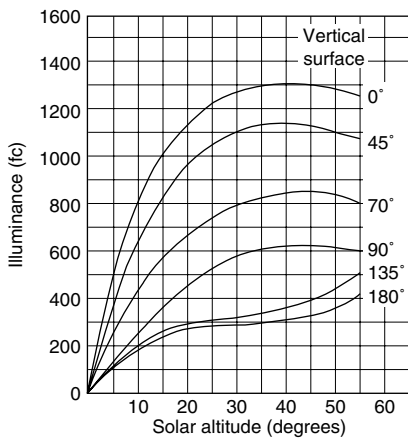
(a) Direct sunlight



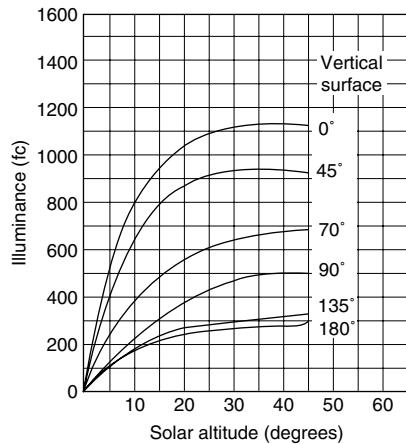
(b) Overcast skylight



(c) Clear summer skylight



(d) Clear autumn/spring skylight



(e) Clear winter skylight

**FIGURE 20.57** Vertical illuminance from (a) direct sunlight and (b-c) skylight, for various sun-window azimuth angle differences. (From IES (Illumination Engineering Society), *Lighting Handbook, Applications Volume*. Illumination Engineering Society, New York, 1987.)

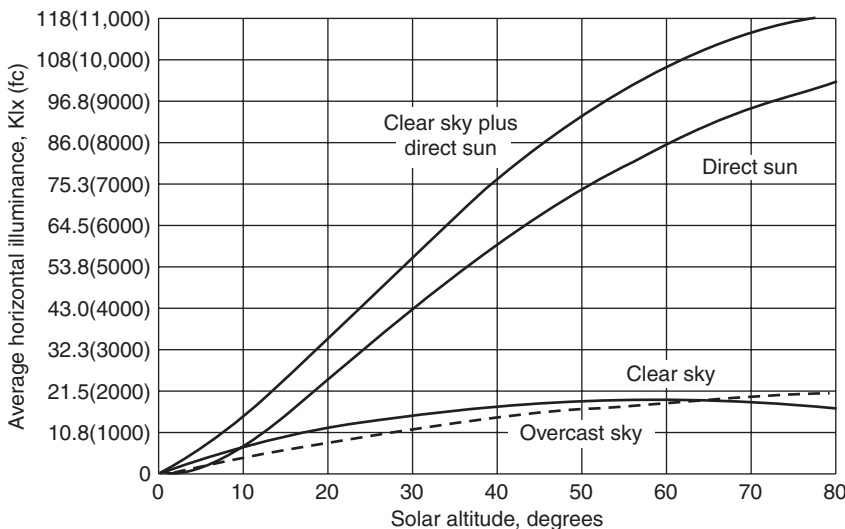


FIGURE 20.58 Horizontal illuminance for overcast sky, clear sky, direct sun, and clear sky plus direct sun. (From Murdoch, J. B., *Illumination Engineering — From Edison’s Lamp to the Laser*, Mac Millan, New York, 1985.)

If the ground surface is considered uniformly reflective from the window outward to the horizon, then the illuminance on the window from ground reflection is

$$E_{gw} = \frac{\rho E_{sg}}{2}. \tag{20.93}$$

A more complicated ground-reflection case is illustrated in Figure 20.59, where multiple “strips” of differently reflecting ground are handled using the angles to the window where a strip’s illuminance on a window is calculated,

$$E_{gw(\text{strip})} = \frac{\rho_{\text{strip}} E_{sg}}{2} (\cos \theta_1 - \cos \theta_2). \tag{20.94}$$

And the total reflected onto the window is the sum of the strip illuminances:

$$E_{gw} = \frac{E_{sg}}{2} [\rho_1 (\cos 0 - \cos \theta_1) + \rho_2 (\cos \theta_1 - \cos \theta_2) + \dots + \rho_n (\cos \theta_{n-1} - \cos 90)]. \tag{20.95}$$

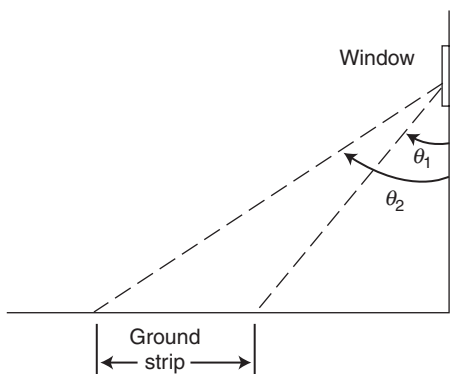


FIGURE 20.59 Geometry for ground “strips”. (From Murdoch, J. B., *Illumination Engineering — From Edison’s Lamp to the Laser*, Mac Millan, New York, 1985.)

**TABLE 20.12** Glass Transmittances

Glass	Thickness (in.)	$\tau$ (%)
Clear	1/3	89
Clear	3/16	88
Clear	1/4	87
Clear	5/16	86
Grey	1/8	61
Grey	3/16	51
Grey	1/4	44
Grey	5/16	35
Bronze	1/8	68
Bronze	3/16	59
Bronze	1/4	52
Bronze	5/16	44
Thermopane	1/8	80
Thermopane	3/16	79
Thermopane	1/4	77

Source: From Murdoch, J. B., *Illumination Engineering—From Edison's Lamp to the Laser*, Macmillan, New York, 1985.

*Step 3: Luminous Flux Entering Space*—The direct sky–sun and ground-reflected luminous fluxes entering the building are attenuated by the transmissivity of the window. Table 20.12 presents the transmittance fraction ( $\tau$ ) of several window glasses. The fluxes entering the space are calculated from the total sun–sky and the ground-reflected illuminances by using the area of the glass,  $A_w$ :

$$\begin{aligned}\phi_{sw} &= E_{sw} \tau A_w, \\ \phi_{gw} &= E_{gw} \tau A_w,\end{aligned}\tag{20.96}$$

*Step 4: Light Loss Factor*—The light loss factor ( $K_m$ ) accounts for the attenuation of luminous flux due to dirt on the window (WDD, window dirt depreciation) and on the room surfaces (RSDD, room surface dirt depreciation). WDD depends on how often the window is cleaned, but a 6-month average for offices is 0.83 and for factories is 0.71 (Murdoch 1985).

The RSDD is a more complex calculation involving time between cleanings, the direct-indirect flux distribution, and room proportions. However, for rooms cleaned regularly, RSDD is around 0.94 and for once-a-year-cleaned dirty rooms, the RSDD would be around 0.84.

The light loss factor is the product of the preceding two fractions:

$$K_m = (\text{WDD})(\text{RSDD}).\tag{20.97}$$

*Step 5: Work-Plane Illuminances*—As discussed earlier, [Figure 20.56](#) illustrates the location of the work-plane illuminances determined with this lumen method of sidelighting. The three illuminances (max, mid, min) are determined using two coefficients of utilization, the  $C$  factor and  $K$  factor. The  $C$  factor depends on room length and width and wall reflectance. The  $K$  factor depends on ceiling–floor height, room width, and wall reflectance. [Table 20.13](#) presents  $C$  and  $K$  values for the three cases of incoming fluxes: sun plus clear sky, overcast sky, and ground-reflected. Assumed ceiling and floor reflectances are given for this case with no window controls (shades, blinds, overhangs, etc.). These further window control complexities can be found in Libbey-Owens-Ford Company (1976); IES (1987), and others. A reflectance of 70% represents light-colored walls, with 30% representing darker walls.

The work-plane max, mid, and min illuminances are each calculated by adding the sun-sky and ground-reflected illuminances, which are given by

$$\begin{aligned} E_{sp} &= \phi_{sw} C_s K_s K_m, \\ E_{gp} &= \phi_{gw} C_g K_g K_m, \end{aligned} \quad (20.98)$$

where the “sp” and “gp” subscripts refer to the sky-to-work-plane and ground-to-work-plane illuminances.

### Example 20.3.9

Determine the clear-sky illuminances for a 30-ft.-long, 30-ft.-wide, 10-ft.-high room with a 20-ft.-long window with a 3-ft. sill. The window faces 10°E of south, the building is at 32°N latitude, and it is January 15 at 2 p.m. The ground cover outside is grass, the glass is 1/4-in clear, and the walls are light colored.

**Solution.** Following the steps in the “sidelighting” method:

Step 1: With  $L=32$ ,  $n=15$ ,  $H=(12-14)60/4=-30$ ,

$$\delta = 23.45 \sin[360(15-81)/365] = -21.3^\circ.$$

Then, Equation 20.89 yields  $\alpha=41.7^\circ$ , Equation 20.91 yields  $\gamma_s=-38.7^\circ$ , and Equation 20.92 yields

$$\Phi = |-38.7 - (+10)| = 48.7^\circ.$$

From Figure 20.57 with  $\alpha=41.7^\circ$  and  $\Phi=48.7^\circ$ :

- (a) For clear sky (winter, no sun):  $E_{kw}=875$  fc.
- (b) For direct sun:  $E_{uw}=4,100$  fc.
- (c) Total clear sky plus direct:  $E_{sw}=4,975$  fc.

(Note: A high  $E_{uw}$  value probably indicates a glare situation!)

Step 2: Horizontal illuminances from Figure 20.58:  $E_{sg}=4007$  fc.

Then Equation 20.93 yields, with  $\rho_{grass}=0.06$ ,  $E_{gw}=222$  fc.

Step 3: From Equation 20.96, with  $\tau=0.87$  and  $A_w=140$  ft.<sup>2</sup>,

$$\Phi_{sw} = 4975(0.87)(140) = 605,955 \text{ lm},$$

$$\Phi_{gw} = 222(0.87)(140) = 27,040 \text{ lm}.$$

Step 4: For a clean office room:

$$K_m = (0.83)(0.94) = 0.78.$$

Step 5: From Table 20.13, for 30' width, 30' length, 10' ceiling, and wall reflectivity 70%,

(a) Clear sky:

$$C_{s, \max} = 0.0137; K_{s, \max} = 0.125,$$

$$C_{s, \text{mid}} = 0.0062; K_{s, \text{mid}} = 0.110,$$

$$C_{s, \min} = 0.0047; K_{s, \min} = 0.107.$$

**TABLE 20.13a** C and K Factors for No Window Controls for Overcast Sky

Illumination by Overcast Sky																			
C: Coefficient of Utilization								K: Coefficient of Utilization											
Room Length (ft.)		20		30		40		Ceiling Height (ft.)		8		10		12		14			
Wall Reflectance (%)		70	30	70	30	70	30	Wall Reflectance (%)		70	30	70	30	70	30	70	30		
Room Width (ft.)		Room Width (ft.)																	
Max	}	20	0.0276	0.0251	0.0191	0.0173	0.0143	0.0137	Max	}	20	0.125	0.129	0.121	0.123	0.111	0.111	0.0991	0.0973
		30	0.0272	0.0248	0.0188	0.0172	0.0137	0.0131			30	0.122	0.131	0.122	0.121	0.111	0.111	0.0945	0.0973
		40	0.0269	0.0246	0.0182	0.0171	0.0133	0.0130			40	0.145	0.133	0.131	0.126	0.111	0.111	0.0973	0.0982
Mid	}	20	0.0159	0.0177	0.0101	0.0087	0.0081	0.0071	Mid	}	20	0.0908	0.0982	0.107	0.115	0.111	0.111	0.105	0.122
		30	0.0058	0.0050	0.0054	0.0040	0.0034	0.0033			30	0.156	0.102	0.0939	0.113	0.111	0.111	0.121	0.134
		40	0.0039	0.0027	0.0030	0.0023	0.0022	0.0019			40	0.106	0.0948	0.123	0.107	0.111	0.111	0.135	0.127
Min	}	20	0.0087	0.0053	0.0063	0.0043	0.0050	0.0037	Min	}	20	0.0908	0.102	0.0951	0.114	0.111	0.111	0.118	0.134
		30	0.0032	0.0019	0.0029	0.0017	0.0020	0.0014			30	0.0924	0.119	0.101	0.114	0.111	0.111	0.125	0.126
		40	0.0019	0.0009	0.0016	0.0009	0.0012	0.0008			40	0.111	0.0926	0.125	0.109	0.111	0.111	0.133	0.130

Source: From IES, 1979.

**TABLE 20.13b** C and K Factors for No Window Controls for Clear Sky

Illumination by Clear Sky																			
C: Coefficient of Utilization								K: Coefficient of Utilization											
Room Length (ft.)		20		30		40		Ceiling Height (ft.)		8		10		12		14			
Wall Reflectance (%)		70	30	70	30	70	30	Wall Reflectance (%)		70	30	70	30	70	30	70	30		
Room Width (ft.)		Room Width (ft.)																	
Max	}	20	0.0206	0.0173	0.0143	0.0123	0.0110	0.0098	Max	}	20	0.145	0.155	0.129	0.132	0.111	0.111	0.101	0.0982
		30	0.0203	0.0173	0.0137	0.0120	0.0098	0.0092			30	0.141	0.149	0.125	0.130	0.111	0.111	0.0954	0.101
		40	0.0200	0.0168	0.0131	0.0119	0.0096	0.0091			40	0.157	0.157	0.135	0.134	0.111	0.111	0.0964	0.0991
Mid	}	20	0.0153	0.0104	0.0100	0.0079	0.0083	0.0067	Mid	}	20	0.110	0.128	0.116	0.126	0.111	0.111	0.103	0.108
		30	0.0082	0.0054	0.0062	0.0043	0.0046	0.0037			30	0.106	0.125	0.110	0.129	0.111	0.111	0.112	0.120
		40	0.0052	0.0032	0.0040	0.0028	0.0029	0.0023			40	0.117	0.118	0.122	0.118	0.111	0.111	0.123	0.122
Min	}	20	0.0106	0.0060	0.0079	0.0049	0.0067	0.0043	Min	}	20	0.105	0.129	0.112	0.130	0.111	0.111	0.111	0.111
		30	0.0054	0.0028	0.0047	0.0023	0.0032	0.0021			30	0.0994	0.144	0.107	0.126	0.111	0.111	0.107	0.124
		40	0.0031	0.0014	0.0027	0.0013	0.0021	0.0012			40	0.119	0.116	0.130	0.118	0.111	0.111	0.120	0.118

Source: From IES, 1979.

**TABLE 20.13c** C and K Factors for No Window Controls for Ground Illumination (Ceiling Reflectance, 80%; Floor Reflectance, 30%)

Ground Illumination																			
C: Coefficient of Utilization								K: Coefficient of Utilization											
Room Length (ft.)		20		30		40		Ceiling Height (ft.)		8		10		12		14			
Wall Reflectance (%)		70	30	70	30	70	30	Wall Reflectance (%)		70	30	70	30	70	30	70	30		
Room Width (ft.)								Room Width (ft.)											
Max	}	20	0.0147	0.0112	0.0102	0.0088	0.0081	0.0071	Max	}	20	0.124	0.206	0.140	0.135	0.111	0.111	0.0909	0.0859
		30	0.0141	0.0012	0.0098	0.0088	0.0077	0.0070			30	0.182	0.188	0.140	0.143	0.111	0.111	0.0918	0.0878
		40	0.0137	0.0112	0.0093	0.0086	0.0072	0.0069			40	0.124	0.182	0.140	0.142	0.111	0.111	0.0936	0.0879
Mid	}	20	0.0128	0.0090	0.0094	0.0071	0.0073	0.0060	Mid	}	20	0.123	0.145	0.122	0.129	0.111	0.111	0.100	0.0945
		30	0.0083	0.0057	0.0062	0.0048	0.0050	0.0041			30	0.0966	0.104	0.107	0.112	0.111	0.111	0.110	0.105
		40	0.0055	0.0037	0.0044	0.0033	0.0042	0.0026			40	0.0790	0.0786	0.0999	0.106	0.111	0.111	0.118	0.118
Min	}	20	0.0106	0.0071	0.0082	0.0054	0.0067	0.0044	Min	}	20	0.0994	0.108	0.110	0.114	0.111	0.111	0.107	0.104
		30	0.0051	0.0026	0.0041	0.0023	0.0033	0.0021			30	0.0816	0.0822	0.0984	0.105	0.111	0.111	0.121	0.116
		40	0.0029	0.0018	0.0026	0.0012	0.0022	0.0011			40	0.0700	0.0656	0.0946	0.0986	0.111	0.111	0.125	0.132

Source: From IES, 1979.



(b) Ground reflected:

$$C_{g, \max} = 0.0098; K_{g, \max} = 0.140.$$

$$C_{g, \text{mid}} = 0.0062; K_{g, \text{mid}} = 0.107.$$

$$C_{g, \min} = 0.0041; K_{g, \min} = 0.0984.$$

Then using Equation 20.98,

$$E_{\text{sp}, \max} = 605,955(0.0137)(0.125)(0.78) = 809 \text{ fc},$$

$$E_{\text{sp}, \text{mid}} = 605,955(0.0062)(0.110)(0.78) = 322 \text{ fc},$$

$$E_{\text{sp}, \min} = 605,955(0.0047)(0.107)(0.78) = 238 \text{ fc},$$

$$E_{\text{gp}, \max} = 27,040(0.0098)(0.140)(0.78) = 29 \text{ fc},$$

$$E_{\text{gp}, \text{mid}} = 27,040(0.0062)(0.107)(0.78) = 14 \text{ fc},$$

$$E_{\text{gp}, \min} = 27,040(0.0041)(0.0984)(0.78) = 9 \text{ fc}.$$

Thus,

$$E_{\max} = 838 \text{ fc},$$

$$E_{\text{mid}} = 336 \text{ fc},$$

$$E_{\min} = 247 \text{ fc}.$$

#### 20.3.5.4.2 Lumen Method of Skylighting

The lumen method of skylighting calculates the average illuminance at the interior work-plane provided by horizontal skylights mounted on the roof. The procedure for skylighting is generally the same as that described above for sidelighting. As with windows, the illuminance from both overcast sky and clear sky plus sun cases are determined for specific days in different seasons and for different times of the day, and a judgment is then made as to the number and size of skylights and any controls needed.

The procedure is presented in four steps: (1) finding the horizontal illuminance on the outside of the skylight; (2) calculating the effective transmittance through the skylight and its well; (3) figuring the interior space light loss factor and the utilization coefficient; and finally, (4) calculating illuminance on the work-plane.

*Step 1: Horizontal Sky and Sun Illuminances*—The horizontal illuminance value for an overcast sky or a clear sky plus sun situation can be determined from [Figure 20.58](#) knowing only the solar altitude.

*Step 2: Net Skylight Transmittance*—The transmittance of the skylight is determined by the transmittance of the skylight cover(s), the reflective efficiency of the skylight well, the net-to-gross skylight area, and the transmittance of any light-control devices (lenses, louvers, etc.).

The transmittance for several flat-sheet plastic materials used in skylight domes is presented in [Table 20.14](#). To get the effective dome transmittance ( $T_D$ ) from the flat-plate transmittance ( $T_F$ ) value (AAMA 1977), use

**TABLE 20.14** Flat-Plate Plastic Material Transmittance for Skylights

Type	Thickness (in.)	Transmittance (%)
Transparent	1/8–3/16	92
Dense translucent	1/3	32
Dense translucent	3/16	24
Medium translucent	1/8	56
Medium translucent	3/16	52
Light translucent	1/8	72
Light translucent	3/16	68

Source: From Murdoch, J. B., *Illumination Engineering—From Edison’s Lamp to the Laser*, Macmillan, New York, 1985.

$$T_D = 1.25T_F(1.18 - 0.416T_F). \tag{20.99}$$

If a double-domed skylight is used, then the single-dome transmittances are combined as follows (Pierson 1962):

$$T_D = \frac{T_{D_1}T_{D_2}}{T_{D_1}T_{D_2} - T_{D_1}T_{D_2}} \tag{20.100}$$

If the diffuse and direct transmittances for solar radiation are available for the skylight glazing material, it is possible to follow this procedure and determine diffuse and direct dome transmittances separately. However, this difference is usually not a significant factor in the overall calculations.

The efficiency of the skylight well ( $N_w$ ) is the fraction of the luminous flux from the dome that enters the room from the well. The well index (WI) is a geometric index (height,  $h$ ; length,  $l$ ; width,  $w$ ) given by

$$WI = \frac{h(w + l)}{2wl}, \tag{20.101}$$

and WI is used with the well-wall reflectance value in Figure 20.60 to determine well efficiency,  $N_w$ .

With  $T_D$  and  $N_w$  determined, the net skylight transmittance for the skylight and well is given by:

$$T_n = T_D N_w R_A T_C, \tag{20.102}$$

where  $R_A$  is the ratio of net to gross skylight areas and  $T_C$  is the transmittance of any light-controlling devices.

*Step 3: Light Loss Factor and Utilization Coefficient*—The light loss factor ( $K_m$ ) is again defined as the product of the room surface dirt depreciation (RSDD) and the skylight direct depreciation (SDD) fractions, similar to Equation 20.97. Following the reasoning for the sidelighting case, the RSDD value for clean rooms is around 0.94 and 0.84 for dirty rooms. Without specific data indicating otherwise, the SDD fraction is often taken as 0.75 for office buildings and 0.65 for industrial areas.

The fraction of the luminous flux on the skylight that reaches the work-plane ( $K_u$ ) is the product of the net transmittance ( $T_n$ ) and the room coefficient of utilization (RCU). Dietz et al. (1981) developed RCU equations for office and warehouse interiors with ceiling, wall, and floor reflectances of 75%, 50%, and 30%, and 50%, 30%, and 20%, respectively.

$$RCU = \frac{1}{1 + A(RCR)^B} \text{ if } RCR < 8, \tag{20.103}$$

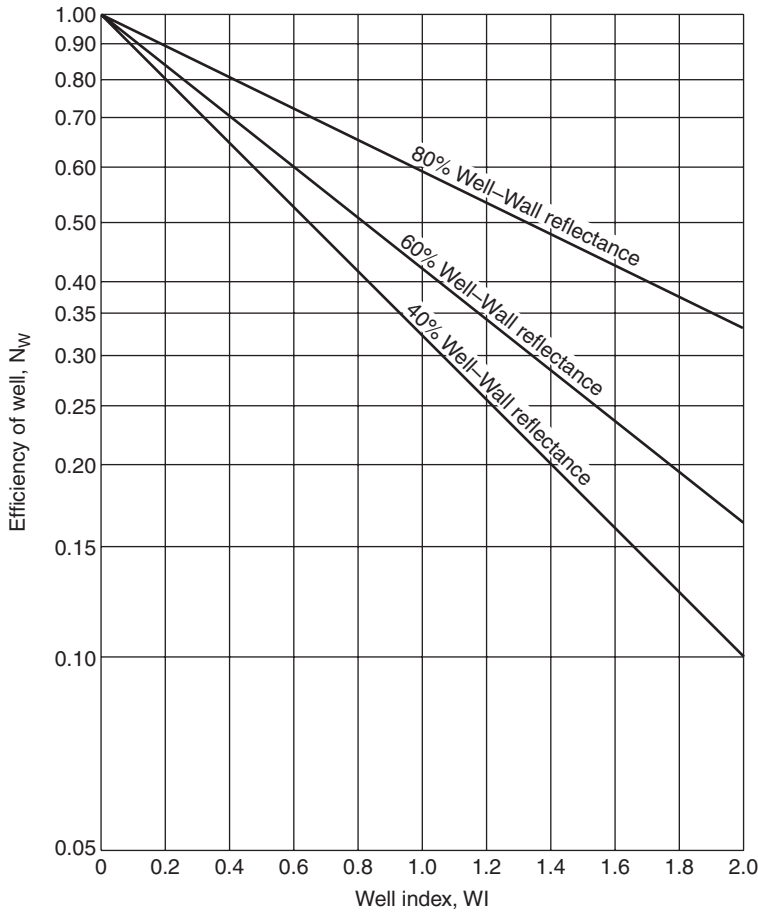


**FIGURE 20.60** Efficiency of well versus well index. (From IES (Illumination Engineering Society), *Lighting Handbook, Applications Volume*. Illumination Engineering Society, New York, 1987.)

where  $A$  is 0.0288 and  $B$  is 1.560 for offices, and  $A$  is 0.0995 and  $B$  is 1.087 for warehouses. Room cavity ratio (RCR) is given by

$$RCR = \frac{5h_c(l + w)}{lw}, \quad (20.104)$$

where  $h_c$  is the ceiling height above the work-plane and  $l$  and  $w$  are the room length and width, respectively.

The RCU is then multiplied by the previously determined  $T_n$  to give the fraction of the external luminous flux passing through the skylight and incident on the workplane:

$$K_u = T_n(RCU). \quad (20.105)$$

*Step 4: Work-Plane Illuminance*—The illuminance at the work-plane ( $E_{TWP}$ ) is given by

$$E_{TWP} = E_H \left( \frac{A_T}{A_{WP}} \right) K_u K_m, \quad (20.106)$$

where  $E_H$  is the horizontal overcast or clear sky plus sun illuminance from Step 1,  $A_T$  is total gross area of the skylights (number of skylights times skylight gross area), and  $A_{WP}$  is the work-plane area (generally room length times width). Note that in Equation 20.106, it is also possible to fix the  $E_{TWP}$  at some desired value and determine the required skylight aread.

Rules of thumb for skylight placement for uniform illumination include 4%–8% of roof area and spacing less than 1.5 times ceiling-to-work-plane distance between skylights (Murdoch 1984).

### Example 20.3.10

Determine the work-plane “clear sky plus sun” illuminance for a  $30 \times 30 \times 10$  ft.<sup>3</sup> office with 75% ceiling, 50% wall, and 30% floor reflectance with four  $4 \times 4$  ft.<sup>2</sup> double-domed skylights at 2:00 p.m. on January 15 at 32° latitude. The skylight well is 1 ft. deep at with 60% reflectance walls, and the outer- and inner-dome flat-plastic transmittances are 0.85 and 0.45, respectively. The net skylight area is 90%.

**Solution.** Follow the four steps in the lumen method for skylighting.

Step 1: Use Figure 20.58 with the solar altitude of 41.7° (calculated from Equation 20.93) for the clear sky plus sun curve to get horizontal illuminance:

$$E_H = 7400 \text{ fc.}$$

Step 2: Use Equation 20.99 to determine domed transmittances from the flat plate plastic transmittances given,

$$T_{D1} = 1.25(0.85)[1.18 - 0.416(0.85)] = 0.89,$$

$$T_{D2}(T_F = 0.45) = 0.56,$$

and use Equation 20.100 to get total dome transmittance from the individual dome transmittances:

$$T_D = \frac{(0.89)(0.56)}{(0.89) + (0.56) - (0.89)(0.56)} = 0.52.$$

To determine well efficiency, use  $WI=0.25$  from Equation 20.101 with 60% wall reflectance in Figure 20.60 to give  $N_w=0.80$ . With  $R_A=0.90$ , use Equation 20.102 to calculate net transmittance:

$$T_n = (0.52)(0.80)(0.90)(1.0) = 0.37.$$

Step 3: The light loss factor is assumed to be from “typical” values in Equation 20.97:  $K_m = (0.75)(0.94) = 0.70$ . The room utilization coefficient is determined using Equation 20.103 and Equation 20.104:

$$RCR = \frac{5(7.5)(30 + 30)}{(30)(30)} = 2.5,$$

$$RCU = [1 + 0.0288(2.5)^{1.560}]^{-1} = 0.89.$$

Equation 20.104 yields  $K_u = (0.37)(0.89) = 0.33$ .

Step 4: The work-plane illuminance is calculated by substituting the above values into Equation 20.106:

$$E_{TWP} = 7400 \left[ \frac{4(16)}{30(30)} \right] 0.33(0.70),$$

$$E_{TWP} = 122 \text{ fc.}$$

### 20.3.5.5 Daylighting Controls and Economics

The economic benefit of daylighting is directly tied to the reduction in lighting electrical energy operating costs. Also, lower cooling-system operating costs are possible due to the reduction in heating caused by the reduced electrical lighting load. The reduction in lighting and cooling system electrical power during peak demand periods could also beneficially affect demand charges.

The reduction of the design cooling load through the use of daylighting can also lead to the reduction of installed or first-cost cooling system dollars. Normally, economics dictate that an automatic lighting control system must take advantage of the reduced lighting/cooling effect, and the control system cost minus any cooling system cost savings should be expressed as a “net” first cost. A payback time for the lighting control system (“net” or not) can be calculated from the ratio of first costs to yearly operating savings. In some cases, these paybacks for daylighting controls have been found to be in the range of 1–5 years for office building spaces (Rundquist 1991).

Controls, both aperture and lighting, directly affect the efficacy of the daylighting system. As shown in Figure 20.61, aperture controls can be architectural (overhangs, light shelves, etc.) and/or window shading devices (blinds, automated louvers, etc.). The aperture controls generally moderate the sunlight entering the space to maximize/minimize solar thermal gain, permit the proper amount of light for visibility, and prevent glare and beam radiation onto the workplace. Photosensor control of electric lighting allows the dimming (or shutting off) of the lights in proportion to the amount of available daylighting illuminance.

In most cases, increasing the solar gain for daylighting purposes, with daylighting controls, saves more in electrical lighting energy and the cooling energy associated with the lighting than is incurred with the added solar gain (Rundquist 1991). In determining the annual energy savings total from daylighting,  $ES_T$ , the annual lighting energy saved from daylighting,  $ES_L$ , is added with the reduction in cooling system energy,  $\Delta ES_C$ , and with the negative of the heating system energy increase  $\Delta ES_H$ :

$$ES_T = ES_L + \Delta ES_C - \Delta ES_H. \quad (20.107)$$

A simple approach to estimating the heating and cooling energy changes associated with the lighting energy reduction is by using the fraction of the year associated with the cooling or heating season ( $f_C, f_H$ ) and the seasonal COP of the cooling or heating equipment. Thus, Equation 20.107 can be

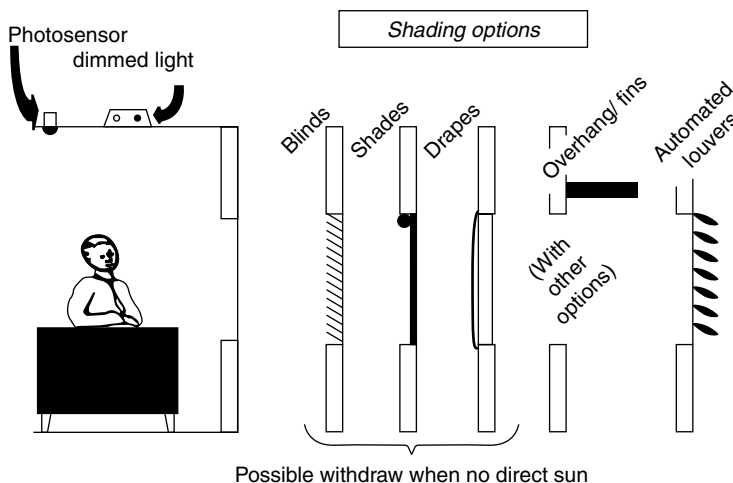


**FIGURE 20.61** Daylighting system controls. (From Rundquist, R. A., Daylighting controls: Orphan of HVAC design. *ASHRAE Journal*, 11 (November), 30–340, 1991.)

expressed as

$$ES_T = ES_L + \frac{f_C ES_L}{COP_c} - \frac{f_H ES_L}{COP_H},$$

$$ES_T = ES_L \left( 1 + \frac{f_C}{COP_c} - \frac{f_H}{COP_H} \right). \quad (20.108)$$

It should be noted that the increased solar gain due to daylighting has not been included here but would reduce summer savings and increase winter savings. If it is assumed that the increased wintertime daylighting solar gain approximately offsets the reduced lighting heat gain, then the last term in Equation 20.108 becomes negligible.

To determine the annual lighting energy saved ( $ES_L$ ), calculations using the lumen method described earlier should be performed on a monthly basis for both clear and overcast days for the space under investigation. Monthly weather data for the site would then be used to prorate clear and overcast lighting energy demands monthly. Subtracting the calculated (controlled) daylighting illuminance from the design illuminance leaves the supplementary lighting needed, which determines the lighting energy required.

This procedure has been computerized and includes many details of controls, daylighting methods, weather, and heating and cooling load calculations. ASHRAE (1989) lists many of the methods and simulation techniques currently used with daylighting and its associated energy effects.

### Example 20.3.11

A  $30 \times 20$  ft.<sup>2</sup> space has a photosensor dimmer control with installed lighting density of 2.0 W/ft.<sup>2</sup>. The required workplace illuminance is 60 fc and the available daylighting illuminance is calculated as 40 fc on the summer peak afternoon. Determine the effect on the cooling system (adapted from Rundquist 1991).

**Solution.** The lighting power reduction is  $(2.0 \text{ W/ft.}^2) (30 \times 20) \text{ ft.}^2 \times (40 \text{ fc}/60 \text{ fc}) = 800 \text{ W}$ . The space cooling load would also be reduced by this amount (assuming  $CLF = 1.0$ ):

$$\frac{800 \text{ W} \times 3.413 \text{ Btu h/W}}{12,000 \text{ Btu h/tn.}} = 0.23 \text{ tn.}$$

Assuming 1.5 tn. nominally installed for 600 ft.<sup>2</sup> of space at \$2200/tn., the 0.23-tn. reduction is “worth”  $0.23 \times \$2200/\text{tn.} = \$506$ . The lighting controls cost about \$1/ft.<sup>2</sup> of controlled area, so the net installed first cost is

$$\text{Net first cost} = \$600 \text{ controls} - \$500 \text{ A/C savings} = \$100.$$

Assuming the day-to-monthly-to-annual illuminance calculations gave a 30% reduction in annual lighting, the associated operating savings can be determined. Lighting energy savings are

$$ES_L = 0.30 \times 2.0 \text{ W/ft.}^2 \times 600 \text{ ft.}^2 \times 2500 \text{ h/year} = 900 \text{ kWh.}$$

Using Equation 20.108 to also include cooling energy saved due to lighting reduction (with  $COP_c = 2.5$ ,  $f_c = 0.5$ , and neglecting heating) gives

$$ES_T = 900(1 + 0.5/2.5 - 0) = 1080 \text{ kWh.}$$

At \$0.10 per kWh, the operating costs savings are  $\$0.10/\text{kWh} \times 1080 \text{ kWh} = \$108/\text{year}$ .

Thus, the simple payback is approximately 1 year ( $100/108$ ) for the “net” situation, and a little over 5.5 years ( $600/108$ ) against the “controls” cost alone. It should also be noted that the 800 W lighting electrical

reduction at peak hours, with an associated cooling energy reduction of  $800 \text{ W}/2.5 \text{ COP} = 320 \text{ W}$ , provides a peak demand reduction for the space of 1.1 kW, which can be used as a “first-cost savings” to offset control system costs.

## Glossary

**Active system:** A system employing a forced (pump or fan) convection heat transfer fluid flow.

**Daylighting:** The use of the sun’s radiant energy for illumination of a building’s interior space.

**Hybrid system:** A system with parallel passive and active flow systems or one using forced convection flow to distribute from thermal storage.

**Illuminance:** The density of luminous flux incident on a unit surface. Illuminance is calculated by dividing the luminous flux (in lumens) by the surface area ( $\text{m}^2$ ,  $\text{ft}^2$ ). Units are lux (lx) ( $\text{lumens}/\text{m}^2$ ) in SI and footcandles (fc) ( $\text{lumens}/\text{ft}^2$ ) in English systems.

**Luminous flux:** The time rate of flow of luminous energy (lumens). A lumen (lm) is the rate which luminous energy from a 1 candela (cd) intensity source is incident on a  $1\text{-m}^2$  surface 1 m from the source.

**Passive cooling system:** A system using natural energy flows to transfer heat to the environmental sinks (ground, air, and sky).

**Passive heating system:** A system in which the sun’s radiant energy is converted to heat by absorption in the system, and the heat is distributed by naturally occurring processes.

**Sidelighting:** Daylighting by light entering through the wall/side of a space.

**Skylight:** The diffuse solar radiation from a clear or overcast sky, excluding the direct radiation from the sun.

**Sunlight:** The direct solar radiation from the sun.

**Toplighting:** Daylighting by light entering through the ceiling area of a space.

## References

- 
- AAMA (Architectural Aluminum Manufacturers Association). 1977. Publication 1602.1.1977, *Voluntary Standard Procedure for Calculating Skylight Annual Energy Balance*. AAMA, Chicago, IL.
- ASHRAE (American Society of Heating, Refrigerating and Air-Conditioning Engineers). 1989. Fundamentals. In *ASHRAE Handbook*. ASHRAE, Atlanta, GA.
- ASHRAE (American Society of Heating, Refrigerating and Air-Conditioning Engineers), 1993. Fundamentals. In *ASHRAE Handbook*. ASHRAE, Atlanta, GA.
- ASHRAE (American Society of Heating, Refrigerating and Air-Conditioning Engineers). 1991. Heating, ventilating, and air-conditioning applications, In *ASHRAE Handbook*. ASHRAE, Atlanta, GA.
- ASHRAE (American Society of Heating, Refrigerating and Air-Conditioning Engineers), 1995. Heating, ventilating, and air-conditioning applications, In *ASHRAE Handbook*, pp. 279–127. ASHRAE, Atlanta, GA.
- Clay, R. A. 2001. Green is good for you. *Monitor on Psychology*, 32, 4, 40–42.
- Close, D. J., Dunkle, R. V., and Robeson, K. A. 1968. Design and performance of a thermal storage air conditioning system. *Mechanical and Chemical Engineering Transactions*, MCA, 45.
- De Paepe, M. and Janssens, A. 2003. Thermo-hydraulic design of earth-air heat exchanger. *Energy and Buildings*, 35, 389–397.
- Dietz, P., Murdoch, J., Pokoski, J., and Boyle, J. 1981. A skylight energy balance analysis procedure. *Journal of the Illuminating Engineering Society*, 11, October, 27–34.
- Duffie, J. A. and Beckman, W. A. 1991. *Solar Engineering of Thermal Processes*. 2nd Ed., Wiley, New York.

- Goswami, D. Y. and Biseli, K. M. 1994. Use of underground air tunnels for heating and cooling agricultural residential buildings. Report EES-78, Florida Energy Extension service, University of Florida, Gainesville, FL. August.
- Goswami, D. Y. and Dhaliwal, A. S. 1985. Heat transfer analysis in environmental control using an underground air tunnel. *J. of Solar Energy Eng.*, 107 (May): 141–45.
- Goswami, D. Y. and Ileslamlou, S. 1990. Performance analysis of a closed-loop climate control system using underground air tunnel. *J. of Solar Energy Eng.* 112 (May): 76–81.
- Givoni, B. 1994. *Passive and Low Energy Cooling of Buildings*, Van Nostrand Reinhold, New York.
- Hay, H. and Yellott, J. 1969. Natural air conditioning with roof ponds and movable insulation. *ASHRAE Transactions*, 75 (1), 165–177.
- Hollmuller, P. and Lachal, B. 2001. Cooling and preheating with buried pipe systems: Monitoring, simulation and economic aspects. *Energy and Buildings*, 33, 509–518.
- IES (Illumination Engineering Society). 1987. *Lighting Handbook, Applications Volume*. Illumination Engineering Society, New York.
- Kinney, L., McCluney, R., Cler, G., and Hutson, J. 2005. New designs in active daylighting: Good ideas whose time has (finally) come. In *Proceedings of the 2005 Solar World Congress*. August 6–12, 2005, ISES, Orlando, FL.
- Krarti, M. and Kreider, J. F. 1996. Analytical model for heat transfer in an underground air tunnel. *Energy Conversion Management*, 37, 10, 1561–1574.
- Kusuda, T. and Achenbach, P. R. 1965. Earth temperature and thermal diffusivity at selected stations in the United States. *ASHRAE Transactions*, 71 (1), 965.
- Labs, K. 1981. Regional analysis of ground and above ground climate. Report ORNL/Sub-81/40451/1, Oak Ridge National Laboratory, Oak Ridge, TN.
- Larson, R., Vignola, F., and West, R. eds. 1992. *Economics of Solar Energy Technologies*. American Solar Energy Society, Orlando, FL.
- Libbey-Owens-Ford Company 1976. *How to Predict Interior Daylight Illumination*. Libbey-Owens-Ford Company, Toledo, OH.
- Martin, M. and Berdahl, P. 1984. Characteristics of infrared sky radiation in the United States. *Solar Energy*, 33, 314, 321–336.
- Marlatt, W., Murray, C., and Squire, S. 1984. Roof Pond Systems Energy Technology Engineering Center. Report No. ETEC 6, April. Rockwell International, New York.
- McCluney, R. 1998. Advanced fenestration daylighting systems. In *International Daylighting Conference '98*, Natural Resources Canada/CETC, Ottawa, Canada.
- McQuiston, P. C. and Parker, J. D. 1994. *Heating, Ventilating, and Air Conditioning. 4th Ed.*, Wiley, New York.
- Murdoch, J. B. 1985. *Illumination Engineering—From Edison's Lamp to the Laser*. Macmillan, New York.
- NCDC (National Climatic Data Center). 1992. *Climatography of the U.S. #81*. NCDC, Asheville, NC.
- Olgay, A. and Olgay, V. 1967. *Solar Control and Shading Devices*, Princeton University Press, Princeton, NJ.
- Pierson, O. 1962. *Acrylics for the Architectural Control of Solar Energy*. Rohm and Haas, Philadelphia, PA.
- Robbins, C. L. 1986. *Daylighting—Design and Analysis*, Van Nostrand, New York.
- Rundquist, R. A. 1991. Daylighting controls: Orphan of HVAC design. *ASHRAE Journal*, 11 (November), 30–34.
- PSDH. 1980. *Passive Solar Design Handbook*. Volume One: Passive Solar Design Concepts, DOE/CS-0127/1, March 1980. Prepared by Total Environmental Action, Inc. (B. Anderson, C. Michal, P. Temple, and D. Lewis); Volume Two: *Passive Solar Design Analysis*, DOE/CS-0127/2, January 1980. Prepared by Los Alamos Scientific Laboratory (J.D. Balcomb, D. Barley, R. McFarland, J. Perry, W. Wray and S. Noll). U.S. Department of Energy, Washington, DC.
- PSDH. 1984. *Passive Solar Design Handbook*. Part One: Total Environmental Action, Inc., Part Two: Los Alamos Scientific Laboratory, Part Three: Los Alamos National Laboratory. Van Nostrand Reinhold, New York.



## For Further Information

The most complete basic reference for passive system heating design is still the Passive Solar Design Handbook, all three parts. Solar Today magazine, published by the American Solar Energy Society, is the most available source for current practice designs and economics, as well as a source for passive system equipment suppliers. The ASHRAE Handbook of Fundamentals is a general introduction to passive cooling techniques and calculations, with an emphasis on evaporative cooling. Passive Solar Buildings and Passive Cooling, both published by MIT Press, contain a large variety of techniques and details concerning passive system designs and economics. All the major building energy simulation codes (DOE-2, EnergyPlus, TRNSYS, TSB13, etc.) now include passive heating and cooling technologies. The Illumination Engineering Society's Lighting Handbook presents the basis for and details of daylighting and artificial lighting design techniques. However, most texts on illumination present simplified format day lighting procedures. Currently used daylighting computer programs include various versions of Lumen Micro, Lightscape, and Radiance Passive Solar Design Strategies: Guidelines for Homebuilders (Passive Solar Industries Council, Washington, DC, 1989) presents a user-friendly approach to passive solar design.

## 20.4 Solar Cooling

---

*D. Yogi Goswami and Sanjay Vijayaraghavan*

In some ways, solar energy is better suited to space cooling and refrigeration than to space heating. The seasonal variation of solar energy is extremely well-suited to the space-cooling requirements of buildings. The principal factors affecting the temperature in a building are the average quantity of radiation received and the environmental air temperature. Because the warmest seasons of the year correspond to periods of high insolation, solar energy is most available when comfort cooling is most needed. Moreover, the efficiency of solar collectors increases with increasing insolation and increasing environmental temperature. Consequently, in the summer, the amount of energy delivered per unit surface area of collector can be larger than that in winter.

Solar cooling using various refrigeration cycles is technically feasible and has been demonstrated several times over past few decades. However, application of these systems has not become popular due to the unfavorable economics. The most widely used methods applied to solar cooling and air conditioning are vapor compression cycles, absorption-cooling cycles, and desiccant cooling. The vapor compression refrigeration cycle is probably the most widely used refrigeration cycle. The vapor compression refrigeration cycle requires energy input into the compressor which may be provided as electricity from a photovoltaic system or as mechanical energy from a solar driven heat engine. Referring to [Figure 20.62](#), the compressor raises the pressure of the refrigerant, which also increases the temperature. The compressed high-temperature refrigerant vapor then transfers heat to the ambient environment in the condenser, where it condenses to a high-pressure liquid at a temperature close to the environmental temperature. The liquid refrigerant is then passed through the expansion valve where the pressure is suddenly reduced, resulting in a vapor-liquid mixture at a much lower temperature. The low-temperature refrigerant is then used to cool air or water in the evaporator where the liquid refrigerant evaporates by absorbing heat from the medium being cooled. The cycle is completed by the vapor returning to the compressor. If water is cooled in the evaporator, the device is usually called a *chiller*. The chilled water could then be used to cool air in a building.

In an absorption system, the refrigerant is evaporated or distilled from a less volatile absorbent, the vapor is condensed in a water- or air-cooled condenser, and the resulting liquid is passed through a pressure-reducing valve to the cooling section (evaporator) of the unit. The refrigerant from the evaporator flows into the absorber, where it is reabsorbed in the stripped absorbing liquid and

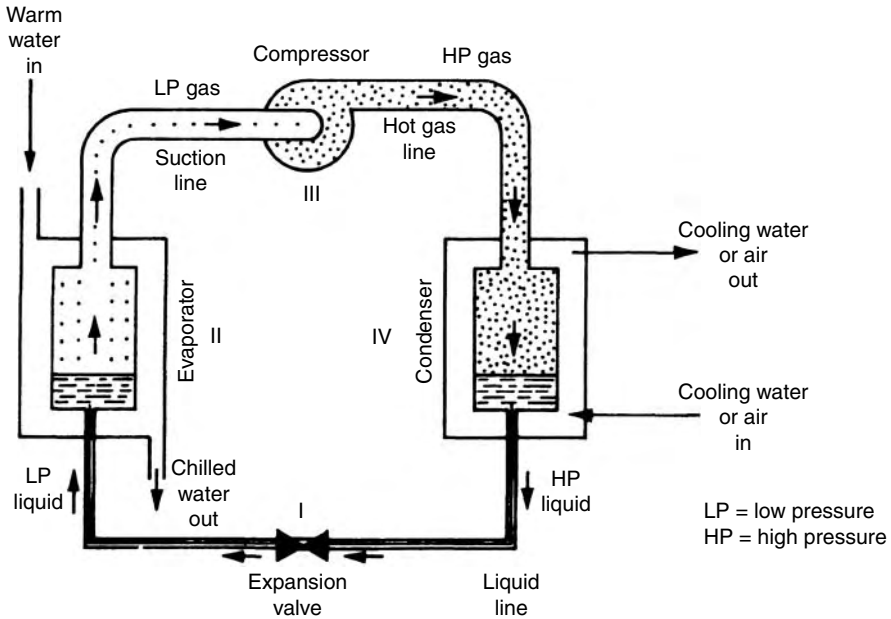


FIGURE 20.62 A schematic diagram showing a typical vapor compression refrigeration cycle.

pumped back to the heated generator. The heat required to evaporate the refrigerant in the generator can be supplied directly from solar energy as shown in Figure 20.63.

In humid climates, removal of moisture from the air represents a major portion of the air-conditioning load. In such climates, desiccant systems can be used for dehumidification, in which solar energy can provide most of the energy requirements. There are several passive space cooling techniques that are

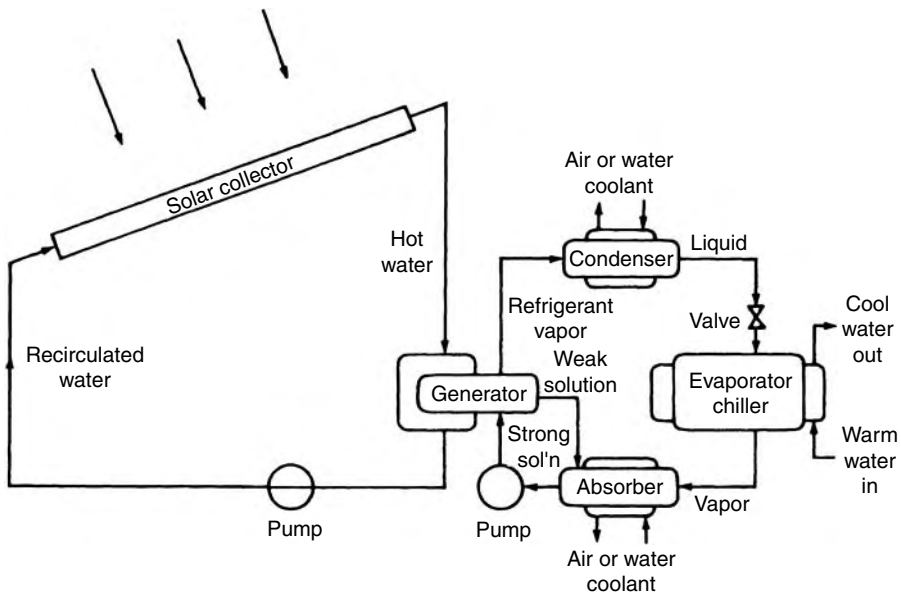


FIGURE 20.63 Figure shows the basic arrangement of a solar driven absorption cycle.

described elsewhere. The present section covers the active solar cooling techniques based on vapor compression and vapor-absorption refrigeration cycles and desiccant humidification.

### 20.4.1 Vapor Compression Cycle

The principle of operation of a vapor compression refrigeration cycle can be illustrated conveniently with the aid of a pressure–enthalpy diagram as shown in Figure 20.64. The ordinate is the pressure of the refrigerant in  $\text{N/m}^2$  absolute, and the abscissa its enthalpy in  $\text{kJ/kg}$ . The roman numerals in Figure 20.64 correspond to the physical locations in the schematic diagram of Figure 20.62. Process I is a throttling process in which hot liquid refrigerant at the condensing pressure  $p_c$  passes through the expansion valve, where its pressure is reduced to the evaporator pressure,  $p_e$ . This is an isenthalpic (constant enthalpy) process in which the temperature of the refrigerant decreases. In this process, some vapor is produced and the state of the mixture of liquid refrigerant and vapor entering the evaporator is shown by point A. Because the expansion process is isenthalpic, the following relation holds:

$$h_{ve}f + h_{lc}(1-f) = h_{lc},$$

where  $f$  is the fraction of mass in vapor state, subscripts “v” and “l” refer to vapor and liquid states, respectively, and “c” and “e” refer to states corresponding to condenser and evaporator pressures, respectively.

Process II represents the vaporization of the remaining liquid. This is the process during which heat is removed from the chiller. Thus, the specific refrigeration effect (per kilogram of refrigerant flow),  $q_r$  is

$$q_r = h_{ve} - h_{lc}, \text{ in kJ/kg.}$$

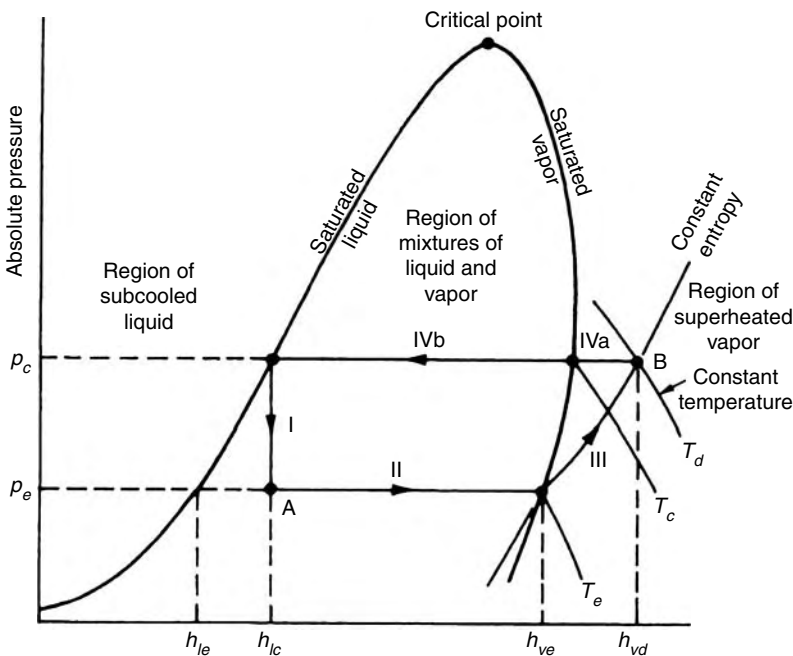


FIGURE 20.64 The thermodynamic state processes of the vapor compression refrigeration cycle shown on a pressure–enthalpy ( $p$ – $h$ ) diagram.

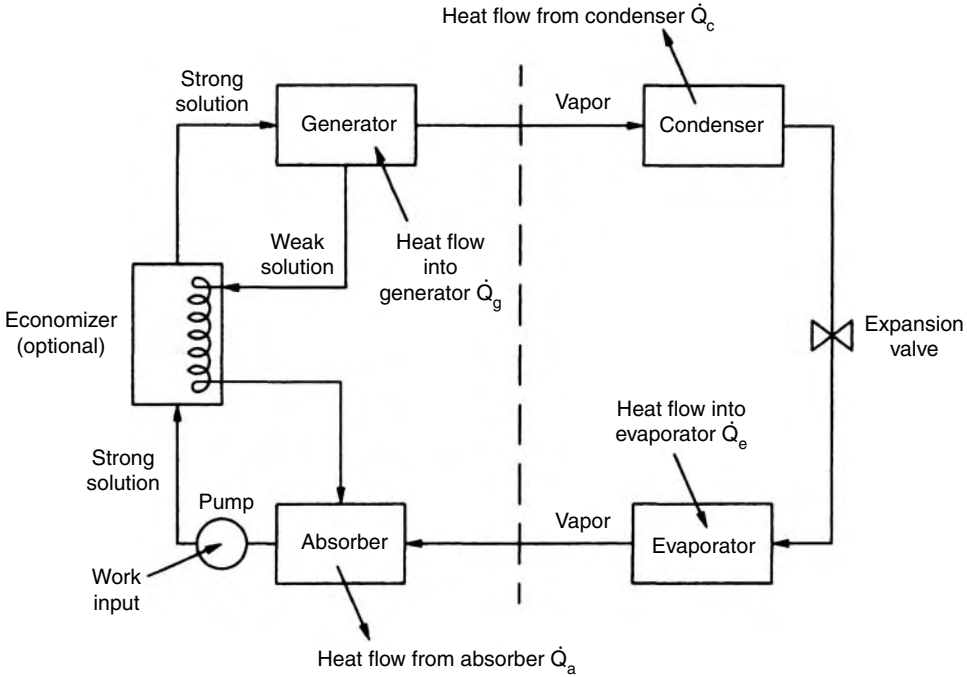


FIGURE 20.65 A typical absorption refrigeration cycle.

In the United States, it is still common practice to measure refrigeration in terms of tons. One ton is the amount of cooling produced if 1 ton of ice is melted over a period of 24 h. One ton of cooling is equivalent to 3.516 kW, or 12,000 Btu/h.

Process III in Figure 20.64 represents the compression of refrigerant from pressure  $p_e$  to pressure  $p_c$ . The process requires work input from an external source, which may be obtained from a solar-driven expander turbine or a solar electrical system. In general, if the heated vapor leaving the compressor is at the condition represented by point B in Figure 20.64, the work of compression is

$$W_c = \dot{m}_r(h_{vd} - h_{ve}).$$

In an idealized cycle analysis, the compression process is usually assumed to be isentropic.

Process IV represents the condensation of the refrigerant. Actually, sensible heat is first removed in subprocess IVa as the vapor is cooled at constant pressure from  $T_d$  to  $T_c$  and latent heat is removed at the condensation temperature  $T_c$  corresponding to the saturation pressure,  $p_c$ , in the condenser. The heat transfer rate in the condenser,  $\dot{Q}_c$ , is

$$\dot{Q}_c = \dot{m}_r(h_{vd} - h_{1c}).$$

This heat must be rejected to the environment, either to cooling water or to the atmosphere if no water is available.

The overall performance of a refrigeration machine is usually expressed as the coefficient of performance that is defined as the ratio of the heat transferred in the evaporator,  $\dot{Q}_r$ , to the shaft work supplied by the compressor:

$$COP = \frac{\dot{Q}_r}{W_c} = \frac{h_{ve} - h_{1c}}{h_{vd} - h_{ve}}.$$

## 20.4.2 Absorption Air Conditioning

Absorption air conditioning is compatible with solar energy because a large fraction of the energy required is thermal energy at temperatures that solar collectors can easily provide. Low- and medium-temperature solar collectors have been used to drive several absorption air conditioning systems (Macriss and Zawacki 1989; Mathur 1989; Manrique 1991; Chinnappa and Wijesundera 1992; Siddiqui 1993; Thornbloom and Nimmo 1994; Hewett 1995). Although single-effect absorption refrigeration systems can be run using solar heated hot water at 80°C, higher temperatures are preferred for better refrigeration cycle performance. The key difference between a conventional gas-fired absorption chiller and one used for solar applications is the larger heat transfer area required to make the cycle work using the lower driving temperatures available in solar applications. Figure 20.65 shows a schematic of an absorption refrigeration system. Absorption refrigeration differs from vapor compression air conditioning only in the method of compressing the refrigerant (left of the dashed line in Figure 20.65). In absorption air conditioning systems, the pressurization is accomplished by first dissolving the refrigerant in a liquid (the absorbent) in the absorber section, then pumping the solution to a high pressure with a liquid pump. The low-boiling refrigerant is then driven from solution by the addition of heat in the generator. By this means, the refrigerant vapor is compressed without the large input of high-grade shaft work that the vapor compression cycle demands.

The effective performance of an absorption cycle depends on the two materials that comprise the refrigerant–absorbent pair. Desirable characteristics for the refrigerant–absorbent pair are as follows:

1. Absence of a solid-phase sorbent
2. A refrigerant more volatile than the absorbent so that separation from the absorbent occurs easily in the generator
3. An absorbent that has a strong affinity for the refrigerant under conditions in which absorption takes place
4. A high degree of stability for long-term operations
5. Nontoxic and nonflammable fluids for residential applications; this requirement is less critical in industrial refrigeration
6. A refrigerant that has a large latent heat so that the circulation rate can be kept low
7. A low fluid viscosity that improves heat and mass transfer and reduces pumping power
8. Fluids that do not have long-term environmental effects

Lithium bromide–water (LiBr–H<sub>2</sub>O) and ammonia–water (NH<sub>3</sub>–H<sub>2</sub>O) are the two pairs that meet most of the requirements and have been used commercially in several applications. In the LiBr–H<sub>2</sub>O system, water is the refrigerant and LiBr is the absorbent, whereas in the ammonia–water system, ammonia is the refrigerant and water is the absorbent. Because the LiBr–H<sub>2</sub>O system has a high-volatility ratio, it can operate at lower pressures and therefore, at the lower generator temperatures achievable by flat-plate collectors. A disadvantage of this system is that LiBr has a tendency to crystallize in the stream returning from the generator. Crystallization is avoided by careful system design and by the use of additives. Furthermore, because the refrigerant is water, the system evaporator cannot be operated at or below the freezing point of water. Therefore, the LiBr–H<sub>2</sub>O system is operated at evaporator temperatures of 5°C or higher. Using a mixture of LiBr with some other salt as the absorbent can overcome the crystallization problem. The ammonia–water system has the advantage that the evaporator can be maintained at very low temperatures. However, for temperatures much below 0°C, water vapor must be removed from ammonia as much as possible to prevent ice crystals from forming. This requires a rectifying column after the boiler. Also, ammonia is a safety code group B2 fluid (ASHRAE Standard 34-1992) that restricts its use indoors (ASHRAE 1997). Consequently, the ammonia–water system cannot use a direct expansion (DX) evaporator. Other refrigerant–absorbent pairs include (Macriss and Zawacki 1989):

- Ammonia–salt
- Methylamine–salt

- Alcohol–salt
- Ammonia–organic solvent
- Sulfur dioxide–organic solvent
- Halogenated hydrocarbons–organic solvent
- Water–alkali nitrate
- Ammonia–water–salt

If the pump work is neglected, the COP of an absorption air conditioner can be calculated from Figure 20.65:

$$\text{COP} = \frac{\text{cooling effect}}{\text{heat input}} = \frac{\dot{Q}_c}{\dot{Q}_g}$$

The COP values for absorption air conditioning range from 0.5 for a small, single-stage unit to 0.85 for a double-stage, steam-fired unit. Another figure of merit for absorption systems is the ratio of the cooling effect to work supplied to the system (circulation pumps, fans, etc.).

Explicit procedures for the mechanical and thermal design as well as the sizing of the heat exchangers are presented in standard heat transfer texts. In large commercial units, it may be possible to use higher concentrations of LiBr, operate at a higher absorber temperature, and thus save on heat-exchanger costs. In a solar-driven unit, this approach would require concentrator-type or high-efficiency flat-plate solar collectors.

#### 20.4.2.1 Ammonia–Water Systems

The main difference between an ammonia–water system and a water–lithium bromide system is that a small amount of absorbent (water) also evaporates along with the refrigerant (ammonia) in the vapor generator. Therefore, ammonia–water systems use a rectifier (also called a *dephlagmator*) after the generator to condense as much water vapor out of the vapor mixture as possible. Figure 20.66 shows a schematic of an  $\text{NH}_3\text{--H}_2\text{O}$  absorption refrigeration system. Because ammonia has a much lower boiling point than water, a very high fraction of ammonia and a very small fraction of water are boiled off in the

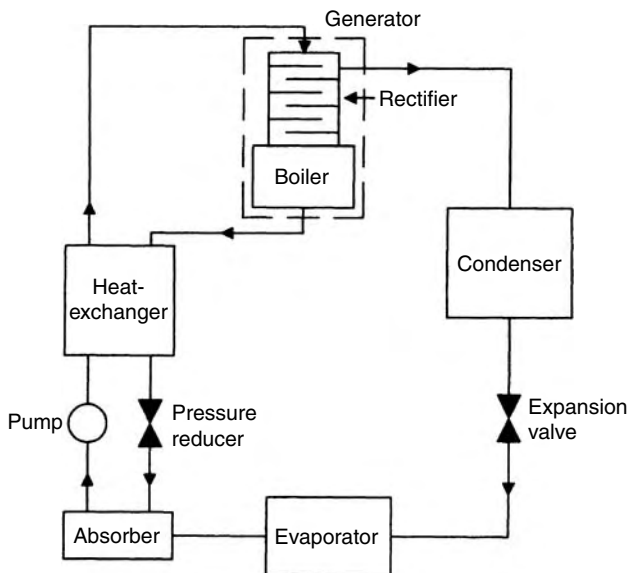


FIGURE 20.66 A diagram showing the arrangement of components for an ammonia-absorption cycle.

boiler. The vapor is cooled as it rises in the rectifier by the countercurrent flow of the strong  $\text{NH}_3\text{-H}_2\text{O}$  solution from the absorber; therefore, some moisture is condensed. The weak ammonia–water solution from the boiler goes through a pressure-reducing valve to the absorber, where it absorbs the ammonia vapor from the evaporator. The high-pressure ammonia from the rectifier is condensed by rejecting heat to the atmosphere. It may be further subcooled before expanding in a throttle valve. The two-phase low-temperature ammonia from the throttle valve provides refrigeration in the evaporator. The vapor from the evaporator is recombined with the weak ammonia solution in the absorber. Operating pressures are primarily controlled by the ambient air temperature for an air-cooled condenser, the evaporator temperature, and the concentration of the ammonia solution in the absorber.

#### 20.4.2.2 Multieffect Systems

A major price component in designing absorption systems is the solar collector field. To improve the economics of a solar absorption system, the efficiency of the solar collectors must be improved in addition to the COP of the absorption system, thus reducing the required collector area. A single-effect absorption system has a typical efficiency of around 0.7. For higher COP, double-effect systems are used. Double-effect systems typically operate at higher temperatures than single-effect systems requiring higher concentration solar collectors to provide the heat input. An example of a typical double-effect lithium bromide system is shown in Figure 20.67.

A double-effect lithium bromide cycle has two generators at two different pressure levels. Vapor is generated using the solar heat source in the first generator. This vapor is condensed in the second generator and the heat of condensation is used to produce more vapor (this arrangement is known as a *condenser-coupled system*). Thus the double-effect absorption cycle is a triple pressure cycle. A double-effect ammonia–water system is configured slightly differently (absorber-coupled), but still uses the same

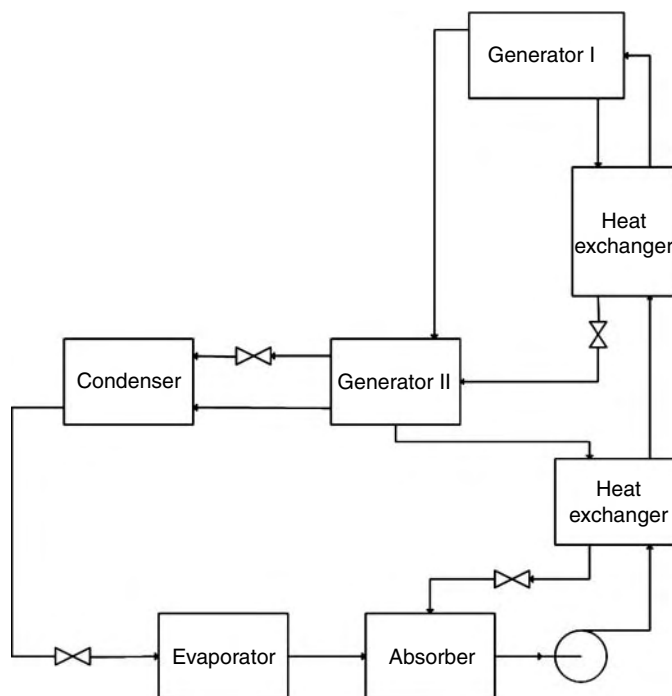


**FIGURE 20.67** A schematic diagram of a condenser coupled double-effect absorption cooling cycle. (Adapted from Wahlig, M., In *Active Solar Systems*, Vol. 6 of *Solar Heat Technologies: Fundamentals and Applications*, MIT Press, Cambridge, MA, 747–854, 1988. With permission.)

principle of internal heat recovery to produce more refrigerant vapor than is possible in a single-effect system. However, it requires a much higher driving temperature (140°C or higher) to operate efficiently.

### 20.4.3 Solar Desiccant Dehumidification

In hot and humid regions of the world experiencing significant latent cooling demand, solar energy may be used for dehumidification using liquid or solid desiccants. Rangarajan, Shirley, and Raustad (1989) compared a number of strategies for ventilation air conditioning for Miami, Florida, and found that a conventional vapor compression system could not even meet the increased ventilation requirements of ASHRAE Standard 62-1989. By pretreating the ventilation air with a desiccant system, proper indoor humidity conditions could be maintained and significant electrical energy could be saved. A number of researchers have shown that a combination of a solar desiccant and a vapor compression system can save from 15 to 80% of the electrical energy requirements in commercial applications such as supermarkets (Meckler 1988; Meckler, Parent, and Pesaran 1993; Meckler 1994; Meckler 1995; Spears and Judge 1997; Oberg and Goswami 1998a, 1998b).

In a desiccant air conditioning system, moisture is removed from the air by bringing it in contact with the desiccant, followed by sensible cooling of the air by a vapor compression cooling system, vapor-absorption cooling system, or evaporative cooling system. The driving force for the process is the water vapor pressure. When the vapor pressure in air is higher than on the desiccant surface, moisture is transferred from the air to the desiccant until an equilibrium is reached (see Figure 20.67). To regenerate the desiccant for reuse, the desiccant is heated, which increases the water vapor pressure on its surface. If air with lower vapor pressure is brought into contact with this desiccant, the moisture passes from the desiccant to the air (Figure 20.68). Two types of desiccants are used: solids such as silica gel and lithium chloride, or liquids such as salt solutions and glycols.

The two solid desiccant materials that have been used in solar systems are silica gel and molecular sieves, a selective absorber. Figure 20.69 shows the equilibrium absorption capacity of several substances. Note that molecular sieves has the highest capacity up to 30% humidity, and silica gel is optimal between 30 and 75%, the typical humidity range for buildings.

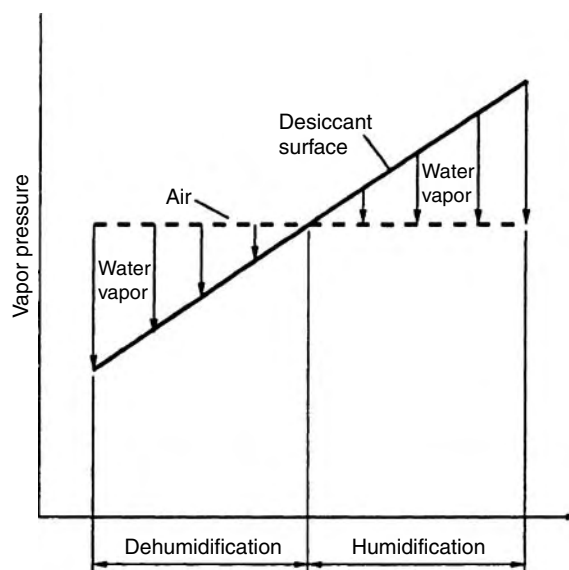


FIGURE 20.68 Vapor pressure vs. temperature and water content for desiccant and air.



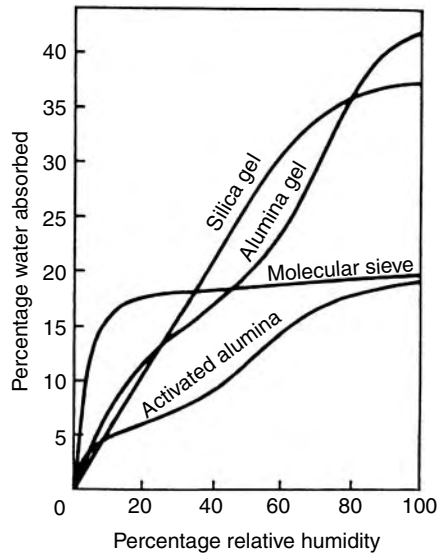


FIGURE 20.69 Equilibrium capacities of common water absorbents.

Figure 20.70 is a schematic diagram of a desiccant cooling ventilation cycle (also known as the Pennington cycle), which achieves both dehumidification and cooling. The desiccant bed is normally a rotary wheel of a honeycomb-type substrate impregnated with the desiccant. As the air passes through the rotating wheel, it is dehumidified while its temperature increases (processes 1 and 2) due to the latent heat of condensation. Simultaneously, a hot air stream passes through the opposite side of the rotating wheel, which removes moisture from the wheel. The hot and dry air at state 2 are cooled in a heat exchanger wheel to condition 3 and further cooled by evaporative cooling to condition 4. Air at condition 3 may be further cooled by vapor compression or vapor absorption systems instead of evaporative cooling. The return air from the conditioned space is cooled by evaporative cooling (processes 5 and 6), which in turn cools the heat exchanger wheel. This air is then heated to condition 7. Using solar heat, it is further heated to condition 8 before going through the desiccant wheel to regenerate the desiccant. A number of researchers have studied this cycle, or an innovative variation of it, and have found thermal COPs in the range of 0.5–2.58 (Pesaran, Penney, and Czandema 1992).

#### 20.4.4 Liquid-Desiccant Cooling System

Liquid desiccants offer a number of advantages over solid desiccants. The ability to pump a liquid desiccant makes it possible to use solar energy for regeneration more efficiently. It also allows several small dehumidifiers to be connected to a single regeneration unit. Because a liquid desiccant does not require simultaneous regeneration, the liquid may be stored for regeneration later when solar heat is available. A major disadvantage is that the vapor pressure of the desiccant itself may be enough to cause some desiccant vapors to mix with the air. This disadvantage, however, may be overcome by proper choice of the desiccant material.

A schematic of a liquid desiccant system is shown in Figure 20.71. Air is brought into contact with concentrated desiccant in a countercurrent flow in a dehumidifier. The dehumidifier may be a spray column or packed bed. The packings provide a very large area for heat and mass transfer between the air and the desiccant. After dehumidification, the air is sensibly cooled before entering the conditioned space. The dilute desiccant exiting the dehumidifier is regenerated by heating and exposing it to a countercurrent flow of a moisture-scavenging air stream. Liquid desiccants commonly used are aqueous solutions of lithium bromide, lithium chloride, calcium chloride, mixtures of these solutions, and

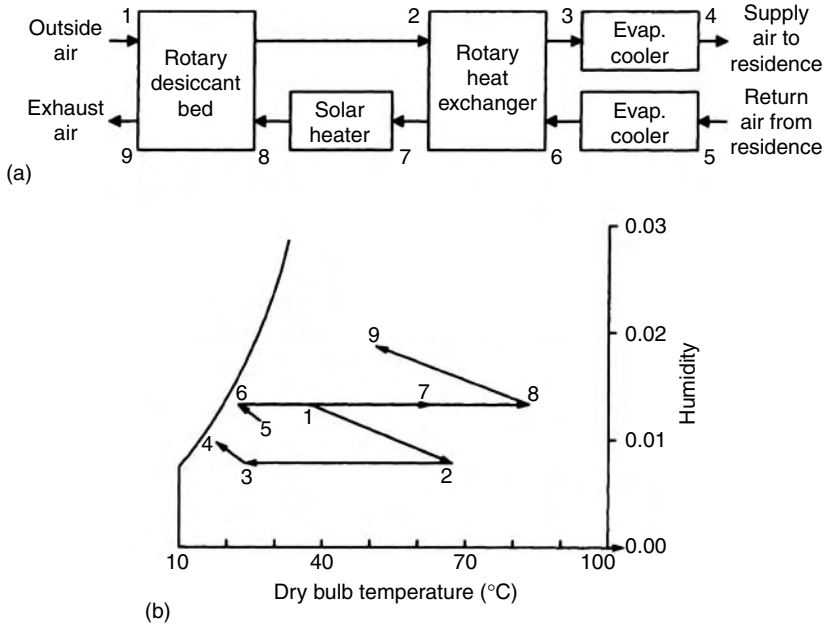


FIGURE 20.70 Schematic of a desiccant cooling ventilation cycle, (a) schematic of air flow, (b) the process on a psychrometric chart.

triethylene glycol (TEG). (See Oberg and Goswami 1998b). Vapor pressures of these common desiccants are shown in Figure 20.72 as a function of concentration and temperature, based on a number of references (Cyprus Foote Mineral Company; Dow Chemical Company 1992, 1996; Ertas, Anderson, and Kiris 1992; Zaytsev and Aseyev 1992). Other physical properties important in the selection of desiccant

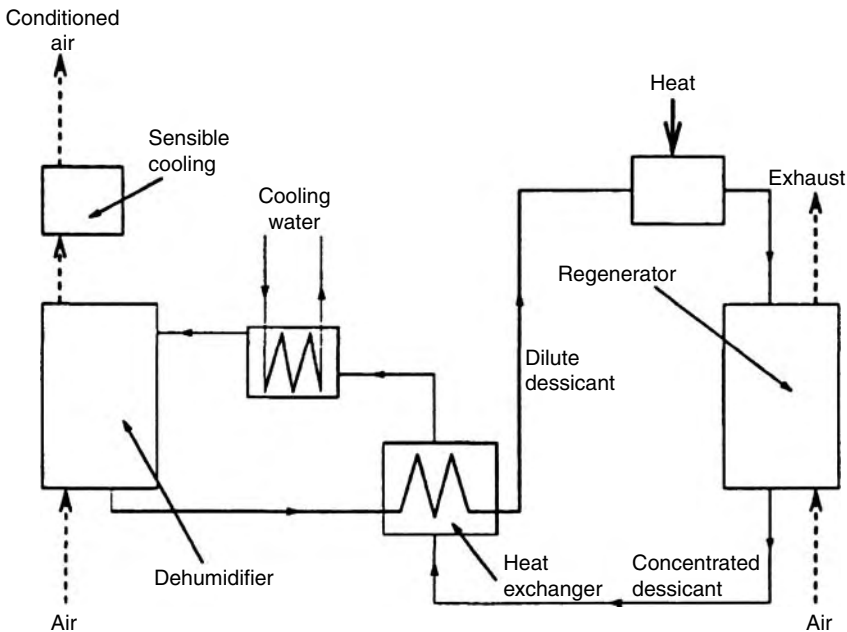


FIGURE 20.71 A conceptual liquid-desiccant cooling system.

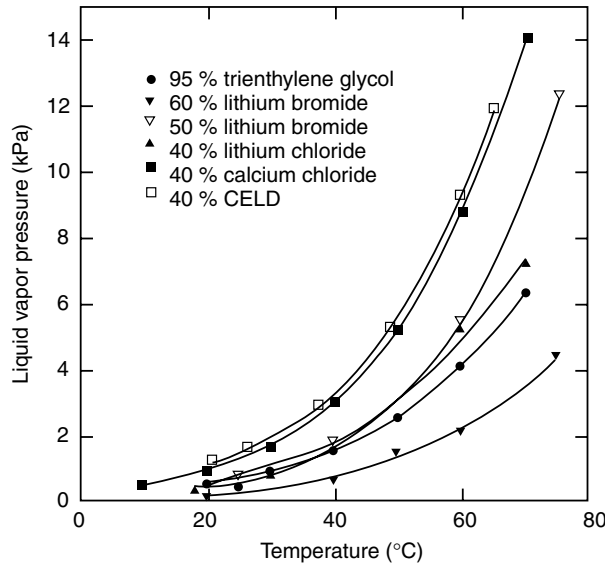


FIGURE 20.72 Vapor pressures of liquid desiccants.

materials are listed in Table 20.15. Although salt solutions and TEG have similar vapor pressures, the salt solutions are corrosive and have higher surface tension. The disadvantage of TEG is that it requires higher pumping power because of its higher viscosity.

Oberg and Goswami (1998b) have presented an in-depth review of liquid-desiccant cooling systems. Based on an extensive numerical modeling and on experimental studies, they have presented correlations for the performance of a packed-bed liquid-desiccant dehumidifier and a regenerator.

The performance of a packed-bed dehumidifier or a regenerator may be represented by a humidity effectiveness,  $\varepsilon_y$ , defined as the ratio of the actual change in humidity of the air to the maximum possible for the operating conditions (Ullah, Kettleborough, and Gandhidasan 1988; Chung 1989; Khan 1994):

$$\varepsilon_y = \frac{Y_{in} - Y_{out}}{Y_{in} - Y_{eq}}$$

where  $Y_{in}$  and  $Y_{out}$  are the humidity ratios of the air inlet and outlet, respectively, and  $Y_{eq}$  is the humidity ratio in equilibrium with the desiccant solution at the local temperature and concentration (Figure 20.73).

In addition to the humidity effectiveness, an enthalpy effectiveness,  $\varepsilon_H$ , is also used as a performance parameter (Khan 1994; Kettleborough and Waugaman 1995):

$$\varepsilon_H = \frac{H_{a,in} - H_{a,out}}{H_{a,in} - H_{a,eq}}$$

where  $H_{a,in}$ ,  $H_{a,out}$ , and  $H_{a,eq}$  are the enthalpies of the air at the inlet and outlet, and in equilibrium with the desiccant, respectively.

Oberg and Goswami (1998a) found the following correlation for  $\varepsilon_y$  and  $\varepsilon_H$ :

$$\varepsilon_y, \varepsilon_H = 1 - C_1(L/G)^a (H_{a,in}/H_{L,out})^b (aZ)^c,$$

**TABLE 20.15** Physical Properties of Liquid Desiccants at 25°C

Desiccant	Density, $\rho \times 10^{-3}$ (kg/m <sup>3</sup> )	Viscosity, $\mu \times 10^3$ (Ns/m <sup>2</sup> )	Surface Tension, $\gamma \times 10^3$ (N/m)	Specific Heat, $c_p$ (kJ/kg °C)	Reference
95% by weight triethylene glycol	1.1	28	46	2.3	Thornbloom and Nimmo (1996)
55% by weight lithium bromide	1.6	6	89	2.1	Gordon and Rabl (1986); Oberg and Goswami (1998a, 1998b)
40% calcium chloride	1.4	7	93	2.5	Gordon and Rabl (1986); Siddiqui (1993); Spears and Judge (1997)
40% by weight lithium chloride	1.2	9	96	2.5	Gordon and Rabl (1986)
40% by weight CELD	1.3	5	—	—	Cyprus Foote Mineral Company

Source: From Oberg, V. and Goswami, D. Y., *Advances in Solar Energy*, 12, 431–470, 1998.

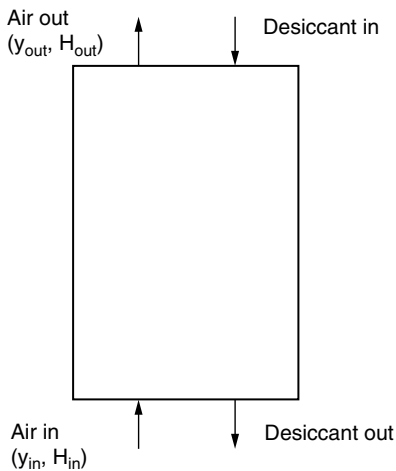


**FIGURE 20.73** Exchange of humidity and moisture between desiccant and air in the tower.

**TABLE 20.16** Constants for Performance Correlations

	$C_1$	$B$	$k_1$	$M_1$	$k_2$	$m_2$
$\epsilon_y$	48.345	-0.751	0.396	-1.573	0.033	-0.906
$\epsilon_H$	3.766	-0.528	0.289	-1.116	0.004	-0.365

where

$$a = k_1 \frac{\gamma_L}{\gamma_c} + m_1,$$

$$c = k_2 \frac{\gamma_L}{\gamma_c} + m_2.$$

Here,  $C_1$ ,  $b_1$ ,  $k_1$ ,  $m_1$ , and  $m_2$  are constants listed in Table 20.16.  $L$  and  $G$  are the liquid and air mass-flow rates, respectively;  $a$  is the packing surface area per unit volume for heat and mass transfer in  $\text{m}^2/\text{m}^3$ ;  $Z$  is the tower height in meters;  $\gamma_L$  is the surface tension of the liquid desiccant; and  $\gamma_c$  is the critical surface tension for the packing material.

Although liquid-desiccant cooling systems are not an off-the-shelf variety currently on the market, there are a number of examples of their use, especially in hybrid combinations with conventional vapor compression systems. In a hybrid system, the liquid desiccant would remove moisture from the air, allowing the vapor compression system to be downsized. Hybrid systems are especially useful in their ability to maintain comfort conditions in hot and humid climates, where conventional high-efficiency systems usually have trouble maintaining low humidity. Mago and Goswami (2003) and Mago (2003a, 2003b) did a simple cost analysis of a hybrid system for a residential building and a supermarket. They found that a house that typically requires a 5-tn. conventional air conditioning unit in Florida could use a hybrid system consisting of a desiccant tower of height 1.1 m, and a vapor compression system of 2 tn.

The total cost of the conventional system was estimated at \$4000, whereas the hybrid system would be \$3250 (\$1000 for the desiccant system + \$2250 for a 2-tn. vapor compression system). A solar system for regeneration of the desiccant was estimated at \$6500, making the total costs of a solar hybrid liquid-desiccant system at \$9780. They estimated that based on the electrical savings, a simple payback period would be 9.5 years. The payback period is high mainly because the solar regeneration system is not utilized throughout the year. For applications where the system can be used year-around, the payback period would be much shorter.

For a commercial application in a supermarket where the hybrid desiccant system and the solar regeneration system would be used throughout the year, the payback period would be less than two years (Mago and Goswami 2003; Mago 2003a). In this application, Mago also estimated that a conventional 13-tn. system, at an estimated cost of \$9300, would be replaced by a hybrid system consisting of a 2-m-high desiccant tower at a cost of \$1500 and a 5-tn. vapor compression system at an estimated cost of \$4000. A solar regeneration system for this desiccant system was estimated at \$9300. The two-year payback period confirmed the estimate of the U.S. Department of Energy (1996) that a simple payback is typically less than five years.

## References

- ASHRAE (American Society of Heating, Refrigerating and Air-Conditioning Engineers). 1997. Fundamentals. In *ASHRAE Handbook*, ASHRAE, Atlanta, GA.
- Chinnappa, J. C. V., and Wijeyesundera, N. E. 1992. Simulation of solar-powered ammonia-water integrated hybrid cooling system. *Journal of Solar Energy Engineering*, 114, 125–127.
- Chung, T. -W. 1989. Predictions of the moisture removal efficiencies for packed-bed dehumidification systems. In *Solar engineering—1989, Proceedings of the 11th Annual ASME Solar Energy Conference*, 371–377, ASME, New York.
- Cyprus Foote Mineral Company. Technical data on lithium bromide and lithium chloride. Bulletins 145 and 151, Cyprus Foote Mineral Company, Kings Mountain, NC.
- Dow Chemical Company. 1996. *Calcium chloride handbook*, Dow Chemical Company, Midland, MI.
- Dow Chemical Company. 1992. *A guide to glycols*, Dow Chemical Company, Midland, MI.
- Ertas, A., Anderson, E. E. and Kiris, I. 1992. Properties of a new liquid desiccant solution—Lithium chloride and calcium chloride mixture. *Solar Energy*, 49, 205–212.

- Hewett, R. 1995. Solar absorption cooling: An innovative use of solar energy. In *AIChE Symposium Series*, No. 306, Vol. 91, AIChE, New York.
- Kettleborough, C. F., and Waughman, D. G. 1995. An alternative desiccant cooling cycle. *Journal of Solar Energy Engineering*, 117, 251–255.
- Khan, A. Y. 1994. Sensitivity analysis and component modeling of a packed-type liquid desiccant system at partial load operating conditions. *International Journal of Energy Research*, 18, 643–655.
- Macriss, R. A., and Zawacki, T. S. 1989. Absorption fluid data survey: 1989 update. Oak Ridge National Laboratory Report, ORNL/Sub84-47989/4.
- Mago, P. J. 2003a. Sistema Hibrido de Enfriamiento como alternativa al sistema convencional de aire acondicionado. *Revista SABER*, 15(1), 39–44.
- Mago, P. J. 2003b. Analisis economico de la utilización de un sistema hibrido enfriamiento liquido secante en aplicaciones residenciales y comerciales. *Revista SABER*, 15(1), 45–50.
- Mago, P. J., and Goswami, D. Y. 2003. Study of the performance of a hybrid liquid desiccant system using lithium chloride. *ASME Journal of Solar Energy Engineering*, 125(1), 129–131.
- Manrique, J. A. 1991. Thermal performance of ammonia-water refrigeration system. *International Communications in Heat and Mass Transfer*, 19(6), 779–789.
- Mathur, G. D. 1989. Solar-operated absorption coolers. *Heating/Piping/Air Conditioning*. (November). 61, 11, 103–108.
- Meckler, M. 1988. Off-peak desiccant cooling and cogeneration combine to maximize gas utilization. *ASHRAE Transactions*, 94(Part 1), 575–596.
- Meckler, H. 1994. Desiccant-assisted air conditioner improves IAQ and comfort. *Heating, Piping & Air Conditioning*, 66(10), 75–84.
- Meckler, M. 1995. Desiccant outdoor air preconditioners maximize heat recovery ventilation potentials. *ASHRAE Transactions*, 101(Part 2), 992–1000.
- Meckler, M., Parent, Y. O. and Pesaran, A. A. 1993. Evaluation of dehumidifiers with polymeric desiccants. Gas Institute Report, Contract No. 5091-246-2247, Gas Research Institute, Chicago, IL.
- Oberg, V., and Goswami, D. Y. 1998a. Experimental study of heat and mass transfer in a packed bed liquid desiccant air dehumidifier. In *Solar engineering*, Morehouse J. H. and Hogan, R. E. ed., ASME, New York, pp. 155–166.
- Oberg, V., and Goswami, D. Y. 1998b. A review of liquid desiccant cooling. *Advances in Solar Energy*, 12, 431–470.
- Pesaran, A. A., Penney, T. R. and Czandema, A. W. 1992. Desiccant cooling: State-of-the-art assessment. Report No. NREL/TP-254-4147, National Renewable Energy Laboratory, Golden, CO.
- Rangarajan, K., Shirley, III, D. B. and Raustad, R. A. 1989. Cost-effective HVAC technologies to meet ASHRAE Standard 62-1989 in hot and human climates. *ASHRAE Transactions*. (Part 1), 166–182.
- Siddiqui, A. M. 1993. Optimum generator temperatures in four absorption cycles using different sources of energy. *Energy Conversion and Management*, 34(4), 251–266
- Spears, J. W., and Judge, J. 1997. Gas-fired desiccant system for retail super center. *ASHRAE Journal*, 39, 65–69.
- Thornbloom, M. and Nimmo, B. 1994. Modification of the absorption cycle for low generator firing temperatures. Solar Engineering 1994, In *Proceedings of the Joint Solar Energy Engineering Conference ASME 1994*, ASME, New York, 367–372.
- Thornbloom, M. and Nimmo, B. 1996. Impact of design parameters on solar open cycle liquid desiccant dehumidification system, In *Solar '96 Proceedings of the 1996 Annual Conference of the American Solar Energy Society*, American Solar Energy Society, Boulder, Colorado, pp. 107–111.
- Ullah, M. R., Kettleborough, C. F., and Gandhidasan, P. 1988. Effectiveness of moisture removal for an adiabatic counterflow packed tower absorber operating with CaCl<sub>2</sub>-air contact system. *Journal of Solar Energy Engineering*, 110, 98–101.
- US Department of Energy. 1996. Desiccant cooling programs. What's new in building energy research. Report DOE/GO-10096-084, Washington, DC.
- Zaytsev, I. O. and Aseyev, G. G. 1992. *Properties of aqueous solutions of electrolytes*, CRC Press, Boca Raton, FL.